



**HELLENIC REPUBLIC
UNIVERSITY OF IOANNINA
SCHOOL OF SCIENCES
DEPARTMENT OF MATERIALS SCIENCE ENGINEERING**

**«MACROMOLECULAR ARCHITECTURE FOR
COMPLEX STRUCTURES OF ELASTOMERS
SYNTHESIS – CHARACTERIZATION - PROPERTIES»**

**NTETSIKAS KONSTANTINOS
MATERIALS SCIENCE ENGINEER, MSc**

PhD THESIS

IOANNINA 2015



**HELLENIC REPUBLIC
UNIVERSITY OF IOANNINA
SCHOOL OF SCIENCES
DEPARTMENT OF MATERIALS SCIENCE ENGINEERING**

**«MACROMOLECULAR ARCHITECTURE FOR
COMPLEX STRUCTURES OF ELASTOMERS
SYNTHESIS – CHARACTERIZATION - PROPERTIES»**

**NTETSIKAS KONSTANTINOS
MATERIALS SCIENCE ENGINEER, MSc**

PhD THESIS

IOANNINA 2015



**ΕΛΛΗΝΙΚΗ ΔΗΜΟΚΡΑΤΙΑ
ΠΑΝΕΠΙΣΤΗΜΙΟ ΙΩΑΝΝΙΝΩΝ
ΣΧΟΛΗ ΘΕΤΙΚΩΝ ΕΠΙΣΤΗΜΩΝ
ΤΜΗΜΑ ΜΗΧΑΝΙΚΩΝ ΕΠΙΣΤΗΜΗΣ ΥΛΙΚΩΝ**

**«ΜΑΚΡΟΜΟΡΙΑΚΗ ΑΡΧΙΤΕΚΤΟΝΙΚΗ
ΠΟΛΥΠΛΟΚΩΝ ΔΟΜΩΝ ΕΛΑΣΤΟΜΕΡΩΝ
ΣΥΝΘΕΣΗ – ΧΑΡΑΚΤΗΡΙΣΜΟΣ - ΙΔΙΟΤΗΤΕΣ»**

**ΝΤΕΤΣΙΚΑΣ ΚΩΝΣΤΑΝΤΙΝΟΣ
ΜΗΧΑΝΙΚΟΣ ΕΠΙΣΤΗΜΗΣ ΥΛΙΚΩΝ, MSc**

ΔΙΔΑΚΤΟΡΙΚΗ ΔΙΑΤΡΙΒΗ

ΙΩΑΝΝΙΝΑ 2015

«Η έγκριση της διδακτορικής διατριβής από το Τμήμα Μηχανικών Επιστήμης Υλικών της Σχολής Θετικών Επιστημών του Πανεπιστημίου Ιωαννίνων, δεν υποδηλώνει αποδοχή των γνωμών του συγγραφέα Ν. 5343, άρθρο 202, παράγραφος 2».

Ημερομηνία αίτησης του κ. Κωνσταντίνου Ντέτσικα: 22/11/2010

Ημερομηνία ορισμού Τριμελούς Συμβουλευτικής Επιτροπής: 22/11/2010

Μέλη Τριμελούς Συμβουλευτικής Επιτροπής:

Επιβλέπων

Αυγερόπουλος Απόστολος, Καθηγητής, Τμήμα Μηχανικών Επιστήμης Υλικών, Πανεπιστήμιο Ιωαννίνων

Μέλη

Ζαφειρόπουλος Νικόλαος, Επίκουρος Καθηγητής, Τμήμα Μηχανικών Επιστήμης Υλικών, Πανεπιστήμιο Ιωαννίνων

Shi-Qing Wang, Kumho Professor, Department of Polymer Science-The University of Akron, Akron, OH, USA

Ημερομηνία ορισμού θέματος: 22/11/2010

«Macromolecular Architecture for Complex Structures of Thermoplastic Elastomers. Synthesis – Characterization – Properties»

«Μακρομοριακή Αρχιτεκτονική Πολύπλοκων Δομών Θερμοπλαστικών Ελαστομερών. Σύνθεση – Χαρακτηρισμός – Ιδιότητες»

Ημερομηνία τροποποίησης θέματος: 25/11/2014

«Μακρομοριακή Αρχιτεκτονική Πολύπλοκων Δομών Ελαστομερών. Σύνθεση – Χαρακτηρισμός – Ιδιότητες»

«Macromolecular Architecture for Complex Structures of Elastomers. Synthesis – Characterization – Properties»

ΛΙΟΡΙΣΜΟΣ ΕΠΤΑΜΕΛΟΥΣ ΕΞΕΤΑΣΤΙΚΗΣ ΕΠΙΤΡΟΠΗΣ : 17/12/2014

Απόστολος Αυγερόπουλος, Καθηγητής Τ.Μ.Ε.Υ., Πανεπιστήμιο Ιωαννίνων
Shi-Qing Wang, Prof., Dept. of Polymer Science-The University of Akron, OH, USA
Μάριος Κοσμάς, Καθηγητής Τμήμα Χημείας, Πανεπιστήμιο Ιωαννίνων
Δημήτριος Γουρνής, Καθηγητής Τ.Μ.Ε.Υ., Πανεπιστήμιο Ιωαννίνων
Κων/νος Μπέλτσιος, Καθηγητής Τ.Μ.Ε.Υ., Πανεπιστήμιο Ιωαννίνων
Νικόλαος Ζαφειρόπουλος, Επίκουρος Καθηγητής Τ.Μ.Ε.Υ., Πανεπιστήμιο Ιωαννίνων
Γεώργιος Σακελλαρίου, Λέκτορας, Τμήμα Χημείας, Ε.Κ.Π.Α.

Έγκριση Διδακτορικής Διατριβής με βαθμό «ΑΡΙΣΤΑ» στις 6/5/2015

Ο Πρόεδρος του Τμήματος

Η Γραμματέας του Τμήματος

**Καρακασίδης Μιχαήλ
Καθηγητής**

Ξανθή Τουτουνζόγλου

Dedicated to my family and to everyone who believed in me...

Knowledge speaks, but wisdom listens...

(Jimi Hendrix)

Acknowledgements

A very big and important chapter of my life has come to an end. It is so hard for me to imprint all the emotions that I feel in a few words. I have been member of this laboratory since February of 2008, when I was finishing my undergraduate studies at DMSE, UOI. From the first day in the lab until now, only good moments and positive emotions overwhelm me. During these 7 years I met and worked with a lot of people and I feel very lucky that I had the opportunity to know them. The least that I could do is to thank them through these words.

Above all I would like, from the deepest parts of my heart, to express my gratitude to my Advisor, Professor Apostolos Avgeropoulos. He was the person who, through his lecturing, inspired me to follow this field. I still remember the impression that I had after the first lecture of ‘Polymeric Materials’ and the first contact with the Polymers Laboratory. All these years, he never stopped guiding me with all his efforts in order to help and support me overcome any difficulties and our discussions were always very interesting and effective. I am grateful to him for providing me with the knowledge and principals in order to become a better scientist and I am truly thankful for giving me the opportunity to travel two times in Spain, to the Autonomous University of Barcelona (UAB) and opening my mind to new perspectives, for making new collaborations as well as for the financial support. This thesis wouldn’t exist without his help and corrections. I owe him a lot for being what I am and it was really honorable to meet him and work together as well as for his friendship.

I would like to express my deep and sincere gratitude to Professor Shi-Qing Wang, Morton Institute of Polymer Science and Engineering, The University of Akron, Ohio, USA who honored me with his presence by accepting the invitation of being a member of my 3-member Advisor Committee as well as being in the 7-member examining committee and for giving me the opportunity to collaborate with his well-known rheology group. He is a distinguished Professor and a hard-working man, with great ideas and theories. Also, I would like to thank Dr. Hao Sun and Gengxin Liu from the Polymer Rheology and Mechanics of Polymer Glasses Group for the rheological measurements in the homopolymers synthesized in this thesis and their help and discussions on the data of uniaxial extension experiments that they have done.

I would like also to thank the other member of the advisory committee, Nikolaos Zafeiropoulos, Assistant Professor at Department of Materials Science Engineering, University of Ioannina, for the fruitful discussions that we’ve had during my presence in the lab, and the remaining members of the 7-member committee, Konstantinos Beltsios and Dimitrios Gournis, Professors in the Department of Materials Science Engineering, University of Ioannina, Marios Kosmas, Professor in the Department of Chemistry, University of Ioannina and Sakellariou George, Lecturer in Department of Chemistry,

National and Kapodistrian University of Athens, for their presence and their useful observations.

I would like to thank Professor Clivia Sotomayor Torres, Catalan Institute of Nanotechnology, Campus de la UAB, Barcelona, Spain who gave me the opportunity to visit her laboratories twice through the collaboration by EU funded proposal (LAMAND) and everyone in the Phononic and Photonic Nanostructure Group for the nice and warm environment. I want to thank especially Dr. Nikos Kehagias and Dr. Claudia Delgado Simao for their hospitality and help in ICN. During my stay there I was trained on nanolithography techniques for diblock and triblock copolymers and I've learnt a lot of things in this field.

The Nuclear Magnetic Resonance (NMR) Center of the Network of Research Support Laboratories at the University of Ioannina is gratefully acknowledged for providing me the possibility to get trained for handling instruments in the specific Center as well as to gain access even after hours in order to run my samples. Dr. Konstantinos Tsiafoulis is the person who helped me to become an independent user in the Center and for that he is acknowledged as well.

I would like also to express my gratefulness to every member of the Polymers Laboratory, either to those who already left or to those who are still there. Their help, to every aspect of my everyday life in the lab, was something more than great and I am thankful for that. I deeply apologize for not mentioning all the names of the people I worked and know all these years. I want to thank especially Liontos George firstly for his friendship through all these years (since 1997, I think...) and then for the close collaboration that we've had since the first day in the lab. Together we have completed numerous projects during our presence in the lab. His assistance during the experiments as well as the characterization of the samples synthesized in this thesis was priceless. Furthermore, I would like to thank Dimitrios Moschovas, George Zapsas, George Polymeropoulos and Apostolos Karanastasis also for their help during the experimental and characterization sections and for the long term discussions that we've made through all these years as well as for their friendship. I feel very lucky and grateful to know and work with them. Moreover, I thank everybody else who made sure to create a nice working environment all these years in the lab. At the end of this route, I am very thankful that I made good friends and as I look back, I have only good moments to remember.

Above all, I am more than grateful to my parents, Tilemachos and Alexandra, and my sister Georgia who have been to my side all these years supporting me with all their strengths. They have taught me to work hard, to never give up my efforts and to be patient for every aspect of my life. They helped me make the right choices when needed and they put always my well-being above themselves. They stood always by me in difficult situations and they made me look things only from the positive point of view. I feel that words are not enough to

express my feelings for them and one thing I know for sure is that their love is overwhelming and unique. Furthermore, I would like to thank all my friends Giannis, Ntinos, Tilemachos and Mary among others, which stood by me and encouraged me to continue my efforts as well as Christine for her undivided love and support and always caring for me. I feel very grateful that all of you are a significant part in my life. Thank you for everything.

Θα ήθελα να εκφράσω την απεριόριστη ευγνωμοσύνη μου και αγάπη στους γονείς μου, Τηλέμαχο και Αλεξάνδρα, καθώς και στην αδερφή μου Γεωργία που βρισκόντουσαν πάντα στον πλευρό μου με όλες τους τις δυνάμεις. Τα εφόδια που μου έδωσαν από μικρό παιδί με βοήθησαν να αντιμετωπίζω τις δύσκολες καταστάσεις και με έκαναν καλύτερο άνθρωπο. Η ανιδιοτέλεια τους είναι μοναδική και πάντα με έβαζαν πάνω από τους εαυτούς τους. Με έμαθαν να δουλεύω σκληρά, να έχω υπομονή, και να βλέπω πάντα τα πράγματα από την θετική τους πλευρά. Η αγάπη τους είναι μοναδική και τα λόγια δεν φτάνουν για να περιγράψουν τα συναισθήματά που νιώθω για την αμέριστη συμπαράσταση όλα αυτά τα χρόνια.

Επίσης, θα ήθελα να ευχαριστήσω τα φιλαράκια μου Γιάννη, Ντίνο, Τηλέμαχο και Μαίρη μεταξύ άλλων για την συμπαράσταση τους και την ενθάρρυνση που μου έδωσαν ώστε να συνεχίσω τις προσπάθειες μου, καθώς και την Χριστίνα για την αμέριστη αγάπη της και συμπαράσταση. Πραγματικά νιώθω πολύ τυχερός που αποτελείτε ένα σημαντικό κομμάτι της ζωής μου. Σας ευχαριστώ για όλα.

Ioannina, April 24th, 2015

Konstantinos Ntetsikas

Abbreviations

a	Statistical segment length
BCC	Body Centered Cubic
1,3-Bd	1,3-Butadiene
Bu₂Mg	Dibutyl Magnesium
CDMSS	4-(Chlorodimethylsilyl)styrene
d	d-spacing of a unit cell
DCMSDPE	4-(dichloromethylsilyl)diphenylethylene
DFI	Difunctional initiator
DG	Double Gyroid
1,1-DPE	1,1-diphenylethylene
DSC	Differential Scanning Calorimetry
DVB	Divinyl Benzene
f	Mass or weight fraction
G	Shear Modulus
G'	Storage Modulus
G''	Loss Modulus
GC-MS	Gas Chromatography-Mass Spectrometry
HDPE	High Density Polyethylene
HEX	Hexagonally closed packed cylinders
¹H-NMR	Proton Nuclear Magnetic Resonance Spectroscopy
I	Polydispersity
i-BuLi	Isobutyl Lithium
Is	Isoprene
ISL	Intermediate Segregation Limit
K	Potassium
k_B	Boltzmann constant
LAM	Alternating Lamellae
LCB	Long Chain Branching
LDPE	Low Density Polyethylene
Li	Lithium
MeOH	Methanol
MFT	Mean Field Theory
\overline{M}_n	Number Average Molecular Weight
Mg	Magnesium
MO	Membrane Osmometry

MST	Microphase Separation Temperature
\overline{M}_w	Weight Average Molecular Weight
MWD	Molecular Weight Distribution
N	Degree of Polymerization
Na	Sodium
n-BuLi	n-Butyl Lithium
OBDD	Ordered Bicontinuous Double Diamond
ODT	Order-Disorder Transition
OOT	Order-Order Transition
PB	Poly(butadiene)
PI	Poly(isoprene)
PL	Perforated Lamellae
PS	Polystyrene
R	Radius of gyration
s	Number of segments per junction point
SANS	Small-Angle Neutron Scattering
SAOS	Small Amplitude Oscillatory Shear
SAXS	Small-Angle X-Ray Scattering
SCFT	Self-Consistent Field Theory
SEC	Size Exclusion Chromatography
sec-BuLi	sec-Butyl Lithium
SSL	Strong Segregation Limit
St	Styrene
t-BuLi	tert-Butyl Lithium
TEM	Transmission Electron Microscopy
T_g	Glass Transition Temperature
THF	Tetrahydrofuran
TGIC	Temperature Gradient Interaction Chromatography
T_m	Melting point temperature
TMEDA	N, N, N', N'-Tetramethylethylenediamine
T_{ODT}	Order-Disorder transition temperature
u	Statistical segment volume
V	Segment volume
VPO	Vapor Pressure Osmometry
WSL	Weak Segregation Limit

α	Constant expressing the enthalpic excess free energy of mixing
β	Constant expressing the entropic excess free energy of mixing
γ	Shear strain
$\dot{\gamma}$	Applied shear rate
δ	Solubility parameter
ε	Elasticity parameter
ζ	Conformational Asymmetry
η	Viscosity
ρ	Density
σ	Shear stress
τ	Relaxation time
$\tau_R(\mathbf{T})$	Rouse relaxation time
φ	Volume fraction
χ	Flory Huggins interaction parameter
ω	Frequency

Table of Contents

CHAPTER 1	5
Introduction	5
1.1 General Information	5
1.2 Scope of this PhD Thesis	7
<i>1.2.1 Linear and Non-Linear Homopolymers of PI_{3,4}</i>	8
<i>1.2.2 Linear Diblock Copolymers (PB-b-PI_{3,4}) and Miktoarm Stars [PB(PI_{3,4})₂ and PB(PI_{3,4})₃]</i>	8
1.3 Overview of the Thesis	10
CHAPTER 2	12
Anionic Polymerization	12
2.1 Basic Concepts	12
2.2 Alkadiene-Based Elastomers	15
2.3 Effect of Polar Additives in Anionic Polymerization of Alkadienes	16
2.4 Polymer Architectures	19
<i>2.4.1 General Information</i>	19
<i>2.4.2 Anionic Polymerization of Non-Linear Homopolymers</i>	21
2.5 Block Copolymers	24
<i>2.5.1 Linear Diblock Copolymers (AB)</i>	25
<i>2.5.2 Miktoarm Star Copolymers (A₂B and A₃B Type)</i>	27
CHAPTER 3	30
Physical Properties of Linear and Non-Linear Block Copolymers	30
3.1 Microphase Separation of Linear Diblock Copolymers	30
<i>3.1.1 Theory Background</i>	30
<i>3.1.2 Strong Segregation Limit (SSL)</i>	33
<i>3.1.3 Weak Segregation Limit (WSL)</i>	34
<i>3.1.4 Intermediate Segregation Limit (ISL)</i>	35
<i>3.1.5 Conformational Asymmetry</i>	36

3.1.6 Phase Diagram of PI- <i>b</i> -PS Diblock Copolymers	38
3.2 Microphase Separation of Non-Linear Block Copolymers	39
3.2.1 General Information	39
3.2.2 Microphase Separation of Miktoarm Star Copolymers	39
3.2.2.1 Theory Background	39
3.2.2.2 Experimental Results	42
3.3 Microphase Separation of Polydienes	43
3.4 Polymer Rheology	46
3.4.1 Introduction	46
3.4.2 Basic Concepts	47
3.4.2.1 Viscoelasticity	47
3.4.2.2 Storage and Loss Moduli	48
3.4.2.3 Non-Linear Viscoelasticity	49
3.4.3 Rheology of Linear and Branched Polymers	49
CHAPTER 4	52
Experimental Section	52
4.1 High Vacuum Technique	52
4.2 Solvent Purification	55
4.3 Monomer Purification	58
4.4 Dilution of the Initiator <i>sec</i> -Butyllithium (<i>sec</i> -BuLi)	60
4.5 Purification of Linking Agents and Other Reagents	62
4.6 Preparation of 4-(Chlorodimethylsilyl)Styrene (CDMSS)	63
4.7 Synthetic Procedures	65
4.7.1 Synthesis of Homopolymers of the $PI_{3,4}$ Type	66
4.7.2 Synthesis of H-type $PI_{3,4}$ Homopolymers	70
4.7.3 Synthesis of Linear Diblock Copolymers	77
4.7.4 Synthesis of Miktoarm Star Copolymers of the A_2B and A_3B Type ...	80
4.8 Molecular Characterization	86
4.8.1 Size Exclusion Chromatography (SEC)	86

4.8.2 Membrane Osmometry.....	86
4.8.3 Proton Nuclear Magnetic Resonance (¹ H-NMR) Spectroscopy	86
4.9 Thermal Analysis	87
4.9.1 Differential Scanning Calorimetry (DSC)	87
4.10 Morphological Characterization	87
4.10.1 Transmission Electron Microscopy (TEM)	87
CHAPTER 5	89
Experimental Results – Discussion – Conclusions – Future Work.....	89
5.1 Molecular Characterization Results of Linear Homopolymers PI _{3,4}	89
5.2 Molecular Characterization Results of Non-Linear Homopolymers PI _{3,4}	94
5.3 Thermal Analysis Results of Non-Linear Homopolymers PI _{3,4}	99
5.4.1 Rheology Results of Linear Homopolymers PI _{3,4}	103
5.4.2 Rheology Results of Non-Linear Homopolymers PI _{3,4}	105
5.5 Molecular Characterization Results of Linear Diblock Copolymers...	106
5.6 Thermal Analysis Results of Linear Diblock Copolymers	116
5.7 Morphological Characterization Results for the Linear Diblock Copolymers.....	121
5.8 Molecular Characterization Results of Miktoarm Star Copolymers...	134
5.9 Thermal Analysis Results of Miktoarm Star Copolymers	142
5.10 Morphological Characterization Results for the Miktoarm Star Copolymers.....	151
5.9.1 Miktoarm Star Copolymers of the PB(PI _{3,4}) ₂ Type	155
5.9.2 Miktoarm Star Copolymers of the PB(PI _{3,4}) ₃ Type	157
5.9.3 Comparison of the Morphological Characterization Results between Linear and Non-Linear Architectures Involving Immiscible Polydienes.	161
5.11 Conclusions-Future Work.....	164
5.11.1 Linear and Non-Linear Homopolymers of PI _{3,4}	165
5.11.2 Linear diblock copolymers (PB-b-PI _{3,4}) and miktoarm stars [PB(PI _{3,4}) ₂ and PB(PI _{3,4}) ₃]	166

References	171
Abstract	176
Περίληψη	178
Curriculum Vitae	180

CHAPTER 1

Introduction

1.1 General Information

Elastomers or elastic polymers are materials which are capable of undergoing large reversible extensions and compressions. A notation for the specific materials by IUPAC is: '*elastomer is a polymer that displays rubber-like elasticity*'.¹ Elastomers are a category of polymers with viscoelasticity (having both viscosity and elasticity) and very weak intermolecular forces, generally exhibiting low Young's modulus and high failure strain compared with other materials. Elastomer based materials are widely used for numerous applications in almost all areas of applied science and engineering.

The most known elastomers and widely used are natural rubber (cis 1,4-polyisoprene) and gutta-percha (trans 1,4-polyisoprene), which can be found in specific plants (*Hevea brasiliensis*, *Palaquium gutta*, etc.).² Based on the applications, elastomers can be divided into two large categories:

- a) *general purpose*, which refers to natural rubber (NR) and to various thermoplastic elastomers (styrenic block copolymers, polyolefin thermoplastic elastomers) and
- b) *special purpose*, which involves elastomers with specific applications in miscellaneous fields [synthetic rubbers of poly(isobutylene) and poly(isoprene)].³

Thermoplastic elastomers (TPEs), or thermoplastic rubbers, are a class of copolymers or physical blends of polymers (usually a plastic and a rubber), which have both thermoplastic and elastomeric properties. TPEs are a very important and popular category of elastomers with numerous applications in different fields. Most of the elastomers are known to be thermosets, even though in some cases they might behave like thermoplastics. The basic difference between thermoset elastomers and thermoplastic elastomers is the type of the crosslinking bond in their structures. All thermoplastic elastomers exhibit characteristic properties of cross-linked elastomers at room temperature, but at higher temperatures they behave as thermoplastics. In contrast with the typical elastomers, another interesting issue concerning TPEs is that they can retrieve their initial shape and therefore they can be used again. Thus, TPEs are considered one of the most important discoveries in the area of elastomers. Famous applications, where TPEs are mainly used, are: car industry, household appliances, shoe soles (styrenic block copolymers), adhesives, coatings and electrical cable jacket/inner insulations.⁴

Alkadiene-based elastomers are a significant category of elastomers involving the majority of total elastomer production worldwide.² The polymers produced from isoprene (or 2-methyl-1,3 butadiene) and 1,3 butadiene are the most well-known and applicable alkadiene-based elastomers. Both of them are conjugated dienes and when polymerized,

macromolecules containing one double bond per monomeric unit (instead of two double bonds in the initial monomer) are formed. The configuration for poly(butadiene) (PB) is dependent on the location of the double bond in the monomeric units and can be: *cis*-1,4, *trans*-1,4 and 1,2-microstructures or geometric isomerisms (Figure 1.1). In the case of isoprene, which is a methyl-substituted 1,3-butadiene, when polymerized it forms as well the *cis*-1,4, *trans*-1,4 and 1,2- microstructures, but due to the methyl-ligand it also adopts the 3,4-microstructure (Figure 1.2). The 3,4-isomerism is a dialkyl-substituted olefin and is thermodynamically more stable than the monoalkyl-substituted -1,2 case. In the presence of polar solvents, anionic polymerization of isoprene can yield up to ~100% 3,4-poly(isoprene).⁵

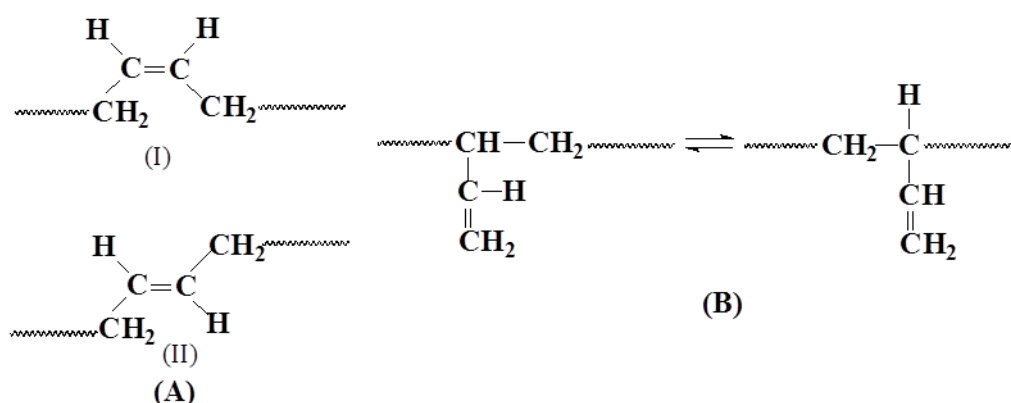


Figure 1.1: Geometric isomerisms of PB: (A): (I) *cis*-1,4, (II) *trans*-1,4, (B): 1,2- (the two cases: -1,2 and -3,4 are identical and only -1,2 is selected and reported in the literature).

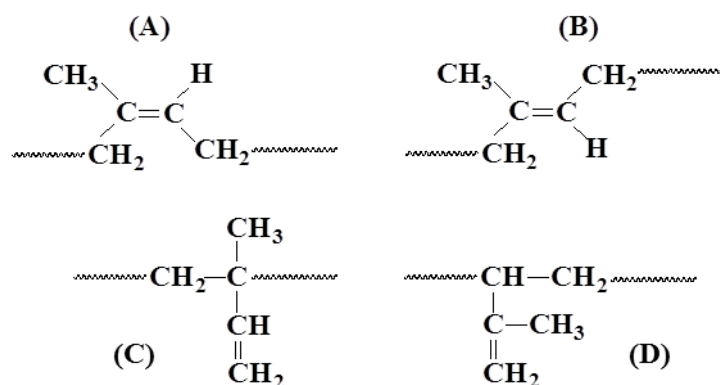


Figure 1.2: Geometric isomerisms of PI: (A): *cis*-1,4, (B) *trans*-1,4, (C): -1,2 and (D): -3,4.

Block copolymers (BCPs) are a significant and large category of polymers with many applications in the last thirty years. Due to easy processing, low cost, variability in chemical functionality and physical properties these materials have played a dominant role in various nowadays applications⁶ (nanofabrication etc.) since they exhibit an important structure/properties relationship attributed to their ability to self-assemble in specific topologies with controlled dimensions and functionalities. All block copolymers refer to a large category of condensed matter, sometimes called soft materials, which are characterized by fluid-like disorder on the molecular scale and by a high degree of order at longer length scales.⁷

Block copolymer macromolecules contain two or more polymer chains linked together by covalent bonds. Linear block copolymers include two or more polymer chains in specific sequence, whereas a star block copolymer contains more than two linear block copolymers attached together at a multifunctional linking point.⁸ There are also different types of star morphology polymers such as symmetric and asymmetric stars. In asymmetric stars, the asymmetry involves: i) the molecular weight (the arms are chemically identical but differ in molecular weight), ii) the chemical nature (miktoarm stars, from the Greek word *μικτός*^{9,10}, meaning mixed) and iii) the topology (the arms are BCPs which may or may not have the same composition and molecular weight, but differ in the relevant segment which is attached to the linking point). Except from these complex architectures, many more have been reported, such as: graft,¹¹ branched^{12,13} (H-type, super H-type), hyper-branched polymers,¹⁴ combs¹⁵ and dendrimers.¹⁶

Anionic polymerization is a powerful tool for polymer scientists, since the synthesized materials are characterized as model polymers with narrow molecular weight distribution and well-controlled molecular characteristics. An additional advantage of anionic polymerization is that through this approach all complex architectures mentioned above for various vinyl and alkadiene monomers with a variety of sequences have been prepared. A disadvantage though, is that it requires good knowledge of glass-blowing techniques for the construction of the necessary apparatuses, where the polymerization procedure takes place, and high vacuum techniques are needed for the purification of all reagents that contribute to the polymerization.

1.2 Scope of this PhD Thesis

For this thesis the basic elastomer studied was poly(isoprene) (PI) with high 3,4-content (55-65%) through preparation of linear and non-linear macromolecular architectures.

A series of linear homopolymers of PI-3,4 (55-65% of 3,4-microstructure) or $PI_{3,4}$ with low and high molecular weights, non-linear H-type $PI_{3,4}$ homopolymers, linear diblock copolymers of the PB-b- $PI_{3,4}$ type [PB: poly(butadiene) with ~90-92% 1,4-microstructure] and asymmetric star copolymers of the $PB(PI_{3,4})_2$ and $PB(PI_{3,4})_3$ types were synthesized. For better understanding of the synthetic procedures and the analysis of molecular and morphological characterization results, all samples prepared in this research thesis are divided in two categories (a and b) as follow:

a) *Linear and non-linear homopolymers of $PI_{3,4}$*

b) *Linear diblock copolymers (PB-b- $PI_{3,4}$) and miktoarm stars [$PB(PI_{3,4})_2$ and $PB(PI_{3,4})_3$]*

1.2.1 Linear and Non-Linear Homopolymers of $PI_{3,4}$

A variety of linear $PI_{3,4}$ homopolymers exhibiting different molecular weights (5,000 g/mol - 350,000 g/mol) were synthesized via anionic polymerization through high vacuum techniques. All polymerizations were performed through special glass apparatuses and the initial solvent used was benzene (at least 200 mL up to 900 mL depending on desired molecular weight). In order to achieve high 3,4-content of PI, a small amount (1 mL to 3 mL depending on the quantity of the benzene) of tetrahydrofuran (THF), which is a polar solvent, was always added.

Furthermore, two (2) samples of non-linear H-type $PI_{3,4}$ homopolymers were synthesized via anionic polymerization and high vacuum techniques, by preparing a macroinitiator through the reaction of 4-(chlorodimethylsilyl)styrene (CDMSS) with linear $PI_{3,4}$ and combination of chlorosilane chemistry. ***It should be mentioned that this type of samples (H-type $PI_{3,4}$) have never been reported in the literature.*** The main purpose for the synthesis of these samples was to investigate the dynamics and rheological properties of long-chain branching (LCB) homopolymers/elastomers through the collaboration with Prof. Shi-Qing Wang from University of Akron (USA).

All samples showed very narrow molecular weight distributions (<1.10) and the molecular characterization results through various techniques led to the conclusion that they exhibit chemical and compositional homogeneity, therefore, can be considered model polymers.

1.2.2 Linear Diblock Copolymers ($PB-b-PI_{3,4}$) and Miktoarm Stars [$PB(PI_{3,4})_2$ and $PB(PI_{3,4})_3$]

Linear diblock copolymers of the $PB-b-PI_{3,4}$ type and asymmetric stars of $PB(PI_{3,4})_2$ and $PB(PI_{3,4})_3$ types were synthesized.

Specifically, five (5) linear diblock copolymers of $PB-b-PI_{3,4}$ were synthesized anionically through high vacuum techniques by using the sequential monomer addition method. As previously mentioned, the 3,4-content of poly(isoprene) was ~55-65%. One of the diblock copolymers exhibited very high molecular weight (~1,000 kg/mol), whereas the other four (4) samples exhibited almost constant number average molecular weight (~100,000 g/mol). These diblock copolymers were synthesized in order to study their molecular and especially their morphological behavior in terms of microphase separation in various molecular weights and volume fractions ranging from 30% v/v up to 70% v/v of the PB block.

Furthermore, four (4) sets, thus eight samples, of miktoarm stars of the $PB(PI_{3,4})_2$ and $PB(PI_{3,4})_3$ type (four samples per sequence) were synthesized using the combination of

anionic polymerization and chlorosilane chemistry. *The preparation and properties of such non-linear copolymers have not been reported in the literature yet.* The volume fraction regime for the PB block as well as the total molecular weight of the star copolymers are approximately equal to those documented for four (4) of the diblock copolymers. The reason for keeping almost constant both total molecular weight and PB block volume fraction in the twelve (12) samples was to compare the star with the linear architecture, especially their structure/properties relationship (self-assembly).

It has been reported in the literature^{17,18} that PB with ~90-92% 1,4 and PI with ~55-65% 3,4-microstructures, microphase separate either in linear triblock terpolymers of SBI or BSI types [where S: polystyrene, B: poly(butadiene) with high (90-92%) 1,4-microstructure and I: poly(isoprene) with high (55-65%) 3,4-content] leading to 3-phase topologies¹⁷ or in [(PB)₂PI]₃ type 2nd generation dendrimers¹⁸. Observing and analyzing the morphological characterization results, it was possible to understand the mechanism of self-assembly for this type of polydiene combination and realize that the interaction parameter is well above zero. Furthermore, it was possible to understand the manner that molecular weight, volume fraction and conformational asymmetry influence the microphase separation of this binary polydiene system.

As stated already for the homopolymers, the linear PB-b-PI_{3,4} and asymmetric star copolymers of PB(PI_{3,4})₂ and PB(PI_{3,4})₃ type can be as well model polymers since they exhibit chemical and compositional homogeneity as concluded from their molecular characteristics with various characterization methods.

Finally, it is very important to mention that in samples where chlorosilane chemistry was combined, the whole synthetic strategy involved time consuming reactions and the formation of byproducts or residue of precursors or both, leading to a timeframe of approximately 3-4 months per sample in order to synthesize a model material.

A schematic presentation of the complex architectures synthesized in this thesis is in Figure 1.3.

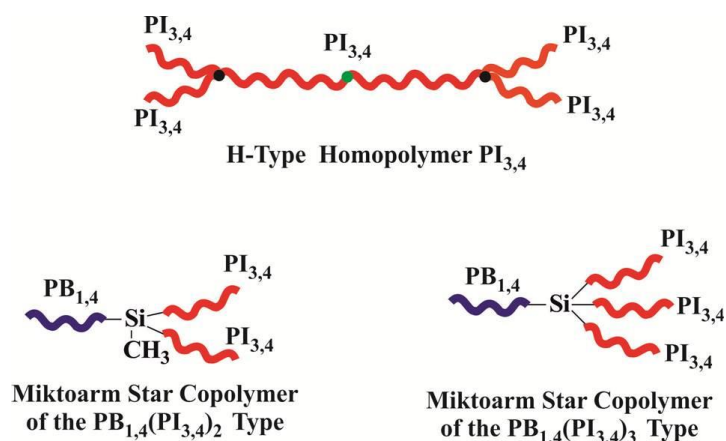


Figure 1.3: Schematic of the complex architectures synthesized in this thesis.

The molecular characterization of the samples was performed through size exclusion chromatography (SEC), in order to confirm the molecular weight distribution, and membrane osmometry (MO) in order to confirm the number average molecular weight, (\overline{M}_n) values. Also, proton nuclear magnetic resonance spectroscopy ($^1\text{H-NMR}$) was adopted to verify the characteristic ratios of stereochemical microstructures for the polydienes as well as to identify the composition of each segment of the linear and non-linear copolymers. Thermal analysis via differential scanning calorimetry (DSC) was also performed in order to examine the variations of glass transition temperatures and their dependence from the molecular weight and the weight fraction of each segment. Morphological characterization was performed through bright field transmission electron microscopy (TEM), in order to verify microphase separation and provide significant information concerning the dependence of the architecture (linear or non-linear) on the adopted morphology. Furthermore, rheological studies were performed in linear and non-linear $\text{PI}_{3,4}$ homopolymers, through the collaboration with Prof. S.-Q. Wang (Morton Institute of Polymer Science and Engineering, The University of Akron, Ohio, USA), leading to new theoretical considerations for the non-linear dynamic behavior of long chain branched (LCB) polymers and their mixtures with the corresponding linear chains in the presence of large external deformations in either simple shear or uniaxial extension.

1.3 Overview of the Thesis

Chapter 2 provides information concerning the fundamentals and the basic principles of anionic polymerization techniques. Furthermore, information for the already reported cases of 1,3-butadiene and isoprene polymerization and their copolymerization with other well studied monomers are provided, as well as information concerning the synthetic routes for linear diblock copolymers and complex architecture polymers such as H-type and miktoarm stars already established.

In *Chapter 3*, information concerning the physical properties of linear block copolymers, miktoarm star copolymers and their microphase separation is given, as well as general information concerning the rheological properties of polymers and dynamic behavior of long chain branched (LCB) polymers.

Chapter 4 provides information on the experimental procedures adopted for the synthesis of the linear homopolymers of the $\text{PI}_{3,4}$ type, the non-linear homopolymers of the H- $\text{PI}_{3,4}$ type, the linear diblock copolymers of the PB-b- $\text{PI}_{3,4}$ type and the miktoarm star copolymers of the $\text{PB}(\text{PI}_{3,4})_2$ and $\text{PB}(\text{PI}_{3,4})_3$ type respectively. Furthermore, detailed description of the purification procedures in order to minimize the traces from unwanted reagents, as well as the instrumentation that was used for the characterization of the samples synthesized for this thesis is thoroughly reported.

In *Chapter 5*, the molecular and morphological characterization results of the synthesized samples as well as the conclusions and future work are presented. Thorough investigation and discussion of the results is performed in order to conclude to the successful synthesis of the linear and non-linear homopolymers of PI_{3,4} and study their rheological properties, as well as to study and compare the observed morphologies for the synthesized linear diblock and star copolymers with systems already mentioned in the literature and especially PS/PI, where PS: polystyrene and PI: poly(isoprene) respectively.

Partial financial support during the framework of the research activities for this PhD thesis was given by the following projects:

- Funded by the European Union under the Call identifier: FP7-NMP-2009-SMALL-3 with Proposal No: CP-FP 245565-2 LAMAND (36 months, 1/7/2010-30/6/2013), title: “Large Area Molecularly Assembled Nanopatterns for Devices” and Acronym: “LAMAND”, as *Researcher*.
- Funded by the European Union under the Call identifier: FP7-NMP-2007-LARGE-1, with Proposal No: CP-IP 213939-1 POCO (48 months, 1/11/2008-31/10/2012) entitled: “Carbon Nanotube Confinement Strategies to Develop Novel Polymer Matrix Composites” and Acronym: “POCO”, as *Researcher*.

CHAPTER 2

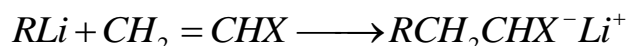
Anionic Polymerization

2.1 Basic Concepts

Anionic polymerization is the most well-known technique for synthesizing well-defined polymers (linear and non-linear) with total control of the molecular characteristics. Initially, Flory divided the polymerization reactions into step-growth and chain reactions, based on their mechanism.¹⁹ Anionic polymerization is a chain reaction and the monomers which can be polymerized are generally vinyl and alkadienes. Although several reports concerning anionic polymerization of vinyl polymers were published in the late 1940s^{20,21}, Michael Szwarc was the first who demonstrated thoroughly the mechanism of anionic polymerization in the mid-1950s, characterized the behavior of this polymerization as “living polymerization” and described the polymers as “living polymers”.^{22,23} The term “living” refers to the ability of the macromolecular chain ends to retain their reactivity for sufficient time, in which they can be used further for polymerizing additional monomer quantities or for reacting with a suitable linking reagent since the termination and/or chain transfer reactions are completely controlled and handled in the specific type of polymerization. It should be mentioned that the term anionic is used to point out that the active chain-ends are negatively charged bearing specific metallic counterions which are positively charged.²⁴ It is clearly understood therefore, that through anionic polymerization, architecture, composition, molecular weight and molecular weight distribution can be controlled.

Since termination and chain transfer reactions are absent under specific conditions, in anionic polymerization only two reaction steps are prominent: initiation and propagation which are exhibited in Figure 2.1:

Initiation



Propagation

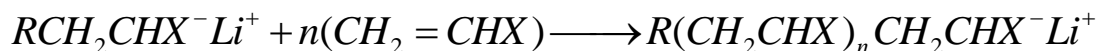


Figure 2.1: Initiation and propagation reactions of living anionic polymerization.

Most industrial polymers are synthesized through free radical polymerization techniques, but they do not exhibit predictable molecular characteristics and narrow molecular weight polydispersity. The reason is that in radical polymerization uncontrolled termination reactions occur through redistribution or conjunction between macromolecular radicals, in contrast with anionic polymerization. Furthermore, a very important issue which limits the use of anionic polymerization in industry and large scale applications/facilities is

that the macroinitiator and the macroanions, due to their reactivity, are very sensitive in oxygen, humidity and carbon dioxide traces. The reactions describing this drawback are shown in Figure 2.2. Therefore, it is very important, during anionic polymerization, that all reactions must take place in the absence of atmospheric air and the reagents involved (initiators, monomers, solvents etc.) must exhibit high purity (> 99.9%). Inert atmosphere or high vacuum conditions (10^{-6} - 10^{-7} mmHg) are adopted for anionically synthesized polymers. Inert atmosphere techniques are simpler and may lead to large quantities of the final materials. On the other hand, high vacuum techniques demand very well purified and suitably modified Pyrex glass vessels, leading to the necessity of scientific glassblowing knowledge. An important drawback is also the preparation of small quantities of the final polymer.

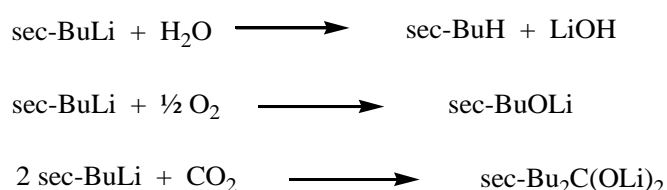


Figure 2.2: Termination reactions of an anionic polymerization initiator with water, oxygen and carbon dioxide.

A very important feature of the polymers synthesized with anionic polymerization is the narrow molecular weight distribution ($I < 1.1$) which ensures the compositional and molecular homogeneity of the final product. Low polydispersities are secured by the proper choice of solvent, monomer and initiator system in combination with the fact that the initiation reaction rate must always be faster than the propagation reaction rate. Moreover, the selected temperature for the reaction and the possible use of polar additives, are crucial parameters for the demanding fast initiation. When these requirements are indulged, polymerization of the monomer units starts simultaneously and almost identical number of monomer units is added to the macromolecular living chains until all quantity is consumed.

The most well-known and useful initiators in anionic polymerization are organometallic compounds, especially alkyllithium reagents, which may be synthesized by the reaction of the corresponding alkyl chloride with lithium. The initiator is always chosen according to its ability to react fast with the monomer and whether it is well soluble in the chosen solvent under the applied reaction conditions. The most important feature of alkyllithium compounds is that the C-Li bond exhibits properties of both covalent and ionic bonds^{25,26}, due to the smallest ion radius and the highest electronegativity among other alkali metals. Usually, organolithium compounds form aggregates in bulk and in solution. The lower the aggregation rate of the initiator, the higher will be the reactivity for the initiation of the polymerization.²⁷ The degree of association is influenced by the structure of the organic moiety, the nature of the solvent, the solution concentration and temperature.²⁸ In Table 2.1

the degree of association of various organolithium compounds, which may be used as anionic polymerization initiators, in hydrocarbon solvents is observed.

Table 2.1: Aggregation states of organolithium compounds in hydrocarbon solvents.

Compound	Solvent	Degree of association	Reference
Ethyllithium (C₂H₅Li)	Benzene	6	29,30
	Cyclohexane	6	29,30
n-Butyllithium (n-C₄H₉Li)	Benzene	6	29-31
	Cyclohexane	6	32
n-Pentyllithium (n-C₅H₁₁Li)	Benzene	6	32
n-Octyllithium (C₈H₁₇Li)	Benzene	6	32
Isopropyllithium (i-C₃H₇Li)	Benzene	4	30
	Cyclohexane	4	30
sec-Butyllithium (sec-C₄H₉Li)	Benzene	4	33
	Cyclohexane	4	33
t-Butyllithium (t-C₄H₉Li)	Benzene	4	34
	Cyclohexane	4	34
Methylithium (CH₃Li)	Benzene	2	35
	Cyclohexane	2	35

Additionally, the reactivity sequence of organolithium initiators for styrene and alkadiene (1,3-butadiene and isoprene) polymerization in a variety of hydrocarbon solvents has been reported in the literature³⁶ and is given below (the degree of aggregation is shown in the parentheses):

Methylithium (2) > secondary butyllithium (*sec*-BuLi) (4) > isopropyllithium (*i*-PrLi) (4-6) > tertiary butyllithium (*tert*-BuLi) (4) > normal butyllithium (*n*-BuLi) (6)

During the propagation step the negatively charged polymer chains with the lithium counterion can also aggregate. The aggregation rate for (polystyryl)lithium [PS⁽⁻⁾Li⁽⁺⁾] in aromatic and aliphatic hydrocarbon solvents has been calculated to be equal to 2.³⁶ Furthermore, the aggregation rate for (polybutadienyl)lithium [PB⁽⁻⁾Li⁽⁺⁾] in hydrocarbon solvents is 4-6 and for (polyisoprenyl)lithium [PI⁽⁻⁾Li⁽⁺⁾] is equal to 3-4 respectively. However, it has been observed that the aggregation rate of initiators and polymer chains is decreased in polar environments. It has been estimated through kinetic studies²⁷ that the aggregation rate of

(polystyryl)lithium in tetrahydrofuran (THF) is decreased from 2 to 1 while for (polybutadienyl)lithium and (polyisoprenyl)lithium the corresponding value is decreased to 2. Such behaviour occurs since a minor quantity of the polar reagent can shift the equilibrium between the aggregated and non-aggregated polymer chains towards the non-aggregated ionic pairs $[\text{PS}^{(-)}\text{Li}^{(+)}]$ leading to a decrease of the solution viscosity while enhancing the kinetics of the polymerization reaction.

The greatest advantage of anionic polymerization is that it can proceed with a yield of 100% in almost all systems (only a few monomers do not apply to this rule). Practically, this means that the polymerization reaction will be completed when all the monomer quantity has been consumed during the propagation reaction. As a result, the molecular weight of the final polymer can be easily estimated by the quantities of the monomer and initiator which were used for the polymerization through the following equation:

$$\overline{M}_n = \frac{g_{\text{monomer}}}{\text{moles}_{\text{initiator}}} \quad (2.1)$$

A large number of monomers have been polymerized through anionic polymerization. The basic feature of these monomers is that they can form stable anionic reactive sites under certain polymerization conditions. For the most studied monomers, styrene and/or styrene derivatives and alkadienes, this means that the two carbon atoms involved in the vinyl bond must bear at least a ligand that can stabilize the negative charge towards nucleophilic attack of other species. These monomers are:

- ❖ Styrene and styrene derivatives (e.g. *a*-methylstyrene, *para*-methylstyrene)³⁷⁻³⁹
- ❖ Alkadienes (e.g. isoprene, 1,3-butadiene, 2-methyl-1,3-pentadiene, 1,3-cyclohexadiene)⁴⁰⁻⁴⁵
- ❖ Methacrylic esters (e.g. methyl methacrylate)⁴⁶
- ❖ Cyclic compounds (e.g. ethylene oxide, hexamethylcyclotrisiloxane and ϵ -caprolactone).⁴⁷⁻⁴⁹

The ability to synthesize well-defined block copolymers and even more complex architectures by anionic polymerization has led significantly to the advancement of the structure/properties relationship in bulk and in solution. Only materials prepared via anionic polymerization have verified older and new theoretical models based on their behaviour in solution and bulk and evidently pioneered the breakthrough of self-assembly and directed self-assembly by combining well-defined block copolymers with specific chemical, physical properties and thermodynamics.

2.2 Alkadiene-Based Elastomers

Alkadienes are vinyl monomers containing two double bonds in their structure. They are considered a significant class of chemical compounds as they exhibit very interesting

physical and chemical properties when polymerized. Poly(isoprene) (PI) and poly(butadiene) (PB) were the first polydienes synthesized and studied extensively for their properties. They belong to the category of elastomers, which are polymers with viscoelasticity (exhibiting both viscosity and elasticity), and very weak inter-molecular interactions, with low Young's modulus and high failure strain when compared to other polymeric materials.

Elastomers are usually thermosets (requiring vulcanization) or thermoplastics. Thermosets are vulcanized polymers (chemically formed networks between polymer chains in the presence of other atoms i.e. sulfur) having the ability to reconfigure in order to distribute an applied external stress. The covalent cross-links ensure that the elastomer will return to its original configuration when the stress is removed. Thermoset elastomers have also low glass transition temperatures (T_g), well below ambient conditions. Specifically, poly(butadiene) with high 1,4-microstructure (~92%) exhibits values of $T_g = -85$ to -90°C , while cis-1,4 poly(isoprene) obtains $T_g = -67^\circ\text{C}$ respectively.^{50,51} Other examples of polydienes anionically synthesized are: poly(2-methyl-1,3-pentadiene) and poly(1,3-cyclohexadiene). Poly(2-methyl-1,3-pentadiene) when hydrogenated is converted (up to >99%) to polypropylene, exhibiting a 100% atactic conformation as well as unique thermal and mechanical properties.⁴² This polydiene exhibits high 1,4-microstructure (~99%) when polymerized via alkyllithium initiators (e.g. *sec*-BuLi) in hydrocarbon solvents (e.g. cyclohexane) and also obtains higher glass transition temperature than the polydienes previously mentioned ($T_g = 4^\circ\text{C}$).⁴³ Poly(1,3-cyclohexadiene) can exhibit very interesting and different, from other polydienes, properties such as increased thermal and chemical stability as well as improved mechanical properties^{52,53} due to its cyclic rings in the main chain. Among these polydienes, poly(isoprene) and poly(butadiene) are the most studied and applicable polydiene-based elastomers with industrial applications already in automobile tires, water proof membranes etc.

2.3 Effect of Polar Additives in Anionic Polymerization of Alkadienes

The carbanion environment affects the kinetics mechanism of anionic polymerization. If the carbon-lithium bond is replaced by a carbon-carbon bond, no active sites remain. When a hydrocarbon solvent is used for the polymerization of a vinyl monomer, the carbanions form a strong ion-pair with metal counterion (usually Li or Na or K). The addition of polar additives, even at very small amounts, such as tetrahydrofuran (THF) or N, N, N', N'-tetramethylethylenediamine (TMEDA) disrupts the alkyllithium aggregates and produces loose ion-pairs. For example a corresponding ion-pair in THF (polar solvent) becomes a free ion. The disruption of the alkyllithium aggregates dramatically increases the kinetics of the reaction (Figure 2.3).



Figure 2.3: A schematic representation of the polar additive effect into the kinetics of anionic polymerization.

The change of the reaction kinetics and environment of lithium carbanion association through polar additives also affects the resulting polydiene microstructure. The effect of a polar solvent (THF) in the polymerization of 1,3-butadiene with *sec*-BuLi as initiator has been reported in the literature⁵⁴ and is shown in Table 2.2. As the amount of THF increases, the 1,2-content of poly(butadiene) also increases. When 1,3-butadiene is polymerized anionically in non-polar hydrocarbon solvents, 1,2-microstructure ranges between 8-10%, while in THF (polar solvent) may reach values up to 90%.⁵⁵ Polydienyl anions provide less chain end association in polar media when compared to their association degree in non-polar hydrocarbon solvents.

Table 2.2: Effect of polar solvent (THF) on the microstructure of poly(butadiene).⁵⁴

Solvent System	THF/ <i>sec</i> BuLi	cis-1,4	trans-1,4	1,2
<i>n</i> -hexanes	0	35	57	8
<i>n</i> -hexanes/THF	1.0	25	40	35
<i>n</i> -hexanes/THF	8.2	21	31	45
<i>n</i> -hexanes/THF	17	14	28	58
<i>n</i> -hexanes/THF	53	7	10	85

Reaction temperature: 30 °C, Initiator: *sec*-BuLi

The 1,2-microstructure of poly(butadiene) affects the properties of the polymer. Approximate values of glass transition (T_g) and melting point (T_m) temperatures of the poly(butadiene) microstructures and conformations of the 1,2-microstructure are summarized in Figure 2.4 and indicate a linear relationship of the glass transition temperature with the percentage of 1,2- vs. 1,4-microstructure in the final poly(butadiene) in each case.⁵⁶

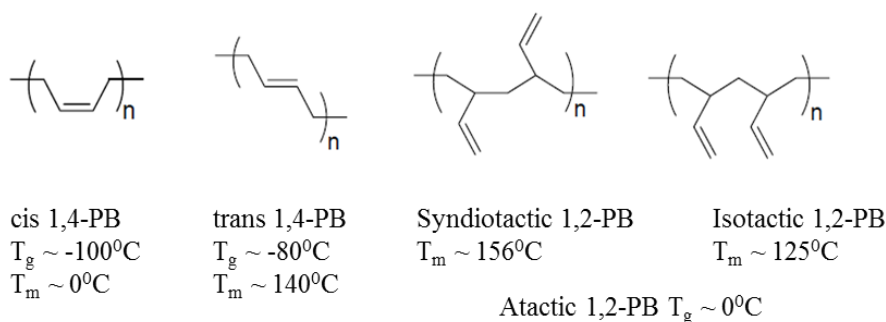


Figure 2.4: Poly(butadiene) microstructures, conformations of the 1,2-microstructure (syndiotactic, isotactic, atactic) and their thermal properties values.⁵⁷

Anionic polymerization of isoprene in a hydrocarbon solvent (benzene, cyclohexane, etc.), using organolithium compounds as initiators, is known to lead to high 1,4-microstructure (>90%) for PI and specifically high *cis*-1,4 PI (~80%), while the -3,4 content is very low (~5%).⁴⁰ The high *cis*-1,4 content is formed due to the presence of the methyl group as a ligand in carbon-2 which distinguishes the specific monomer from 1,3-butadiene. The methyl group modifies the configuration of either the anion or the approaching monomer. The presence of ethers (THF) or amines (TMEDA) during the polymerization of isoprene has been reported to affect drastically the microstructure of the polymer produced.^{58,59} It also increases the initiation and propagation rates, as concluded from kinetic studies reported by Bywater and Worsfold.⁶⁰ The produced PI had high vinyl content and less 1,4-microstructure (Table 2.3) as indicated by the ¹H-NMR spectra data. The transition to a solution rich in THF causes the PI polymer to progressively enrich the 3,4-microstructure whereas in pure THF it is reported that the 1,4-microstructure is no longer evident.

Table 2.3: Variation of poly(isoprene) microstructures in the presence of THF.⁵⁸

Polyisoprene microstructures					
Initiator*	Solvent	Structure (%)			
		<i>cis</i> 1:4	<i>trans</i> 1:4	3:4	1:2
Butyllithium	Cyclohexane	80	15	5	—
Butyllithium + 2 moles THF	Cyclohexane	68	19	13	—
Butyllithium + 15 moles THF	Cyclohexane	69	26	31	—
Butyllithium	Cyclohexane + 10% THF			66	9
Butyllithium	THF	—	—	74	26
Butyllithium + lithium hydroxide	Cyclohexane	68	27	5	—
Butyllithium + lithium butoxide	Cyclohexane	69	26	5	—
Sodium	Cyclohexane	29	29	42	—
Sodium	THF	—	—	82	18
Emulsion	Water (50°)	30	65	5	—

*Butyllithium concentration ca. $3 \times 10^{-4} M$.

More studies were reported for the polymerization of isoprene in the presence of dioxane and diethyl ether or exclusively in these solvents.⁶¹⁻⁶³ In all cases the synthesized PI, exhibited high 3,4-microstructure (>50%) despite the addition of only small amounts of the polar additives. Furthermore, it was reported that *cis*-1,4 is the more stable 1,4-microstructure for all alkali metals (Li, Na, K) in polar solvents when compared to the *trans*, whereas with

lithium as the metal counterion in hydrocarbon solvents the *trans*-1,4 microstructure is most dominant (Table 2.4).

Table 2.4: Ratio of the PI microstructures as formed in ether at -20°C .⁶³

counterion	% 1,4 ^a	% 1,2 ^a	% 3,4 ^a
Li ⁺	35 (7, 14)	13 (17, 18)	52 (76, 68)
Na ⁺	17 (9)	22 (12)	61 (78)
K ⁺	38 (38, 36)	19 (12, 14)	43 (50, 50)
Cs ⁺	52 (47)	16 (12)	32 (41)

^aNumber in parentheses are from ref. 60 and 61, for polymerizations in dioxane.

Hsu and Halasa reported a patent⁶⁴ for the synthesis of crystallizable PI_{3,4} (3,4-content approximately equal to 80-85%) and isoprene-butadiene copolymers having high vinyl content utilizing a catalyst system which is comprised from: a) an alkyliron compound (soluble in organic solvents), b) a partially hydrolyzed organoaluminum compound prepared by adding a protonic compound (water or alcohols) and c) an aromatic amine in ratio with the alkyliron compound equal to 0.1:1. The polymerization reaction was accomplished in an organic solvent at a temperature range within 10-30^oC for 1-2 hours. The prepared crystallizable PI_{3,4} exhibited a T_g within the range of 4-8^oC, and the molecular weight distributions were quite high (2 < I < 3). These PI macromolecules are very useful for making tire tread rubber compositions since they may provide good rolling resistance while offering outstanding wet and dry traction characteristics.

2.4 Polymer Architectures

2.4.1 General Information

The physical properties of a polymer are determined by the configuration of the constituent atoms and the molecular weight. The configuration is partly dependent on the main chain, and partly on the various side groups. Many side chain groups cause steric hindrance and restrictions in the free rotation of the ligands attached to the carbon atoms bearing the double bond. The structure of a macromolecule includes the topology and the arrangement of the monomer (homopolymers) or different monomers (copolymers, terpolymers, etc.). In Figure 2.5 some of the most important architectures of homopolymers are summarized including linear, different kinds of branched polymers as well as cross-linked architectures. Except from the linear and cyclic cases, the remaining structures exhibiting chains as ligands indicate the significance of branching in the final properties of the resulting architecture.

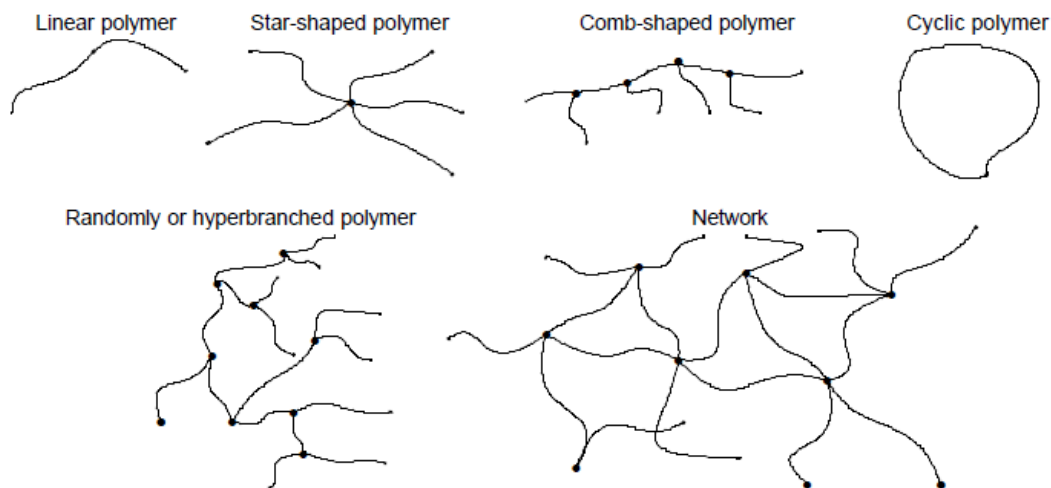


Figure 2.5: Various architectures of linear and non-linear homopolymers.

Depending on the monomer chemical structure and the number of chemically different monomeric units employed in the final material, polymers can be divided to homopolymers, if there is only one type of monomeric unit, copolymers (two types of chemically different monomeric units), terpolymers (three types of chemically different monomeric units) etc.⁶⁵ Copolymers are also categorized depending on the manner the different monomers are arranged in the final polymer to: block, random, alternating and graft copolymers (Figure 2.6).

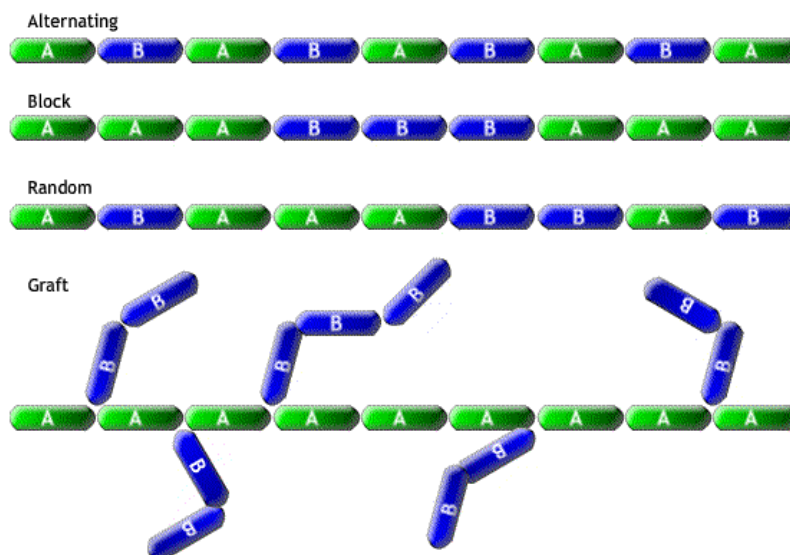


Figure 2.6: Different categories of a copolymer depending on the arrangement of the two types of chemically different monomeric units within the final material.

2.4.2 Anionic Polymerization of Non-Linear Homopolymers

The combination of anionic polymerization techniques and chlorosilane chemistry⁶⁶ can lead to the formation of well-defined homopolymers with complex architectures such as stars, H-shaped, super H-shaped, graft, dendrimers etc. The synthesis and characterization of H-shaped PI_{1,4} has been reported,⁶⁷ using anionic polymerization via high vacuum techniques and chlorosilane chemistry. The polymerization of isoprene was carried out in benzene and *sec*-BuLi was used as initiator. The final H-type PI was prepared using a difunctional initiator resulting from the reaction of *sec*-BuLi with 1,2-bis[4-(1-phenylethenyl)phenyl]ethane which initially polymerized isoprene and then the difunctional living PI was coupled with trichloromethylsilane (CH₃SiCl₃), followed by condensation with monofunctional poly(isoprenyllithium).

A different synthetic approach was reported for the synthesis of well-defined symmetric H-type poly(butadienes) by Mays' research group.⁶⁸ This synthetic strategy involved anionic polymerization techniques in combination with a difunctional linking agent, 4-(dichloromethylsilyl)diphenylethylene (DCMSDPE). The synthesis was performed by following specific steps which were: a) growing of a living PB⁽⁻⁾Li⁽⁺⁾ chain using *sec*-BuLi as initiator in benzene, b) titration of DCMSDPE with the living PB⁽⁻⁾Li⁽⁺⁾, c) addition of *sec*-BuLi in order to activate the double bond of the substituted DPE, d) subsequent addition of butadiene in order to form a living "half-H architecture", a structure identical to a 3-arm star homopolymer, which exhibited two chains linked into a macromolecule bearing living sites and with half the molecular weight of the final connector and e) final coupling of the two "half-H architecture" macromolecules with dichlorodimethylsilane [(CH₃)₂SiCl₂] in order to prepare the final H-type PB_{1,4} homopolymer (Figure 2.7). These polymers were also studied⁶⁹ with temperature gradient interaction chromatography (TGIC), where a lot of byproducts were obtained. Rheological measurements of this type of polymers were used in order to validate or not the "tube" model for long-chain branched polymers.

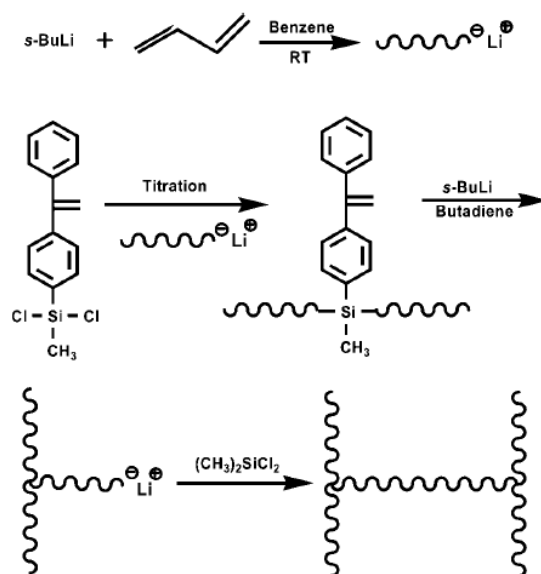


Figure 2.7: Synthetic route for the preparation of symmetric H-shaped poly(butadiene) with high 1,4-microstructure.⁶⁸

The same group also reported the synthesis, molecular characterization and linear rheological measurements of four different asymmetric H-type PB_{1,4} homopolymers utilizing again DCMSDPE as the linking agent.^{70,71} The synthetic procedure was slightly different than the one reported above. In this case, living PB⁽⁻⁾Li⁽⁺⁾ is added into DCMSDPE in order to replace both chlorine atoms. The result was an in-chain DPE with two short arms. Subsequent addition of *sec*-BuLi and Bd monomer led to a living three arm asymmetric star. Another in-chain DPE with two long arms was synthesized separately and mixed with the first one bearing the short arms in the presence of THF in order to obtain the desirable asymmetric H-type PB homopolymer (Figure 2.8).

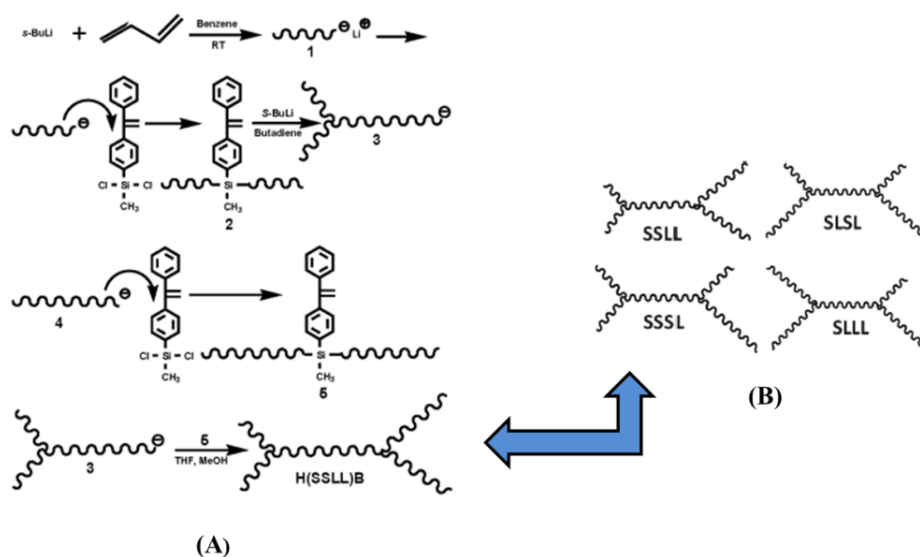


Figure 2.8: (A): Reactions for the synthesis of asymmetric H-type PB_{1,4} homopolymer (B): scheme of the different architectures of asymmetric H-type PB_{1,4} homopolymer (S: short chain, L: large chain, for the arms attached to the connector).⁷⁰

Polystyrene with dendritic branching prepared by the convergent method and living anionic polymerization were reported⁷² using another linking agent, 4-(chlorodimethylsilyl)styrene (CDMSS). The coupling agent CDMSS comprised from a polymerizable group and a moiety capable of quantitatively coupling with a living chain. A series of dendritic polystyrenes with different branch lengths were synthesized, utilizing this method. The same group in a similar manner managed to synthesize graft copolymers of PS-g-(hyper)PS, PMMA-g-(star)PS and PMMA-g-(hyper)PS types from star-shaped and hyperbranched polystyrene macromonomers respectively⁷³ (Figure 2.9).

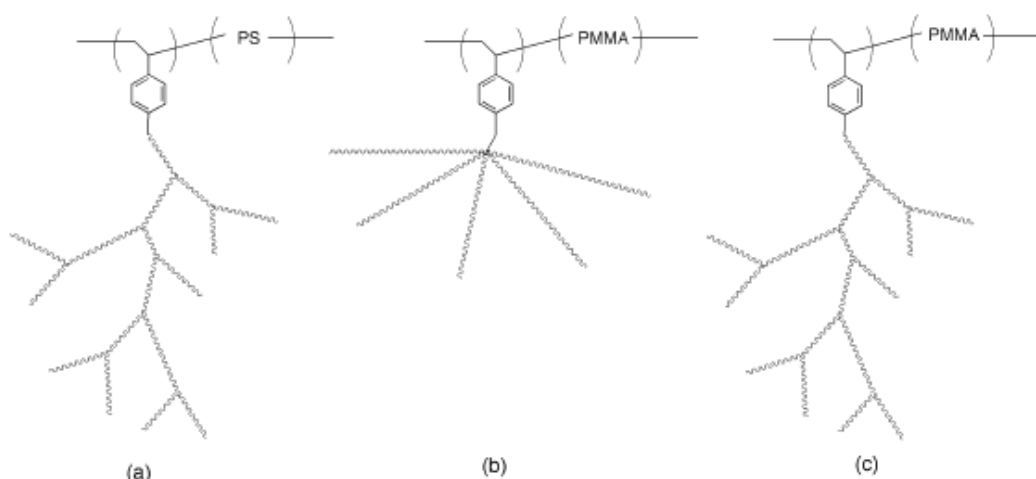


Figure 2.9: Representation of (a) polystyrene-graft-(hyperbranched polystyrene), (b) PMMA-graft-(star polystyrene), and (c) PMMA-graft-(hyperbranched polystyrene).⁷³

By using the same linking agent (CDMSS) Hadjichristidis' research group reported⁷⁴ the synthesis and characterization of a variety of novel complex macromolecular architectures based on styrenic polymacromonomers of PI, PB and PS-b-PI by selective reaction of $\text{PI}^{\ominus}\text{Li}^{(+)}$, $\text{PB}^{\ominus}\text{Li}^{(+)}$, and $\text{PS-b-PI}^{\ominus}\text{Li}^{(+)}$ with the chlorine atom of 4-(chlorodimethylsilyl)styrene. These macromonomers and conventional monomers (styrene, isoprene, and 1,3-butadiene) were homopolymerized or block copolymerized, by anionic polymerization high-vacuum techniques. Well-defined second generation dendritic polymers of isoprene and styrene were also reported⁷⁵, utilizing this synthetic procedure (Figure 2.10).

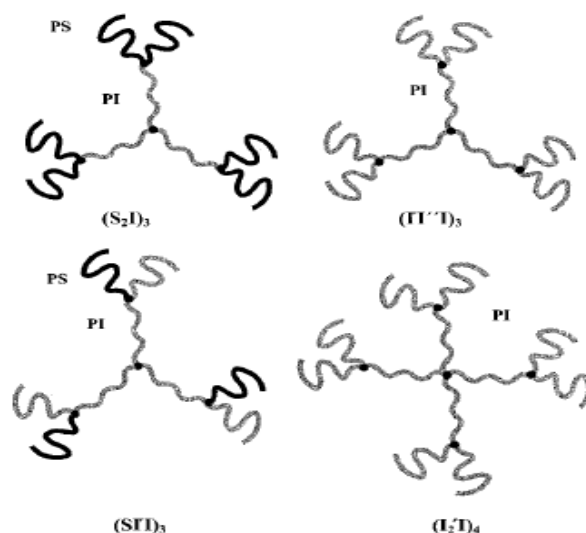


Figure 2.10: Schematic presentation of second-generation symmetric and non-symmetric dendritic homo- and copolymers of the $(II'I)_3$, $(I_2'I)_4$, $(S_2I)_3$, and $(SI'I)_3$ types.⁷⁵

2.5 Block Copolymers

A block copolymer macromolecule contains two or more polymer chains linked together with covalent bonds in which only two chemically different monomeric units are involved. Linear block copolymers include two or more polymer chains in a specific sequence, whereas a star block copolymer contains more than two linear block copolymers attached together to a multifunctional linking point. In most cases, the different polymeric chains of block copolymers are thermodynamically incompatible giving rise to a variety of morphologies when studied in bulk and in solution. Therefore, the obtained topologies are highly coupled to the chemical and physical characteristics of the molecules of each block and materials with applications ranging from thermoplastic elastomers and high-impact plastics to pressure-sensitive adhesives, additives, foams etc. can be created.⁷⁶ Furthermore, block copolymers are excellent candidates for potential applications in advanced materials technologies such as nanolithography and nanofabrication⁷⁷⁻⁷⁹, magnetic media storage⁸⁰, drug delivery⁸¹ and photonic crystals.⁸²

Anionic polymerization is the most reliable technique for the synthesis of well-defined block copolymers but it requires high purity reagents and the use of high vacuum techniques to prevent accidental termination or transfer reactions due to the presence of any type of impurities. Following specific experimental conditions^{28,83}, due to the absence of termination and chain transfer reactions, carbanions remain active after complete consumption of the first monomer and the formation of block copolymers is successful by introducing a second monomer into the polymerization mixture. The need to combine more properties in block copolymer systems has directed recent advances in the synthesis of block

copolymers with complex architectures, such as miktoarm stars¹⁰, H-shaped⁸⁴, super H-shaped¹³, graft¹¹ and dendrimers¹⁸ (Figure 2.11).

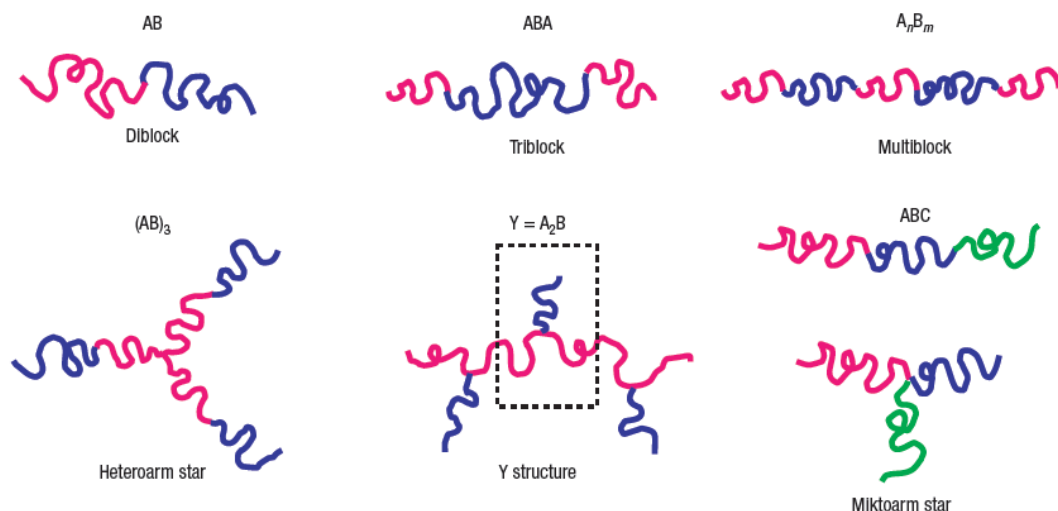


Figure 2.11: Block copolymer architectures.⁸⁵

2.5.1 Linear Diblock Copolymers (AB)

Linear diblock copolymers⁸⁶ are the simplest case of copolymers since only two chemically different blocks are linked together via a common junction point (Figure 2.12) corresponding to a carbon-carbon covalent bond. The most general method in order to synthesize diblock copolymers is the sequential monomer addition, where one of the two monomers is polymerized first and the second monomer is added and polymerized through the living macroanions of the first block until its complete consumption. Then, a termination reagent is added and the diblock copolymer is precipitated in a non-solvent, dried and collected.



Figure 2.12: Schematic representation of a diblock copolymer.

The most important parameters that must be fulfilled in order to achieve the synthesis of well-defined diblock copolymers are:

- (a) The macroanion of the first monomer must be a stronger nucleophile than the one obtained from the second monomer in order to be able to initiate the polymerization of the second monomer.
- (b) The initiation rate for the polymerization of the second monomer by the macroanions of the first monomer must be higher than the propagation rate during the polymerization of the second monomer in order to ensure narrow molecular weight distribution and molecular homogeneity.

- (c) The purity of the second monomer must be equally high with that of the first monomer. Otherwise, macroanions of the first monomer can be partially terminated leading to the presence of homopolymer in the final material. Furthermore, there will be no control of the molecular weight of the final diblock copolymer, the composition in mass fraction between the two blocks will not be the requested one due to the decrease in the concentration of the active centers leading to higher molecular weight for the final product.

The most widely studied diblock copolymers are those consisting from polystyrene and a polydiene (either PI or PB).^{5,57} The polystyrene anionic centers can initiate efficiently the polymerization of either isoprene or 1,3-butadiene in hydrocarbon solvents. Additionally, by using organolithium initiators, high percentage of 1,4-microstructure is achieved for the polydienes leading to copolymers with relatively good elastomeric properties. Alternatively, copolymerization of dienes as the first block in hydrocarbon solvents with styrene as the second block is possible by adding a small amount of a polar additive (THF) prior to the initiation of styrene polymerization. The presence of polar reagents alters the stereochemistry and the reactivity of the polydiene macroanions, enabling a fast initiation rate for the second monomer (styrene) and leading to diblock copolymers with predictable molecular weights and narrow molecular weight distributions.⁸⁷ Except from the copolymerization of styrene with isoprene or 1,3-butadiene, other alkadienes have also been copolymerized with styrene, such as 2-methyl-1,3-pentadiene⁴² and 1,3-cyclohexadiene,⁸⁸ leading to diblock copolymers with well-defined molecular weights, narrow molecular weight distributions and structural/compositional homogeneity.

The synthesis of diblock copolymers containing styrene/styrenic monomers or dienes (isoprene, 1,3-butadiene) and (meth)acrylic monomers has also been reported in the literature.⁸⁹ These diblock copolymers are synthesized by polymerizing first the most reactive monomer (styrenic or alkadiene) and then the (meth)acrylic monomer. Polymerization of (meth)acrylic monomers requires low polymerization temperatures (-78°C), polar solvents (usually THF)⁴⁶ and relatively less active and more sterically hindered initiators in order to avoid side reactions of the carboanions with the active carbonyl group of the acrylic monomer. For this reason, a non homopolymerizable reagent such as 1,1-diphenylethylene (1,1-DPE) is usually used together with additives like LiCl, enhancing the control of the polymerization of (meth)acrylic monomers even in higher temperatures (e.g. -30°C).⁸⁹

Another class of significant diblock copolymers involves siloxane monomers and especially hexamethylcyclotrisiloxane. The last two decades, siloxane containing polymers are widely used in numerous applications, mainly in the area of nanotechnology, and especially nanostructuring and nanofabrication through self-assembly in bulk and directed self-assembly from thin films. Anionic polymerization of cyclosiloxanes has been

investigated for synthesizing diblock copolymers with either styrene or alkadienes as the first block.⁹⁰ Initiators containing Li as the counterion have been used under specific conditions and taking into consideration the high purity of the siloxane monomer together with the elimination of back-biting and/or redistribution reactions, well-defined diblock copolymers have been synthesized exhibiting variable molecular weights and compositions (Figure 2.13).⁴⁸ Model copolymers of PB and poly(dimethylsiloxane) (PDMS) were also synthesized through sequential monomer addition. By homogeneous hydrogenation of PB-b-PDMS, the PB chains were almost quantitatively transformed to poly(ethylene) and diblock copolymers of the PE-b-PDMS type were obtained.⁹¹

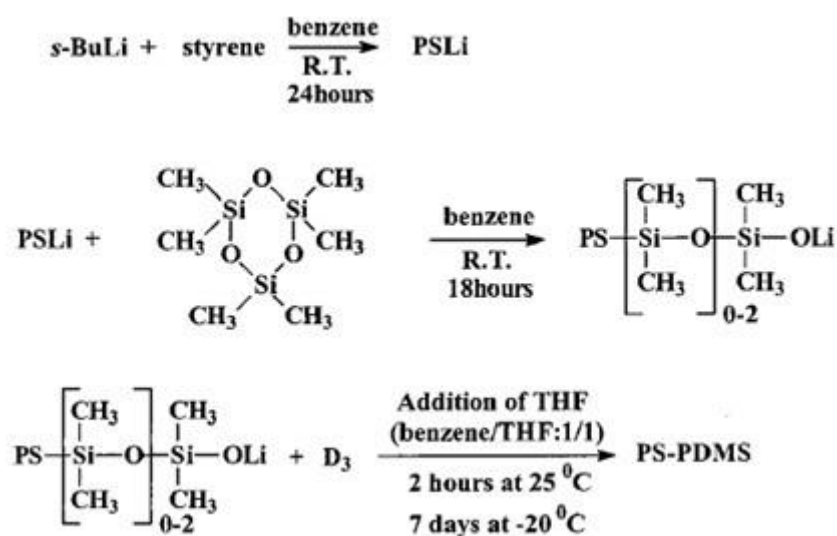


Figure 2.13: Reaction mechanism for the synthesis of PS-b-PDMS diblock copolymers.⁴⁸

2.5.2 Miktoarm Star Copolymers (A_2B and A_3B Type)

Star copolymers in general are divided to symmetric and asymmetric. In asymmetric star copolymers, the asymmetry involves: i) the molecular weight (the arms differ in molecular weight), ii) the chemical nature (miktoarm star copolymers) and iii) the topology (the arms are block copolymers which may or may not have the same composition and molecular weight, but differ in the relevant segment which is attached to the linking point).¹⁰

The word miktoarm¹⁰ (mikto from the Greek word $\mu\kappa\tau\acute{o}\varsigma$ meaning mixed) is an international term which has been adopted to describe exclusively star polymers consisting of chemically different chains. The number of different arms may vary together with the total number of arms, in order to prepare a variety of miktoarm stars such as: A_2B , A_3B , A_5B (or generally A_nB) and A_nB_n (Figure 2.14).

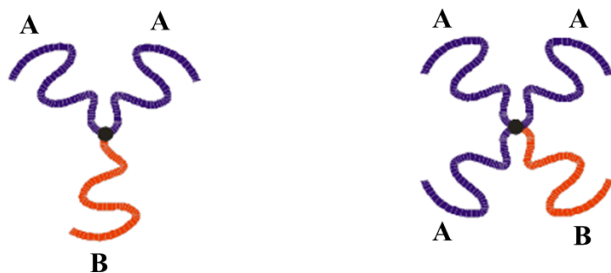


Figure 2.14: Schematic presentation of the architectures corresponding to miktoarm star copolymers of the A_2B and A_3B type.

Although there are several individual methods for the synthesis of miktoarm stars four general methodologies have been referred in the literature. Three of them are based on anionic polymerization and the fourth on cationic. In all of them the use of appropriate linking agents is necessary. These methods are: anionic polymerization with: a) divinylbenzene (DVB), b) diphenylethylenes (DPE), c) combination of chlorosilane chemistry and the fourth method involving living cationic polymerization.

The first, almost monodisperse, miktoarm star copolymer of the A_2B type where A was PI and B was PS was reported by Mays et al.⁹², using trichloromethylsilane (CH_3SiCl_3) as the linking reagent. A very important issue in the synthesis of these types of star polymers involves the incorporation of the linking reagent. Living B chains are reacted with a large excess of CH_3SiCl_3 in order to selectively substitute only one chlorine atom of the silane, therefore, the specific active sites should be the most sterically hindered (e.g. $\text{PS}^{(-)}\text{Li}^{(+)}$). By employing this synthetic procedure the advantage is that no side reactions occur, such as the formation of a dimer, tetramer or even a gel, but the disadvantage is that the excess of the relative chlorosilane should be removed prior to the addition of the second type chemically different chains. In order to ensure the complete substitution of the two remaining chlorine atoms, a small excess of the A living ends is added and therefore fractionation in a mixture of solvent/non solvent is needed to remove the residual non incorporated living ends (Figure 2.15).

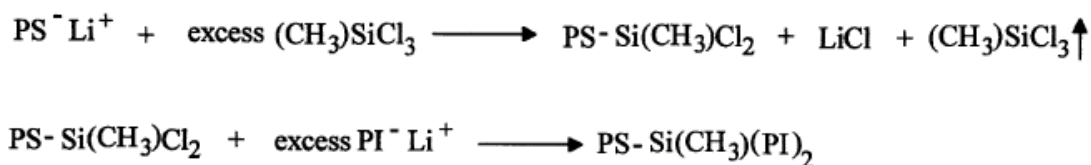


Figure 2.15: Reactions scheme for the synthesis of $\text{PS}(\text{PI})_2$ miktoarm star copolymer.

This synthetic procedure was further developed by the Hadjichristidis' group.⁹³ All possible combinations of A_2B polymers with A and B being PS, PI or PB were prepared. High degrees of molecular, structural and compositional homogeneity were achieved by this

technique, as was evidenced by the combination of all molecular characterization data reported in the literature.

The chlorosilane method was adopted for the synthesis of miktoarm stars of the type B(A-*b*-B)₂ where A is PI and B is PS.⁹⁴ The synthetic procedure was similar to that used for the preparation of A₂B stars except that two of the arms were diblock copolymers, as is shown in Figure 2.16. Extensive characterization data were given to confirm the synthesis of the well-defined copolymers.

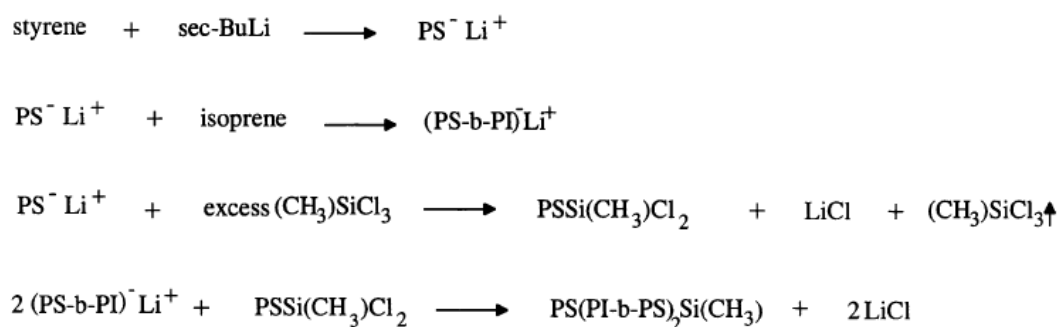


Figure 2.16: Synthetic route for B(A-*b*-B)₂ star copolymer.

For the synthesis of A₃B miktoarm star copolymers the only difference is on the linking reagent (SiCl₄ instead of CH₃SiCl₃). Living PS chains were reacted with an excess of the linking agent for the preparation of the trichlorosilane end-capped PS. After removal of the SiCl₄ excess the macromolecular linking agent was added to a slight excess of living PI⁽⁻⁾Li⁽⁺⁾ chains and the A₃B miktoarm star was prepared. The reactions of all steps involved were monitored by SEC. The products after extensive characterization exhibited high degree of molecular and compositional homogeneity.⁹⁵ This type of chlorosilanes, due to their low boiling points, can be easily removed from the solution of the chlorosilane-capped B polymer. The solvent, usually benzene, and the chlorosilane are removed in a high vacuum line until the sample is completely dried, whereas the remaining product is re-dissolved in benzene. A similar procedure was followed for the synthesis of miktoarm stars of the type B(A-*b*-B)₃, in which again A corresponded to PI and B to PS.⁹⁴

CHAPTER 3

Physical Properties of Linear and Non-Linear Block Copolymers

3.1 Microphase Separation of Linear Diblock Copolymers

3.1.1 Theory Background

Block copolymers consist of incompatible polymer segments which are chemically connected to each other with covalent bonds. The value of the Gibbs free energy (ΔG_M) for the simplest case, which is the mixing of two chemically different homopolymers, is given by the following equation:

$$\Delta G_M = \Delta H_M - T\Delta S_M \quad (3.1)$$

where ΔH_M and ΔS_M are the enthalpy and entropy variations due to mixing, respectively. For the phase separation of a linear diblock copolymer, the final free energy F is given by the following equation:

$$\frac{F}{kT} = \chi_{AB}\phi_A\phi_B + \left(\frac{\phi_A}{N_A}\right) \ln(\phi_A) + \left(\frac{\phi_B}{N_B}\right) \ln(\phi_B) \quad (3.2)$$

where ϕ_A and ϕ_B correspond to the volume fraction of block A and B respectively, N_A and N_B are the degree of polymerization of block A and B respectively which are always proportional to the molecular weight of each relative block and χ is the Flory-Huggins interaction parameter between the A and B polymer segments. The first two factors, ϕ and N , are related to the composition of the copolymer and affect the entropy of mixing while χ is a parameter related to the enthalpic interaction of the blocks and is inversely proportional to the temperature according to the following equation⁹⁶:

$$\chi = \frac{\alpha}{T} + \beta \quad (3.3)$$

where α contains the enthalpic excess free energy of mixing and β contains the entropic excess free energy of mixing (the units α and β are typically Kelvin and do not bear any units, respectively).⁹⁷ It is easily understood, from equation 3.2, that entropic interactions are related to N^{-1} and enthalpic interactions are related to χ and since $\chi \ll N$, the microphase separation exclusively depends on the χN value.

Thermodynamics of block copolymers depend also on the fact that chains tend to maintain their unperturbed dimensions. Entropic interactions tend to favor the mixing of the two blocks while the enthalpic interactions promote their separation. Consequently, the phase behavior of linear block copolymers (diblock is the simplest case) is determined by three experimental controllable parameters:

- the total degree of polymerization N ,
- the volume fraction ϕ
- the A/B segment-segment Flory-Huggins interaction parameter χ .

At equilibrium, polymer chains tend to form such structures that the total free energy of the system is minimized. When the interaction parameter χ is increased (e.g. by lowering the temperature) the junction points (covalent bonds joining together the two blocks) between A and B are less favored. If the value of degree of polymerization N is relatively high, then the junction points of A and B blocks are even less favored leading to the decrease of the chain conformation entropy. The result is that the chains do not maintain anymore their unperturbed dimensions and the enthalpy requirement for minimizing the junction points between dissimilar chain segments leads to a local phase separation which is called microphase separation (Figure 3.1).

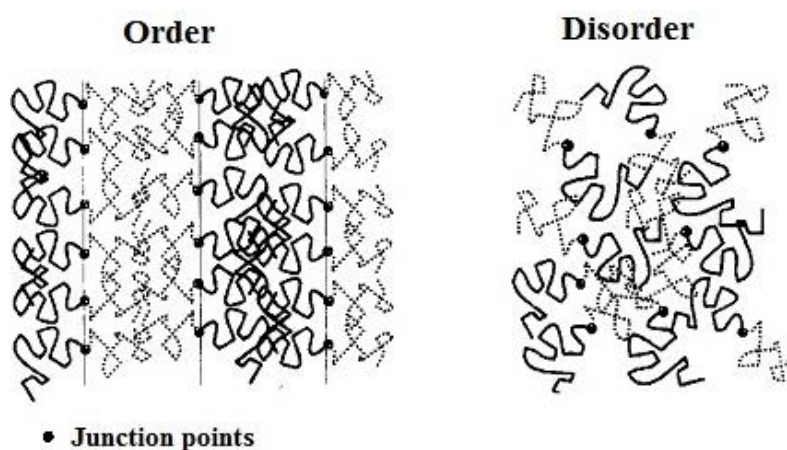


Figure 3.1: Ordered state (left) and disordered state (right) of a symmetric linear diblock copolymer, exhibiting alternating lamellar structure (left image). The ordered state consists of separated microphases of the two components with the junction points located on the interface.⁹⁶

In the case where χ or N decrease significantly, the entropic factors will dominate, leading the system to the disorder state. The change related to a transition from a disorder state to an ordered state is called microphase separation transition (MST) or order-disorder transition (ODT) and the temperature where this change happens is called order-disorder temperature (T_{ODT}). Mean-field theory (MFT) calculations by Leibler⁹⁸ predicted that the order-disorder transition (ODT) for a symmetric diblock copolymer ($\phi_A = \phi_B = 0.5$) is observed when $\chi N = 10.5$.

The separated microphases assemble forming various structures. The morphology that will be adopted by the copolymer melt, when it microphase separates, is determined by the entropic and enthalpic factors adjusting the total free energy value. The enthalpic term is related to the interaction energy and favors the minimization of the interface size which separates the two different blocks. The entropic term is related to the extension energy of the

chains and favors chain conformations in both sides of the interface. The adopted morphology of the copolymer at equilibrium is a combination of both entropic and enthalpic parameters. For a symmetric diblock copolymer ($\phi_A = \phi_B = 0.5$), the chains located in both sides of the interface will have almost the same size (almost identical conformation) leading to the formation of alternating lamellar. While the asymmetry between the blocks in both sides of the interface is increased ($\phi_A > 0.5$, $\phi_B < 0.5$), the asymmetry between the chain size is also increased resulting to the formation of more curved interfaces towards the block with the lowest content (ϕ_B) (Figure 3.2).

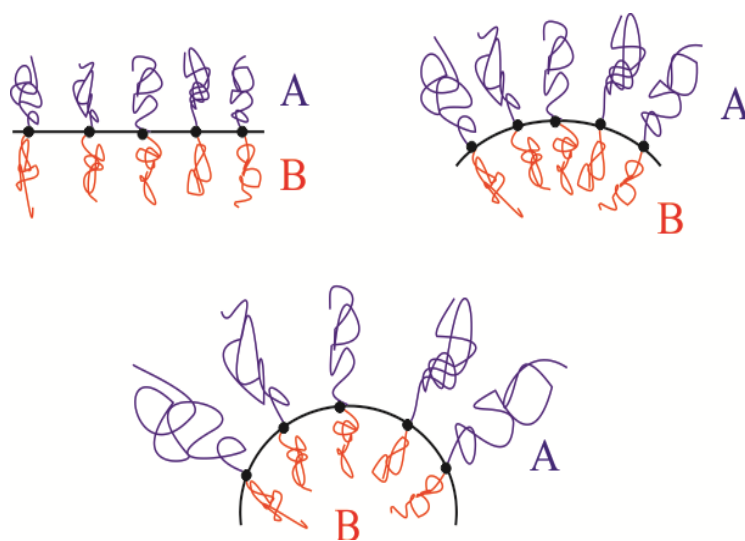


Figure 3.2: *The effect of asymmetry between the blocks on the interface curvature in a diblock copolymer. The more asymmetric the macromonomer is, the larger the curvature of the interface becomes. The overall morphology of the system depends on the local curvature of the interface.*

At the beginning of microphase separation, the system goes through the ODT to the weak segregation limit (WSL) when $\chi N \sim 10.5$. In WSL, the thickness of the interface is not small but significantly large, due to the high mixing of the two blocks inside the interface and the macromolecular conformations are similar to the unperturbed dimensions. The other regime which has been reported in the literature is the strong segregation limit (SSL) for cases in which $\chi N > 100$, where the interactions between the asymmetric blocks are so strong that the chains are almost immediately separated in homogenous microdomains divided by very thin interfaces on which the junction points are located. Each microphase contains exclusively only one of the two components and by moving from one microphase to another there is a sharp change in composition. It is important to emphasize that the dimensions of the intermediate surface in the strong segregation limit are negligible in contrast with the case of weak segregation limit. Consequently, the enthalpic term of the free energy is related only to the area of the interface since this is the domain where the junction points between the two different blocks are located. The enthalpic term is significantly reduced by the stretching of the chains away from the interface (the macromolecular conformations are far from the

unperturbed dimensions), resulting to absolute absence of mixing between the blocks. The third regime is the intermediate segregation limit (ISL) for which the χN value is varying accordingly: $30 < \chi N < 100$.

3.1.2 Strong Segregation Limit (SSL)

Many theories were developed in order to describe the strong segregation limit for block copolymer microphase separation. Two of the most important are described.

The first was developed by Helfand and Wasserman⁹⁹⁻¹⁰¹ who introduced a self-consistent field theory (SCFT) with three principal contributions to the free energy: a) contact enthalpy between the A and B microdomains at the interface, b) minimization of entropy due to stretching of chains and c) confinement entropy due to localization of the junction points at the interface. Their result for the microdomain thickness was:

$$d \sim a N^\delta \chi^\nu \quad (3.4)$$

where $\delta \sim 9/14$, $\nu = 1/7$ and a is the statistical segment length.

The second theoretical study was developed by Semenov¹⁰² who estimated the free energy in the asymptotic limit arguing that polymer chains are strongly stretched. This situation resembles grafted polymer brushes as well as surfactant interfaces and estimates that the microdomain size in the asymptotic limit is given by the following equation:

$$d \sim a N^{2/3} \chi^{1/6} \quad (3.5)$$

The above equation predicts a strong dependence on the microdomain size on N and a weak dependence on χ . Since there is weak dependence of the interaction parameter χ , the experimental verification of this equation was a difficult task, however experiments in symmetric diblock copolymers¹⁰³ have shown a weaker dependence as $d \sim N^{0.6}$, for $\chi N > 29$, with a strange N -dependence ($d \sim N^{0.8}$) at weaker segregation, implying that this SSL predictions of $d \sim N^{2/3}$ are only correct for $\chi N > 100$, as expected.

Changes in volume fraction, ϕ primarily affect the shape and packing symmetry of the ordered microstructure, except near the ODT, and are almost uncorrelated with χN . Reducing or increasing ϕ , leads to unequal packing and chain stretching constraints on each side of a diblock copolymer molecule and leads to new ordered-phase symmetries over specific ranges in composition. Seven ordered phases have been identified in the polystyrene/poly(isoprene) diblock copolymers (PS-*b*-PI), as illustrated in Figure 3.3, where ϕ indicates the volume fraction of polystyrene.¹⁰⁴

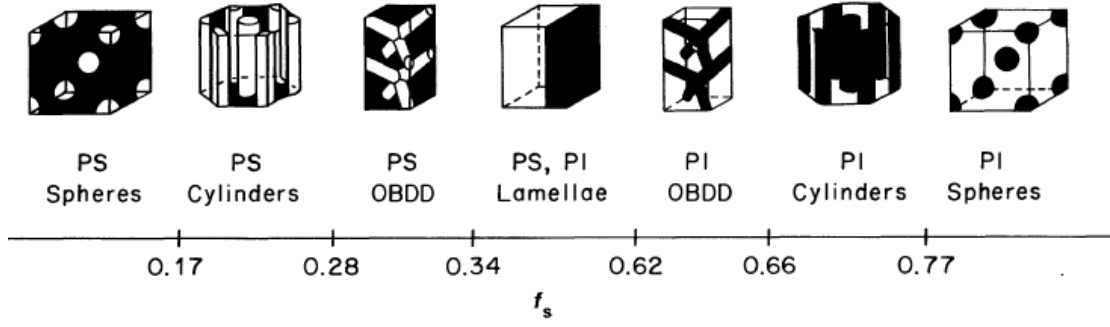


Figure 3.3: Effect of varying composition on the ordered-phase symmetry in polystyrene-*b*-poly(isoprene) (PS-*b*-PI) block copolymer, where f refers to the overall volume fraction of polystyrene.

For $\phi_{PS} < 0.17$, microspheres of polystyrene are ordered on a body-centered cubic (BCC) lattice in a matrix of poly(isoprene). Increasing the composition to $0.17 < \phi_{PS} < 0.28$ leads to hexagonally packed (HEX) cylindrical PS microdomains. An ordered bicontinuous double diamond (OBDD) PS microstructure embedded in a continuous PI microphase appears where $0.28 < \phi_{PS} < 0.34$. It should be noted that OBDD has been replaced since the mid 90's by the double gyroid (DG), where it was found to be more stable predominant structure. Between $\phi_{PS} = 0.34$ and 0.62 these materials display an alternating lamellae microstructure (LAM). Increasing ϕ_{PS} further, leads to the corresponding inverted ordered phases, in which PS is the matrix and PI the minority component.

3.1.3 Weak Segregation Limit (WSL)

This is the regime where most of the experiments were accomplished, when χN is slightly larger than 10.5. Leibler⁹⁸ was the first who considered a monodisperse linear diblock copolymer (AB) with equal monomer volumes and statistical segment lengths ($\alpha_A = \alpha_B$). The conclusion was that the morphological behavior is related to the interaction parameter χ , the degree of polymerization N and the volume fraction ϕ , which is a fraction of the copolymer molecular composition f , according to the equation:

$$\phi_A = \frac{f_A d_B}{f_A d_B + f_B d_A} \quad (3.6)$$

where ϕ_A is the volume fraction of block A, d_A and d_B are the densities of A and B blocks respectively and f_A and f_B are the molecular fraction or mass fraction values of A and B blocks respectively. The molecular fraction of block A is given by the following equation:

$$f_A = \frac{\overline{M}_{n,A}}{\overline{M}_{n,A} + \overline{M}_{n,B}} \quad (3.7)$$

The phase diagram obtained is shown in Figure 3.4. The phase limits are more curved with the volume fraction as the segregation becomes weaker. For a symmetric copolymer with volume fraction $\phi = 0,5$ the order-disorder transition is predicted that occurs when $\chi N = 10.495$, where a second order transition from the disordered phase to alternating lamellar domains occurs. For a specific range of compositions and χN values larger than 10.5, for systems exhibiting large asymmetry between the two blocks, Leibler predicted that at the ODT the system undergoes a first order transition from the disorder phase to a body centered cubic (BCC) sphere phase.

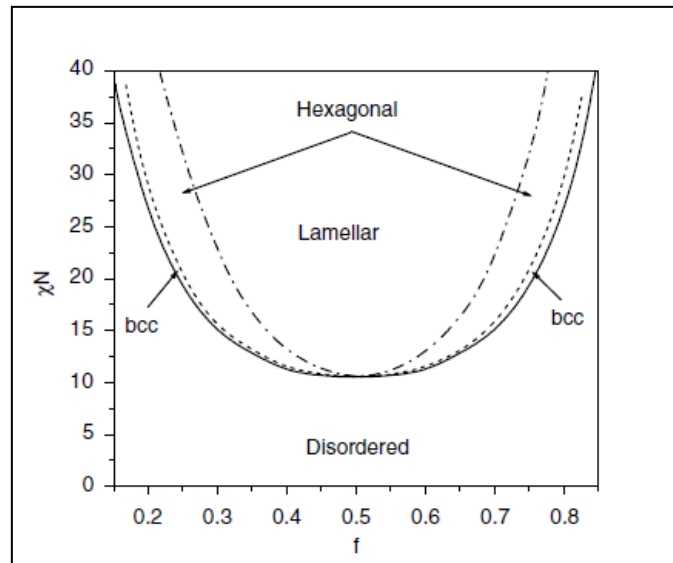


Figure 3.4: Theoretical phase diagram for linear diblock copolymers within the mean-field theory assuming equal monomer volumes and statistical segment lengths for the two blocks. On this phase diagram, f corresponds to the volume fraction.⁹⁸

By further increase of χN at specific volume fractions, and by using the mean-field theory (MFT) calculations, the system undergoes a transition to hexagonally packed cylinder (hpc) phase and then to the lamellar phase. Mayes and Olvera de la Cruz¹⁰⁵ used the Hartree approximation which resulted in the following equation:

$$(\chi N)_{\text{ODT}} = 10,495 + 39,053 N^{-1/2} \quad (3.8)$$

As it can be concluded and in contrast with strong segregation limit theory where $d \sim N^{2/3}$, at weak segregation limit theory the microdomain size (d) of the adopted unit cell in each case is analogous to $N^{1/2}$.

3.1.4 Intermediate Segregation Limit (ISL)

The previously reported approaches from Helfand, Leibler and Semenov were very successful in predicting the three classical phases but failed to account for the more complex ones. Matsen¹⁰⁶ showed self-consistent field theory (SCFT) results, for intermediate segregation, in more complex structures as it can be observed by the phase diagram given in Figure 3.5. The most important aspect of this phase diagram is the existence of a new phase,

the double gyroid phase, in addition to the usual lamellar, hexagonal and spherical phases predicted from Leibler's work.

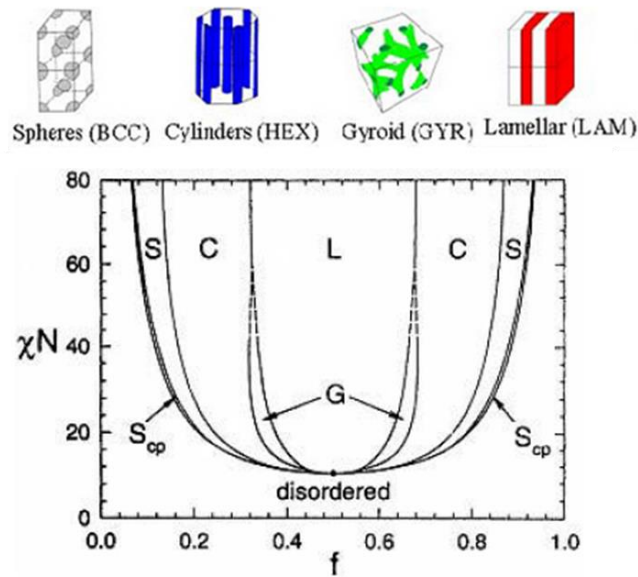


Figure 3.5: Mean field phase diagram within the SCFT approximation for conformationally symmetric diblock copolymers constructed by Matsen. The different phases are: L: lamellar, C: hexagonally packed cylinders, S: spheres packed in a bcc lattice, G: bicontinuous Ia3d cubic (double gyroid), S_{cp}: closed packed spheres.¹⁰⁷

The SCFT predicts for intermediate segregation the sequence of lamellar-gyroid-hexagonal-spheres-disordered phases when ϕ progresses from 0.5 to 0 or 1. Both perforated lamellar (PL) phase¹⁰⁸ and the ordered bicontinuous double diamond (OBDD) are absent from the diagram since they were considered unstable and/or metastable phases.

3.1.5 Conformational Asymmetry

Matsen and Bates¹⁰⁹ reported, through SCFT calculations, that conformational asymmetry (ζ) plays a significant role to the order-order and order-disorder phase boundaries. By compiling the free energy values found for classic and more complex diblock copolymers, very interesting phase diagrams were produced corresponding to the cases where $\alpha_A/\alpha_B = 1.5$ and $\alpha_A/\alpha_B = 2$ (Figure 3.6), where α is the statistical segment length. The main effect of conformational asymmetry is to shift the phase boundaries towards compositions richer in the blocks exhibiting the higher asymmetry. This asymmetry has been attributed to differences in monomer volume and in chain flexibilities of the blocks, leading to an overall conformational asymmetry described by equation 3.9:

$$\zeta = \frac{\alpha_A^2 / 6u_A}{\alpha_B^2 / 6u_B} \quad (3.9)$$

where u is the statistical segment volume and a the statistical segment length.

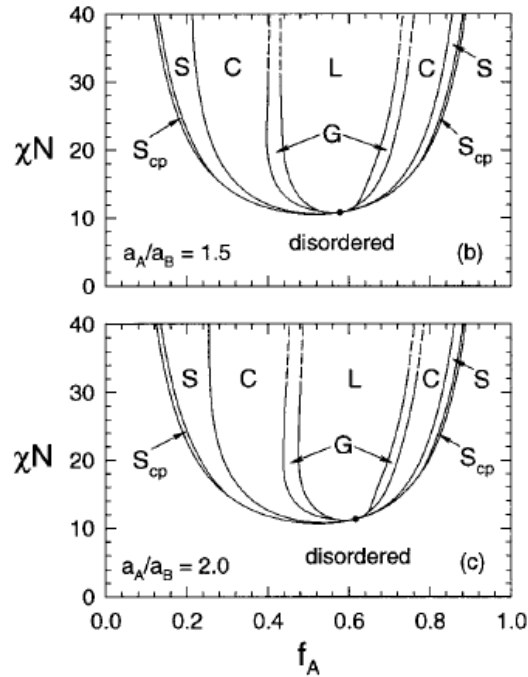


Figure 3.6: Phase diagrams for linear diblock copolymers with different conformational asymmetries within the SCFT and $f_A =$ volume fraction. Top: $a_A/a_B = 1,5$; Bottom: $a_A/a_B = 2$: The ordered phases are L (lamellar), G (gyroid), C (hexagonally packed cylinders), S (spheres in bcc lattice), and S_{cp} (spheres in fcc lattice).¹⁰⁹

As it can be easily observed from Figure 3.6, the conformational asymmetry has a greater impact on the order-order transitions (OOT) than on the order-disorder transitions (ODT) producing larger shifts. The larger shifts in the OOT can be explained from the fact that as a_A/a_B increases, the A blocks become easier to stretch, while the opposite happens for the B blocks leading to a larger asymmetry in the phase diagram when the value of a_A/a_B is equal to 2. The interface acquires the tendency to curve towards the A blocks, while allowing the B blocks to relax at the expense of A segments. At a certain composition ϕ_A or f_A , the lamellar phase will tend to transform to the hexagonal one where cylinders of A blocks will be embedded in a matrix of B blocks. This tendency causes the OOT to shift towards larger A-block volume fractions. On the other hand, the effect of conformational asymmetry on the ODT is much smaller. For example, disorder from spherical structure formed by A block requires a thermal energy applied on the blocks forming the spheres which is approximately equal to the value of $\chi N \phi_A$, therefore independent from the statistical segment lengths a_A and a_B . The ODT is relatively unaffected by the conformational asymmetry. Apart from the differences on the phase state, conformational asymmetry strongly affects the relative domain spacing between structures along their boundaries. This is expected to affect the kinetics of the respective order - order transitions.

3.1.6 Phase Diagram of PI-b-PS Diblock Copolymers

The most investigated system in bulk for diblock copolymers is the poly(isoprene)-b-polystyrene (PI-b-PS), where sixteen (16) samples were prepared and examined.¹¹⁰ For the PI-b-PS phase diagram (Figure 3.7) the morphologies that were observed are:

- ✓ Spheres of the minority component arranged in a body centered cubic (BCC) lattice in a matrix of the majority component ($Im\bar{3}m$).
- ✓ Hexagonally packed cylinders of the minority component in a matrix of the majority component (HEX).
- ✓ Double gyroid, where two independently interpenetrating and not interconnected bicontinuous networks of the minority component are formed in a matrix of the majority component ($Ia\bar{3}d$).
- ✓ Hexagonally perforated layers (HPL).
- ✓ Alternating lamellae of the two components (LAM).

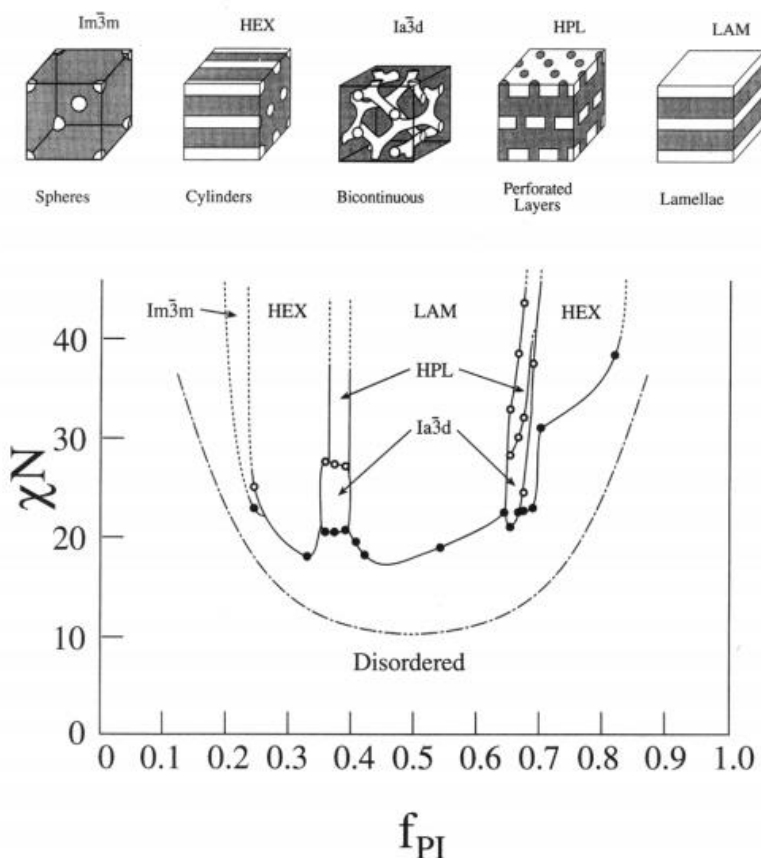


Figure 3.7: Phase diagram of χN vs f_{PI} indicating the equilibrium morphologies experimentally observed for linear diblock copolymers of the PI-b-PS type. The dashed line gives the spinodal line from Leibler's MFT predictions, where f_{PI} =volume fraction of poly(isoprene).¹¹⁰

As it can be observed, the phase diagram is asymmetric around $\phi = 1/2$. Furthermore, the gyroid phase is stabilized for a narrow range of compositions, from 0.27 to 0.34 and from 0.64 to 0.69 respectively indicating the stability of the specific phase even when the matrix becomes the channels and vice-versa which is considered of major importance.

3.2 Microphase Separation of Non-Linear Block Copolymers

3.2.1 General Information

Miscellaneous architectures of block copolymers, except from the linear ones, have been explored, due to the expectation of different morphologies and/or physical properties induced by different molecular architectures such as: miktoarm star, star-shaped, graft copolymers etc.¹¹¹ These complex architectures of block copolymers have shown enhanced mechanical and viscoelastic properties and can be used at least as compatibilizers in polymer blends.¹¹²

By chemically joining two homopolymers in order to form a diblock copolymer, increases the compatibility, which is reflected in the reduction of the critical temperature for phase separation when compared to the homopolymer blend. Compatibility can be further increased by changing the molecular architecture. For this purpose, triblock, star, graft and miktoarm star copolymers have been synthesized and theoretical¹¹³⁻¹¹⁶ as well as experimental^{95,117-122} efforts revealed that in general:

$$(\chi N_t)_{c, blend} < (\chi N_t)_{ODT, diblock} < (\chi N_t)_{ODT, graft} < (\chi N_t)_{ODT, triblock} < (\chi N_t)_{ODT, star}$$

where $(\chi N_t)_c$ or $_{ODT}$ is the critical value of χN_t corresponding to the stability of the disordered state (N_t is the total degree of polymerization). This means that a melt of a triblock or a star copolymer will remain in the homogeneous (disordered) phase for temperatures where a melt of linear diblock copolymer is already microphase separated.

3.2.2 Microphase Separation of Miktoarm Star Copolymers

3.2.2.1 Theory Background

Olvera de la Cruz and Sanchez¹¹³ were the first researchers to report theoretical calculations concerning the phase stability of graft and miktoarm star copolymers of the A_nB_n type with equal numbers of A and B branches. They predicted that a simple graft has no critical point for any volume fraction ϕ . Irrespective of the position of the branch point, the minimum value of the spinodal appears at a volume fraction equal to: $\phi = 0.5$. For the case of an A_2B miktoarm star it is concluded that ODT occurs when $\chi N = 13.5$ and $\phi = 0.5$. Therefore, it is more difficult for the chains to phase separate in such architecture when compared to the simpler case of linear block copolymers. Miktoarm star copolymers of the A_nB_n type are

predicted to have critical point $(\chi N)_c=10.5$ (as for the diblocks when $\phi = 0.5$), which signifies that the microphase separation of nearly symmetrical miktoarm stars depends only on the molecular weight of the associate block copolymer N_0 and not on the whole star number of chains.

A few years later, Milner¹¹⁵ concluded to a theoretical phase diagram for A_nB_n miktoarm star copolymers in the strong segregation limit, in which the interface between the two blocks is considered relatively sharp. In this study a new parameter was incorporated for calculating the phase diagram and it was attributed as the elasticity parameter (ε) (equation 3.10). The morphologies are determined by the competition between the increase of stretching free energy as each arm stretches away from the interface and the reduction of interfacial tension. In Figure 3.8 this phase diagram corresponding to miktoarm star copolymers for the elasticity parameter as a function of volume fraction of B (ϕ_B) is given. By increasing ε , the phase boundary between different microdomains is moved toward ϕ_B .

$$\varepsilon = (n_A/n_B)(I_A/I_B)^{1/2} \quad (3.10)$$

where n_A and n_B are the numbers of A and B blocks and I_A, I_B are characteristic lengths (Kuhn lengths) of A and B respectively.

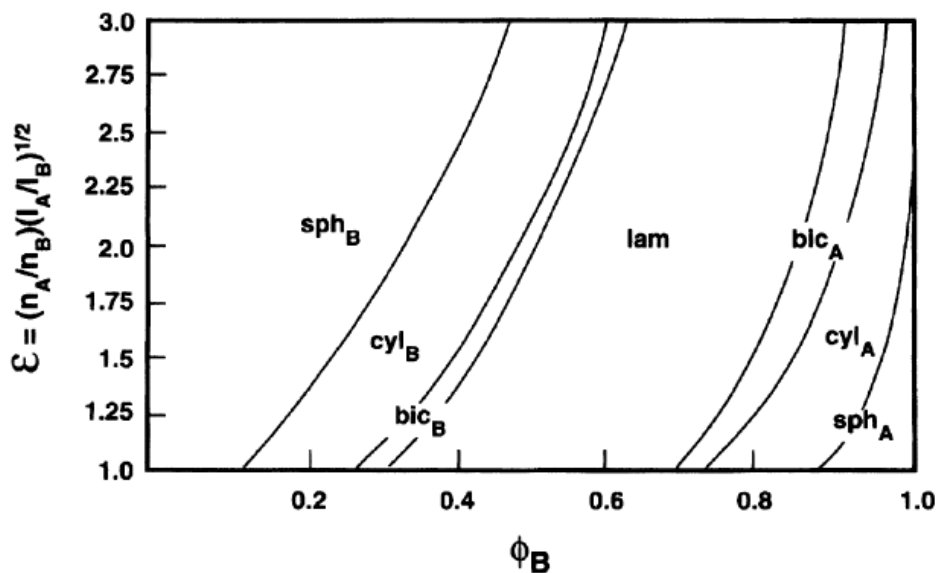


Figure 3.8: Phase diagram in the strong segregation limit for star block copolymers with n_A : A arms and n_B : B arms as a function of the volume fraction for B domains.¹¹⁵

Floudas et al.¹²³ predicted the microphase separation for diblock and AB_n miktoarm star copolymer based on mean field theory (as Leibler did in his initial studies at the weak segregation regime). Spinodal curves were calculated for the AB_n miktoarm star copolymers

with n up to 100 [Figure 3.9(a)]. Microphase separation of AB_n miktoarm star copolymers becomes more difficult when compared with linear block copolymers, due to the critical value of χN_t ($N_t = N_A + nN_B$) being higher for the AB_n complex architecture [Figure 3.9(b)]. In addition, the spinodal curves are asymmetric when plotted for f_A due to the asymmetry of miktoarm star copolymers. Interestingly, the maximum critical value of χN_t in AB_n miktoarm star copolymers appeared when n was equal to 3, attributed possibly to the balance between the stretching free energies of A and B arms. The theoretical predictions on phase boundaries are consistent with experimental results by small angle X-ray scattering (SAXS) measurements for relative AB_3 miktoarm star copolymers of the PS(PI)₃ type.

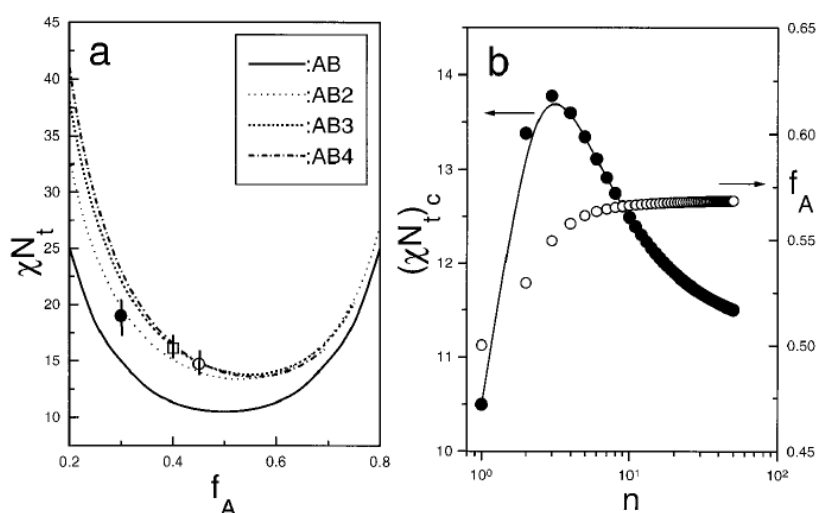


Figure 3.9: (a) Comparison of the spinodal curves $\chi N_t(f_A)$ for diblock and different AB_n miktoarm copolymers with $n = 2, 3,$ and 4 . The experimental results from an AB_2 and two AB_3 miktoarm stars are shown simultaneously with the investigated temperature range (vertical lines). (b) Critical values of χN_t , plotted as a function of the number of arms of the B blocks. The dependence of the optimal composition corresponding to the minima of the spinodal curves is also shown.¹²³

Grason and Kamien¹²⁴ reported the phase behavior of AB_n miktoarm star copolymers in SSL, using a self-consistent field theory (SCFT) approach. All phase diagrams were not symmetric, which means that the shape of the interfaces is curved toward the A block due to the asymmetry of the non-linear architecture. They also found that the interface between two blocks is highly distorted when the number of B arms is higher than 3. As a result, increasing the number of B arms enhances the stability of A15 phase (sphere-like micelles) which is not observed for linear diblock copolymers.

Recently, Matsen¹²⁵ calculated equilibrium phase diagrams for a selection of two component block copolymer architectures (comb and star-like) using as well SCFT. He reported that the topology of the phase diagrams is relatively unaffected by differences in architecture, but the phase boundaries shift significantly due to composition. Although the complex phase windows continue to be dominated by the gyroid (G) phase, the regions of the newly discovered $Fddd$ (O^{70} , orthorhombic and single-network structure)^{126,127} phase become

considerably evident for certain architectures, the comb copolymer exhibits a stable region for A15 spheres (S_{A15}) in the same vicinity that Grason and Kamien¹²⁴ have predicted for AB_2 stars (as mentioned above) and the perforated-lamellar (PL) phase becomes stable when the complex phase shifts toward high compositional asymmetry (Figure 3.10).

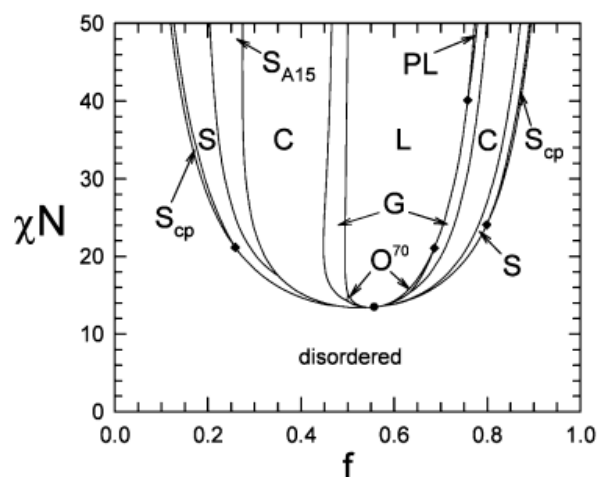


Figure 3.10: Theoretical phase diagram of AB_2 miktoarm star copolymer. PL, $Fddd$ are additionally shown.¹²⁵

3.2.2.2 Experimental Results

In the first microphase separation study of A_2B miktoarm stars¹²⁸ where A and B are PS or PI respectively, by Hadjichristidis and collaborators, a $PS(PI)_2$ sample with 37 vol.% PS was found, by transmission electron microscopy (TEM) studies, to microphase separate exhibiting PS cylinders in the PI matrix in contrast to an alternating lamellae structure expected for a linear diblock copolymer with the same volume fraction. Subsequently, more studies^{95,122,129} with a larger number of samples and covering a wider range of compositions showed that differences exist in the phase diagram for miktoarm star copolymers in comparison to what is predicted and expected for linear diblock copolymers. The boundaries of the morphologies usually expected in diblock copolymers (as mentioned previously in the discussion for the strong segregation limit) are shifted towards higher compositions of B in the A_nB complex architecture. At constant composition the miktoarm star copolymer adopts a highly curved topology, when compared with the relative diblock attributed to the overcrowding of the A chains and overstretching of the B component in the miktoarm star A_2B architecture.

Analogous shifts were also observed in the case of A_3B (A:PI and B:PS) miktoarm stars.⁹⁵ These findings are in qualitative agreement with the theoretical predictions made by Milner¹¹⁵, which were made just after the first experimental findings.¹²⁸ However, some discrepancies in terms of the exact location of the morphology boundaries do exist between theoretical predictions and experimental results. For example a I_2S sample with 53 vol.% PS

formed experimentally a tricontinuous double gyroid structure with networks of PI in a PS matrix whereas an alternating lamellae structure was expected from the theoretical predictions (Figure 3.11). Another I₂S sample with high PS content, (81% by vol.), exhibited microphase separation without long range order. This randomly oriented wormlike morphology of PI “cylindrical” micelles in a matrix of PS, was concluded to be an equilibrium structure by employing selective solvent casting and annealing experiments.



Figure 3.11: Bright field TEM micrograph of I₂S miktoarm star with 53 vol.% PS exhibiting a tricontinuous double gyroid morphology with PI networks (black) in PS matrix (white). The differentiation between the blocks is evident due to staining/cross-linking of the PI domains with vapors of OsO₄ aqueous solution.⁹⁵

Furthermore, the experimentally determined phase diagram for the I₃S miktoarm stars did not show any spherical morphology for high PS content up to 92%. The micrographs of a I₃S sample with 39 vol.% PS had the structure of PS cylinders instead of spheres as theoretically predicted, whereas a sample with 86 vol.% PS exhibited PI cylinders instead of alternating lamellae and finally a sample having 92 vol.% in PS showed disordered PI cylinders in a PS matrix instead of PI bcc spheres in a PS matrix as expected theoretically. It is obvious that as the number of arms in A_nB type samples increases significant discrepancies between the theoretical expectations and experimental results are more prominent.

3.3 Microphase Separation of Polydienes

In general, the possible combinations of microstructures for PB and PI in a diblock copolymer sequence are significant and are given below:

- PB_{1,4}/PI_{1,4}
- PB_{1,2}/PI_{1,4}
- PB_{1,2}/PI_{3,4} (high content in 3,4-)
- PB_{1,4}/PI_{3,4} (high content in 3,4-)

For diblock copolymers or triblock terpolymers, the type and relative amount of the specific stereoisomers should always be considered since local structure influences the segment-segment interaction parameter. The possible segment microstructures for PB are 1,4-*cis*, 1,4-*trans* and 1,2-, while for PI they are: 1,4-*cis*, 1,4-*trans*, 3,4- and 1,2-, respectively. When the 3,4-microstructure of PI is significantly increased (~55-60%), then the 1,2-microstructure is increased as well (15-25%).

The first three combinations of polydiene pairs given above have been explored and the interaction parameters were found sufficiently small such that either copolymers or even blends of the polydiene pairs form mixed homogeneous phases for typical molecular weights. The segment-segment interaction parameter of diblock copolymers of predominantly 1,4-PB and predominantly *cis*-1,4 PI with either or both of the corresponding linear homopolymers has been studied.¹³⁰ Cohen and Wilfong¹³¹ calculated χ for different diene pairs, obtaining room temperature values of 0.081 and 0.048 for 1,4-PI/1,4-PB and 1,4PI/1,2-PB, respectively.

The synthesis and morphological characterization of a terpolymer containing PB and PI have been reported for the first time by Neumann et al.^{132,133} The results of this study showed that the triblock material behaved essentially as a pseudo-diblock copolymer since it consisted of a mixed 1,4-PI/1,2-PB block segregated by a PS block.

Avgeropoulos et al.¹⁷ reported for the first time the anionically synthesized and morphological characterization of ABC terpolymers with two polydiene blocks and PS with the difference being in the 3,4-microstructure content of the PI (~55% 3,4-content) whereas the PB block was the usual one with high 1,4-microstructure (~92%). A three-component microphase separated system occurred, leading to the conclusion that the 1,4-PB/3,4-PI polydiene combination has a larger χ interaction parameter than the other three possible combinations. The morphological characterization of the samples was performed through transmission electron microscopy (TEM) (Figure 3.12) and small angle X-ray scattering (SAXS). What is of major importance in this study is that by altering the block sequence from BSI to SBI but keeping the volume fraction ratio constant, they obtained that morphology remained the same, leading to the conclusion that the adopted topologies were equilibrium structures (since the block sequence did not alter the morphology as already reported in SIV vs. ISV by Thomas and Mogi respectively).^{134,135}

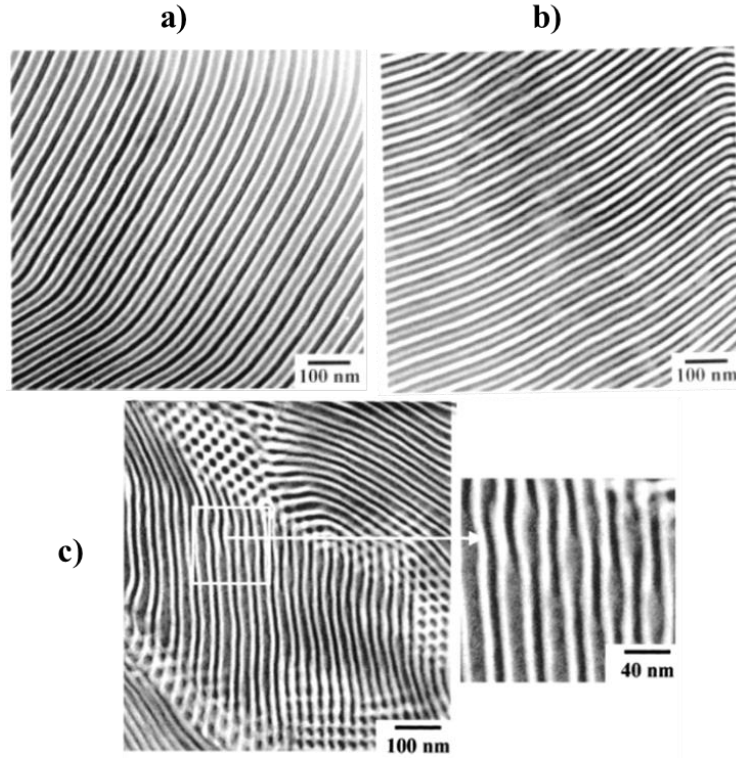


Figure 3.12: a) Bright field TEM image of the three-phase four-layer lamellae of the BSI-25/28/32, b) bright field TEM image of the three-phase four-layer of the SBI-45/48/40, c) bright field TEM image of the BSI-37/80/32 sample, showing cylindrical morphology. The darkest diene phase corresponds to the PB and the gray contrast regions correspond to the PI.¹⁷

A schematic of the three-phase four-layer BSI-25/28/32 and SBI-45/48/40 lamellar morphologies and the cylindrical structure of BSI-37/80/32 exhibiting typical chain conformation are shown for all three samples in Figure 3.13.

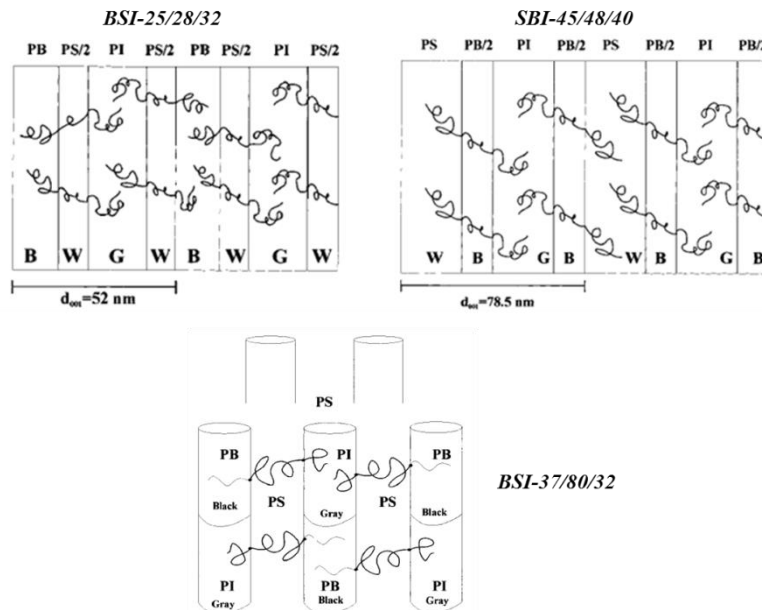


Figure 3.13: Schematics of the three-phase four-layer lamellar and cylindrical morphologies of BSI and SBI samples as reported in the literature.¹⁷

Additionally, a very recent study by Avgeropoulos' group¹³⁶ showed the coexistence of core-shell double gyroid and three-phase four-layer lamellar morphologies for similar SBI triblock terpolymers (S: PS, B: PB_{1,4} and I: PI_{3,4}), as verified by TEM. SAXS results led to the conclusion that the 3-phase 4-layer lamellae is most predominant despite the relatively long range order and the observations of both structures by bright field TEM images (Figure 3.14). Diblock copolymers of the PB-b-PI_{3,4} type were also synthesized in order to verify the microphase separation and immiscibility of these two polydienes in lower and very high molecular weights.

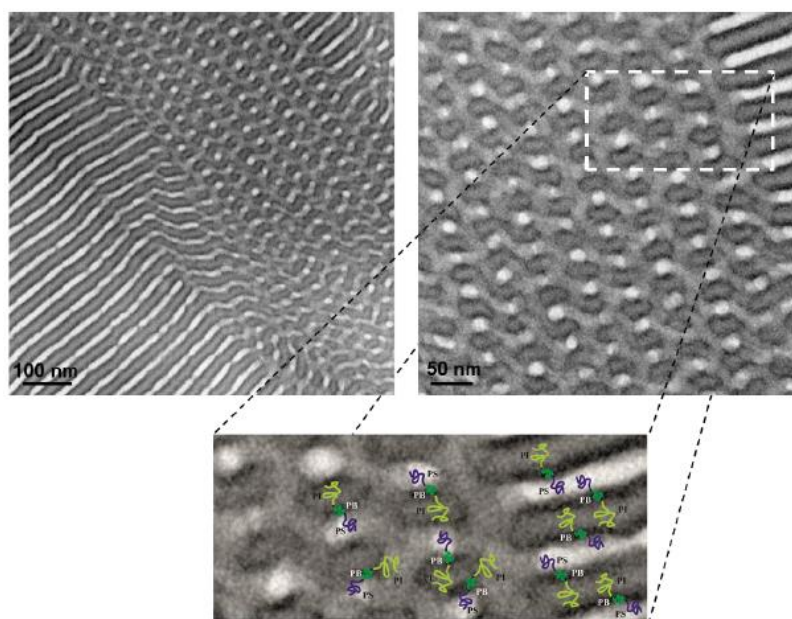


Figure 3.14: Bright field TEM images exhibiting grains with coexistence of a 2-fold projection for a core-shell double gyroid with three-phase four-layer lamellae domains where PS is the core, PB is surrounding the core of the networks and PI is the matrix.¹³⁶

3.4 Polymer Rheology

3.4.1 Introduction

Rheology is defined as the science of flow and deformations of materials resulting from an applied stress.¹³⁷ The foundations of rheology are associated with the terms of elasticity and viscosity. Polymers exhibit non-Newtonian behavior in the melt state, which is attributed to both elastic effects and shear-rate-dependent viscosity leading to time and rate effects during polymer processing. Elastomers are materials which are capable of undergoing large reversible extensions and compressions. As already mentioned in Chapter 1 of this thesis, elastomers are a category of polymers with viscoelasticity (having both viscosity and elasticity) and very weak inter-molecular interactions, which exhibit low Young's modulus and high failure strain when compared with other materials.

Long chain branching (LCB) is a very important feature in polymer science, due to its influence on the rheological properties of polymers. For polymer melts used in commercial applications, large differences in the processability and rheological behavior have been noticed between LCB polymers and linear ones.

3.4.2 Basic Concepts

3.4.2.1 Viscoelasticity

An introduction to viscoelasticity is given by Larson¹³⁸ and Rohn¹³⁹, where the origins of viscoelastic behavior are derived from Hooke's and Newton's Laws. The spring and dashpot model¹⁴⁰ combines the solid and liquid behavior from the two classic models into a system that exhibits solid and liquid like behavior. In simple deformations, the shear stress, σ (N/m²), is given by the shear force applied to the sample per unit area of the surface as shown in the following equation:

$$\sigma = \frac{F}{A} \quad (3.11)$$

Deformation of a solid is measured by the shear strain, γ and the deformation rate is specified by the shear rate derivative with respect to time, $\dot{\gamma}$. The shear viscosity may then be defined as:

$$\eta = \frac{\sigma}{\dot{\gamma}} \quad (3.12)$$

Hooke's Law accurately describes behavior of solids, where the tensile stress in extension is directly proportional to the strain and for simple cases shear can be derived from the equation:

$$\sigma = G \cdot \gamma \quad (3.13)$$

where G is the shear modulus. For fluids, Newton's Law of viscosity accurately predicts that the force is directly proportional to the rate of strain:

$$\sigma(t) = \eta \cdot \dot{\gamma}(t) \quad (3.14)$$

In viscoelastic materials the loading time of the substance is critical, the material behaves as a solid for rapid loading and as a liquid for slow loading. For a solid obeying Hooke's law, when shear strain γ_0 is applied, the stress would be constant. For a liquid, the stress would be zero since the strain rate is zero. Viscoelastic materials would show a stress value that decreases with time until it reaches equilibrium. A small strain applied to the material may result in a linear response, called the shear stress relaxation modulus $G(t)$ which is calculated by the equation

$$G(t) = \frac{\sigma(t)}{\gamma_0} \quad (3.15)$$

When the strain and strain rates are small enough, so that the molecules are not disturbed far away from their equilibrium state, the relaxation modulus is independent from the specific strain or strain rate. This behavior is called linear viscoelasticity.

3.4.2.2 Storage and Loss Moduli

Small amplitude oscillatory shear (SAOS) is a method for determining the dynamics of viscoelastic systems.^{138,139} The in-phase and the out-of-phase components of the shear stress are measured as a function of frequency, ω (rad s^{-1}) as described in the following equation:

$$\gamma(t) = \gamma_0 \sin \omega t \Rightarrow \frac{\sigma(t)}{\gamma_0} = G'(\omega) \sin \omega t + G''(\omega) \cos \omega t \quad (3.16)$$

where G' expresses the dynamic storage modulus and G'' the dynamic loss modulus, γ_0 is the strain amplitude and is normally kept low (< 1) to ensure that linear response for the material is achieved, leading therefore to valid relaxation times being recorded in equilibrium. The response is of a sinusoidal nature due to the origin of the applied stress. The storage modulus represents the storage of elastic energy, while the loss term comes from the loss of the energy due to the viscosity of the material. The ratio of the loss to the storage modulus (G''/G') is called the loss tangent ($\tan \delta$) and is high (>1) for liquid like materials and low (< 1) for solid like materials. Figure 3.15 shows the G' and G'' mastercurve for a polymer melt dynamic experiment.

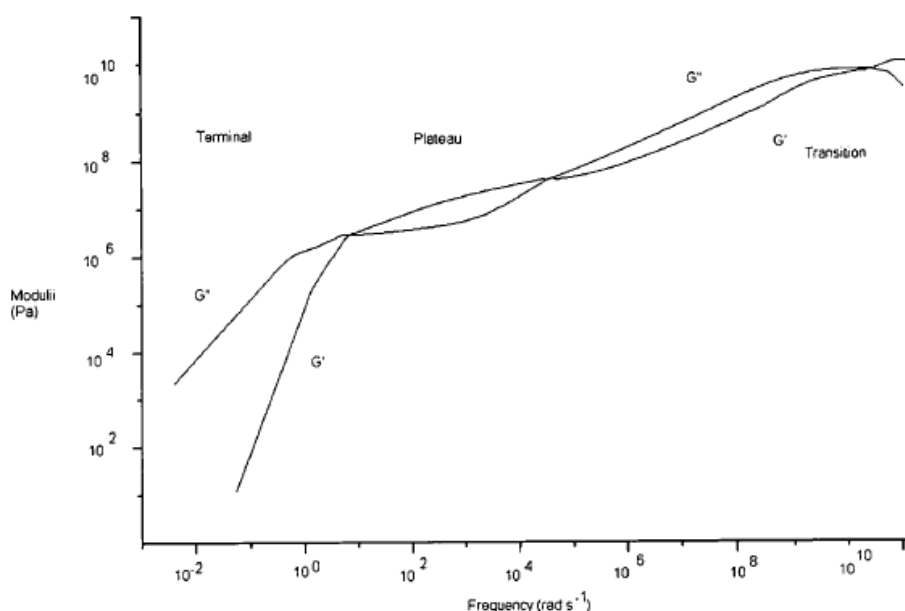


Figure 3.15: Small amplitude oscillatory shear measurements of a high molecular weight polymer melt.¹³⁸

The lower frequencies shown in Figure 3.15, in which G'' is larger than G' , indicate where the viscous (liquid-like) properties of the melt are observed. Increasing the frequency

causes G'' and G' to cross and the response from the material enters the plateau region. The plateau region is where factors such as chain entanglements and other complex mechanisms occur, where G' is larger than G'' . At higher frequencies G'' crosses G' as the diagram enters the transition zone, where the response to the strain from the solid glassy like is observed. In the plateau region where the liquid like behavior becomes more solid like in appearance (viscoelastic region), the moduli crossover can be used as a reference point. This happens since ω_c corresponds to the value of the inverse of characteristic relaxation time τ , hence $\tau \sim \omega_c^{-1}$, which can be a useful guide for material properties. At the $G' = G''$ crossover the characteristic modulus G may be defined, as the modulus at the crossover point. The zero shear viscosity can then be estimated from the data, by multiplying the relaxation time τ , and the characteristic modulus G through the following equation

$$\eta_0 \approx G\tau \quad (3.17)$$

3.4.2.3 Non-Linear Viscoelasticity

The above concepts correspond in the case for the behavior of fluids in the linear regime, where small and slow deformations allow the material to return back to its equilibrium state. However, this is not the case when dealing with large deformations, where the chains are displaced significantly from their equilibrium conformations. Furthermore, the relaxation modulus $G(t)$ is no longer independent of the strain since the following equation is now prominent:

$$\sigma(t, \gamma) = \gamma \cdot G(t, \gamma) \quad (3.18)$$

However, for many polymeric liquids, stress relaxation following a sudden imposition of shear is depending on strain-dependent and time-dependent functions as it is evident in equation 3.19:

$$\sigma(t, \gamma) = \gamma \cdot h(\gamma)G(t) \quad (3.19)$$

where $h(\gamma)$ is known as the dumping function. This is not normally observed at all times following step strain.¹⁴¹

3.4.3 Rheology of Linear and Branched Polymers

Rheological behavior of polymeric materials is an important aspect of physical properties. The most well-known theoretical report in the past three decades is the reptation-tube theory by de Gennes-Doi-Edwards¹⁴² for polymer dynamics and rheology.^{143,144} It is the first molecular theory that can be used to evaluate most dynamical properties of entangled linear polymers including nonlinear behavior. On the contrary, it has not provided any reliable predictions concerning the nonlinear responses of linear polymers to sudden external

deformation. Very recently studies by Wang's group have settled serious questions on the reptation-tube model, concerning whether the discovered shear inhomogeneity during start-up shear¹⁴⁵⁻¹⁴⁷ is a steady-state property of entangled polymers under fast shear.

A lot of research groups have been looking continuously for new ways to improve the various properties of different polymers. Long chain branching (LCB) is the most important parameter to control the dynamic behavior of a polymer without significant changes in specific characteristics such as the glass transition temperature, crystallization temperature and other thermodynamic properties including its compatibility with other polymers. Anionic polymerization methods have allowed rubber polymers such as poly(butadienes) and styrene-butadiene copolymers to be synthesized with controlled chain architectures.^{16,18,69,148}

The best known polymer containing LCB is low density polyethylene (LDPE) whose dynamic properties have been extensively studied in the literature.¹⁴⁹⁻¹⁵² Due to the significant amount of LCB in LDPE, better resistance to localized yielding in uniaxial extension is evident in LDPE when compared to high density PE (HDPE) whereas the shear deformation behavior is plagued with the potential complication of interfacial failure. Comparing to HDPE, LDPE can be stretched to a thinner dimension, which causes the true stress (i.e., the tensile force divided by the shrinking cross-sectional area) to rise with increasing extension even after yielding has occurred. The transient viscosity rises above the values reported in the zero-rate limit. Many scientists involved with rheology characterized this behavior "strain hardening" and believed that the observed difference between shear and extensional behaviors, i.e. "softening shear yet hardening in extension", is rooted in the presence of LCB in LDPE.¹⁵³

McLeish studied¹⁵⁴⁻¹⁵⁶ linear and some nonlinear dynamic properties of model LCB polymers such as H-shaped architectures. The main constraint on the flow of the molecule is the branch points between the polymer chains, which may in some cases be considered as two 3 armed stars, for which the flow properties are relatively well understood. The model is mainly based on Rouse type theories with additional constraints, notably however that reptation is not the main relaxation process due to the linking of the polymer branch points and the constraints on the entanglements. Frequency-dependent rheological data on a series of poly(isoprene) H-polymers are in good agreement with the tube model theory that combines path-length fluctuation (like that of star polymer melts) at high frequency, with reptation of the self-entangled "cross-bars" at low frequencies (like that of linear polymer melts) (Figure 3.16).

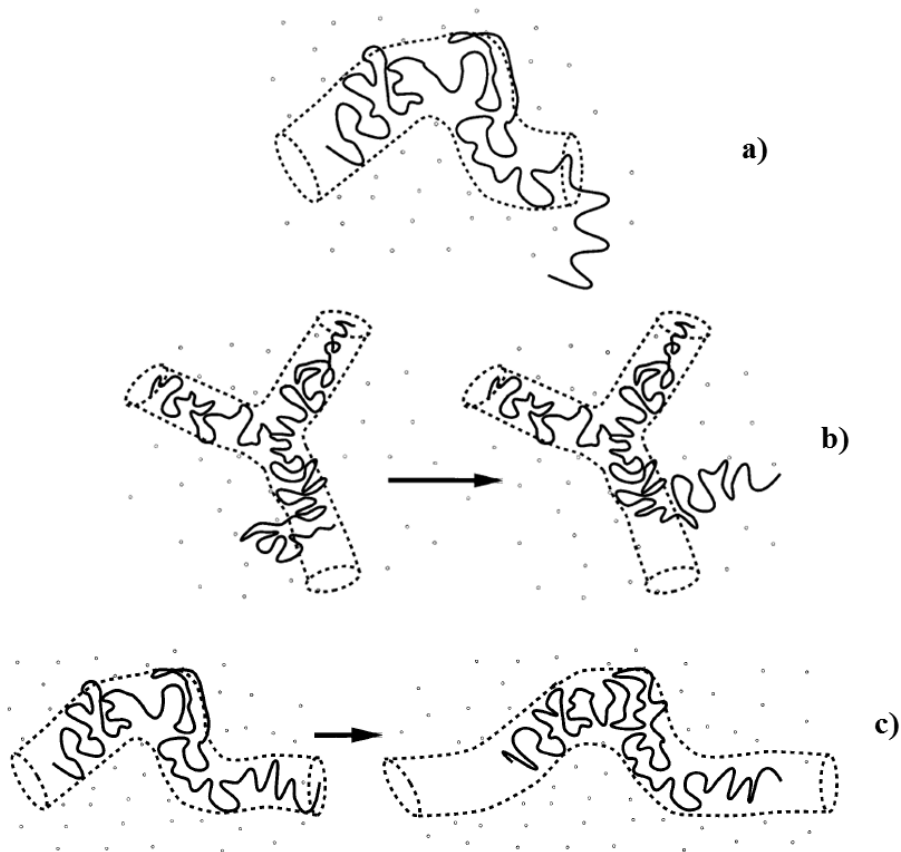


Figure 3.16: Schematic presentation of the processes of a) reptation, b) arm retraction via fluctuations for stress relaxation in linear and branched polymers, respectively and c) retraction of chain in an extending tube in a nonlinear flow.¹⁵⁵

Extensive observations of strain localization upon startup or after stepwise shear and a conceptual framework for nonlinear rheology of entangled polymers appears to have emerged leading to the discovery of new considerations, which were not previously predicted by the standard tube model.¹⁵⁷ Therefore, the field of nonlinear rheology of entangled polymers is a crucial area in which further experimental and theoretical studies are needed.

CHAPTER 4

Experimental Section

For this thesis a series of linear homopolymers of PI-3,4 (55-65% of -3,4 microstructure) or PI_{3,4} with low and high molecular weights, non-linear H-type PI_{3,4} homopolymers, linear diblock copolymers of the PB-b-PI_{3,4} type [PB: poly(butadiene) with ~90-92% -1,4] and asymmetric star polymers of PB(PI_{3,4})₂ and PB(PI_{3,4})₃ types were synthesized. In order to achieve well-defined homopolymers and copolymers with narrow molecular weight distributions it was necessary to adopt anionic polymerization, high vacuum techniques, well-known purifying procedures for all reagents and solvents as well as chlorosilane chemistry.^{28,83}

4.1 High Vacuum Technique

High vacuum technique is very important and plays a significant role for the successful synthesis of all homo- and co-polymers prepared in this thesis and is used in order to remove impurities such as oxygen, carbon dioxide and moisture from all reagents involved in the polymerization process. These impurities, during the polymerization, can react rapidly with the initiator or the living anionic sites, according to the following reactions (Figure 4.1), leading to undesirable termination or/and transfer reactions.

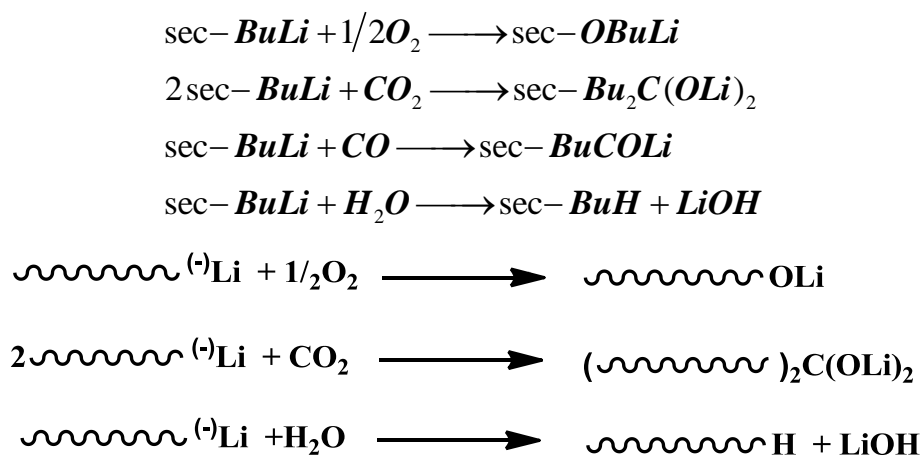


Figure 4.1: Termination reactions of the initiator *sec*-BuLi and the living macroanions with O₂, CO₂ and H₂O.

High vacuum is accomplished through a high vacuum line which is constructed from Pyrex glass and mounted onto a stainless steel frame (Figure 4.2). The main parts of a high vacuum line are: the oil pump (A), the mercury diffusion pump (B), the liquid nitrogen trap (C), the upper (D) and lower (E) glass tube rigs and the stopcocks. The length of a high vacuum line is approximately 2.0-2.5 meters, since it is difficult to work if the vacuum ports are spaced more than 30 cm apart especially when dealing with non-volatile reagents and distillation from one port to another is difficult or even impossible.

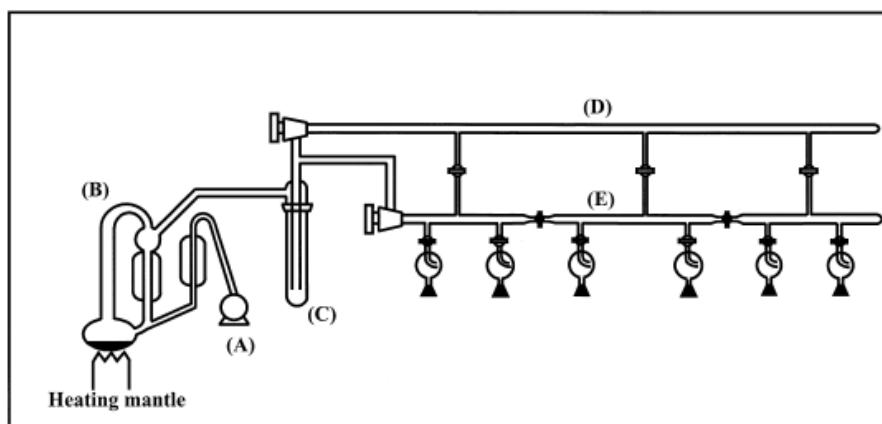


Figure 4.2: Schematic presentation of a high vacuum line.

The oil pump is used in order to reduce the pressure in the system at approximately 10^{-2} mm Hg, where the mercury inside the diffusion pump starts to evaporate by heating through a heating mantle. After mercury distillation is achieved the mercury diffusion pump can bring the pressure to a value of approximately 10^{-6} mm Hg. The operation of the diffusion pump is based on the diffusion of mercury vapors through a very narrow section (Figure 4.3) which creates an increase in the speed of mercury molecules and therefore sub-pressure according to Bernoulli's law, leading to high vacuum ($\sim 10^{-6}$ mm Hg). During the contact of mercury with the condenser walls, it condenses and returns back in the heated part of the diffusion pump where the procedure is repeated. A liquid nitrogen trap is used to condense any volatile compounds incorporated in the system and in order to protect the oil and the diffusion pump from contamination. The diffusion pump is connected through glass tubes (Pyrex) with the main part of the high vacuum line. The upper rig is separated from the lower one by high vacuum Teflon stopcocks and is used to connect the parts of the lower rig to the vacuum separately. By this way it is possible to use the parts of the lower rig to perform different procedures (e.g. distillations, degassing) at the same time. The high vacuum stopcocks are constructed by a Pyrex glass frame and a Teflon piston. Reactors and other glass apparatuses are attached to the vacuum line through the lower rig via high vacuum 'o' ring stopcocks and ground joints. The use of high vacuum grease is necessary in order to avoid friction between ground joints and apparatuses, since both are constructed from Pyrex glass and to make use of vacuum seal joints to all the flasks and apparatuses that are attached to the vacuum line without any introduction of environmental impurities.

A Tesla coil is a very useful and convenient tool, in order to check the level of the vacuum in the vacuum line and verify the absence of any pinholes in any apparatus used for purification and/or polymerization. When the vacuum line is properly evacuated, the sound of the Tesla coil becomes silent when it is attached next to the glass. In contrast, the Tesla coil is very noisy when pinholes are evident in an apparatus or volatile compounds are still present

in the vacuum line. The noise is gradually confined after a few minutes indicating high vacuum in the line and the apparatus involved during degassing.

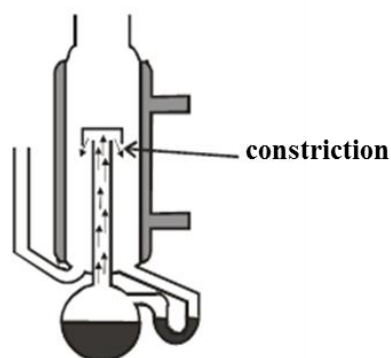


Figure 4.3: Schematic of a diffusion pump. The liquid indicated in the flask with dark grey color corresponds to the mercury.

The most commonly used fluids inside the diffusion pump are silicone oil and mercury (Hg). In our case mercury diffusion pumps were used due to Hg properties, therefore a stream of its vapor has a large momentum which is desirable in such an application for creating high vacuum conditions, however, as it is well known, Hg is extremely dangerous and hazardous. Silicone-oil diffusion pumps are as well affective and can be considered less unsafe. Furthermore, turbo molecular pumps are also used instead of a combination of oil and diffusion pumps, but they are easily contaminated with volatile reagents (solvents, monomers, chlorosilanes) which are commonly used in anionic polymerization, leading to fast and cost-effective damage of such pumps since they are more expensive when compared to the diffusion pumps.

It is important to mention that the vacuum line must be kept clean from any reagent otherwise in most cases its efficiency is compromised. The oil in the mechanical pump should be often changed and some parts of the lower rigs on the vacuum line should be replaced or cut-off when contaminated and should be cleaned with solvents and/or hydrofluoric acid 1M. In order to avoid contamination of various vacuum line parts it is suggested to use short-path distillation apparatuses which are constructed by glass blowing of Pyrex glass flasks and tubes. Finally, special safety precautions must be taken into account while working on the high vacuum line (safety glasses, lab robe, working together with other people familiar with the vacuum line functionality), as well as great care must be given during its use when specific reactions are taking place involving hazardous, flammable and volatile reagents.

All polymerization reactors, dilution apparatuses and ampules are constructed from Pyrex glass flasks and tubes, so it is necessary and important to know glass-blowing. In addition to outstanding resistance in heat and thermal shocks, Pyrex glasses are known for their chemical durability and low coefficients of thermal expansion.¹⁵⁸ Scientific glassblowing

is one of the most basic skills that a scientist has to develop in order to respond efficiently to anionic polymerization requirements. For the introduction of reagents under vacuum conditions into the main reactor, break-seals are used. They are constructed with a thin glass tip, which is easily ruptured with a cylindrical magnet encapsulated in a Pyrex glass tube (Figure 4.4 left). In order to remove an apparatus or an ampule from the vacuum line, constrictions are used, which are heat sealed by a torch (Figure 4.4 right).

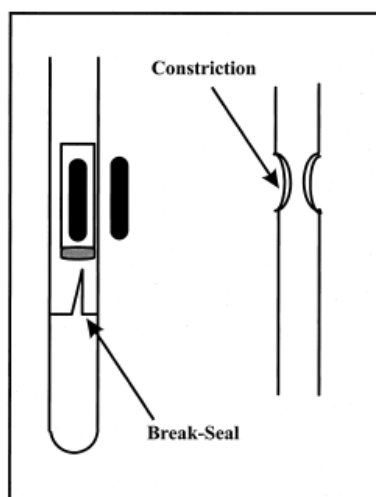
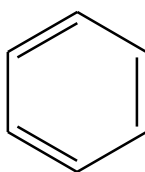


Figure 4.4: Schematic representation of breaker with break-seal (left) and a constriction prior the heat sealing (right).

4.2 Solvent Purification

Benzene, Ben (C₆H₆)



Commercially available benzene is usually free of thiophenes and substituted phenyl-derivatives such as toluene and vinyl compounds. Nevertheless, if some of the above exist in benzene as purchased, then it is necessary to purify it by stirring over concentrated sulfuric acid (H₂SO₄) for a week in a conical flask inside a hood and then washed with an aqueous solution of NaOH. Furthermore, a round bottom flask which contains the appropriate amount of benzene, finely grounded calcium hydride (CaH₂) and a magnetic stirrer is attached to the vacuum line where it is degassed in order to remove CO, CO₂ and O₂ and left under stirring overnight. Calcium hydride is the most commonly used drying agent since it reacts sufficiently with moisture (Figure 4.5). The next day, the solvent is degassed for at least two times and it is distilled in a calibrated cylinder containing *n*-BuLi and styrene in approximately 7:1 ratio, which simultaneously react under vacuum creating PS⁽⁻⁾Li⁽⁺⁾ living

ends. $\text{PS}^{(-)}\text{Li}^{(+)}$ gives to benzene a characteristic orange-red color which is a purity indication for the solvent (Figure 4.6). Various quantities of the purified benzene are distilled into the polymerization reactor or initiator dilution apparatus or even into other type of apparatuses when necessary.

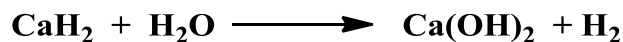
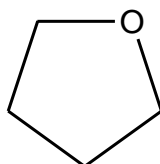


Figure 4.5: Reaction of CaH_2 with moisture.



Figure 4.6: Picture of a cylinder with (polystyryl)lithium living ends in benzene attached to the vacuum line, indicating the high purity of the solvent due to the orange-red color observed.

Tetrahydrofuran, THF ($\text{C}_4\text{H}_8\text{O}$)



A more complex procedure from that used for benzene is followed for the purification of tetrahydrofuran. Initially, the solvent is left under reflux for at least three hours in the presence of Na small pieces and then it is collected in a round flask which contains finely grounded calcium hydride (CaH_2). The flask is attached to the vacuum line where is degassed and left under stirring overnight. The next day, THF is degassed at least three times, distilled to a flask containing sodium/potassium (Na/K) reactive alloy in a 1:3 ratio and stirred rapidly. The formation of a bright blue color is the indication of the solvent's purity (Figure 4.7), due to the free movement of electrons between potassium, leading to the conclusion that major unwanted impurities have been eliminated.

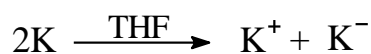




Figure 4.7: Picture of the flask with THF in Na/K alloy attached on the vacuum line. The observation of blue color indicates high purity for the specific solvent.

Methanol, MeOH (CH₃OH)



Methanol is transferred in a round bottom flask containing fresh finely grounded CaH₂, attached in the vacuum line, degassed and left under stirring overnight, for reaction of moisture with CaH₂. The following day is degassed again 3-4 times and distilled in small quantities (~ 1mL) into the necessary ampoules (Figure 4.8).

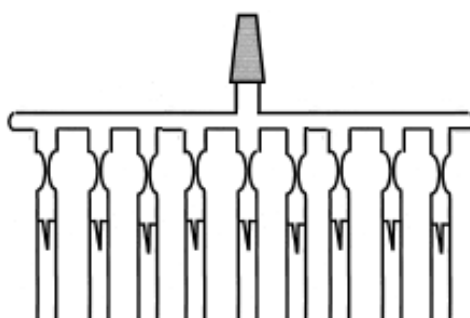


Figure 4.8: Apparatus for the distillation of purified methanol into ampoules.

Methanol is used as a termination reagent for anionic polymerization due to the following reaction (Figure 4.9):

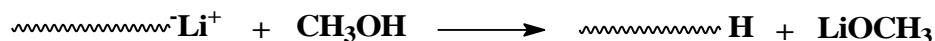
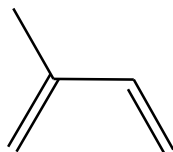


Figure 4.9: Termination reaction of macroanions with methanol.

4.3 Monomer Purification

Isoprene (2-Methyl-1,3-Butadiene), Is (C₅H₈)



Initially, proper amount of as commercially received isoprene (or 2-methyl-1,3-butadiene) is transferred in a round bottom flask containing fresh finely grounded CaH₂, attached on the vacuum line, degassed and left under stirring, for the reaction of even traces of moisture with CaH₂, overnight. The next day, isoprene is degassed twice and distilled into a new flask which contains proper amount of *n*-butyl lithium (*n*-BuLi) in hexane (commercially available) and is left under stirring for approximately thirty minutes (30') at ~ 0°C. *n*-BuLi is an initiator for isoprene at room temperature, so it is necessary to lower the temperature to 0°C, in order to prevent the polymerization of the monomer and was left to react with impurities. This procedure is repeated again in a new flask and then pure isoprene is distilled in pre-calibrated ampoules equipped with break-seals. It should be noted that between the distillations of isoprene in the flasks which contained *n*-BuLi, several degasses took place. Afterwards, the ampoules with the purified isoprene are stored at -20°C and it must be used for polymerization within one month.

1,3-Butadiene, Bd (C₄H₆)



For the purification of 1,3-butadiene, *n*-BuLi is also used for the removal of impurities as already reported for Is. Initially, a stainless steel cylinder containing 1,3-butadiene, which is a gas at room temperature (b.p.: -4°C), is attached to the vacuum line and then the desirable quantity of the monomer is condensed in a pre-calibrated cylinder that contains *n*-BuLi at -78°C [Figure 4.10, (A)], using a liquid nitrogen/isopropanol bath. The monomer is stirred for 30' at -10°C (ice/salt bath) and then is distilled into another flask [Figure 4.10, (B)], which also contains *n*-BuLi and again is left under stirring for 30'. Finally, the pure monomer is distilled in a calibrated ampule, already attached on the polymerization apparatus. Polymerization of 1,3-butadiene must be performed immediately after the apparatus is sealed off from the vacuum line.

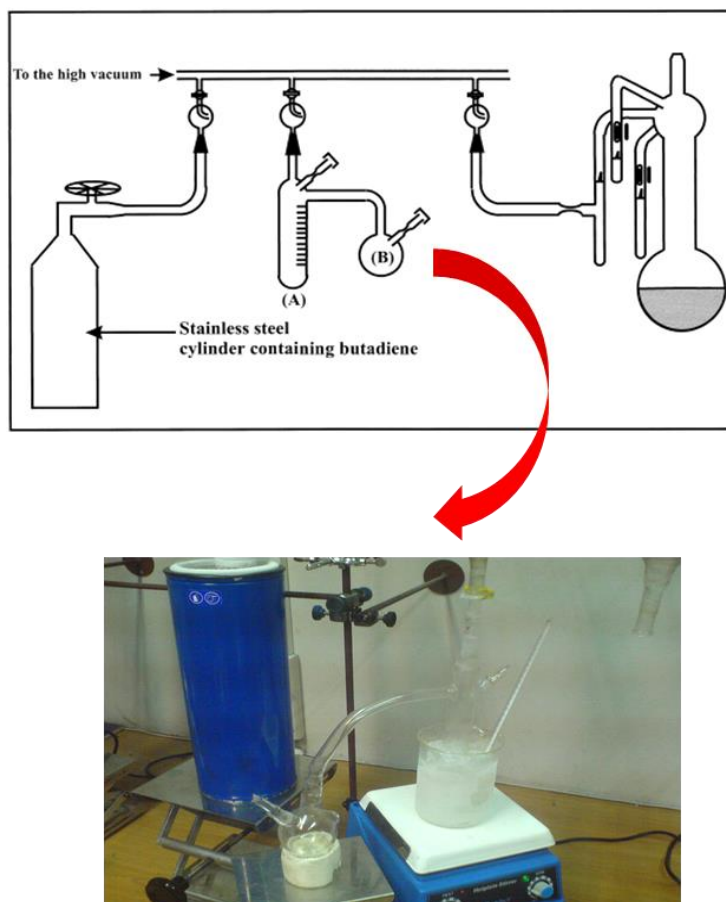
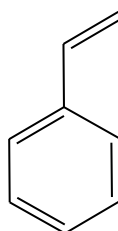


Figure 4.10: Purification procedure of 1,3-butadiene and distillation to the ampule prior to polymerization.

Styrene, St (C₈H₈)



Proper amount of styrene as commercially received is transferred in a round bottom flask containing fresh finely grounded CaH₂, which is attached on the vacuum line through a short path distillation apparatus [Figure 4.11, (A)]. It is degassed once and stirred overnight in order for the CaH₂ to react with any traces of moisture. Then it is degassed again twice and distilled in a new round bottom flask containing an appropriate amount of dibutylmagnesium (Bu₂Mg) in heptane ([monomer]/[Bu₂Mg] = 25/1) which has been introduced via a pyrex attachment through an elastic septum. Styrene is left to react with Bu₂Mg for at least 3 hours over stirring at low temperature (0⁰C-10⁰C), it is degassed once more and it is finally distilled in calibrated ampoules [Figure 4.11, (B)] and is kept at -20⁰C. The compound Bu₂Mg for the final purification step is preferred due to its higher solubility in hydrocarbon solvents. It is

also important to mention that styrene should not remain in the Bu_2Mg solution more than 3 hours, since the specific purifying reagent is an organometallic compound and initiates the polymerization of styrene (low initiation rate and decreases further at temperatures below ambient conditions).

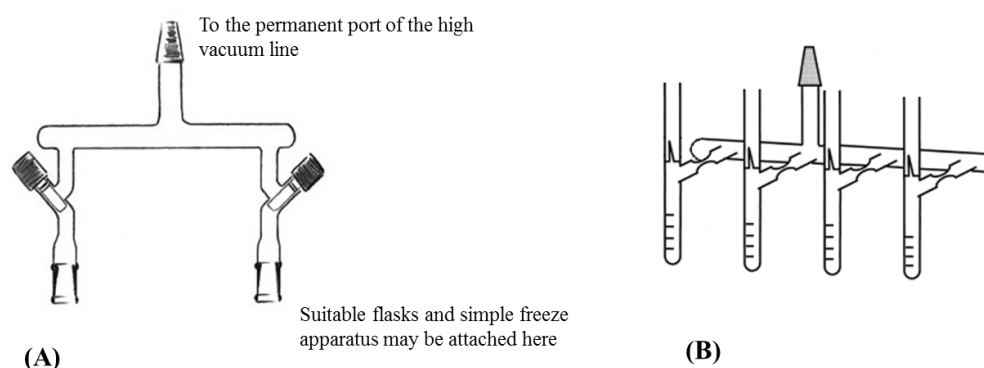


Figure 4.11: (A): Short-path apparatus used for the purification of styrene⁸³ and (B): apparatus of calibrated ampules for distillation of purified styrene.

Preparation of St End-Capping Solution

Styrene was used as a coupling agent (St end-capping) of living $\text{PB}^{(-)}\text{Li}^{(+)}$, prior to the reaction with the suitable chlorosilane, as it will be described below. For the preparation of St end-capping solution, an ampule of purified styrene is attached on an apparatus with calibrated ampules and after high vacuum is achieved, a proper amount of benzene is distilled. The mixture is degassed and the apparatus is heat-sealed from the vacuum line. Afterwards, the break-seal of the styrene ampule is ruptured and mixed with the benzene in order to create a homogeneous solution of styrene exhibiting very low concentration in order to be used for end-capping of the $\text{PB}^{(-)}\text{Li}^{(+)}$ and control the coupling reactions accordingly.

4.4 Dilution of the Initiator *sec*-Butyllithium (*sec*-BuLi)

For the synthesis of the homopolymers, linear diblock copolymers and the initial precursors for star copolymers, *sec*-BuLi is used as the initiator of the polymerization. This organometallic compound is very reactive, especially with air components such as CO_2 , O_2 and H_2O as it was indicated with specific reaction in a prior section of this chapter. These undesirable reagents can lead to deactivation of the initiator, and therefore, uncontrolled polymerization might take place leading to non-model polymers, as well as to increased molecular weights and molecular weight distributions. The initiator *sec*-BuLi, as commercially received, is in high concentration (1.4M in hexane or cyclohexane solution) and a dilute solution is needed in order to be used sufficiently for the required experiments. The dilution of the initiator is accomplished in a suitable apparatus with pre-calibrated ampules as shown in Figure 4.12.

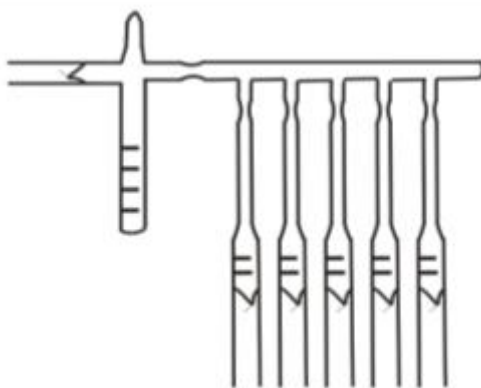


Figure 4.12: Schematic of the apparatus used for the dilution of *sec*-BuLi with benzene. The same apparatus is also used for *St* end-capping.

Initially, the apparatus is connected through a ground joint to the vacuum line in order to achieve high vacuum. An amount of *sec*-BuLi (1.4M) is injected into the apparatus through a proper elastic septum and the hexane of the solution is removed. Then, the appropriate amount of benzene is distilled, the mixture is degassed and the apparatus is removed from the vacuum line through sealing-off the appropriate constriction. The amount of benzene needed for the desirable concentration is calculated through the following equation:

$$C_1V_1 = C_2V_2 \quad (4.1)$$

where C_1 is the initial concentration of *sec*-BuLi (usually 1.4M), V_1 the initial volume in mL of *sec*-BuLi injected in the apparatus, C_2 the final concentration needed and V_2 the appropriate volume in mL of benzene in order to achieve the desired concentration.

The procedure that was described above refers to dilute solutions of initiator *sec*-BuLi with concentrations approximately equal or higher to 0.1 mol/L (0.1 mmol/mL). If the desired concentration of the initiator is lower, in order to synthesize polymers with high molecular weights, then a different and more complicated procedure should be followed.

Initially, an apparatus, as exhibited in Figure 4.13 must be constructed through scientific glass blowing, where A corresponds to the ampule of the concentrated *sec*-BuLi solution. The apparatus is connected to the vacuum line through ground joint B. Degassing is carried out until high vacuum is achieved and afterwards a small amount of the purging agent (2-3 mL), namely *n*-BuLi solution in 1.6 M in hexane, is introduced through the elastic septum C, by a glass syringe. After the removal of hexane (solvent of the *n*-BuLi solution) the constriction D is heat-sealed and the required amount of benzene is distilled through the vacuum line into flask E, followed by degassing of the solution by freeze drying with liquid nitrogen and the reactor is heat sealed in constriction F and removed from the vacuum line. Furthermore, the apparatus is washed with the *n*-BuLi solution and then it is rinsed thoroughly, by condensing benzene through freezing with liquid N₂ the Pyrex parts of the

apparatus. Finally, the benzene is distilled from flask E into the calibrated cylinder G and the purge section is heat-sealed at constriction H. The break-seal A is ruptured and the concentrated *sec*-BuLi solution is allowed to drain into the cylinder which already contains the additional amount of benzene. Ampule A is rinsed several times with the solution, in order that all quantity of the initiator is transferred into the cylinder and the ampules followed by removal from the apparatus by heat sealing constriction J. The new dilute solution of the initiator is distributed covering all the Pyrex parts of the apparatus and it is stored at -20°C for future use according to the experimental needs.

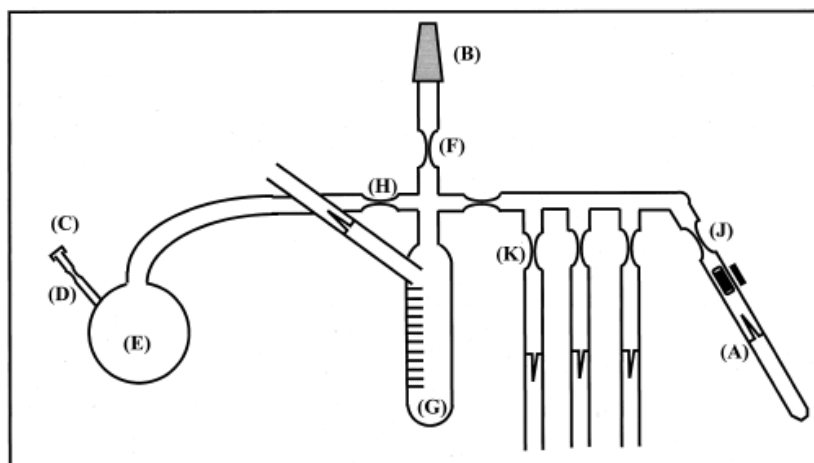


Figure 4.13: Apparatus for the dilution of concentrated *sec*-BuLi with benzene.

4.5 Purification of Linking Agents and Other Reagents

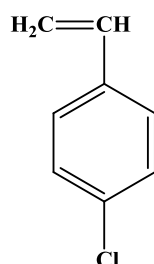
Dichlorodimethylsilane $[(\text{CH}_3)_2\text{SiCl}_2]$ - *Trichloromethylsilane* $(\text{CH}_3)\text{SiCl}_3$ - *Tetrachlorosilane* (SiCl_4)

The linking agents dichlorodimethylsilane, trichloromethylsilane and tetrachlorosilane are purified by adopting exactly the same procedure since all these chlorosilanes are volatile reagents. Initially, appropriate amount of each silane is transferred into a round bottom flask containing fresh finely grounded CaH_2 and a stirrer (Teflon). Then, it is attached on the vacuum line, degassed and left for reaction of moisture with CaH_2 overnight. The next day, the round bottom flask is degassed again at least three times and a small amount is distilled into the whole apparatus with the calibrated ampoules in order for the corresponding silane to react with any possible impurities that may exist in the glass ampule apparatus and to deactivate them. The remaining amount which has already reacted is distilled in the nitrogen trap through the vacuum line. After the completion of this procedure, the proper amount of the indicative silane is distilled into calibrated ampoules and stored at -20°C for future use.

In the case of dichlorodimethylsilane, a dilute solution in benzene was needed in order to be used sufficiently for the required experiments. The procedure adopted for the

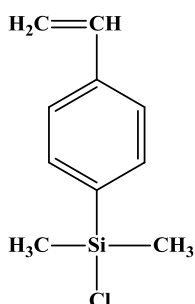
purification of the specific silane, is exactly the same as that described already for St end-capping.

p-Chlorostyrene (C_8H_7Cl)



The *p*-chlorostyrene or 4-chlorostyrene is transferred into a round bottom flask containing fresh finely grounded CaH_2 . Then, it is attached on the vacuum line, degassed and left to react with CaH_2 overnight in order to remove the moisture. The following day, it is degassed additionally 2-3 times, distilled in calibrated ampoules (Figure 4.11, B) and finally stored at $-20^{\circ}C$ until further use.

4.6 Preparation of 4-(Chlorodimethylsilyl)Styrene (CDMSS)



CDMSS was synthesized from purified *p*-chlorostyrene and dichlorodimethylsilane through a Grignard reaction (Figure 4.14), under high vacuum techniques. The magnesium (Mg) used in the Grignard reaction was dried in a vacuum oven at $40^{\circ}C$ for approximately two days in order to completely remove any humidity traces prior to use. A specially designed glass apparatus consisting of a flask, a glass filter and a condenser was used for the preparation of the Grignard reagent (Figure 4.15).

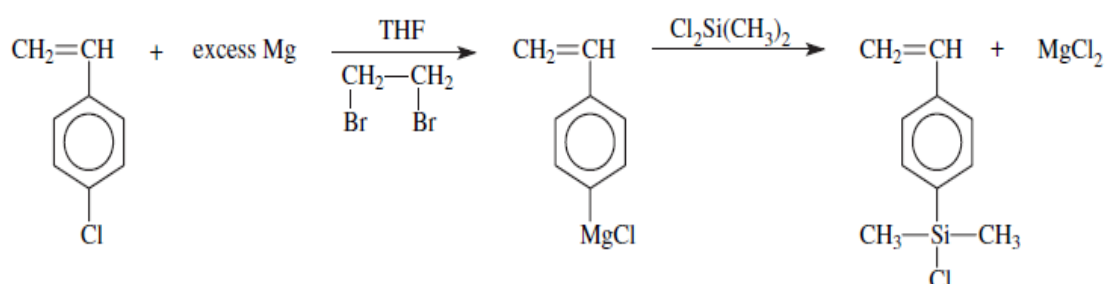


Figure 4.14: Synthesis reaction of 4-(chlorodimethylsilyl)styrene (CDMSS) for 4-chlorostyrene and dichlorodimethylsilane through the Grignard reaction.

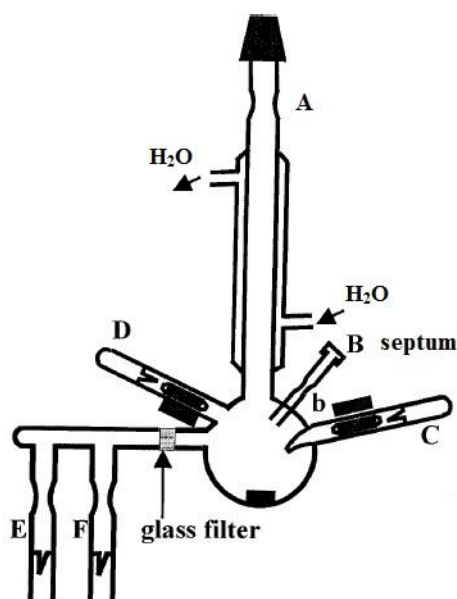


Figure 4.15: Glass apparatus for the preparation of the Grignard reagent.

After introducing magnesium turnings (0.5 g or 20 mmol) through the Pyrex glass tube B, the tube was shut with an elastic septum, the apparatus was attached to the vacuum line through a ground joint, evacuated and sealed-off at B. A solution of a few drops of 1,2-dibromoethane in THF was added from the ampule D to the flask, through breakage of the corresponding break-seal and the mixture was stirred for a few minutes in order to activate the magnesium. Afterwards, the apparatus was evacuated and sealed-off at A. Purified *p*-chlorostyrene was introduced dropwise to the flask after breaking the break-seal of ampule C, while maintaining the reflux of THF by external heating at approximately 50°C. The *p*-chlorostyrene was added in approximately 3 h and the reaction was allowed to proceed for another 2 h. The yield of the reaction is ~ 70%, according to the literature.⁷² The Grignard reagent was filtered through the glass filter to ampoules E and F which are equipped with break-seals. Then, ampule E was attached to another apparatus (Figure 4.16), which was already equipped with ampule G containing dichlorodimethylsilane (2.66 g or 21 mmol) diluted in 10 mL of THF.

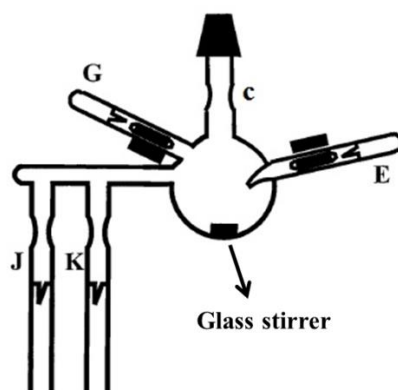


Figure 4.16: Glass apparatus for the preparation of the 4-(chlorodimethylsilyl)styrene reagent.

After evacuating and detaching the apparatus shown in Figure 4.16 from the vacuum line, by sealing off at constriction c, the chlorosilane solution was first introduced to the main flask and by cooling at 0°C, the Grignard reagent was added dropwise in approximately 90 min. The quantity of dichlorodimethylsilane was quite larger than that of the Grignard reagent (~1.5:1 ratio), in order to ensure that the yield of the reaction is high. The produced 4-(chlorodimethylsilyl)styrene or CDMSS was transferred to another apparatus (Figure 4.17) through ampule K, which was sealed-off from the previous apparatus. The new apparatus was evacuated, CDMSS was purified through fractional distillation, diluted with proper amount of benzene, leading to the desirable concentration, and stored at -20°C in ampules equipped with break-seals. The completion of the reaction and the successful synthesis of the required CDMSS were observed via gas chromatography-mass spectroscopy (GC-MS), where no traces of the initial reactants were observed.

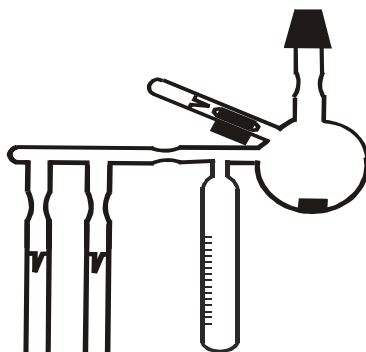


Figure 4.17: Glass apparatus for the purification of CDMSS.

4.7 Synthetic Procedures

The main scope of this thesis was to synthesize and study different architectures of poly(isoprene) (PI) with high 3,4-content (55-65%), including linear and non-linear homopolymers of PI_{3,4}, diblock copolymers of the PB-b-PI_{3,4} type [PB: poly(butadiene) with ~90-92% -1,4] and asymmetric star polymers of PB(PI_{3,4})₂ and PB(PI_{3,4})₃ type respectively.

Initially, synthetic procedures of linear and non-linear homopolymers of PI_{3,4} and H-type PI_{3,4} will be described, using anionic polymerization techniques, 4-(chlorodimethylsilyl)styrene (CDMSS) for the preparation of macromonomers and appropriate combination with chlorosilane chemistry, in order to synthesize the non-linear H-PI_{3,4}. Six (6) samples were synthesized in total: four (4) samples of linear homopolymers of the PI_{3,4} type and two (2) samples of the non-linear H-type PI_{3,4} homopolymers respectively. All samples exhibited very narrow molecular weight polydispersities (PDI < 1.10) and the molecular characterization results through various techniques led to the conclusion that they exhibit chemical and compositional homogeneity, therefore they can be considered model polymers.

Subsequently, synthetic procedures of linear diblock copolymers of the PB-b-PI_{3,4} type and asymmetric star polymers of PB(PI_{3,4})₂ and PB(PI_{3,4})₃ type will be described through anionic polymerization techniques via sequential monomer addition (for the case of the diblock copolymers) and combination again with chlorosilane chemistry via coupling reactions (for the case of the miktoarm star copolymers). Thirteen (13) samples were synthesized: five (5) samples of the PB-b-PI_{3,4} type and eight (8) samples of miktoarm star copolymers of PB(PI_{3,4})₂ and PB(PI_{3,4})₃ types (four samples per sequence) respectively. The results from molecular characterization showed that these samples also exhibit chemical and compositional homogeneity and can be considered as well model polymers.

4.7.1 Synthesis of Homopolymers of the PI_{3,4} Type

The synthesis of linear homopolymers of poly(isoprene) with high -3,4 content (55-65%) was accomplished by the use of anionic polymerization and high vacuum techniques. The main scope of the synthetic route adopted, was to synthesize homopolymers of PI_{3,4} with narrow molecular weight distributions, predictable molecular weights and high 3,4-microstructure. All polymerizations were accomplished by using benzene as solvent, *sec*-BuLi as the initiator and methanol as the termination reagent. In order to obtain the high 3,4-content in all samples, it was essential to use a small amount (~1 mL) of tetrahydrofuran (THF), which alters the aggregation degree of PI from 4-6 in non-polar hydrocarbon solvents to a value of 2 in polar solvents or in their mixtures. The synthetic route that was adopted is shown in Figure 4.18 and the apparatus for the polymerization can be observed in Figure 4.19.

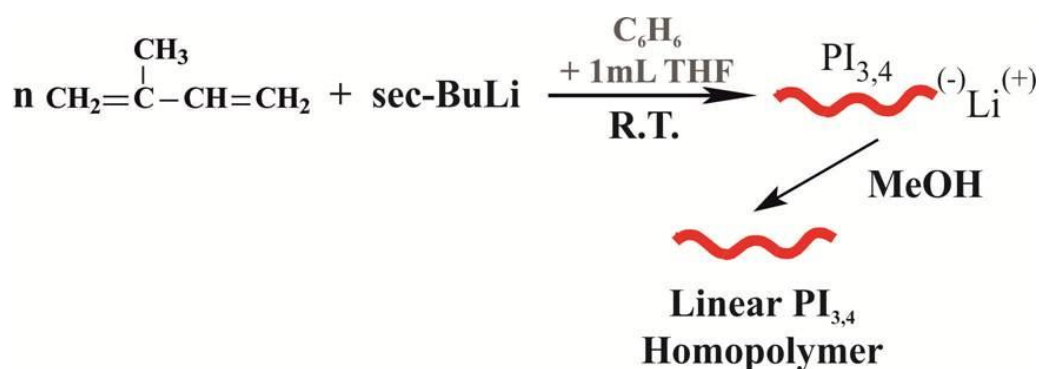


Figure 4.18: Synthetic route for the synthesis of PI_{3,4} homopolymers.

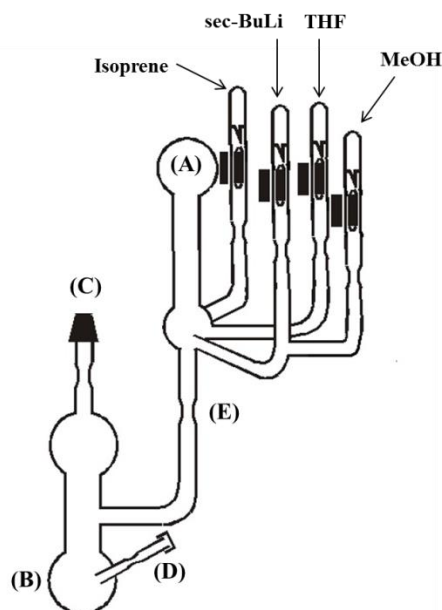


Figure 4.19: Pyrex glass apparatus used for the synthesis of the $PI_{3,4}$ homopolymers.

Initially, the appropriate scientific glass blowing is performed and the ampules of the monomer, the initiator, the small amount of THF and the termination reagent are attached on the apparatus. Then, the apparatus is attached to the vacuum line through a ground joint C, checked for pinholes by use of the Tesla coil and evacuated. It is very important to mention that the flame drying technique, by a hand torch, is very useful at this point in order to accelerate degassing and remove any moisture traces. Flame drying is repeated 2-3 times, until no sound from the Tesla coil is ensured. After completion of the degassing, a small amount (3-4 mL, depending on the solvent volume) of purging agent (*n*-BuLi in hexane) is added via a syringe through the elastic septum D. The elastic septum is rinsed and detached afterwards by sealing-off the constriction and the small amount of hexane is removed to the nitrogen trap through the vacuum line. The appropriate amount of benzene (solvent) is distilled from a purified reservoir, by using liquid nitrogen, into the spherical flask B through the vacuum line and as soon as the mixture is degassed, it is detached from the vacuum line by sealing off the appropriate constriction. The solution of *n*-BuLi and benzene is thawed and transferred 2-3 times to all the inner glass surface of the apparatus very carefully. In this manner, *n*-BuLi reacts with impurities that might exist in the apparatus and were not removed during its purification at ambient conditions. Furthermore, the solution is collected in the purge section flask B which is placed into a warm water bath ($\sim 50^{\circ}\text{C}$) in order to rinse the apparatus by condensation of the solvent. Following this procedure the solvent is collected in the major reactor flask A and poured back into the purge section by carefully tilting the apparatus. Repeating this procedure periodically and approximately 10 times allows the collection of the remaining *n*-BuLi, along with its reaction products with impurities on the surface of the glass, back to the purge section which will be eventually removed and these

impurities will not affect the polymerization reaction. In order to collect the pure solvent in the major reactor the purge section B is immersed in a water bath ($\sim 50^{\circ}\text{C}$) and the reactor flask A in an ice bath ($\sim 0^{\circ}\text{C}$), following a procedure shown in Figure 4.20.

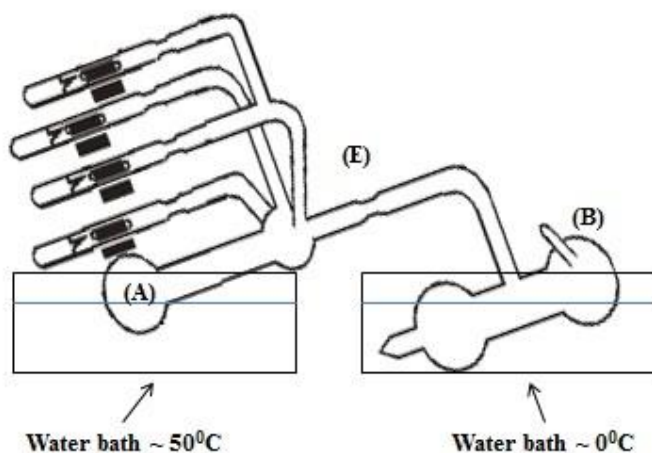


Figure 4.20: Procedure adopted for distilling the pure solvent in the major polymerization flask.

After the complete distillation of the pure solvent, the purge section part B is detached from the apparatus by heat sealing the proper constriction. The final polymerization reactor is shown in Figure 4.21. When the solvent is heated to room temperature, the break seals of the necessary reagents are ruptured through magnets sealed in Pyrex glass (breakers) which are controlled by outside magnetic rods.

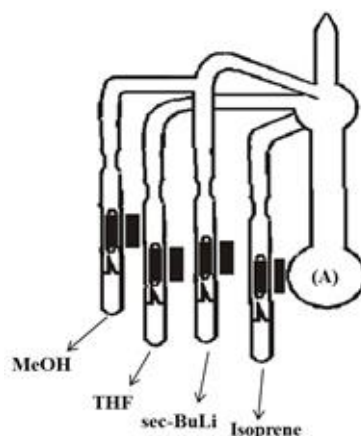


Figure 4.21: The final polymerization reactor for the synthesis of $PI_{3,4}$ homopolymers.

Initially, the break-seal of the ampule containing THF is ruptured and the quantity is allowed for ~ 10 min in order to form a homogeneous solution with benzene. It is known from the literature^{58,60}, that the presence of THF has a marked effect on the microstructure of poly(isoprene), produced with lithium based initiators, and specifically increases the 3,4-content. It is experimentally proven that even a small amount of THF (~ 1 mL) can lead to poly(isoprene) with high 3,4-content (55-60%). The break-seal of the ampule of isoprene is

then ruptured, the quantity of the monomer is distilled into the reactor A, using an ice bath ($\sim 0^{\circ}\text{C}$), the empty ampule of isoprene is heat sealed at the proper constriction and finally *sec*-BuLi is introduced into the reactor in order to initiate the polymerization of isoprene. It is important to mention that the ampule containing the isoprene (high volatile reagent) was always cooled prior the rupture of the break seal in order to minimize surface tension and avoid abrupt movement of the breaker leading to its rupture. As soon as *sec*-BuLi is introduced in the reactor, a bright yellow color is obtained in the solution immediately, indicating the initiation of polymerization. The reaction is left to proceed at least for 24 h or more in room temperature, depending on the targeted molecular weight. By completion of the polymerization, the break-seal of the MeOH ampule is ruptured, the living anions are deactivated and the solution immediately is discolored. The desired homopolymer is precipitated in a large excess of methanol stabilized with a proper antioxidant reagent (Figure 4.22) and the obtained homopolymer is dried under vacuum for at least 24 h in a drying oven set at 50°C .

According to the method previously described, four (4) $\text{PI}_{3,4}$ homopolymers were synthesized with various molecular weights, ranging from 10,000-400,000 g/mol. The quantity of the polymer in each case was at least 10 g in order to be enough for all the characterization studies and rheology experiments carried out in this thesis. The amount of benzene used for the polymerization reactions varied from 200-250 mL (for the lower molecular weights) up to 600-700 mL (for the higher molecular weights) respectively. In all cases the solutions concentrations was kept low and always lower than 5% w/v. The calculations for the required quantities of isoprene and *sec*-BuLi were based on the following equations (4.2 and 4.3):

$$\overline{M}_n = \frac{g_{\text{monomer}}}{\text{moles}_{\text{initiator}}} \quad (4.2)$$

$$C_{\text{sec-BuLi}} = \frac{n}{V} \quad (4.3)$$



Figure 4.22: Image of precipitated $\text{PI}_{3,4}$ in a large excess of methanol.

4.7.2 Synthesis of H-type $PI_{3,4}$ Homopolymers

For the synthesis of the H-type $PI_{3,4}$ homopolymers, the first step was to synthesize poly(isoprene) living chains with high 3,4-content with the aforementioned procedure. The solution of the living $PI_{3,4}^{(-)}Li^{(+)}$ was divided stoichiometrically to two flasks. The living ends in one of the flasks were end-capped with a few styrenic monomeric units (St end-capping) and were introduced via a titration reaction into an appropriately prepared CDMSS solution [4-(chlorodimethylsilyl)-styrene/benzene] with a molar ratio of $PI_{3,4}^{(-)}Li^{(+)}$:CDMSS equal to 1:1, in order to form a macromonomer, through the substitution of a chlorine atom by the living ends. Then, the solution of the macromonomer is introduced again via titration into the other flask, containing an excess (~5-10%) of living $PI_{3,4}^{(-)}Li^{(+)}$ chains, in order to form a macroinitiator, through the addition of the living ends to the vinyl bond of the macromonomer. Finally, specific quantity of isoprene is added and followed by polymerization in order to synthesize a 3-arm star homopolymer of the $[(PI_{3,4})_2(PI'_{3,4})]$ type which corresponds to the half molecule of the desirable H-type $PI_{3,4}$ homopolymer. In order to prepare the desired H-type homopolymer dichlorodimethylsilane $[(CH_3)_2SiCl_2]$ diluted in benzene to a desirable concentration is added and approximately in one month the linking reaction is completed. All the reactions were handled in room temperature and small aliquots were taken during all the steps of the synthetic route, in order to monitor the synthetic procedure. The synthetic route adopted for the preparation of the H-type $PI_{3,4}$ homopolymers is shown in Figure 4.23.

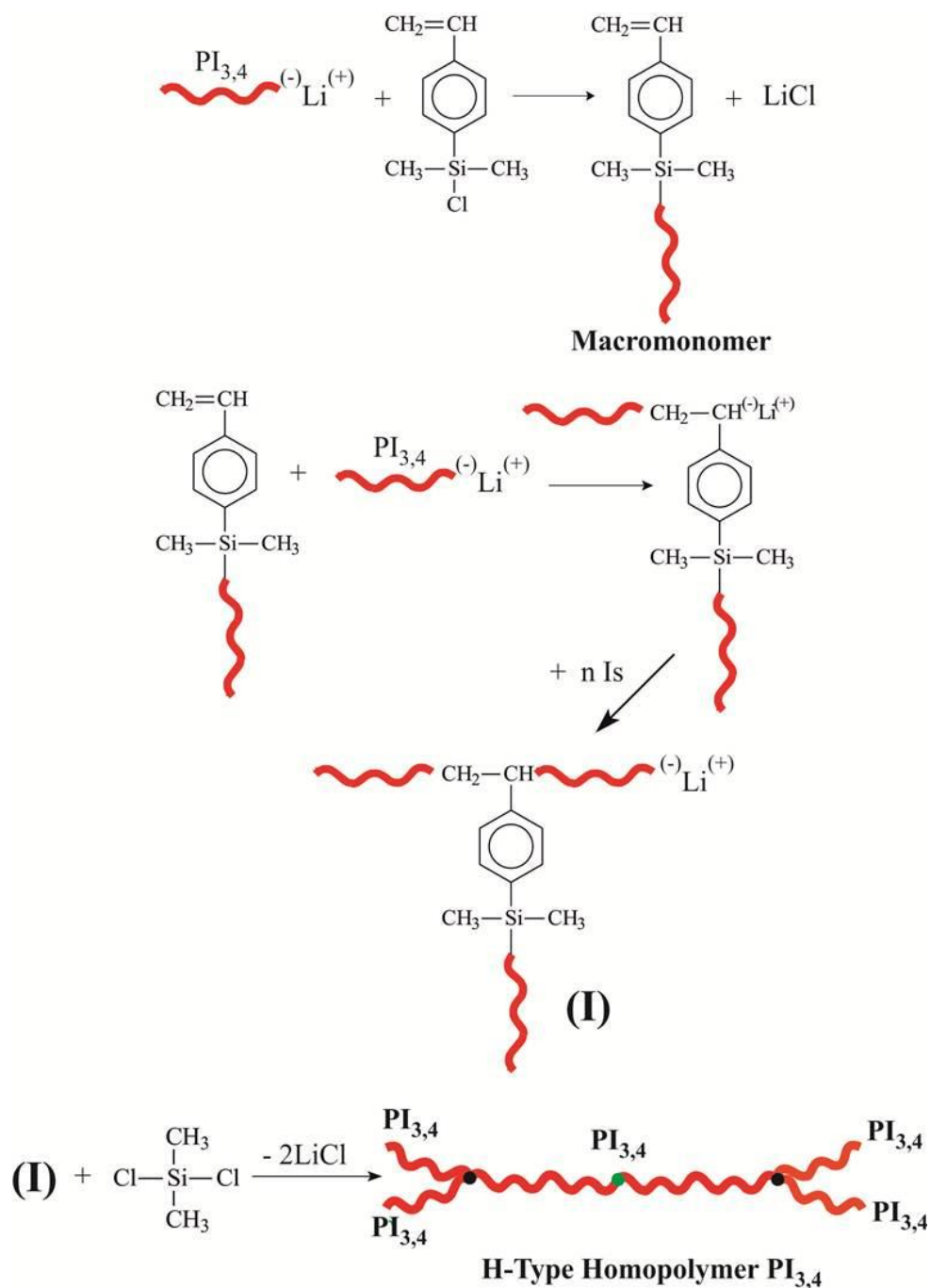


Figure 4.23: Analytical reactions for the synthesis of H-type $\text{PI}_{3,4}$ homopolymers.

The apparatus used for the synthesis of the initial arms for the preparation of the H-type homopolymers of $\text{PI}_{3,4}$ is shown in Figure 4.24.

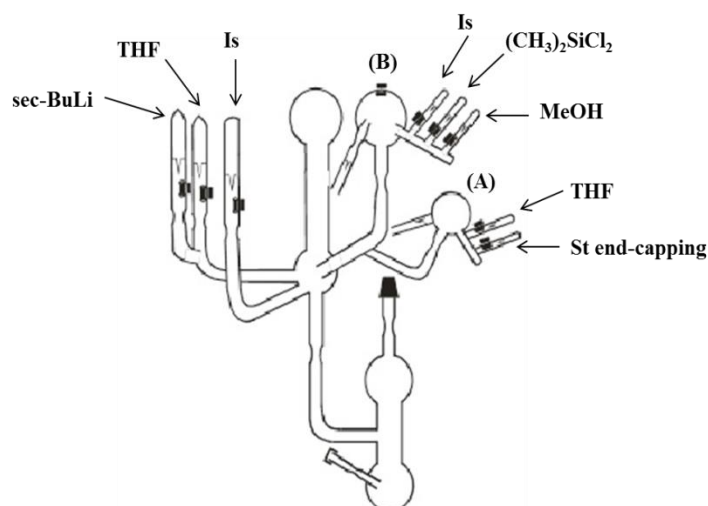


Figure 4.24: Apparatus for the synthesis of the initial $PI_{3,4}$ living chains which were used for the preparation of the final H-type $PI_{3,4}$ homopolymers.

In Figure 4.24 flask A is equipped with two (2) ampoules containing St end-capping and THF, while flask B contains three (3) ampoules of isoprene, linking agent dichlorodimethylsilane $[(CH_3)_2SiCl_2]$ and methanol respectively. By completing the polymerization of isoprene, an aliquot ($\sim 0.5g$) for molecular characterization via size exclusion chromatography (SEC) and membrane osmometry (MO) is obtained and the solution of living chains $PI_{3,4}^{(-)}Li^{(+)}$ is divided stoichiometrically between the two flasks. These flasks are then removed from the main reaction apparatus by heat sealing the proper constrictions. In flask B the quantity of the living ends is larger ($\sim 5-10\%$ in excess) for the reason already mentioned above during the description of the synthesis reaction of the H-type homopolymers.

Concurrently another apparatus is prepared (Figure 4.25), equipped with an ampoule of 4-(chlorodimethylsilyl)styrene (CDMSS), a difunctional reagent in order to prepare the macromonomer, and flask A which contains a part of the $PI_{3,4}^{(-)}Li^{(+)}$ living chains. This apparatus consisted of a purge section B and the main reactor C in which the macromonomer will be synthesized.

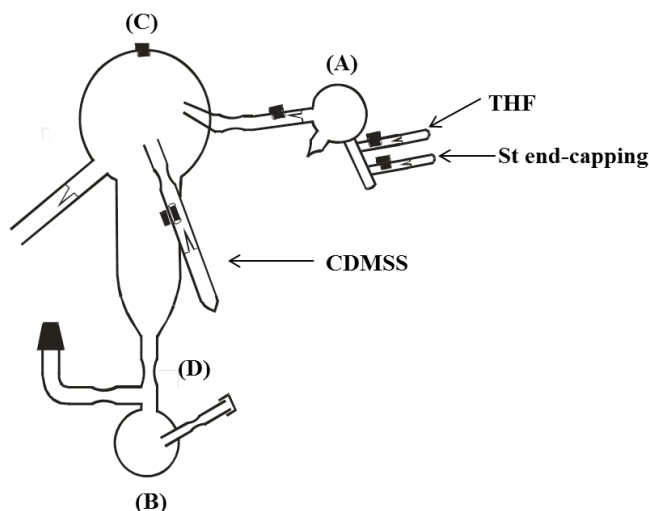


Figure 4.25: Apparatus for the synthesis of the intermediate macromonomer.

Initially, the apparatus is attached on the vacuum line through a ground joint, degassed and a small amount of *n*-BuLi (2-3 mL) is introduced from the elastic septum, rinsed and sealed off. The apparatus is degassed again and approximately 50 mL of benzene are distilled into the purge section, frozen with liquid nitrogen and degassed again. The apparatus is detached from the vacuum line by sealing off the appropriate constriction, the benzene solution is thawed and the solution of benzene and *n*-BuLi is transferred in the inner Pyrex glass surface of the apparatus as already described previously. Then, the apparatus is rinsed by continuous benzene reflux in order to remove traces of *n*-BuLi as well as its reaction products with impurities. Approximately half amount (25 mL) of the solvent is left in the main reactor C in order to reduce the vapor pressure of the volatile reagent (CDMSS) during the introduction of the living anions $\text{PI}_{3,4}^{(-)}\text{Li}^{(+)}$ and the purge section B is removed by sealing off the appropriate constriction D. Then, the protection of the living ends of $\text{PI}_{3,4}^{(-)}\text{Li}^{(+)}$ is achieved through end-capping with 2-4 monomeric units of styrene (St end-capping), by rupturing first the ampule of THF and then the ampule containing the St for the end-capping. The color of the solution turned into orange, indicating the alteration of $\text{PI}_{3,4}^{(-)}\text{Li}^{(+)}$ to $\text{PS}^{(-)}\text{Li}^{(+)}$, leading to better control of the linking reaction due to steric hindrance effects. Furthermore, the ampule of CDMSS is ruptured, the solution is homogenized, the empty ampule is sealed off and the solution is left under vigorous stirring (Figure 4.26).

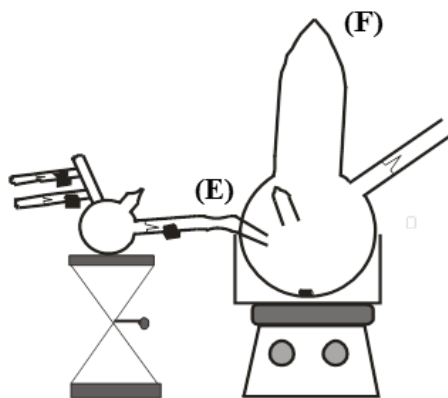


Figure 4.26: Final apparatus for performing the linking reaction and the preparation of the intermediate macromonomer.

The next step was to rupture the break-seal of the flask containing the living polymer and the quantity was added dropwise in the CDMSS solution. It should be indicated that the molar ratio of $\text{PI}_{3,4}^{(-)}\text{Li}^{(+)}$ /CDMSS was approximately equal to 1:1. The macromonomer is formed through the substitution of a chlorine atom by the living polymer ends. The addition of the end-capped poly(isoprene) living chains with 2-4 monomeric units of styrene was accomplished via titration (stoichiometry), controlled and verified by collecting aliquots during the reaction and monitoring through SEC. The procedure was performed with great caution and very slowly, in order to avoid the addition of living chains to the vinyl bond of the CDMSS, which is an unwanted reaction at the current synthesis step. As soon as the living chains are added to the CDMSS solution, the color changed immediately from orange to colorless indicating the controlled substitution of $-\text{Cl}$ and the formation of LiCl . In a period of approximately 2 h the procedure is completed. Then, the flask was removed from the apparatus F by heat-sealing the constriction E and the reactor containing the macromonomer is attached to another apparatus with the initial flask B which contained the remaining quantity of the $\text{PI}_{3,4}^{(-)}\text{Li}^{(+)}$ living chains (Figure 4.27).

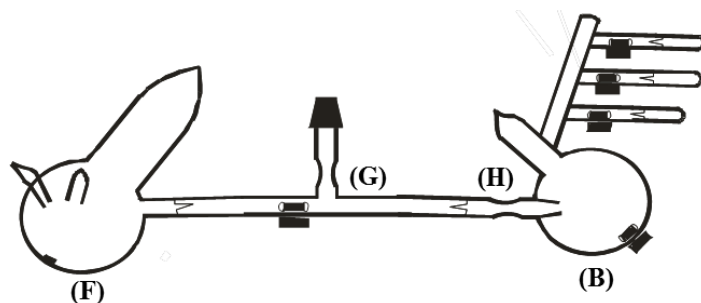


Figure 4.27: Apparatus for the synthesis of the intermediate macroinitiator.

The apparatus shown in Figure 4.27, is attached to the vacuum line, flame dried, degassed and heat-sealed at constriction G. Furthermore, the apparatus is left under stirring, the corresponding break-seals of flasks F and B are ruptured and the macromonomer is added dropwise to the solution of $\text{PI}_{3,4}^{(-)}\text{Li}^{(+)}$ living chains (Figure 4.28).

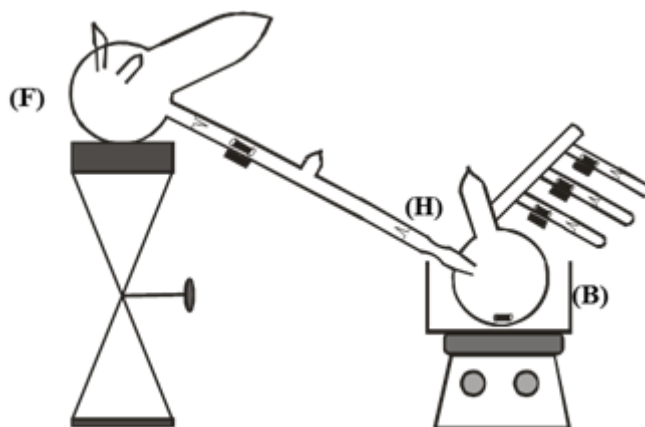


Figure 4.28: Final apparatus for the synthesis of the intermediate macroinitiator.

The solution of living ends was in excess (~5-10%), compared to the macromonomer, since in that manner, the addition through the vinyl bond of the macromonomer is achieved successfully. The substitution of the chlorosilyl group is easier than the addition of the vinyl bond and this is the reason why the second addition is much slower as already mentioned in the literature.⁷² The color of the solution changed from bright yellow ($\text{PI}_{3,4}^{(-)}\text{Li}^{(+)}$) to orange, indicating the successful reaction of the living polymer with the vinyl bond of the macromonomer. The second titration was also controlled by collecting aliquots during the reaction and monitoring the reaction progress through SEC. After completion of the reaction, flask B was removed by heat-sealing the appropriate constriction H.

Finally, inside the apparatus, shown in Figure 4.29, which contains the formed macroinitiator, the ampule with the appropriate quantity of isoprene is ruptured, the monomer is distilled in the reactor and the polymerization of isoprene is initiated from the living ends of the macroinitiator. The desired 3,4-microstructure of poly(isoprene) is achieved by the already incorporated amount of THF used for the end-capping, as already mentioned. The polymerization is completed after ~24 h and the linking agent dichlorodimethylsilane $[(\text{CH}_3)_2\text{SiCl}_2]$ was introduced in the reactor. The linking reaction is completed in approximately one (1) month and was inspected by taking aliquots in periodic timeframes and analyzing them by SEC. When no further change in the progress of the linking reaction was verified by the SEC studies, the MeOH ampule was ruptured in order to terminate the reaction and deactivate any living ends involved.

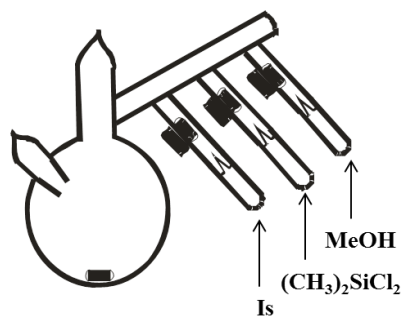


Figure 4.29: Apparatus for the synthesis of the star homopolymer $(PI_2)PI'$ and the final H type- $PI_{3,4}$ homopolymer.

Mass fractionation procedure in a mixture of solvent/non-solvent (toluene/methanol) was adopted, in order to remove any unreacted intermediate products such as $PI_{3,4}^{(-)Li^{(+)}}$ that was in excess during the synthesis of the macroinitiator and any unreacted macromonomer. After the fractionation, the final H-type $PI_{3,4}$ homopolymer was precipitated in a large excess of stabilized methanol and dried under vacuum.

Mass Fractionation

Mass fractionation is a separation process in which a certain quantity of a mixture (solid/liquid) is divided to a number of smaller quantities (fractions) in which the polymer compositions and molecular characteristics are different.¹⁵⁹ In this case, the mixture comprises of the desired non-linear homopolymer with the unwanted byproducts (which should be removed), a solvent and a non-solvent. Depending on the type of polymer chains, various systems of solvent/non-solvent can be adopted. Fractionation is performed in a separation flask equipped with a stopcock. Initially, the polymer mixture that needs fractionation is diluted in the chosen solvent under stirring, creating usually a solution of 2% w/v or less, depending on the molecular characteristics of the polymer mixture. The separation flask, without the stopcock, is placed in an annealing oven at approximately 150°C and remains there until the following procedure is completed. The non-solvent (usually methanol) is added carefully to the diluted polymer mixture until the solution becomes cloudy, a procedure which depends exclusively on what are the molecular characteristics of the unwanted byproducts. Then, the mixture is warmed up until it becomes transparent again, the separation flask is removed from the annealing oven, the stopcock is placed back again, the mixture is transferred to the warm separation flask and is left to cool down slowly to room temperature. During the introduction into the separation flask, the mixture should not touch the walls of the flask in order to maintain its homogeneity and avoid any evaporation of the non-solvent (MeOH exhibits very low boiling point and may evaporate if the flask is warmer than it should be). The temperature of the mixture and the separation flask should be approximately the same during the introduction of the mixture into the separation flask. In this manner, the higher molecular weight macromolecules will precipitate first by forming a lower layer of a

more concentrated phase, while the lower molecular weight macromolecules will form an overlying phase (Figure 4.30). The quantity of the desired polymer in each phase depends on the molecular weight and the chemical composition. This type of fractionation is called “successive precipitation fractionation” and its success is monitored by usually extracting small aliquots of the lower and upper phase for molecular characterization via SEC. If the results are not satisfactory, the lower phase is collected and fractionated again until the complete elimination of the undesirable products is verified.



Figure 4.30: Images of a separation flask used for the fractionation procedure, indicating the formation of the lower and the upper phase of the mixture (right image).

4.7.3 Synthesis of Linear Diblock Copolymers

The synthesis of the linear diblock copolymers of the PB-*b*-PI_{3,4} type was accomplished by using anionic polymerization and high vacuum techniques via sequential monomer addition. The main scope of the synthetic route adopted, was to synthesize diblock copolymers with narrow molecular weight distributions and predictable molecular weights, consisting of poly(butadiene) of high 1,4-microstructure (~92%) and poly(isoprene) with relatively high 3,4-content (55-65%). Five (5) diblock copolymers were synthesized with variable molecular weights and volume fractions between the two chemically different blocks. One of the diblock copolymers exhibited very high molecular weight (~1,000 kg/mol), whereas the other four samples had almost constant number average molecular weight (100,000 g/mol) and variable volume fractions. All polymerizations were accomplished by using benzene as solvent, *sec*-BuLi as the initiator and methanol as the termination reagent. For the successful polymerization of isoprene with relatively high 3,4-content, a small amount of THF was used, for the reasons already mentioned previously in this chapter. The synthetic route that was adopted for the synthesis of PB-*b*-PI_{3,4} is shown in Figure 4.31.

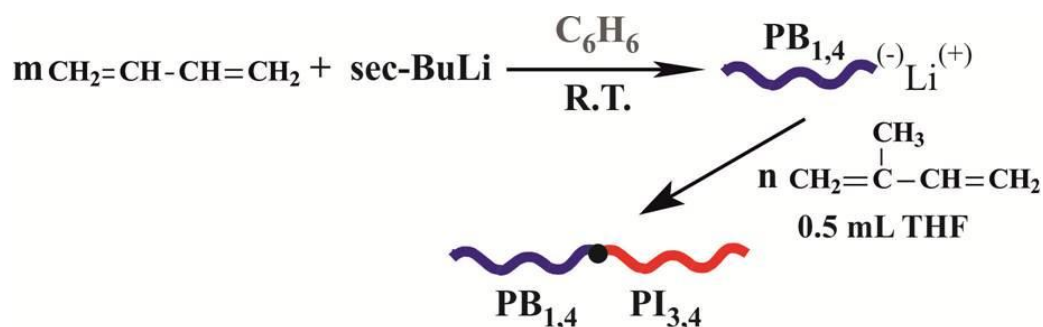


Figure 4.31: Synthetic route for the synthesis of PB-*b*-PI_{3,4} diblock copolymers.

The appropriate scientific glassblowing is performed and the ampules of the monomers, the initiator, THF and the terminating agent are attached on the apparatus (Figure 4.32). Through the ground joint the apparatus is attached on the vacuum line, degassed and a small amount of *n*-BuLi is introduced from the elastic septum, rinsed and sealed. It is degassed again and the proper amount of benzene (~200 mL) is distilled, through the vacuum line, into flask A. The system is degassed again and is detached from the vacuum line by heat sealing constriction C. The apparatus is rinsed by the same procedure described previously for the case of the PI_{3,4} homopolymer samples and the purge section A is removed through sealing off constriction D.

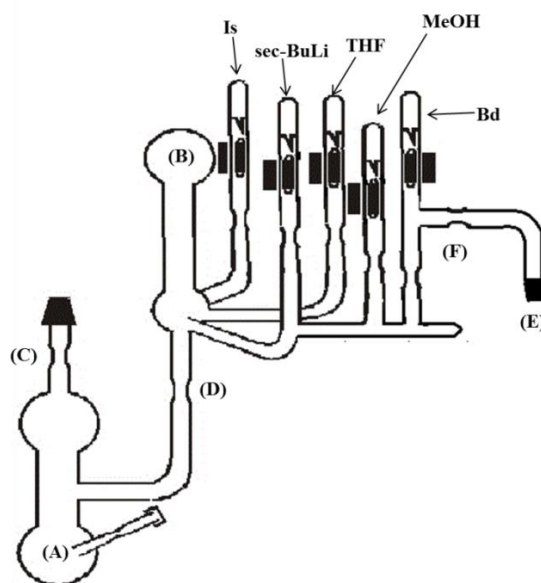


Figure 4.32: Apparatus for the synthesis of linear PB-*b*-PI_{3,4} linear diblock copolymers.

As it was mentioned already for 1,3-butadiene it requires immediate polymerization after being purified. For this reason, when the pure solvent is distilled from the purge section A to the main reactor B, in a period of 2-3 h, the purification of butadiene is performed simultaneously in another vacuum line. After the procedure is completed, the apparatus is attached on the vacuum line through the ground joint E that the empty ampule for Bd bears and is thoroughly degassed (Figure 4.33). The exact amount of the pure monomer is distilled

into the ampule using a liquid nitrogen/isopropanol bath (-78°C) and the apparatus is removed from the vacuum line through constriction F.

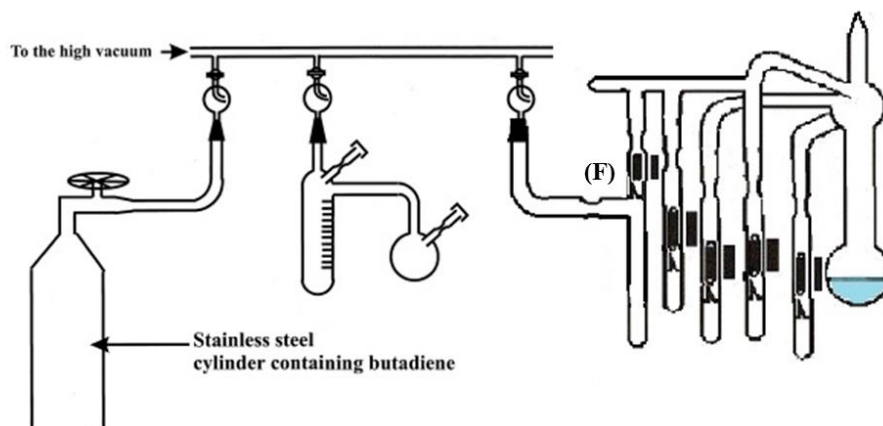


Figure 4.33: Distillation of pure butadiene into the apparatus, prior to polymerization.

The break-seal of the ampule of butadiene is ruptured, the monomer is distilled into the main reactor and the ampule is removed by heat sealing of the appropriate constriction. Then, *sec*-BuLi is introduced to the solution and initiates the polymerization of butadiene. This polymerization is completed in 24 h and a small aliquot is taken for molecular characterization via SEC, MO and $^1\text{H-NMR}$. Prior to the initiation of isoprene polymerization the small amount of THF is introduced in the solution. The color of the solution turned into pale yellow from almost colorless, since the degree of association between the solvent and the $\text{PB}^{(-)}\text{Li}^{(+)}$ living ends is decreased from 6 to 2 as already mentioned previously. It should be pointed out that the requirement in these experiments was to introduce specific ratios of polydiene microstructure [poly(butadiene) of high 1,4-microstructure ($\sim 92\%$) and poly(isoprene) with relatively high 3,4-content (55-65%)] in order to obtain eventually successful self-assembly between the two blocks. This is the reason why the 1,3-butadiene is polymerized first and the isoprene is introduced as the second monomer. According to the literature¹⁷ the resulting microstructure following this specific route is such that leads to microphase separation during studies with Transmission Electron Microscopy (TEM).

After approximately 10 min from the THF addition in the solution, isoprene was added and polymerized. The color turned to bright yellow, indicating the initiation of polymerization for the second monomer. The polymerization is also completed in 24 h (depending on the desirable molecular weights), the ampule of methanol is ruptured and the termination of the polymerization is achieved. The desired diblock copolymer is precipitated into an excess of methanol stabilized with a proper antioxidant reagent, dried under vacuum for at least 24 hours in a drying oven set at 50°C .

In the case of the diblock copolymer with high molecular weight ($\sim 1,000$ kg/mol), the amount of benzene and THF used were approximately 800-850 mL and ~ 3 mL respectively.

All samples exhibited very narrow molecular weight distributions (PDI <1.1) and predictable molecular weights, as confirmed from SEC and MO.

4.7.4 Synthesis of Mikroarm Star Copolymers of the A₂B and A₃B Type

The synthesis of mikroarm star copolymers of the A₂B and A₃B type, where A is PI_{3,4} (3,4-content: ~55-65%) and B is PB_{1,4} (~90-92% 1,4-microstructure), was accomplished through anionic polymerization techniques and high vacuum techniques in combination with chlorosilane chemistry. The solvent used was benzene, *sec*-BuLi as the initiator, THF for the achievement of the desirable high 3,4-microstructure of PI, trichloromethylsilane (CH₃SiCl₃) and tetrachlorosilane (SiCl₄) as the linking agents and methanol as the terminating agent for all the polymerizations. *Such mikroarm star copolymers were synthesized for the first time and have never been reported in the literature.*

Eight (8) samples were prepared, divided to four (4) sets (four samples per sequence), according to the similarities in volume fractions. The volume fraction regime for the PB block as well as the total molecular weight of the non-linear copolymers are approximately equal to those documented for the four (4) of the diblock copolymers, thus each diblock copolymer corresponds to a set of mikroarm star copolymers with approximately equal number average molecular weights and volume fractions. The reason for keeping almost constant both total molecular weight and PB block volume fraction in the linear diblock and in the non-linear copolymers was to compare their structure/properties relationship and verify in such systems the influence of non-linear architecture in self-assembly. *It should be noted here that it is the first time such a study is performed in exclusively 100% elastomers.*

The synthetic route used for the preparation of PB(PI_{3,4})₂ and PB(PI_{3,4})₃ mikroarm star copolymers is shown in Figures 4.34 and 4.35 respectively.

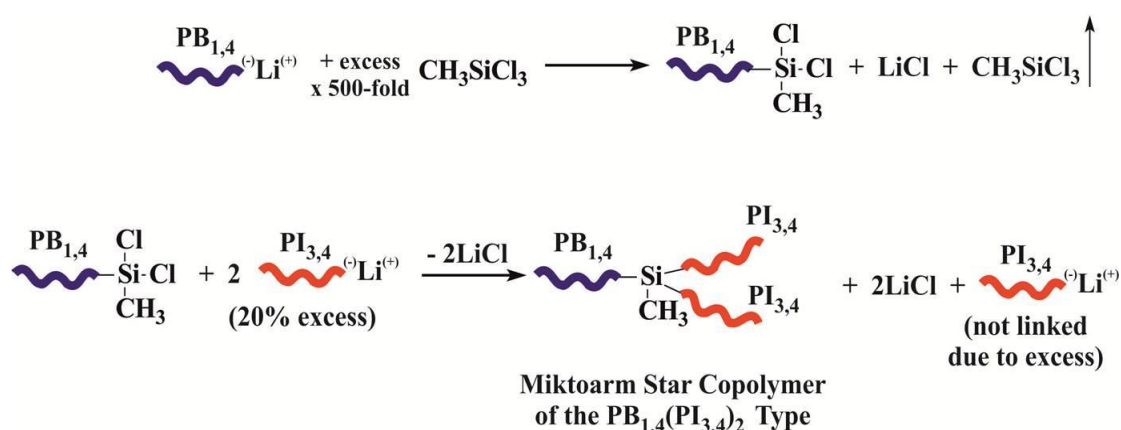


Figure 4.34: Synthetic route for the synthesis of mikroarm star copolymers of the PB(PI_{3,4})₂ type.

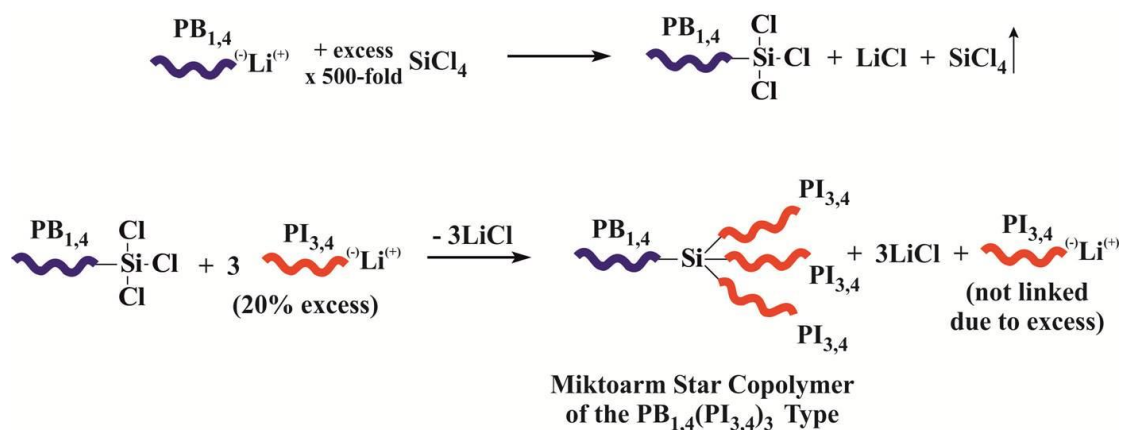


Figure 4.35: Synthetic route for the synthesis of miktoarm star copolymers of the $\text{PB}(\text{PI}_{3,4})_3$ type.

Initially, $\text{PB}^{-}\text{Li}^{(+)}$ living chains are synthesized through anionic polymerization, as already mentioned. Benzene is used as the solvent and *sec*-BuLi as the initiator. The apparatus used for this polymerization is different from the already described previously and is shown in Figure 4.36:

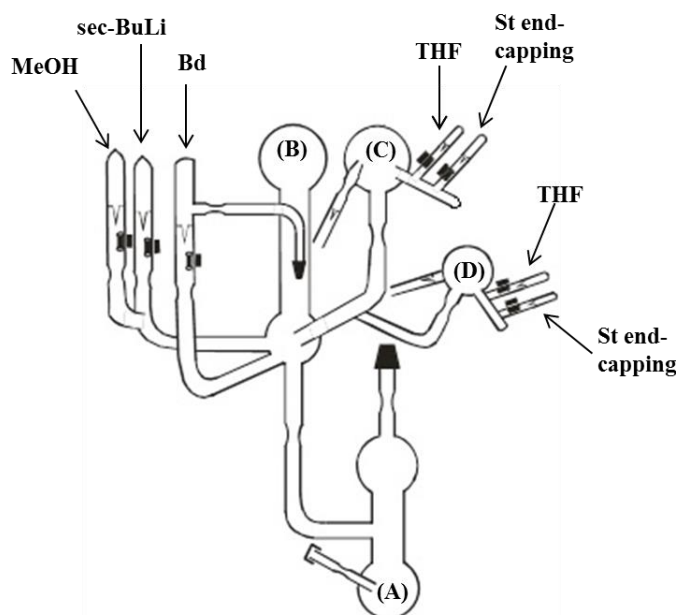


Figure 4.36: Apparatus for the synthesis of $\text{PB}^{-}\text{Li}^{(+)}$ prior to the linking reactions with chlorosilanes.

The apparatus is attached on the vacuum line, flame dried, degassed, a small amount of *n*-BuLi is injected through the elastic septum, rinsed and removed from the apparatus. Appropriate amount of benzene (300-400 mL) is distilled in flask A, the system is degassed again and finally removed from the vacuum line. The purification procedure of the apparatus is the same as previously reported, and the purge section flask A is removed, leading only to pure benzene in the main reactor B. The apparatus is attached to the vacuum line again and the distillation of pure butadiene is achieved through the appropriate setup as described previously (Figure 4.33). Following the aforementioned procedure, polymerization of butadiene is completed after 24 h and the solution of living $\text{PB}^{-}\text{Li}^{(+)}$ is divided

stoichiometrically into flasks C and D respectively which are sealed off from the apparatus accordingly. An appropriate amount of living $\text{PB}^{(-)}\text{Li}^{(+)}$ is left in the apparatus (~ 0.5 g) in order to perform molecular characterization through SEC, MO and $^1\text{H-NMR}$. Methanol is introduced in the apparatus for the deactivation of the small amount living ends. In both flasks C and D, ampules of THF and St for end-capping are attached in order to alter the reactivity of the living ends to $\text{PS}^{(-)}\text{Li}^{(+)}$, leading to better control of the linking reaction. The ampule of THF is ruptured first, the color of the solution turned into yellow and after a while is followed by the rupture of the St end-capping ampule and the color turned into light orange verifying the alteration of the living ends as needed.

For the linking reaction of trichloromethylsilane (CH_3SiCl_3) or tetrachlorosilane (SiCl_4) with the new $\text{PS}^{(-)}\text{Li}^{(+)}$ living ends of the protected PB, the apparatus used is exhibited in Figure 4.37.

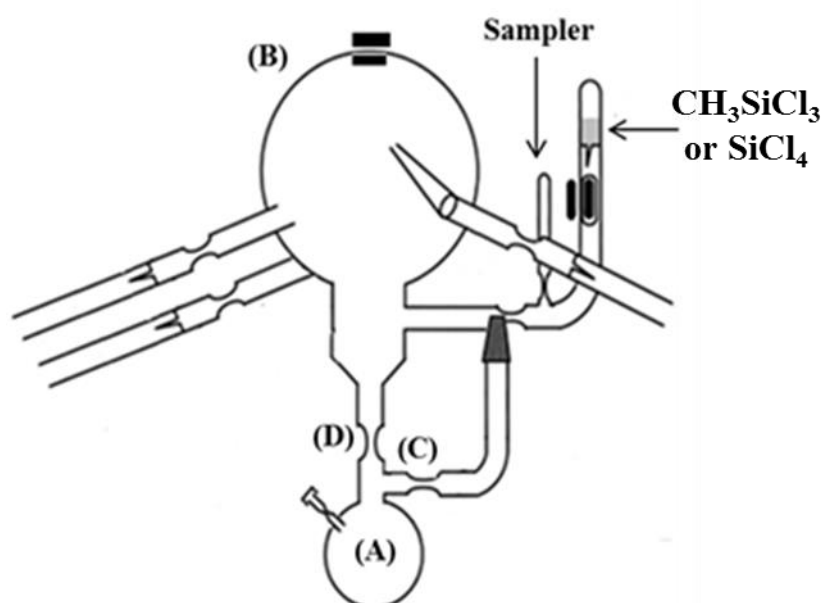


Figure 4.37: Apparatus for the linking reaction of the chlorosilane with the living ends.

This apparatus consisted of the purge section A and the main reactor B which will be used for the linking reaction. Initially, the apparatus is attached on the vacuum line through the appropriate ground joint, degassed and a small amount of $n\text{-BuLi}$ is introduced from an elastic septum, rinsed and sealed-off. The apparatus is degassed again and approximately 50 mL of benzene are distilled into the purge section, cooled with liquid nitrogen and degassed again. The apparatus is detached from the vacuum line by sealing-off the constriction C, the benzene solution is thawed and the solution of benzene and $n\text{-BuLi}$ is transferred in the inner Pyrex glass surface of the apparatus as already described. Then, the apparatus is rinsed by continuous benzene reflux in order to remove traces of $n\text{-BuLi}$ as well as its reaction products with impurities. Approximately half amount (25 mL) of the solvent is left in the main reactor in order to reduce the vapor pressure of the volatile linking agent during the introduction of

the living anions and the purge section A is removed. The ampule of the linking agent is ruptured, the solution is homogenized and the empty ampule of the silane is sealed off as well. The break-seal of the collection flask with the St end-capped PB living ends is attached to the one side arm of the linking apparatus which bears a break-seal connected to constriction with a glass nozzle as indicated in Figure 4.38. The connection part is degassed very carefully on the vacuum line by flame drying 2-3 times, the apparatus is detached by sealing off constriction A and is left under stirring prior to the linking reaction in an ice bath (0°C in order again to minimize the vapor pressure of the volatile chlorosilane).

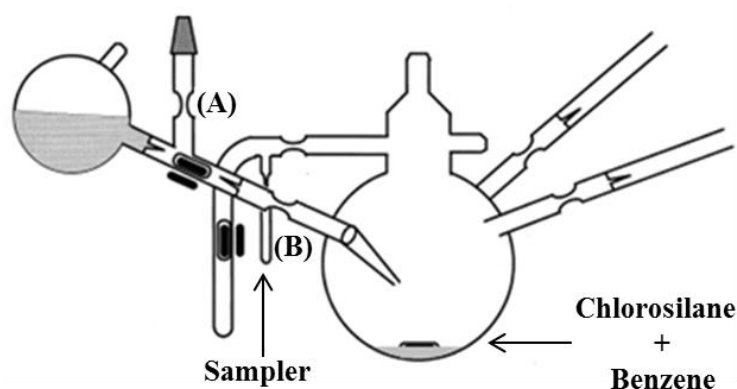


Figure 4.38: Schematic of the reactor constructed for the linking reaction which is connected with the collection flask containing the St end-capped poly(butadienyl) living ends.

At this point of the synthetic procedure any error in the handling of the apparatus could lead to unwanted results and the linking reaction of the silane with the living ends will not be successful. Two parameters are very important:

- a) The amount of the chlorosilane linking agent must be in a large excess when compared with the amount of the active polymer chains (at least 400- to 500-fold excess).
- b) The solution of the active polymer must be added to the chlorosilane as quickly as possible, without permitting any vapors of the chlorosilane to transfer back to the connection part, or even worse, back to the flask with the living ends leading eventually to cross-linking reactions and to gelation.

The linking reactor with the linking agent in benzene is placed into an ice bath (0-4°C) under soft stirring, the flask with the active polymer chains is warmed up to 75-80°C and both break-seals are ruptured if possible simultaneously. The apparatus is tilted and a towel soaked in hot water is placed on the flask with the active polymer in order to help the insertion of the solution into the linking reactor as fast as possible. The living polymer is, therefore, added in one continuous motion into the linking reactor where vigorous stirring is applied and in order for the reaction to be successful the loss of color (from the living ends) should be evident as soon as the solution is inserted to the reactor bearing the chlorosilane solution. After the

addition is completed, the apparatus is left under stirring for at least one (1) hour at room temperature. The most crucial aspect of this linking reaction is the substitution by the living chains of only one chlorine atom, leading therefore to the intermediate product PB-Si-Cl₂ or PB-Si-Cl₃ (according to the chlorosilane used in each case).

An important procedure for the successful synthesis of the final miktoarm star copolymers is the removal of the excess of the linking agent since even a small amount of unreacted chlorosilane could lead to undesirable products in the final material. This volatile reagent is removed by adopting a specified procedure in the high vacuum line. The apparatus of Figure 4.39 is attached on the vacuum line through one of the two remaining break-seal entries in which a ground joint C was attached.

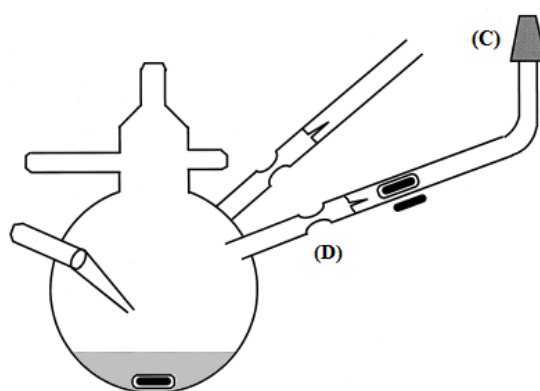


Figure 4.39: Apparatus for the quantitative removal of the unreacted chlorosilane linking agent.

After the specific apparatus (Figure 4.39) is degassed on the vacuum line, the corresponding break-seal is ruptured and the contents (benzene, chlorosilane) are distilled to a waste collection flask attached on the high vacuum line until the solution becomes enough viscous to stir. Freshly purified benzene (50-70 mL) is distilled into the linking reactor, through the vacuum line, and the contents are stirred for 30 minutes at approximately 30⁰C in order to fully dilute again the PB-Si-Cl₂ or PB-Si-Cl₃ polymer. By this manner, the inner Pyrex glass surface of the apparatus is rinsed from the remaining chlorosilane traces. The contents are again distilled to the waste collection flask and the procedure is repeated for at least two more times. After the third distillation of the contents to the waste collection flask, the reactor may be opened to the vacuum line for a large period of time until no volatile residues are evident in the apparatus (through the elimination of the Tesla coil noise). Depending on the amount of chlorosilane and the molecular weight of the polymer, this period of time can last from 5-10 days. The reactor is usually warmed up to ~30-35⁰C in order to enhance the evaporation of the trapped volatile residues.

The distillation of freshly purified benzene into the reactor was performed with a liquid nitrogen/isopropanol bath and not directly with liquid nitrogen in order to prevent any

crack in the glassware of the reactor through stresses acquired by overheating and overfreezing. The existence of high vacuum is an indication that all the chlorosilane quantity has been removed from the apparatus. Purified benzene is again distilled into the reactor (~150-200 mL, depending on the molecular weight and the quantity of the polymer) and the apparatus is detached from the vacuum line by sealing-off constriction D (Figure 4.39). Then, the reactor is connected, through the last break-seal entry, with the polymerization reactor of the living $\text{PI}_{3,4}^{(-)}\text{Li}^{(+)}$ by constructing a new apparatus shown in Figure 4.40. The living chains of $\text{PI}_{3,4}^{(-)}\text{Li}^{(+)}$ should be in ~20% excess compared to the Si-Cl living ends of the PB-Si-Cl₂ or PB-Si-Cl₃ in order to verify that all the remaining chlorine atoms will be substituted by the PI chains, leading eventually to the desired PB($\text{PI}_{3,4}$)₂ and PB($\text{PI}_{3,4}$)₃ miktoarm star copolymers respectively.

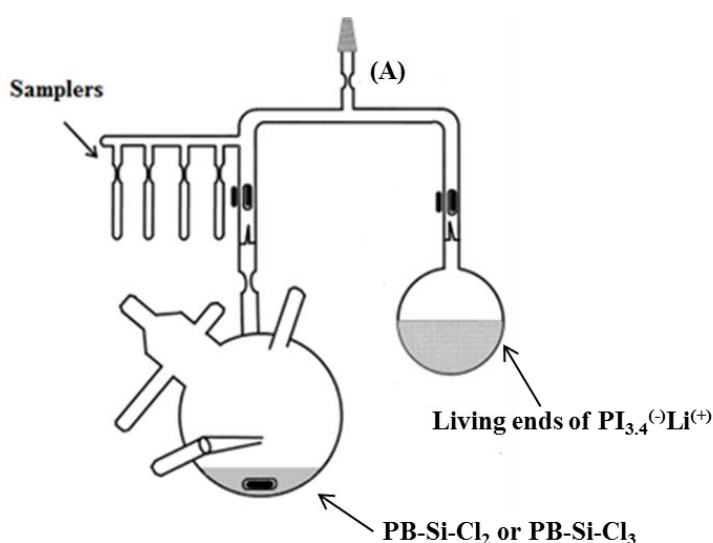


Figure 4.40: Apparatus for the linking of the living $\text{PI}_{3,4}^{(-)}\text{Li}^{(+)}$ with PB-Si-Cl₂ or PB-Si-Cl₃ respectively in order to prepare the desired miktoarm star copolymer.

The apparatus observed in Figure 4.40 is attached carefully on the vacuum line through a ground joint, is evacuated for ~1 h and then is detached from the vacuum line by sealing-off the appropriate constriction A. Then, the break-seal of the living $\text{PI}_{3,4}$ ends, which are in excess, is ruptured and the solution is transferred to the inner Pyrex glass surface of the apparatus. The excess of the living anions reacts with any impurities and deactivates them since it is not possible to purify this apparatus by incorporating a purge section as described in previous cases. Afterwards, the break seal of the PB-Si-Cl₂ or PB-Si-Cl₃ is ruptured and the two solutions are mixed thoroughly. An indication of the linking reaction is the change of the color of the living arms from bright yellow to an almost colorless solution (a pale color sometimes is obtained due to the excess of the living arms). The final mixture is collected to the reactor of the PB-Si-Cl₂ or PB-Si-Cl₃ and the final linking reaction is left to proceed for approximately one (1) month. During this linking procedure, small aliquots of the mixture for molecular characterization via SEC are extracted in order to monitor the progress of the

linking reaction. After completion of the linking reaction, the homopolymer (PI_{3,4}) and non-linear copolymer mixture is precipitated in stabilized methanol and dried under vacuum at room temperature for at least 24 h. Finally, due to the excess of the PI_{3,4}⁽⁻⁾Li⁽⁺⁾ living ends used in order to ensure complete substitution of the remaining chlorine atoms by the living chains, fractionation was necessary for the homopolymer excess removal. The solvent/non solvent system adopted was toluene/methanol, due to the very good solubility of both PB and PI_{3,4} in toluene.

The same synthetic procedure and apparatuses, as described above, was used for both types of miktoarm star copolymers.

4.8 Molecular Characterization

4.8.1 Size Exclusion Chromatography (SEC)

A size exclusion chromatograph (SEC), equipped with an isocratic pump (SpectraSystem P1000), column oven (LabAlliance) heated at 30⁰C, three columns in series (PLgel 5 mm Mixed-C, 300×7.5 mm), refractive index (RI, Shodex RI-101), ultraviolet absorbance (UV, SpectraSystem UV1000) detectors and tetrahydrofuran (THF) as the eluent, was calibrated with eight PS standards (Mp: 4.300 to 3.000.000 g/mol). In every case, prior to calculating the polydispersity index (PDI) of the synthesized polymers as well as prior to make an estimation on the average molecular weights (\overline{M}_n and \overline{M}_w), a series of standard PS solutions were always tested in order to examine the accuracy of the measurements. All measurements were performed at the Polymers Laboratory, Department of Materials Science Engineering, University of Ioannina since the specific equipment is necessary for the molecular characterization of synthesized linear and non-linear polymer samples.

4.8.2 Membrane Osmometry

Membrane osmometry (MO) was adopted to determine the number average molecular weight \overline{M}_n by using a Gonotec Osmomat 090 in 35⁰C. The solvent used was toluene, distilled from CaH₂, while the membrane was from regenerated cellulose. The number average molecular weight was estimated by creating a graph of $(\pi/c)^{1/2}$ as a function of c, where π is the osmotic pressure and c the concentration of the corresponding solution in g/ml. All measurements were performed at the Polymers Laboratory, Department of Materials Science Engineering, University of Ioannina since the specific equipment is necessary for the molecular characterization of synthesized linear and non-linear polymer samples.

4.8.3 Proton Nuclear Magnetic Resonance (¹H-NMR) Spectroscopy

Proton nuclear magnetic resonance (¹H-NMR) spectroscopy was used for determining the composition and the isomeric microstructures of poly(butadiene) and poly(isoprene)

blocks respectively, and was carried out in CDCl_3 at 25°C using a Bruker AVANCE II 250 MHz spectrometer, located at the Chemistry Department in the University of Ioannina. Data were processed using UxNMR (Bruker) software. The Network of Research Supporting Laboratories at the University of Ioannina is highly acknowledged in this case since the equipment (Center of Nuclear Magnetic Resonance) is located at the Department of Chemistry, University of Ioannina.

4.9 Thermal Analysis

4.9.1 Differential Scanning Calorimetry (DSC)

For the calculation of glass transition temperatures values of the materials, differential scanning calorimetry (DSC) was employed. The measurements were accomplished with a Q20 TA instrument. The heating ramp was $5^\circ\text{C}/\text{min}$ and the temperature range from -120°C to 40°C . A small amount of 2-5 mg was used from each sample and placed in an aluminum pan, which was sealed properly and introduced into the sample holder of the instrument. Two heating and one cooling cycles were performed and the results of the second heating were reported and analyzed using Advantage v5.4.0 (TA instruments) software. All measurements were performed at the Polymers Laboratory, Department of Materials Science Engineering, University of Ioannina since the specific equipment is necessary for identifying thermal properties and transitions of synthesized linear and non-linear polymer samples.

4.10 Morphological Characterization

4.10.1 Transmission Electron Microscopy (TEM)

The observation of the samples was performed in a JEOL JEM-2100 transmission electron microscope (TEM) operating at 200 kV in bright field mode equipped with a LaB_6 filament. In order to study the morphology of the copolymers prepared in the framework of this thesis, the preparation of thin films that exhibit microphase separation was required. Thermodynamic equilibrium ensures enhanced self-assembly of the sample, leading eventually to distinguishable microphase separation. The preparation of the samples and the observation via TEM of the equilibrium morphologies were performed in the Department of Materials Science Engineering, University of Ioannina at the Electron Microscopy Unit.

Casting-Annealing: Initially, for the preparation of the thin films, a 5% w/v solution of each sample in toluene was prepared. The solvent should be non-selective for both blocks of the copolymer. The samples were casted for approximately 5-7 days in a properly established saturated environment under a beaker in a hood. In this manner, the solvent is evaporated slowly from the solution. Thin films with thickness approximately 1 mm were formed and half parts of them were placed in an oven for thermal annealing (50°C) for 5 days. Then, each film was removed from the annealing oven and immersed in liquid nitrogen for a

few seconds (quenching). This procedure was adopted since there is a possibility that the formed morphology might alter, if the sample is cooled slowly to room temperature, especially if the molecular characteristics of the sample are low and WSL theories are adopted.

Ultramicrotomy: For the research work involved in this thesis, cryo-ultramicrotomy was performed in a Leica EM UC7 Ultramicrotome, located in the Polymers Laboratory, Department of Materials Science Engineering, University of Ioannina. Cryogenic conditions (-100°C) were employed for the reason that the hardness of each sample was improved, since the microtomy was accomplished below the lowest T_g of both PB and PI_{3,4} (-90°C and -10°C respectively).

CHAPTER 5

Experimental Results – Discussion – Conclusions – Future Work

5.1 Molecular Characterization Results of Linear Homopolymers PI_{3,4}

The molecular characterization results are presented and discussed for the four (4) linear homopolymers of the PI_{3,4} type synthesized for this thesis. All samples, as already mentioned were synthesized via anionic polymerization through high vacuum techniques. High 3,4-content (55-65%) was adopted in all four samples, using a small amount of a polar additive (THF), prior to the polymerization of isoprene. All polymerizations were performed by using *sec*-BuLi as initiator, benzene as the solvent and methanol as the terminating agent of the polymerization.

Molecular characterization of the samples was performed through size exclusion chromatography (SEC), membrane osmometry (MO), vapor pressure osmometry (VPO) when the number average molecular weight was low and proton nuclear magnetic resonance spectroscopy (¹H-NMR). SEC with THF as the eluent at 30⁰C was used extensively in order to verify the narrow molecular weight distributions of the polymers and to receive information concerning the number average molecular weights. The instrument was always calibrated with PS standards and the number average molecular weights are not accurate for the PI_{3,4} homopolymer samples.

The reason for calibrating the SEC equipment is to define the relationship between the molecular weight and elution volume or elution time (since in the equipment the flow rate in all experiments was set at 1mL/min) in the selective permeation range of the column set used and to calculate the number and weight average molecular weights of the sample with unknown molecular characteristics. In order to verify the number average molecular weight values for each sample, membrane osmometry and vapor pressure osmometry in toluene at 35⁰C and 50 ⁰C respectively for the MO measurements. Square root plots $(\pi/c)^{1/2}$ vs c (π : osmotic pressure and c : concentration) were used in order to calculate the \overline{M}_n values minimizing therefore the plot curvature due to the third virial coefficient especially in the cases where the \overline{M}_n values are high (bimolecular interactions between adjacent chains are strong even in dilute solutions leading to significant values of the third Virial coefficient). By combining the results from the above characterization methods and using them in the polydispersity equation: $I = \frac{\overline{M}_w}{\overline{M}_n}$, relative information concerning the \overline{M}_w value of the final materials may be obtained.

Furthermore, another method used for the molecular characterization of the samples, and especially to verify the high 3,4-microstructure for the PI_{3,4} homopolymer samples, was

proton nuclear magnetic resonance ($^1\text{H-NMR}$) spectroscopy in CDCl_3 at room temperature ($\sim 25^\circ\text{C}$).

In Table 5.1 the most significant molecular characteristics of the four homopolymers are summarized. Four (4) homopolymer samples of the $\text{PI}_{3,4}$ type in different molecular weights (ranging from 5,000 g/mol to 330,000 g/mol) were synthesized. The characteristic ratios of the stereochemical microstructures were calculated by the corresponding $^1\text{H-NMR}$ spectra and in all cases the 3,4-content was found to be higher than 55% and lower or equal to 60%.

Table 5.1: Molecular characterization results for the linear homopolymers of the $\text{PI}_{3,4}$ type.

Samples	$(\overline{M}_n)_{PI}^a$ (g/mol)	I^b	$(\overline{M}_w)_{PI}^c$ (g/mol)	% 3,4 ^d microstructure	% 1,4 ^d microstructure	% 1,2 ^d microstructure
PI_{3,4}-1	5,500 ^{VPO}	1.05	5,800	58	30	12
PI_{3,4}-2	14,500 ^{VPO}	1.03	14,900	59	29	12
PI_{3,4}-3	210,000	1.07	225,000	60	30	10
PI_{3,4}-4	330,000	1.08	356,000	58	30	12

^aMO in toluene at 35°C or VPO in toluene at 50°C , ^bSEC in THF at 30°C , ^cFrom combination of SEC and MO measurements through the equation $I = \overline{M}_w / \overline{M}_n$, ^dFrom $^1\text{H-NMR}$ measurements in CDCl_3 at 25°C .

A variety of results can be concluded from Table 5.1. The lowest number average molecular weight of the $\text{PI}_{3,4}$ is 5,500 g/mol while the highest is 330,000 g/mol. The molecular weight distributions are narrow in all cases, implying that the samples exhibit chemical and compositional homogeneity. Furthermore, the 3,4-content in all cases varies in the regime 58%-60%, as a result of utilizing a polar additive (THF) prior to the polymerization of isoprene. The theoretical calculations for \overline{M}_n values of the $\text{PI}_{3,4}$ homopolymer samples were always in accordance with the experimental results from SEC and MO. VPO measurements were needed in the cases of the two lower molecular weight samples ($\text{PI}_{3,4}$ -1 and $\text{PI}_{3,4}$ -2 as denoted in Table 5.1).

In Figure 5.1 the SEC chromatographs of all four samples are presented, following the notations adopted for Table 5.1. Prior to every measurement, the SEC instrument was calibrated with PS standards solutions exhibiting well-known molecular weights. The values obtained for the number average molecular weight of the samples are not accurate. For this reason membrane osmometry and/or vapor pressure osmometry were used in order to verify precisely the number average molecular weight of each sample. The results from the above mentioned techniques indicated that the values of number average molecular weight differed between size exclusion chromatography and osmometry by a ratio 1.29-1.31 in all cases and specifically the values from SEC were always larger by this ratio. This is due to the fact that

size exclusion chromatography was calibrated with PS standards and therefore the chemical structure of the $PI_{3,4}$ homopolymer samples is completely different from that of linear PS. The hydrodynamic volume of the $PI_{3,4}$ is larger leading to the conclusion that for these specific homopolymers the number and weight average molecular weights should always be divided by the value 1.30 as derived from the osmometry measurements (MO and VPO).

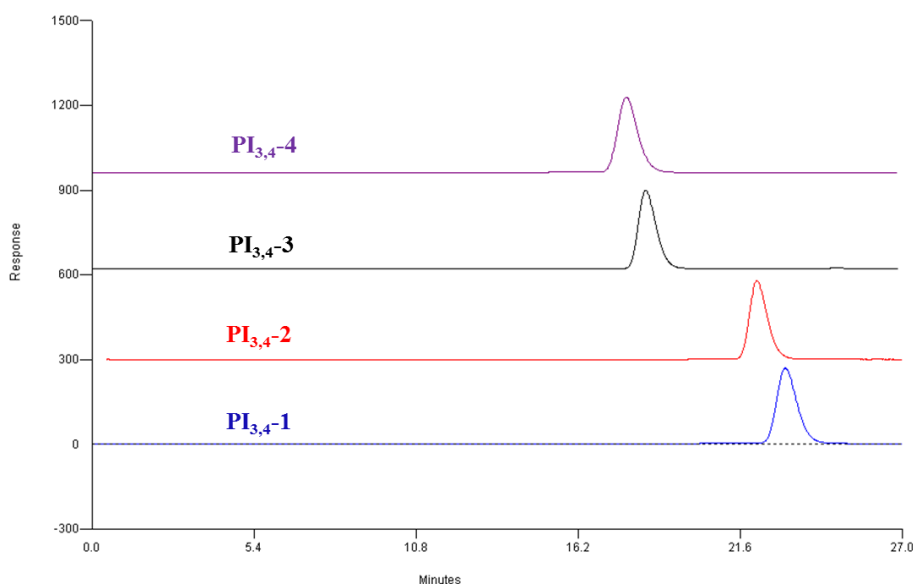


Figure 5.1: SEC chromatographs of the linear homopolymers of the $PI_{3,4}$ type, where the blue color corresponds to $PI_{3,4-1}$, red to $PI_{3,4-2}$, black to $PI_{3,4-3}$ and purple to $PI_{3,4-4}$ respectively.

By observing the SEC chromatographs of all homopolymers, it is clearly understood that their molecular weight distributions are monomodal. The presence of only one peak and their low polydispersity indices indicate their molecular homogeneity as well as the absence of any side and/or termination reactions during the polymerization of isoprene. The chromatographs of the higher molecular weight samples ($PI_{3,4-3}$ and $PI_{3,4-4}$) eluted at lower elution times in contrast with the lower molecular weight samples.

In order to calculate the characteristic ratios of stereochemical microstructures of each sample, 1H -NMR spectra in $CDCl_3$ at $25^\circ C$ were obtained. As it was mentioned in the experimental section (Chapter 4), THF was used prior to the polymerization of isoprene, leading to PI samples with enriched 3,4-microstructure. The lower 1,4-content is due to the delocalization of the negative charge among the three final carbons of the living chain (loose ion pairs).

The most characteristic feature of a 1H -NMR spectrum is its proton chemical shifts which correspond to specific protons located in carbons of the monomeric units. In Table 5.2 the theoretical proton chemical shifts for each microstructure of PI are given. As it is evident, the ratio of each microstructure can be estimated via 1H -NMR spectroscopy since, according to Table 5.2, different protons generate different chemical shifts in a 1H -NMR spectrum.

Table 5.2: Type and number of protons with the corresponding chemical shifts for protons incorporated in the monomeric units of poly(isoprene).

Geometric Isomerism	Type and Number of Protons	Chemical Shift (ppm)
1,4	Olefinic (1)	5,12
3,4	Olefinic (2)	4,70
1,2	Olefinic (1)	5,82
	Olefinic (2)	5,00

More specifically, olefinic proton chemical shifts appear above 4 ppm while the aliphatic appear at lower values (> 2 ppm). Olefinic proton chemical shifts usually attract greater interest since they correspond to protons related with the double bond carbons in polydienes. These shifts are the most important for the calculation of the ratio of the microstructures of PI. The chemical shift at 4,70 ppm corresponds to the hydrogen atoms (2) connected with the double bond carbon (carbon 1) in the 3,4-microstructure of poly(isoprene), the chemical shift at 5,12 ppm corresponds to the hydrogen atom (1) of the double bond carbon (carbon 2) in the 1,4-microstructure and the chemical shifts at 5,00 and 5,82 ppm correspond to the hydrogen atoms (2) of carbon 4 and the hydrogen atom (1) of carbon 3 in the 1,2-microstructure respectively.

In Figure 5.2 the $^1\text{H-NMR}$ spectrum of $\text{PI}_{3,4-3}$ linear homopolymer, where the characteristic chemical shifts for all protons (in red) of all the microstructures for the $\text{PI}_{3,4-3}$ homopolymer sample is presented.

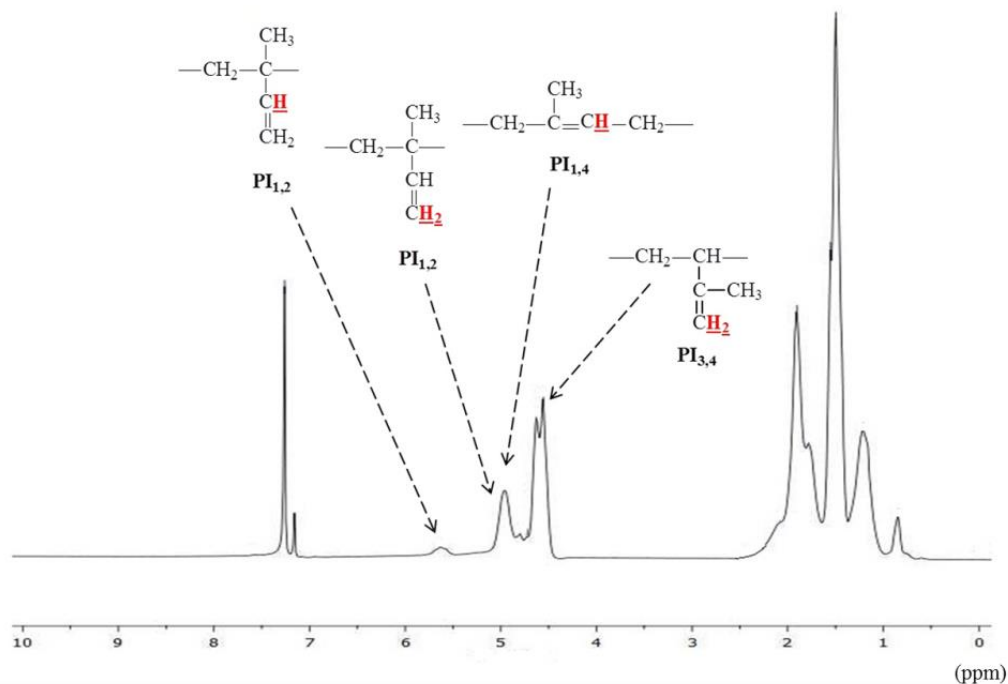


Figure 5.2: ¹H-NMR spectrum of PI_{3,4-3} linear homopolymer.

As it can be easily observed, in the ¹H-NMR spectra of the PI_{3,4-3} linear homopolymer, the experimental results are verifying the theoretically expected. Chemical shifts at 5,6-5,8 ppm corresponding to the olefinic proton of the 1,2-microstructure are evident, as well as at 5-5,2 ppm the two olefinic protons of the 1,2-microstructure and the olefinic proton of the 1,4-microstructure are exhibited and finally at 4,6-4,7 ppm the two olefinic protons of the 3,4-microstructure of PI are observed as well.

The proton chemical shifts evident at approximately 7,2-7,3 ppm correspond to the deuterated chloroform (CDCl₃) which is the solvent used to dilute the sample. The intensity of the ¹H-NMR signals is being displayed along axis y of the spectrum and is proportional to the molar concentration of the sample in the final solution studied. All the above are characteristic proton chemical shifts which confirm the high purity and homogeneity of the final materials, as well as the high 3,4-content (58-60% in all cases) of PI. Identical ¹H-NMR spectra were obtained in all four homopolymers of the PI_{3,4} type in this thesis.

The characteristic ratios of the stereochemical microstructures of PI were calculated through the integration of the area of the chemical shifts, corresponding to each microstructure. The results are in good agreement with the theoretical calculations of the chemical shifts for each microstructure and the successful synthetic procedure was confirmed. Summarizing the results of the molecular characterization of linear homopolymers of the PI_{3,4} type through SEC, MO and ¹H-NMR, the successful synthesis of all samples and the high 3,4-content was confirmed.

It is very important to mention that these samples were sent to the Morton Institute of Polymer Science and Engineering, The University of Akron, Ohio, USA, in Professor Wang's group where rheological measurements were performed along with the H-type PI_{3,4} samples whose molecular characterization results are given below.

5.2 Molecular Characterization Results of Non-Linear Homopolymers PI_{3,4}

The molecular characterization results are presented and discussed for the two (2) non-linear homopolymers PI_{3,4} of the H-type synthesized for this thesis. The synthetic procedure as mentioned in Chapter 4 involved anionic polymerization techniques and chlorosilane chemistry. In order to synthesize this type of samples it was necessary to use CDMSS [(4-chlorodimethylsilyl)styrene] as a difunctional reagent, and sequential titrations of living PI_{3,4}. After the synthesis of a 3-arm star homopolymer of the (PI₂)PI' type, dichlorodimethylsilane [(CH₃)₂SiCl₂] was used for the coupling reaction and the final preparation of the desired H-type PI_{3,4} was performed. Following the termination of the coupling reaction (approximately after 4 weeks), mass fractionation in a solvent/non-solvent (toluene/methanol) system was adopted for removal of the unreacted intermediate products. Great caution was taken in all steps of the synthetic procedure in order to achieve homogeneous and model polymers with low polydispersities.

Molecular characterization of the samples was performed again through size exclusion chromatography (SEC), membrane osmometry (MO) and proton nuclear magnetic resonance spectroscopy (¹H-NMR) as in the case of the PI_{3,4} linear homopolymers. The conditions of each technique and the solvents used were the same as described above.

SEC was used during the whole synthetic procedure in order to monitor the linking reactions in every step of the procedure and through MO the number average molecular weight of the initial arms, intermediate products and the final polymers was calculated. ¹H-NMR was used in order to confirm the desirable high 3,4-microstructure of the samples. In Table 5.3 the molecular characteristics of the precursors, intermediate products and final fractionated samples of the H-type PI_{3,4} are summarized.

Table 5.3: Molecular characteristics of the precursors, intermediates (3-arm star $PI_{3,4}$) and fractionated H-shaped poly(isoprenes).

Samples	$(\overline{M}_n)_{arm}^a$ (g/mol)	$(\overline{M}_n)_{PI_2PI'}^a$ (g/mol)	$(\overline{M}_n)_{connector}^b$ (g/mol)	$(\overline{M}_n)_{total}^a$ (g/mol)	I_{total}^c	$(\overline{M}_w)_{total}^d$ (g/mol)
H-PI_{3,4}-1	25,200	104,800	110,000	210,800	1,10	231,900
H-PI_{3,4}-2	30,600	96,000	69,900	192,300	1,06	203,800

^aMO in toluene at 35^oC, ^b $(\overline{M}_n)_{connector}$ was calculated through the equation: $(\overline{M}_n)_{connector} = [(\overline{M}_n)_{total} - (\overline{M}_n)_{arm} \cdot x4]$, ^cSEC in THF at 30^oC, ^dFrom combination of SEC and MO measurements.

As it can be observed from Table 5.3, two samples of the H-type $PI_{3,4}$ were synthesized with sufficiently high number average molecular weights, ~192,300 g/mol and 210,800 g/mol respectively. In the case of H-PI_{3,4}-1 the number average molecular weight of each arm was calculated through MO to be approximately equal to 25,000 g/mol and that of the connector ~110,000 g/mol, while in H-PI_{3,4}-2 the number average molecular weight was experimentally calculated ~30,000 g/mol and that of the connector ~96,000 g/mol respectively. The polydispersity indices in both cases were quite low, especially in H-PI_{3,4}-2 sample, indicating the homogeneity of the samples. A representative example, corresponding to sample H-PI_{3,4}-1, is given in Figure 5.3, where the chromatographs of the precursors, intermediates, unfractionated and fractionated H-PI_{3,4}-1 are shown analytically, while in Figure 5.4 the chromatographs of the final fractionated H-PI_{3,4}-1 and H-PI_{3,4}-2 are presented. The results from one sample were chosen to be presented thoroughly, due to the fact that the chromatographs of both H-type $PI_{3,4}$ homopolymers were almost identical.

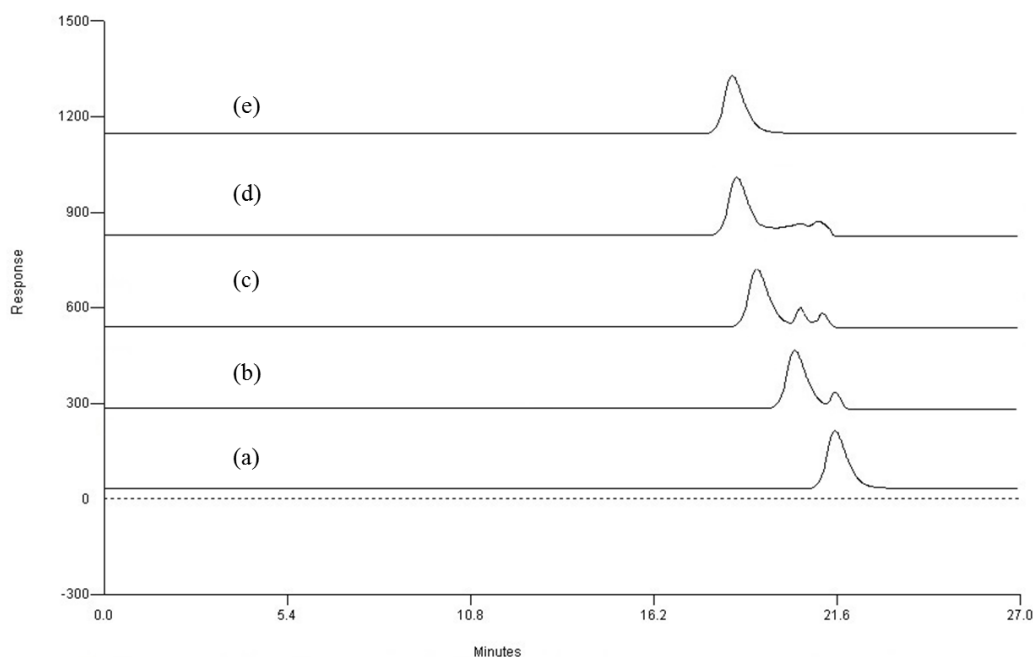


Figure 5.3: SEC chromatographs of aliquots during the synthetic procedure of H-type $PI_{3,4-1}$, where: a) corresponds to linear $PI_{3,4}$ arms, b) to macroinitiator $(PI_{3,4})_2$, c) to 3-arm star homopolymer of the $(PI_{3,4})_2PI_{3,4}'$ type, d) to unfractionated H-type $PI_{3,4-1}$ and e) to the final H-type $PI_{3,4-1}$ sample after fractionation.

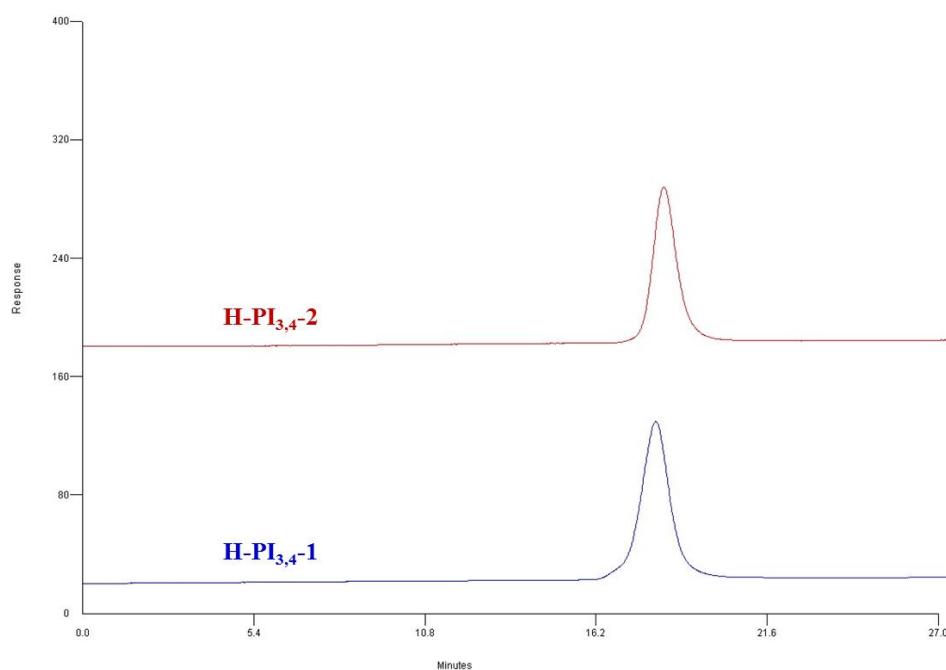


Figure 5.4: SEC chromatographs of the final fractionated H- $PI_{3,4-1}$ (indicated in blue color) and H- $PI_{3,4-2}$ (indicated in red color) respectively.

The synthesis of H-type $PI_{3,4}$ samples involved the preparation and polymerization of vinyl-functionalized monomers or macromonomers, which were synthesized by the direct termination of living polymers with a functionalized reagent.¹⁶⁰ The key factor for the

synthesis of this type of polymers was the fast reaction of the living $PI_{3,4}$ (protected through end-capping with 2-4 monomeric units of styrene) with the chlorine atom located in CDMSS than with its double bond. Previous research has shown that the nucleophilic substitution reaction of polystyryllithium with the halogens in chlorosilyl and chloromethyl groups is much faster than the addition reaction to the vinyl double bond, allowing the use of these compounds in the synthesis of macromonomers.⁷² In order to produce only the macromonomer and not a mixture of macromonomer and in-chain living polymer, the living polymer was added to the CDMSS solution dropwise in a molar ratio of $PI_{3,4}^{(-)Li^{(+)}}$ /CDMSS equal to 1:1. In that manner, a controllable substitution of the chlorine atom of CDMSS was achieved.

The next step was the addition via a second titration of the macromonomer to the living chain of $PI_{3,4}$ and not the opposite, as in the first titration. The solution of the living ends was in excess (~5-10%), compared to the macromonomer molar quantity, since in that manner, the addition through the vinyl bond of the macromonomer is successfully achieved. It should be noted that the second titration were performed very slow and under continuous stirring. As shown in the SEC chromatograph Figure 5.3(b) the successful synthesis of the macroinitiator was achieved following this technique. Nevertheless, a small amount of the living $PI_{3,4}$ was always evident due to the initial excess of the living chains of $PI_{3,4}$.

After the addition of isoprene and the completion of the polymerization (at least for 24 h), a 3-arm star of the $(PI_{3,4})_2PI_{3,4}'$ was obtained with number average molecular weight approximately equal to 105,000 g/mol [Figure 5.3(c) SEC chromatograph]. As mentioned above a small portion of undesired reactions due to the excess of living ends are also observed. The final step was the linking reaction of the living $(PI_{3,4})_2PI_{3,4}'$ star with $(CH_3)_2SiCl_2$ which is a very slow procedure (~1 month), resulting to the desired H-type $PI_{3,4}$ [Figure 5.3(d) SEC chromatograph]. It is clearly understood from the SEC chromatographs in Figure 5.3 that in order to obtain the final H-type $PI_{3,4}$ samples, fractionation techniques were adopted using a solvent (toluene)/non-solvent (methanol) system. This procedure is repeated until the complete elimination of all undesirable products is verified, as it is shown in Figure 5.4, where the chromatographs of the final fractionated H-type $PI_{3,4}$ for both samples are presented.

By observing the SEC chromatographs (Figure 5.4) of the final polymers, it is clearly understood that their molecular weight distributions are monomodal. The presence of only one peak and their low polydispersity indices indicates their chemical and compositional homogeneity as well as the absence of any undesired products from the synthetic procedure.

In order to calculate the characteristic ratios of stereochemical microstructures of each sample, 1H -NMR measurements in $CDCl_3$ at $25^{\circ}C$ were performed. As it was mentioned in the case of the linear $PI_{3,4}$ homopolymers, the ratio of each microstructure can be estimated

via $^1\text{H-NMR}$ spectroscopy (Table 5.2) due to the variable chemical shifts of different protons located at specific carbon atoms of the PI monomeric unit, corresponding to each geometric microstructure.

In Figure 5.5 the $^1\text{H-NMR}$ spectra of both final H-type homopolymers are given, where the characteristic chemical shifts of each microstructure are presented.

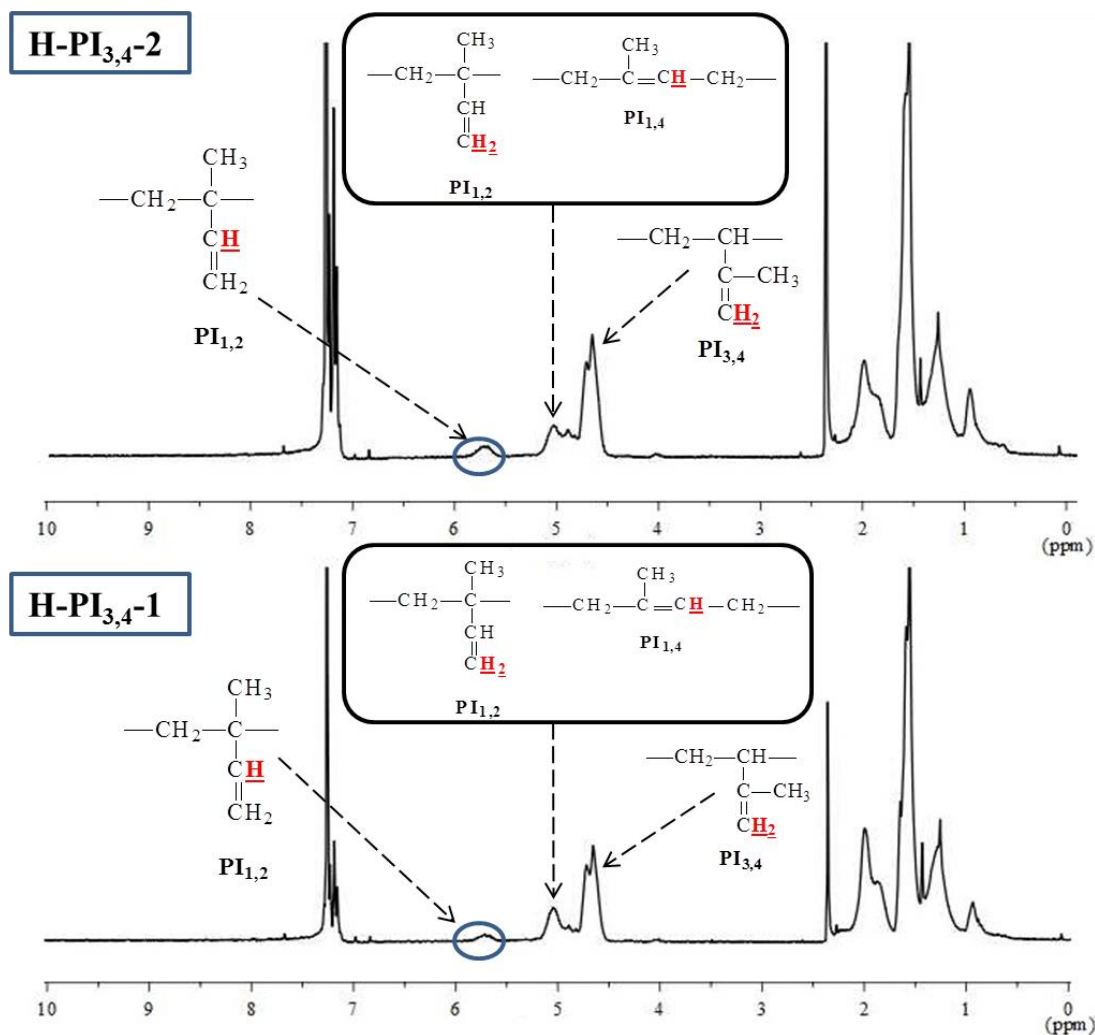


Figure 5.5: $^1\text{H-NMR}$ spectra of H-PI_{3,4}-1 and H-PI_{3,4}-2 samples respectively.

It is clearly understood from the above $^1\text{H-NMR}$ spectra that both samples exhibit high 3,4-content and through calculations of the integration of the area that corresponds to each proton chemical shift, H-PI_{3,4}-1 sample is enriched in 3,4-microstructure by a value of approximately 61%, while H-PI_{3,4}-2 exhibits ~63% 3,4-content respectively. It should be noted that the $^1\text{H-NMR}$ spectra for the final polymers are identical with those of the intermediate 3-arm stars as well as those spectra corresponding to the linear PI_{3,4} homopolymers therefore the chemical shifts are not analytically described. It should also be mentioned that the proton chemical shifts appearing at approximately 7,2-7,3 ppm correspond to the deuterated chloroform (CDCl₃) which is the solvent used to dilute each sample,

whereas the chemical shifts at 7-7,2 ppm correspond to the aromatic hydrogen atoms of CDMSS or/and to the St end-capping that was used for the protection of the initial living PI_{3,4}. In Table 5.4 the characteristic ratios of geometric isomerisms or stereochemical microstructures of each H-type sample is reported.

Table 5.4: Characteristic ratios of the different microstructures of H-type PI_{3,4} samples as were calculated by ¹H-NMR spectra.

Samples	% 3,4 microstructure	% 1,4 microstructure	% 1,2 microstructure
H-PI _{3,4} -1	61	25	14
H-PI _{3,4} -2	63	22	15

5.3 Thermal Analysis Results of Non-Linear Homopolymers PI_{3,4}

Differential scanning calorimetry is a thermo-analytical technique in which a physical property of the sample is monitored as a function of temperature, while the sample and the reference undergo a thermal treatment, either heating or cooling. DSC can provide very useful information concerning the glass transition temperature, melting point and the crystallization of a polymeric material. The glass transition temperature is referred to amorphous polymers or semicrystalline polymers with amorphous regions and is the temperature where a reversible transition occurs from an amorphous, hard and relatively brittle state into an elastomeric, rubber-like state. The transition from the glassy state to the elastomeric state is endothermic and it is not considered a phase transition. In the amorphous state, partial movements of the polymer chains in a large scale are difficult to occur. By heating the amorphous material up to the glass transition temperature, the sectional movements of the polymer chains are activated (but in total the polymer chains remain freezed) and this transition is monitored and expressed via a characteristic curve in a DSC thermograph.

The glass transition temperature (T_g) of high content *cis*-1,4 poly(isoprene) is ranging from -70⁰C to -60⁰C depending always on the ratio of *cis*- and *trans*- configurations. It has been reported in the literature¹⁶¹ that the T_g value of PI depends on the microstructure and specifically it increases linearly with increased 3,4-content and hence decreases when the 1,4-content is increased (Figure 5.6). Several factors relating to the chemical structure of polymers are known to affect the glass transition temperature. The most important is chain stiffness, which depends on the molecular weight and configuration of the polymer. In the case of poly(isoprene), molecular weight does not play a significant role and different T_g correspond to different microstructures.

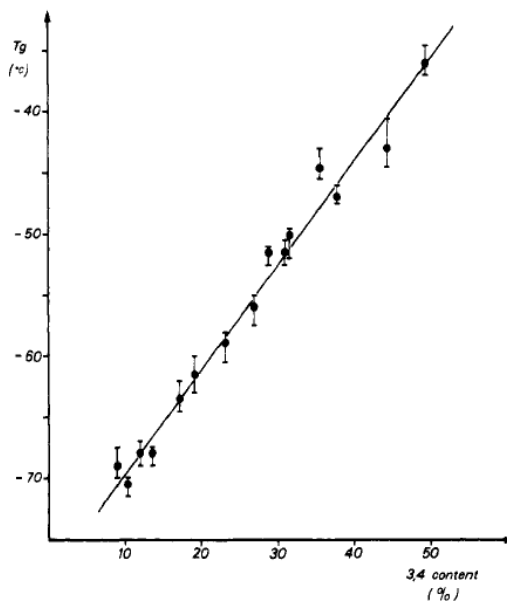


Figure 5.6: Glass transition temperature as a function of 3,4-microstructure of poly(isoprene).¹⁶¹

Concerning PI with high 3,4-content, the T_g increasement could be explained due to the steric hindrance from the side-chain vinyl group which contributes to increasing the stiffness of the polymer chains. In contrast, the high 1,4-microstructure PI exhibits low T_g values leading to more flexible polymer chains.

The thermal analysis results through DSC for the two H-type $PI_{3,4}$ homopolymers are given and discussed below. The measurements were accomplished with a Q20 TA instrument. The heating ramp was $5^{\circ}C/min$ and the temperature range from $-120^{\circ}C$ to $40^{\circ}C$. In Figures 5.7 and 5.8 the DSC thermographs for the two $PI_{3,4}$ homopolymers of the H-type are exhibited. The displayed thermographs correspond to the second heating process of each measurement which involves two heating and one cooling procedures. The first heating was performed in order to erase the history of the sample at an increased rate (commonly $10^{\circ}C/min$).

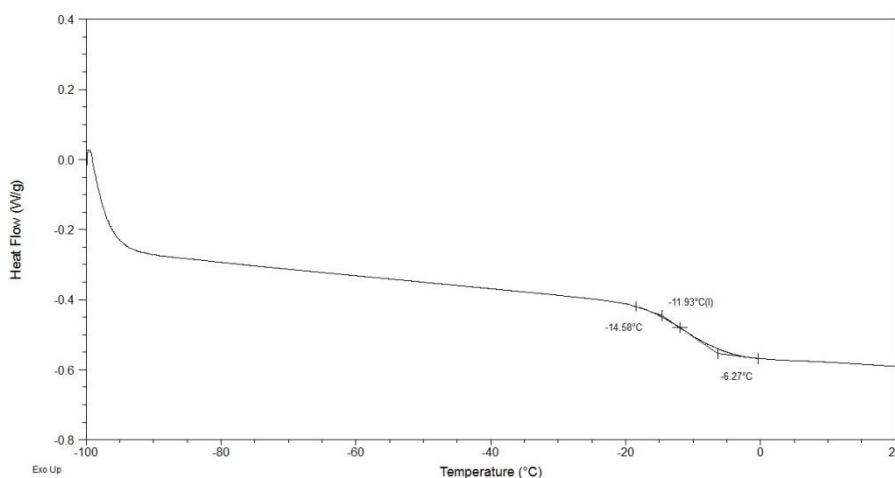


Figure 5.7: DSC thermograph of the H- $PI_{3,4-1}$ homopolymer indicating a T_g equal to $-11,93^{\circ}C$.

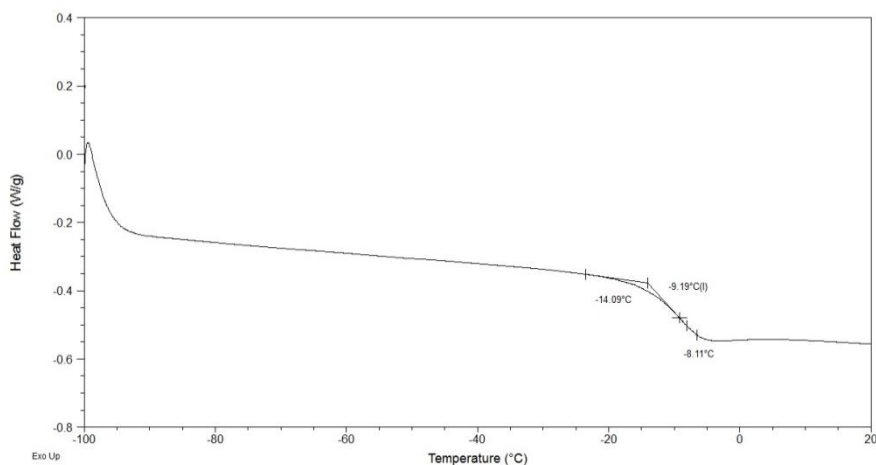


Figure 5.8: DSC thermograph of the H-PI_{3,4}-2 homopolymer indicating a T_g equal to $-9,19^{\circ}\text{C}$.

Analyzing the DSC result for the H-PI_{3,4}-1 homopolymer (Figure 5.7), an endothermic transition at approximately -12°C is observed which corresponds to glass transition temperature. No crystallization was observed but also no melting temperature (T_m) is evident, since most of the polydienes synthesized by anionic polymerization exhibit a high yield in atactic conformations and only T_g is observed in the DSC thermographs. It has been reported¹⁷ that PI with high 3,4-content ($\sim 55\%$) exhibited T_g values approximately equal to -30°C . The examined system was a linear triblock terpolymer of the BSI or SIB type where B corresponds to poly(butadiene), S to polystyrene and I to poly(isoprene) enriched in 3,4-microstructure. H-PI_{3,4}-1 sample showed increased T_g , probably due to the higher content of 3,4-microstructure ($\sim 61\%$) and the complexity of the homopolymer architecture. Similar results were obtained for the case of H-PI_{3,4}-2 homopolymer, where an endothermic transition at approximately -9°C is observed, which correspond to the glass transition temperature. In this sample the ratio of 3,4-microstructure was calculated to be equal to 63% not that significantly different from sample H-PI_{3,4}-1 but the content is well above the $\sim 55\%$ reported for the SBI sample in the literature. The glass transition temperatures along with the molecular characteristics of the non-linear homopolymers of the H-type PI_{3,4} are given in Table 5.5.

Table 5.5: Glass transition temperatures of the H-type PI_{3,4} homopolymers along with their molecular characteristics.

Samples	$(\overline{M}_n)_{arm}^a$ (g/mol)	$(\overline{M}_n)_{PI_2,PI'}^a$ (g/mol)	$(\overline{M}_n)_{total}^a$ (g/mol)	I_{total}^c	$(\overline{M}_w)_{total}^d$ (g/mol)	% 3,4 ^e microstructure	% 1,4 ^e microstructure	% 1,2 ^e microstructure	T _g ^f (°C)
H-PI_{3,4}-1	25,200	104,800	210,800	1,10	231,900	61	25	14	-11,93
H-PI_{3,4}-2	30,600	96,000	192,300	1,06	203,800	63	22	15	-9,19

^aMO in toluene at 35^oC, ^b $(\overline{M}_n)_{connector}$ was calculated through the equation: $(\overline{M}_n)_{connector} = [(\overline{M}_n)_{total} - (\overline{M}_n)_{arm} \times 4]$, ^cFrom SEC in THF at 30^oC, ^dFrom combination of SEC and MO measurements, ^e¹H-NMR measurements in CDCl₃ at 25^oC and ^fFrom DSC experiments

5.4 Rheology Results of Linear and Non-Linear Homopolymers PI_{3,4}

The rheological measurements of the high molecular weight linear homopolymers PI_{3,4} and the H-shaped PI_{3,4} homopolymers, synthesized in this thesis, are presented and discussed. It is very important to mention that all the measurements, as well as the theoretical considerations were conducted by Professor Wang's group at the Morton Institute of Polymer Science and Engineering, The University of Akron, Ohio, USA. This collaboration included rheological studies that were performed in linear and non-linear PI_{3,4} homopolymers, leading to new theoretical considerations for the non-linear dynamic behavior of long chain branching (LCB) polymers and their mixtures with the corresponding linear chains in the presence of large external deformations in either simple shear or uniaxial extension.

5.4.1 Rheology Results of Linear Homopolymers PI_{3,4}

Uniaxial extension experiments were performed in the high molecular weight linear homopolymer PI_{3,4-4} (notation given in a previous subchapter, Table 5.1), utilizing small amplitude oscillatory shear (SAOS) measurements, using a Physica MCR 301 rotational rheometer equipped with 15 mm parallel plates. All the uniaxial extension experiments were carried out in room temperature (approximately 23⁰C) using a first generation SER fixture mounted on a Physica MCR 301 rotational rheometer or a strain control rheometer ARES-LS at a constant Hencky strain rate $\dot{\epsilon}$, as well as an Instron Material Testing System (model 5543, maximum velocity: 1000 mm/min) that stretches the samples according to the literature.¹⁶²

The specimens for extension experiments were made by initially preparing solutions based on toluene followed by their casting on a PTFE plate at room temperature. The cast solutions were left under a hood for days in order to allow slow solvent evaporation prior to placing them in a vacuum oven to remove residual toluene. The typical dimensions of the sample were 21 mm × 2 mm × 0.4 mm. The molecular characteristics along with rheological properties of the PI_{3,4-4} linear homopolymer are listed in Table 5.6.

Table 5.6: Molecular characteristics and rheological properties of the PI_{3,4-4} linear homopolymer.

Sample	\overline{M}_n (g/mol)	\overline{M}_w (g/mol)	M_e (g/mol)	$\overline{M}_w / \overline{M}_n$	% 3,4- microstructure	τ (s)	G_N^0 (MPa)	Z
PI _{3,4-4}	330,000	356,000	7,100	1.08	58	2533	0.32	50

In Figure 5.9 the results from the SAOS experiments are given and exhibit the dynamic storage and loss moduli G' and G'' respectively as a function of the oscillation frequency ω , obtaining basic linear viscoelastic characteristics such as the reptation time τ and the elastic modulus G_N^0 as listed in Table 5.6 above. The number of entanglements per chain Z can be estimated as:

$$Z = \frac{\overline{M}_w}{M_e} = \frac{\overline{M}_w}{(\rho RT/G_N^0)} \quad (5.1)$$

In equation (5.1) the symbols M_e and \overline{M}_w correspond to the entanglement molecular weight and the weight average molecular weight respectively of the examined sample.

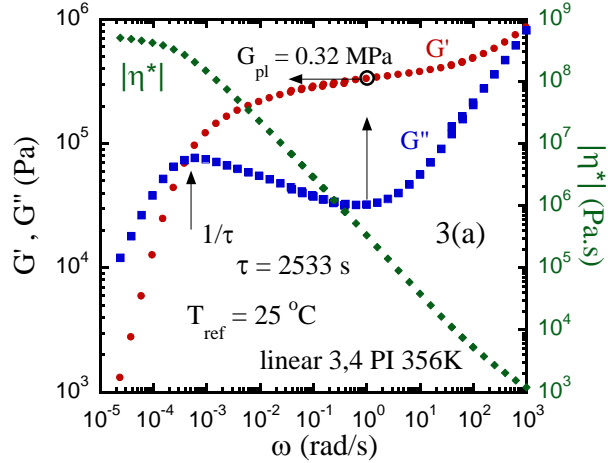


Figure 5.9: Small amplitude oscillatory shear measurements of the $PI_{3,4}$ linear homopolymer.

Through theoretical calculations and experimental results based on the above mentioned linear $PI_{3,4}$ homopolymer, a dendritic $PI_{3,4}$ homopolymer¹⁶ and a linear styrene-butadiene rubber (SBR), Prof. Wang's group¹⁶² studied the origin of 'strain hardening' when comparing the transient stress response of entangled melts to uniaxial extension with that of a simple shear. The phenomenon originates from the difference in the kinematics between shear and extension. Both linear chains and polymers containing long chain branches (LCB), show strain hardening when the uniaxial extension involves sufficiently high strain rate. The theoretical analysis showed that polymer melts would always exhibit strain hardening at sufficient high Hencky rates, due to the fact that the entanglement network can be effectively strengthened during extension and can only be weakened during shear.

Additionally, stress relaxation experiments were carried out in the linear response regime for different temperatures. Typical data are shown in Figure 5.10. The stepwise shear was produced with a high rate corresponding to the Rouse-Weissenberg number $Wi_R = \dot{\gamma}\tau_R(T) = 5$ and 2.5 respectively, where $\dot{\gamma}$ is the applied shear rate and $\tau_R(T)$ is the Rouse relaxation time at the measurement temperature T . The collapse in the four sets of stress relaxation data in Figure 5.10 confirms that the chain relaxation dynamics showed the same temperature dependence as observed from SAOS measurements. In other words, over 3 orders of magnitude in time scales, the relaxation dynamics have the same temperature dependence.¹⁶³

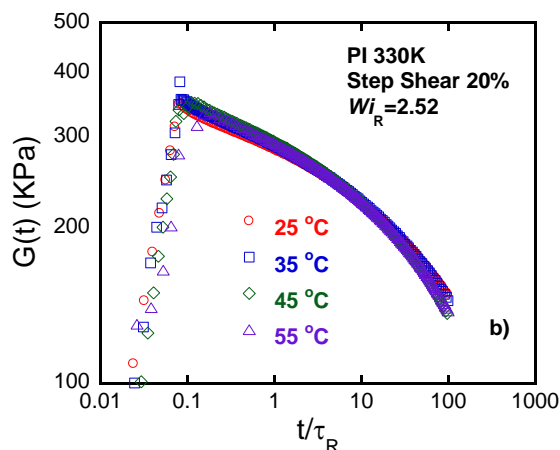


Figure 5.10: Stress relaxation curves of linear $PI_{3,4-4}$ homopolymer at four different temperatures with amplitude of 20%.

5.4.2 Rheology Results of Non-Linear Homopolymers $PI_{3,4}$

Uniaxial extension experiments were performed in the H- $PI_{3,4-1}$ homopolymer utilizing small amplitude oscillatory shear (SAOS) measurements as already reported above for the linear $PI_{3,4}$ homopolymer. The measurements were performed by Prof. Wang's group at the Department of Polymer Science, College of Polymer Science and Polymer Engineering, University of Akron, USA.

The stretching of the sample was carried out at different temperatures not a lot higher than its glass transition temperature, using a first generation SER fixture^{164,165} mounted on the ARES-LS rotational rheometer equipped with a Rheometric Scientific Oven accurate to 0.1°C. The H- $PI_{3,4}$ specimens were made from a dense H- $PI_{3,4}$ /THF solution that slowly evaporated inside a glass ring (3 cm radius) on the Kapton film. The polymer film was placed in a vacuum oven for several days, in order to remove any residual solvent prior to cutting them into dimensions of 20 mm × 2 mm × 0.5 (0.1) mm. The transient stress-strain curves of SAOS were recorded on an ARES-G2 rotational rheometer from TA Instruments, based on a pair of 8 mm parallel plates. The molecular and rheological characteristics of the sample are listed in Table 5.7.

Table 5.7: Molecular and rheological characteristics of the H- $PI_{3,4-1}$ homopolymer.

Sample	$(\overline{M}_n)_{arm}$ (g/mol)	$(\overline{M}_n)_{connector}$ (g/mol)	$(\overline{M}_n)_{Total}$ (g/mol)	M_e (g/mol)	$\overline{M}_w/\overline{M}_n$	% 3,4- microstructure	G_N^0 (MPa)	T_g (°C)
H- $PI_{3,4-1}$	25,200	110,000	210,800	7,000	1.10	61	0.28	-12

In Figure 5.11, the SAOS measurements are presented and the value of G_N^0 is obtained as G' at the frequency ω_{min} where the $\tan \delta = G''(\omega_{min})/G'(\omega_{min})$ shows a minimum. The shaded regime in the plot represents the range of effective (Hencky) rates

applied in startup extension experiments. G' and G'' are also plotted against De_e (Deborah number) as the X axis, where $De_e = \omega\tau_e$.

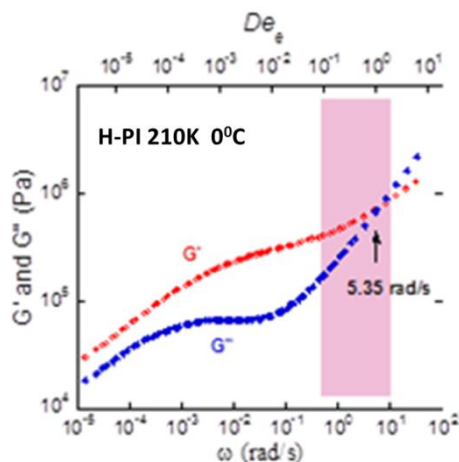


Figure 5.11: Small amplitude oscillatory shear measurements of the H-PI_{3,4}-1 homopolymer.

5.5 Molecular Characterization Results of Linear Diblock Copolymers

The molecular characterization results are presented and discussed for the five (5) linear diblock copolymers of the PB-b-PI_{3,4} type synthesized for this thesis. All samples, as already mentioned, were synthesized through anionic polymerization by using the sequential monomer addition method and high vacuum techniques. High 3,4-microstructure was adopted for all PI blocks by using a small amount (~1 mL) of a polar additive (THF). All polymerizations were performed utilizing *sec*-BuLi as initiator, benzene as the solvent and methanol as the terminating agent of the polymerization.

As it was mentioned in Chapter 4, several methods were adopted for the molecular characterization of these samples. Size exclusion chromatography (SEC) with THF as the eluent at 30°C was used extensively in order to verify the narrow molecular weight distributions of the first blocks, as well as of the final linear diblock copolymers. The instrument was always calibrated with PS standards and the results concerning the initial PB blocks and the final PB-b-PI_{3,4} diblock copolymers are not reliable. In order to verify the total number average molecular weight values for each sample, as well as the values for each PI_{3,4} block, membrane osmometry (MO) in toluene at 35°C was adopted. By combining the results

from these two characterization methods and using them in equation $I = \frac{\overline{M}_w}{\overline{M}_n}$, information

concerning the weight average molecular weight of the initial PB homopolymers and the final diblocks was obtained. Furthermore, another method used for the molecular characterization of the samples, and especially to verify the high 3,4-microstructure for the PI blocks (~55-

65%) as well as the molecular and compositional homogeneity of the samples, was proton nuclear magnetic resonance ($^1\text{H-NMR}$) spectroscopy in CDCl_3 at 25°C .

In Table 5.8 the molecular characteristics for the synthesized linear diblock copolymers are summarized. The molecular composition or mass fraction, f , was calculated via $^1\text{H-NMR}$ measurements and by using the following equations it was possible to determine the volume fraction φ of each block respectively:

$$\varphi_{PB} = \frac{f_{PB}\rho_{PI}}{f_{PB}\rho_{PI} + (1 - f_{PB})\rho_{PI}} \quad (5.2)$$

$$\varphi_{PB} + \varphi_{PI} = 1 \quad (5.3)$$

where φ_{PB} , φ_{PI} are the volume fractions of polybutadiene and poly(isoprene), f_{PB} is the mass fraction of polybutadiene and ρ_{PB} , ρ_{PI} are the densities of polybutadiene and poly(isoprene) respectively.

Table 5.8: Molecular characterization results for the linear diblock copolymers of the PB-b-PI_{3,4} type.

Samples	$(\overline{M}_n)_{PB}^a$ (g/mol)	$(\overline{M}_n)_{PI}^a$ (g/mol)	$(\overline{M}_n)_{Total}^a$ (g/mol)	I_{Total}^b	$(\overline{M}_w)_{Total}^c$ (g/mol)	f_{PB}^d	φ_{PB}^e
PB-b-PI_{3,4}-1	38,200	55,400	93,600	1.06	99,200	0,42	0,42
PB-b-PI_{3,4}-2	65,100	27,300	92,400	1.05	97,000	0,71	0,71
PB-b-PI_{3,4}-3	58,300	40,200	98,500	1.06	104,400	0,59	0,59
PB-b-PI_{3,4}-4	35,500	72,400	107,900	1.07	115,600	0,32	0,32
PB-b-PI_{3,4}-5	590,200	420,300	1,010,500	1.10	1,111,500	0,59	0,59

^aMO in toluene at 35°C , ^bSEC in THF at 30°C , ^cFrom combination of SEC and MO measurements,

^dFrom $^1\text{H-NMR}$ measurements in CDCl_3 at 25°C and ^eFrom the equation $\varphi_{PB} = \frac{f_{PB}\rho_{PI}}{f_{PB}\rho_{PI} + (1 - f_{PB})\rho_{PI}}$.

$(\overline{M}_n)_{PI}$ was calculated through the equation: $(\overline{M}_n)_{PI} = (\overline{M}_n)_{Total} - (\overline{M}_n)_{PB}$.

A variety of results can be concluded from the values in Table 5.8. The aim of this study, concerning the molecular weight of the polymers, was to keep constant the total number average molecular weight of the copolymers approximately at 100,000 g/mol. The reason was the molecular and morphological comparison of the linear diblock copolymers with the star copolymers that will be discussed later.

Furthermore, it is the first time in the literature that such diblock copolymers with the specific segments and microstructure content have been synthesized and studied morphologically with transmission electron microscopy. The only drawback that these

diblock copolymers exhibited is that they can not be studied with small-angle X-ray scattering (SAXS) due to the similar and almost identical electron density of the two segments involved.

Four of the diblock copolymers have an almost similar total number average molecular weight which varies in the region of 93,000-105,000 g/mol, while the fifth sample (PB-b-PI_{3,4}-5) exhibited high number average molecular weight (~1,000,000 g/mol). Furthermore, a variety of compositions ranging from 32% up to 71% in mass fraction for the PB block were observed in order to compare their morphological behavior with that of the well-studied PS-b-PI diblock copolymer.

The volume fractions (φ) for the two chemically different chains are approximately equal with the mass fractions (f), as they were calculated from ¹H-NMR, since the densities of PB and PI segments are almost identical (0,900 g/mL and 0,903 g/mL respectively).¹⁶⁵ There is no information in the literature concerning PI with increased 3,4-microstructure, therefore, the density used for the PI segments in this thesis is the one corresponding to PI with 90% 1,4- and 10% 3,4/1,2- microstructures. In order to verify this comment two samples (PB-b-PI_{3,4}-2 and PB-b-PI_{3,4}-3) of the five diblock copolymers synthesized were prepared as needed in order to perform small angle X-ray scattering (SAXS) experiments. The requirements were thin films with specific dimensions (thickness x diameter equal to 0.1 cm x 1 cm) and were inserted in the appropriate SAXS equipment but no matter the duration of the experiment no contrast was evident. Also, another reason for synthesizing such high molecular weights was to secure the microphase separation of the two domains during the morphological characterization since the Flory-Huggins interaction parameter, χ , of this sequence has never been calculated or reported in the literature. The only research work involving such blocks is mentioned by Avgeropoulos et al. in the literature^{17,18,136} for linear triblock terpolymers or dendritic type block co- and terpolymers respectively in which the third segment was always polystyrene.

In all cases PB was the first block, due to the fact that it is not possible to synthesize PI_{3,4}-b-PB_{1,4} taking into account all the requirements necessary in order to synthesize well-defined block copolymers as described previously in the basic concepts for anionic polymerization in Chapter 2 of this thesis. Actually, the presence of THF from the beginning of the polymerization would increase the 1,2-microstructure of PB and no microphase separation would be observed since as mentioned in section 3.3 of Chapter 3 only when the 3,4-microstructure of the PI is high (~55%) and that of the PB block was the usual one with high 1,4-microstructure (~92%) microphase separation between the two blocks could be observed (by selective and controlled staining of both chains).

The theoretical calculations for \overline{M}_n values (Equation 5.4) of the PB block were always in accordance with the experimental results obtained by membrane osmometry (MO).

$$\overline{M}_n = \frac{g_{monomer}}{moles_{initiator}} \quad (5.4)$$

Three representative examples, corresponding to samples PB-b-PI_{3,4}-3 , PB-b-PI_{3,4}-4 and PB-b-PI_{3,4}-5, are given in Figures 5.12-5.14, where the SEC chromatographs of the first PB blocks and the final diblock copolymers are shown. The initial PB blocks are indicated in blue color, while the final diblock copolymers are indicated in red color respectively.

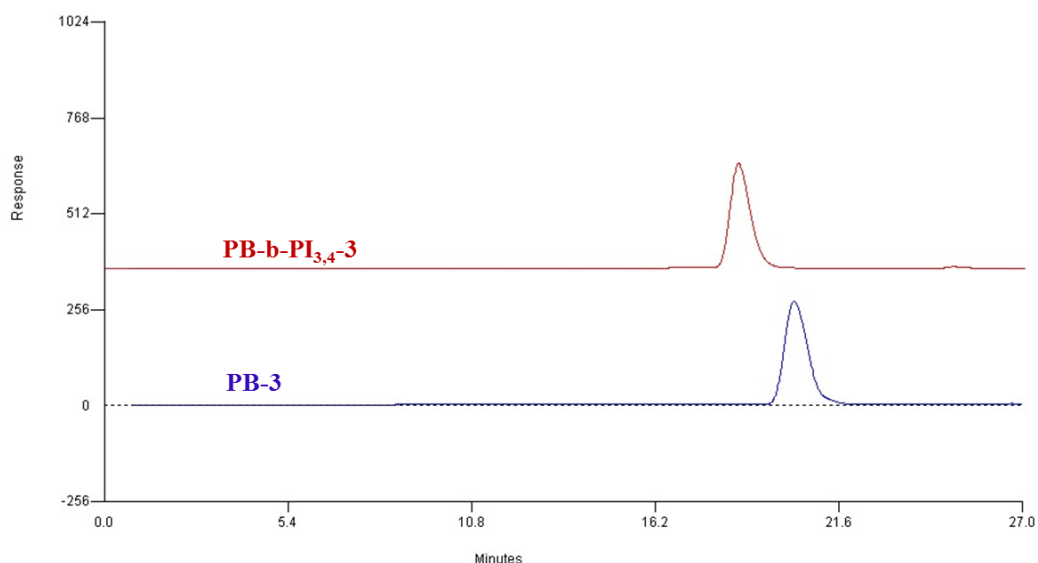


Figure 5.12: SEC chromatographs of homopolymer PB-3 (indicated in blue color) and the final diblock copolymer PB-b-PI_{3,4}-3 (indicated in red color).

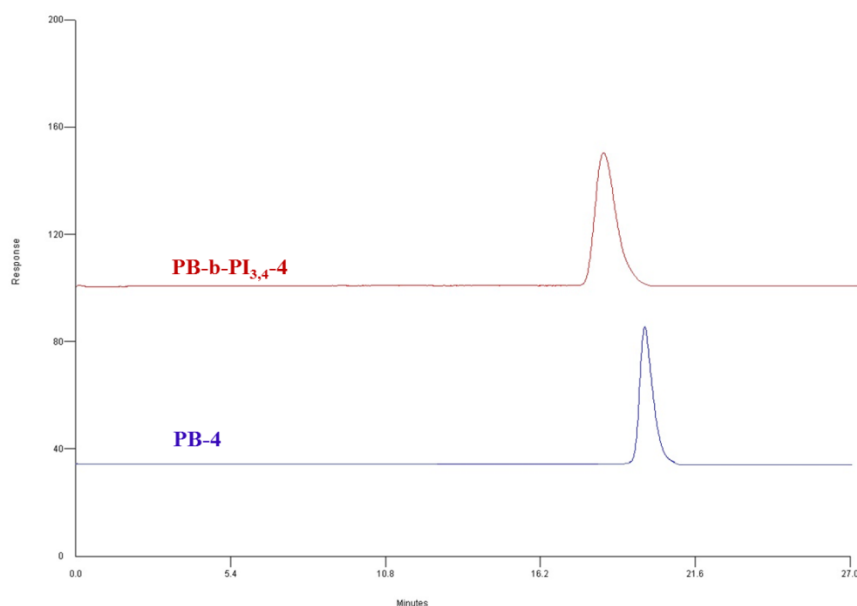


Figure 5.13: SEC chromatographs of homopolymer PB-4 (indicated in blue color) and the final diblock copolymer PB-b-PI_{3,4}-4 (indicated in red color).

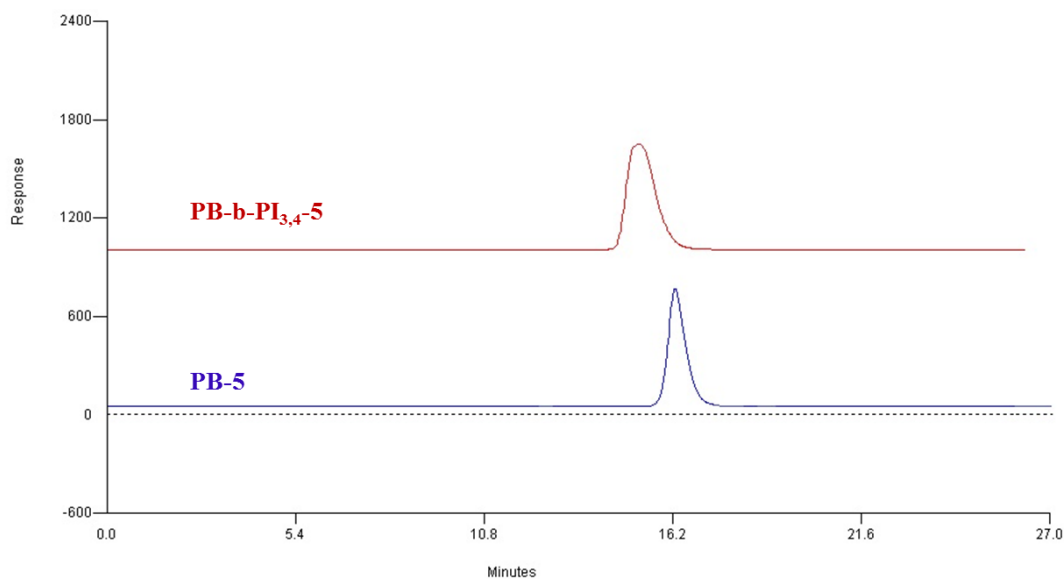


Figure 5.14: SEC chromatographs of homopolymer PB-5 (indicated in blue color) and the final diblock copolymer PB-b-PI_{3,4}-5 (indicated in red color).

By observing the SEC chromatographs (Figures 5.12-5.14) of these three linear diblock copolymers (PB-b-PI_{3,4}-3, -4 and -5), it is evident that their molecular weight distributions are monomodal. The presence of only one peak and their low polydispersity indices indicates their molecular and compositional homogeneity as well as the absence of any side and/or termination reactions during the polymerization of isoprene. In the case of PB-b-PI_{3,4}-5, the polydispersity index of the final diblock copolymer was increased compared to the other diblock copolymers, since the total number average molecular weight of the sample was sufficient high (~1,000,000 g/mol). The polymerization time was ~48 h for the formation of the PB block and another 48 h at least for completion of the isoprene polymerization. The chromatographs of the final copolymers were eluted in lower elution times compared to those of the corresponding PB blocks, indicating the successful initiation and propagation of the polymerization of the second monomer (higher final molecular weight is produced when compared with the initial PB precursor). Similar results are derived for samples PB-b-PI_{3,4}-1 and PB-b-PI_{3,4}-2 respectively.

In Figure 5.15 the SEC chromatographs of all the final diblock copolymers of the PB-b-PI_{3,4} sequence are presented.

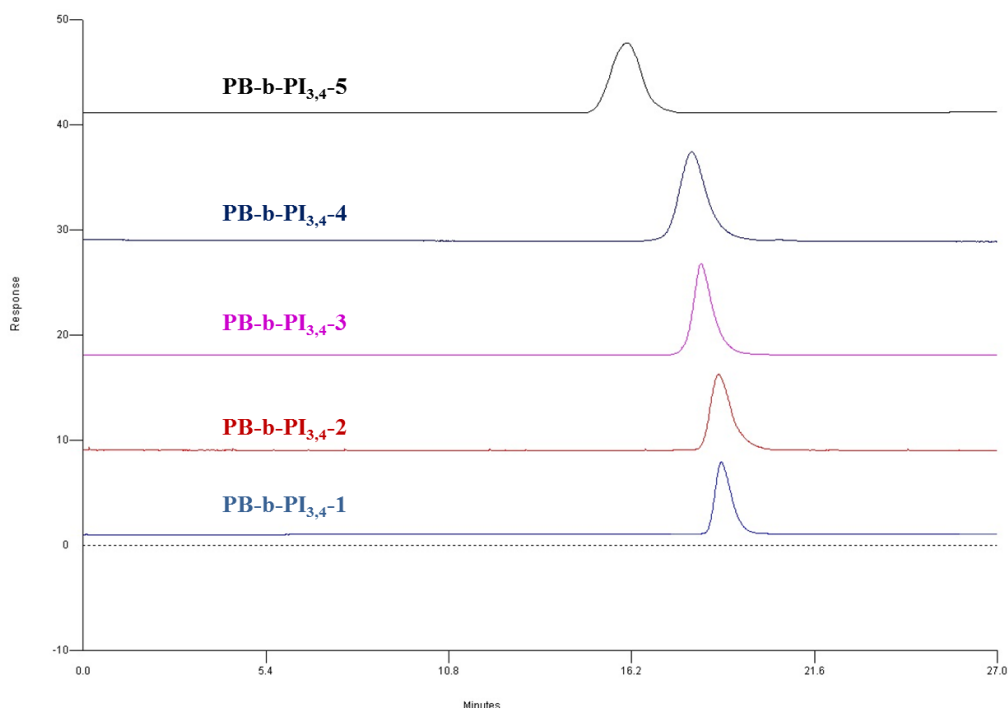


Figure 5.15: SEC chromatographs of all final diblock copolymers of the PB-b-PI_{3,4} sequence.

The monomodal molecular weight distributions of the five linear diblock copolymers of the PB-b-PI_{3,4} type, indicating high molecular and compositional homogeneity for all samples, as well as the absence of any undesired products during the synthetic procedure, are observed in Figure 5.15. It is important to mention that *this type of block copolymers are reported for the first time and have never been reported previously in the literature.*

The molecular characterization via proton nuclear magnetic resonance (¹H-NMR) spectroscopy was necessary in order to verify the composition results as produced by the average molecular weights of both blocks by combining the results from SEC and MO since the calculation of the mass fraction (f) can be derived from the ¹H-NMR spectra, as well as to confirm the existence of the desirable 3,4-microstructure at high values (> 55%) for the PI segments of the linear diblock copolymers.

In Table 5.9 all the proton chemical shifts for PB and PI are given. As it is evident, the ratio of each microstructure can be estimated via ¹H-NMR spectroscopy since, according to Table 5.9, different protons generate different chemical shifts in a corresponding ¹H-NMR spectrum.

Table 5.9: Type and number of protons with the corresponding chemical shifts for protons incorporated in the monomeric units of polybutadiene and poly(isoprene).

Polymeric chain	Geometric Isomerism	Type and Number of Protons	Chemical Shift (ppm)
PB	1,4	Olefinic (2)	5,35
		Olefinic (1)	5,60
	1,2	Olefinic (2)	4,95
PI	1,4	Olefinic (1)	5,12
	3,4	Olefinic (2)	4,70
		Olefinic (1)	5,82
	1,2	Olefinic (2)	5,00

High 3,4-microstructure (60-65%) was obtained for the PI blocks of the five linear diblock copolymers, while all PB blocks were enriched in 1,4-microstructure (90-92%) as it expected, through $^1\text{H-NMR}$ measurements. Specifically, in the synthesis procedure via anionic polymerization in the absence of polar solvent media, the resultant microstructure of PB segments is 90-92% 1,4- and 8-10% 1,2-, while for PI segments is 90% 1,4- (usually 70% *cis*- and 20% *trans*-) and 10% 3,4- as already reported in the literature. After the completion of the polymerization of 1,3-butadiene and prior to the polymerization of isoprene, a small amount of THF (~1 mL) was added in the solution. The resultant microstructure of the PI segments is enriched in 3,4-content and the 1,2-microstructure is increased as well (10-15%), while the 1,4-microstructure is sufficiently decreased (25-30%).

A $^1\text{H-NMR}$ spectrum, except from the molar ratio of the microstructure, can also provide information for the composition of a copolymer since through specific proton chemical shifts the molar ratio for the segments maybe calculated and therefore eventually the calculation of the number average molecular weight is possible. Such a procedure is possible by calculating the molar ratio (% moles) of each block through the following equation:

$$X_A = \frac{\alpha_A}{\beta} \quad (5.5)$$

where X_A is the molar ratio (% moles) of A block, α_A is the area of the peaks corresponding to the specific proton chemical shifts in the $^1\text{H-NMR}$ spectrum for A block and β is the number of protons that cause the particular chemical shift. Specifically in the case of PB-b-PI_{3,4} diblock copolymers, overlapping effect is unavoidable in some proton chemical shifts, especially for those corresponding to the one olefinic proton of 1,2-PB at ~5,60 ppm with the one olefinic proton of 1,2-PI at ~5,82 ppm. Furthermore, the chemical shifts that correspond

to the one olefinic proton of 1,4-PI at ~5,12 ppm, the two olefinic protons of 1,2-PI at ~5,00 ppm and the two olefinic protons of 1,2-PB at ~4,95 ppm are as well overlapped leading to rather difficult calculations of the various microstructures content for each segment. Despite the overlapping by using the data from Table 5.9 in equation 5.5 and well resolved proton chemical shifts in the ¹H-NMR spectra, the following equations can be derived:

$$X_{PB_{1,4}} = \frac{a_{5,35}}{2} \quad (5.6)$$

$$X_{PB_{1,2}} + X_{PI_{1,2}} = \frac{a_{5,60-5,82}}{2} \quad (5.7)$$

$$X_{PI_{3,4}} = \frac{a_{4,70}}{2} \quad (5.8)$$

$$X_{PI_{1,4}} + X_{PI_{1,2}} + X_{PB_{1,2}} = \frac{a_{4,95-5,12}}{5} \quad (5.9)$$

$$X_{PB} = X_{PB_{1,4}} + X_{PB_{1,2}} \quad (5.10)$$

$$X_{PI} = X_{PI_{1,4}} + X_{PI_{3,4}} + X_{PI_{1,2}} \quad (5.11)$$

Through the combination of the above equations (there are six equations with only five unknown values which should be calculated) the 1,2-, 1,4-content of both blocks and the 3,4-content of PI segment can be calculated. From the ¹H-NMR results of the initial PB block involving the molar ratios of the 1,4- and 1,2-microstructures, the determination of the weight ratio (% wt) or mass fraction (*f*) is possible, by multiplying each *X* value with the molecular weight of the corresponding monomer unit according to the equation:

$$\% \text{ wt} = \frac{X_A \times MW_A}{C} \quad (5.12)$$

where *MW_A* is the molecular weight of the monomer unit for A block and parameter *C* is given by $C = X_{PB} \times MW_{PB} + X_{PI} \times MW_{PI}$, with *MW_{PB}* = 54 g/mol and *MW_{PI}* = 68 g/mol respectively. The mass fractions of PB and PI as calculated by ¹H-NMR along with the characteristic microstructure content of each block are presented in Table 5.10. In all samples, the 3,4-microstructure of PI is ranging from 57% to 62%, while the mass fraction of the PB block obtained values ranging from 0,32 up to 0,71.

Table 5.10: Mass fractions and characteristic microstructures content of each block, as calculated by $^1\text{H-NMR}$ spectroscopy results.

Samples	f_{PB}	f_{PI}	% 1,4-PB	% 1,2-PB	% 3,4-PI	% 1,4-PI	% 1,2-PI
PB-b-PI _{3,4} -1	0,42	0,58	91	9	58	29	13
PB-b-PI _{3,4} -2	0,71	0,29	92	8	57	30	13
PB-b-PI _{3,4} -3	0,59	0,41	92	8	60	28	12
PB-b-PI _{3,4} -4	0,32	0,68	90	10	62	23	15
PB-b-PI _{3,4} -5	0,59	0,41	91	8	57	31	12

Two representative examples, corresponding to samples PB-b-PI_{3,4}-2 and PB-b-PI_{3,4}-4 are given in Figures 5.16 and 5.17, where the $^1\text{H-NMR}$ spectra of the initial PB blocks and the final diblock copolymers are presented. The choice of these samples was made in order to present a $^1\text{H-NMR}$ spectrum of a diblock copolymer with high values of PB mass fraction (PB-b-PI_{3,4}-2) and the other being a sample with high values of PI mass fraction (PB-b-PI_{3,4}-4) in order to observe the differences in the height of the specific proton chemical shifts in each case through which the molar fraction is calculated.

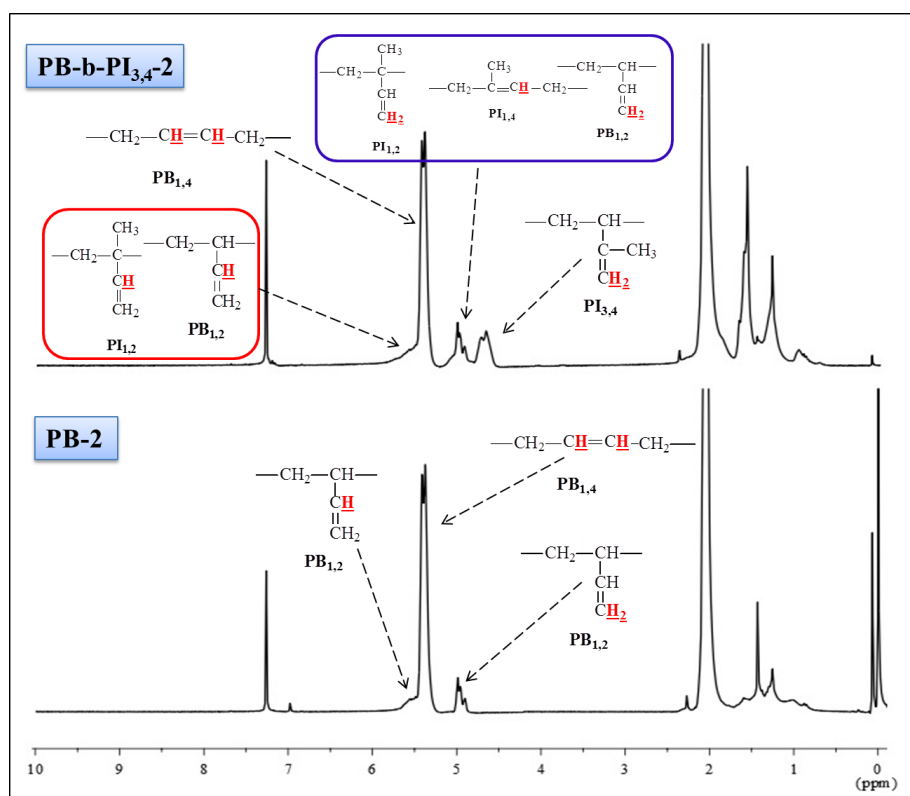


Figure 5.16: $^1\text{H-NMR}$ spectra of the initial homopolymer PB-2 and the final diblock copolymer PB-b-PI_{3,4}-2.

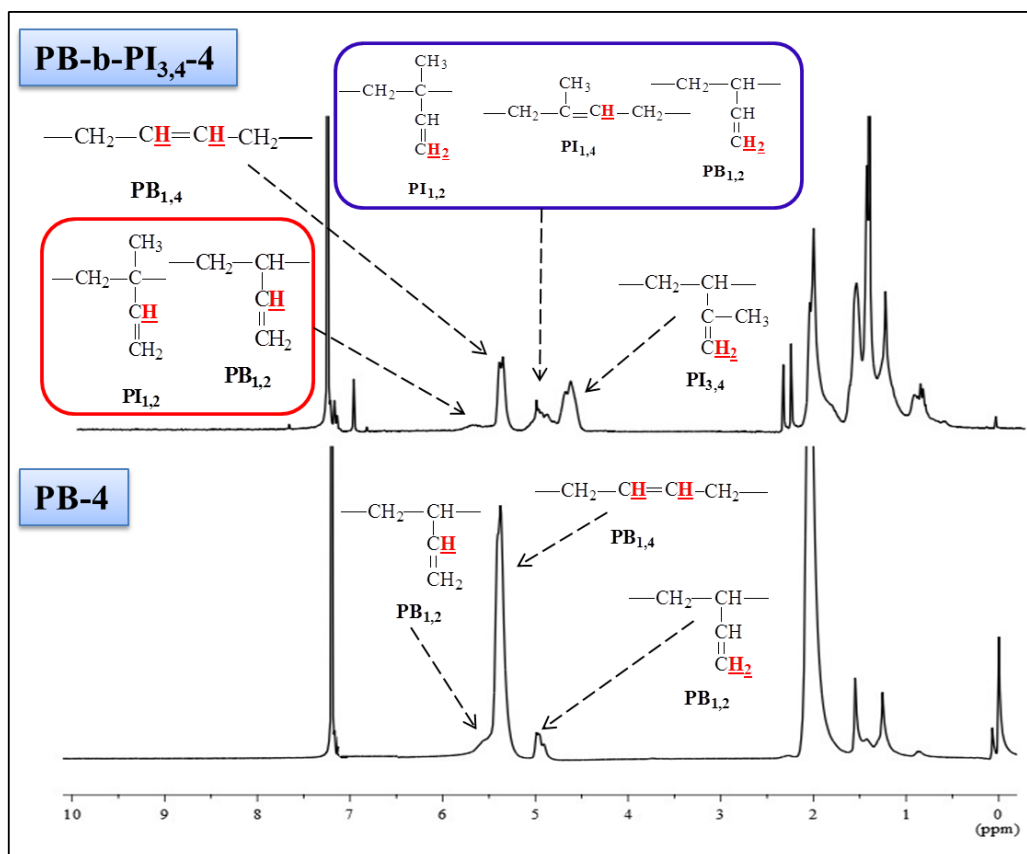


Figure 5.17: $^1\text{H-NMR}$ spectra of the initial homopolymer PB-4 and the final diblock copolymer $\text{PB-b-PI}_{3,4-4}$.

The intensity of the $^1\text{H-NMR}$ signals is displayed along the vertical axis of a spectrum and is proportional to the molar concentration of the sample. It is clearly understood from the above $^1\text{H-NMR}$ spectra that in both linear diblock copolymers, PI exhibits high 3,4-content and through calculations by using the equations mentioned above (equations 5.6-5.12), $\text{PB-b-PI}_{3,4-2}$ sample is enriched in 3,4-microstructure by a value of approximately 57%, while $\text{PB-b-PI}_{3,4-4}$ exhibits ~62% 3,4-content respectively.

Furthermore, the PB block exhibits high 1,4-microstructure ~92% in sample $\text{PB-b-PI}_{3,4-2}$, whereas in $\text{PB-b-PI}_{3,4-4}$ the PB block exhibits ~90% 1,4-content. The values of mass fractions of PB for $\text{PB-b-PI}_{3,4-2}$ and $\text{PB-b-PI}_{3,4-4}$ were calculated to be 0,71 and 0,32 respectively. It should be mentioned that the proton chemical shifts appearing at approximately 7,2-7,3 ppm correspond to the deuterated chloroform (CDCl_3) which is the solvent used to dilute each sample. Similar $^1\text{H-NMR}$ spectra were obtained for the remaining three linear diblock copolymers of the $\text{PB-b-PI}_{3,4}$ type and the obtained results are thoroughly exhibited in Table 5.10.

5.6 Thermal Analysis Results of Linear Diblock Copolymers

Differential scanning calorimetry was employed for the thermal analysis of the five linear diblock copolymers of the PB-b-PI_{3,4} type. DSC can provide very useful information concerning the glass transition temperature, melting point and the crystallization of a polymeric material. The specific technique may also provide useful information concerning the glass transition temperature of block copolymers and conclusions concerning the miscibility of the blocks involved in the examined material can be derived. More specifically for a diblock copolymer, if two glass transition temperatures exist, similar in value to the glass transition temperatures of the corresponding homopolymers, then the two different blocks are considered immiscible and during self-assembly they will lead to well-defined microphase separation. If three different glass transition temperatures exist (two slightly different from the values for the corresponding homopolymers and one somewhere in between), then the two blocks are miscible and the morphological studies will lead to weakly separated phases due to partial mixing. Finally, when only one glass transition temperature appears with a value between the glass transition temperature of the two blocks, it indicates that there is a homogenous mixture of these two components with no phase separation.

Fox and Flory¹⁶⁷ established a relationship between T_g and the number average molecular weight of a polymer. This equation is presented below:

$$T_g = T_g^\infty - K \overline{M}_n^{-1} \quad (5.13)$$

where, T_g^∞ is the glass transition temperature of a polymer with infinite \overline{M}_n and K is a constant characteristic of a given polymer. This equation indicates that beyond a significant value of \overline{M}_n (~20,000 g/mol), the T_g of a polymer is equal to T_g^∞ and therefore will not be affected by the number average molecular weight when that is relatively high in value (as is evident from the molecular characteristics for both blocks in Table 5.8 the lowest \overline{M}_n for the PB block is 35.500 g/mol and 27.300 g/mol for the PI, therefore no dependence from the molecular weight should be evident for the T_g values of both blocks for all five diblock copolymers of the PB-b-PI_{3,4} sequence.

The glass transition temperature (T_g) of PB_{1,4} (90-92% 1,4-microstructure) is ranging from -90⁰C to -85⁰C, while the T_g of PI varies from -30⁰C to -10⁰C, depending on the high content of the 3,4-microstructure of the PI blocks, as already mentioned. For comparison reason the T_g value of PI blocks synthesized in non-polar solvent media, therefore exhibiting high 1,4-microstructure (90-92%), is approximately equal to -60⁰C, well below to the value for the PI_{3,4} blocks synthesized in all samples of this thesis.

The measurements were accomplished with a Q20 TA instrument. The heating ramp was 5⁰C/min and the temperature range from -120⁰C to 40⁰C for all heating and cooling cycles.

In Figures 5.18-5.22 the DSC thermographs for the five linear diblock copolymers synthesized for this thesis are given. The displayed thermographs correspond to the second heating procedure of each measurement. The first heating was performed in order to erase the history of the sample at a specific rate (commonly 10⁰C/min).

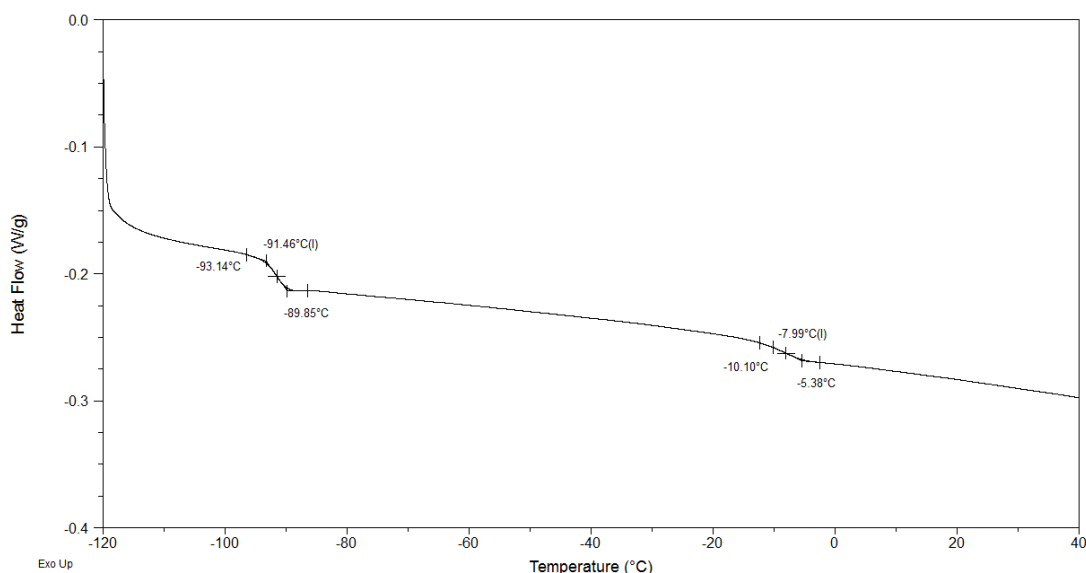


Figure 5.18: DSC thermograph of the PB-b-PI_{3,4}-1 diblock copolymer indicating T_g of PB equal to -91,46⁰C and T_g of PI_{3,4} equal to -7,99⁰C respectively.

Analyzing the DSC results for sample PB-b-PI_{3,4}-1 (Figure 5.18), two endothermic transitions at approximately -91⁰C and -8⁰C are observed which correspond to the glass transition temperatures of PB and PI_{3,4} respectively. The relatively high value of the T_g of PI_{3,4} is due to the high 3,4-content (~57%). Crystallization and melting point temperature (T_m) are not evident in the thermograph, in the temperature regime used for the DSC experiment. The existence of two glass transition temperatures, similar to the glass transition temperatures of the corresponding homopolymers, leads to the conclusion that the two different blocks are totally immiscible.

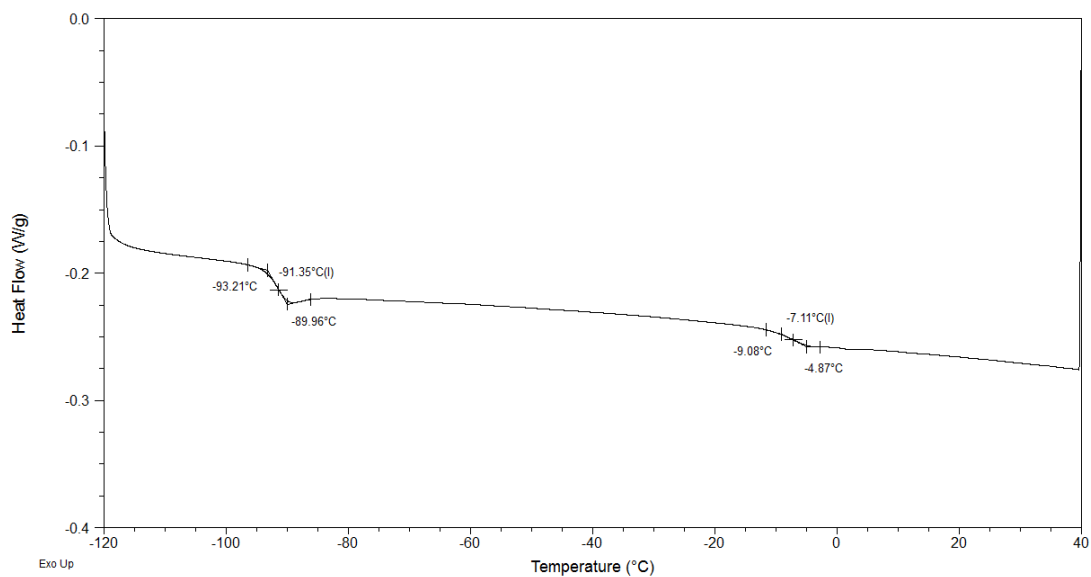


Figure 5.19: DSC thermograph of the PB-*b*-PI_{3,4}-2 diblock copolymer indicating T_g of PB equal to $-91,35^{\circ}\text{C}$ and T_g of PI_{3,4} equal to $-7,11^{\circ}\text{C}$ respectively.

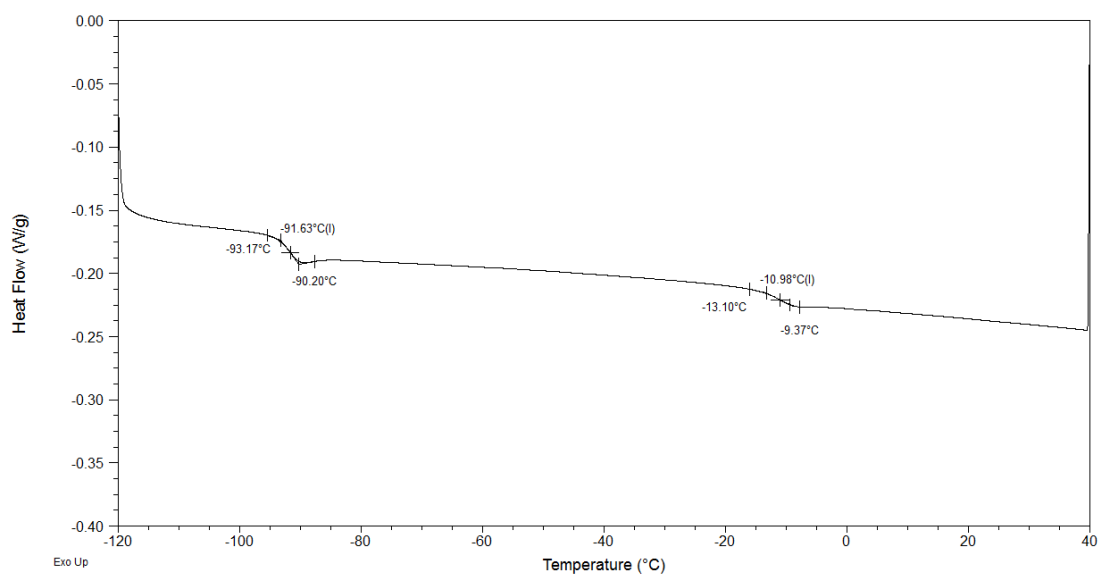


Figure 5.20: DSC thermograph of the PB-*b*-PI_{3,4}-3 diblock copolymer indicating T_g of PB equal to $-91,63^{\circ}\text{C}$ and T_g of PI_{3,4} equal to $-10,98^{\circ}\text{C}$ respectively.

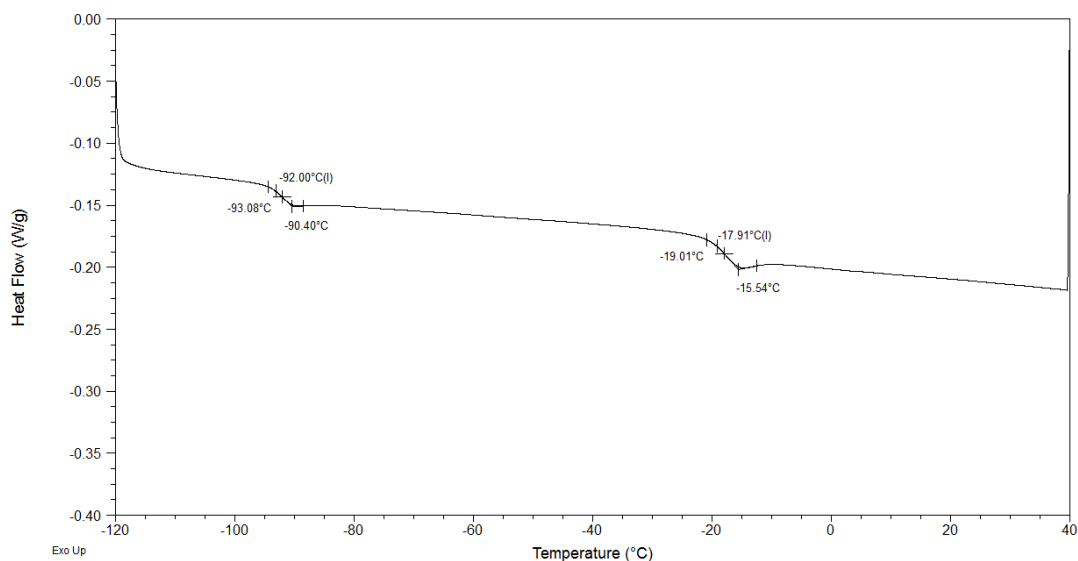


Figure 5.21: DSC thermograph of the PB-b-PI_{3,4}-4 diblock copolymer indicating T_g of PB equal to -92°C and T_g of PI_{3,4} equal to $-17,91^{\circ}\text{C}$ respectively.

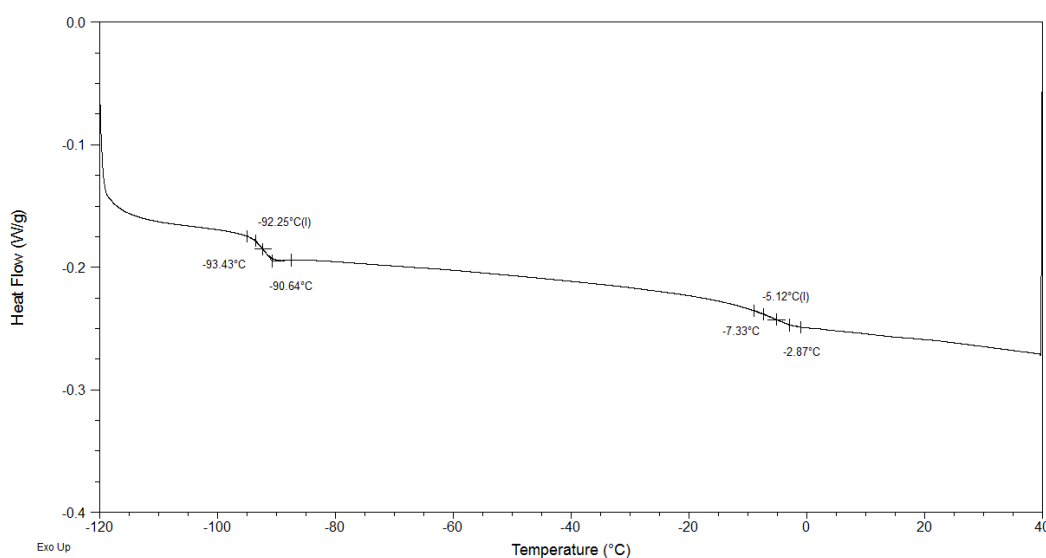


Figure 5.22: DSC thermograph of the PB-b-PI_{3,4}-5 diblock copolymer indicating T_g of PB equal to $-92,25^{\circ}\text{C}$ and T_g of PI_{3,4} equal to $-5,12^{\circ}\text{C}$ respectively.

Analyzing the DSC results for the other four samples (PB-b-PI_{3,4}-2, PB-b-PI_{3,4}-3, PB-b-PI_{3,4}-4 and PB-b-PI_{3,4}-5) (Figures 5.19-5.22) two endothermic transitions were obtained as well in each case, corresponding to the glass transition temperatures of PB and PI_{3,4} respectively.

A major discrepancy to the glass transition temperature of the PI block is exhibited for sample PB-b-PI_{3,4}-4 where the T_g value of PI_{3,4} was calculated approximately equal to -18°C . This low value, maybe attributed to the fact that this sample is the only one with very high volume fraction in PI, (0,68). The 3,4-content for the PI in this case is approximately 62% (the highest among the other diblock copolymers, Table 5.10) and it was expected to

obtain a higher $(T_g)_{PI}$ value in controversy to what was observed for the corresponding values in the other three diblock copolymers with similar number average molecular weights. This differentiation in value may also be attributed to the fact that the PI in the specific sample exhibits the lowest 1,4-content (23%) and the highest -1,2 (15%), when compared with the other diblock copolymers. Furthermore, the T_g values obtained for the high molecular weight PB-b-PI_{3,4} sample were approximately equal to those of the aforementioned similar in block sequence diblocks. Two glass transitions were evident: -92°C for the PB block and -5°C for the PI block respectively (Figure 5.22). Therefore, although the total number average molecular weight of the sample is sufficient high, approximately an order of magnitude, it is evident that due to the flexibility of the chains and the basic property of the specific materials (100% elastomers) the glass transitions are not affected. These results led to the conclusion that in very high molecular weights, the T_g is still independent from the number average molecular weight, as described by Fox and Flory equation (Equation 5.13) despite the questionable effect of the limited configurational rotations of the larger chain segments without interfering with the chain in total, due to the increased molecular characteristics of the sample.

In all samples, the existence of two glass transition temperatures, led to the conclusion that the two different blocks are completely immiscible. The glass transition temperatures along with the molecular characteristics of the linear diblock copolymers of the PB-b-PI_{3,4} type are summarized in Table 5.11.

Table 5.11: Glass transition temperatures (T_g) of the linear diblock copolymers along with their molecular characteristics.

Samples	$(\overline{M}_n)_{PB}^a$ (g/mol)	$(\overline{M}_n)_{PI}^a$ (g/mol)	$(\overline{M}_n)_{Total}^a$ (g/mol)	$(\overline{M}_w)_{Total}^c$ (g/mol)	I_{Total}^b	f_{PB}^d	φ_{PB}^e	$(T_g)_{PB}^f$ (°C)	$(T_g)_{PI}^f$ (°C)
PB-b-PI_{3,4}-1	38,200	55,400	93,600	99,200	1.06	0,42	0,42	-91,46	-7,99
PB-b-PI_{3,4}-2	65,100	27,300	92,400	97,000	1.05	0,71	0,71	-91,35	-7,11
PB-b-PI_{3,4}-3	58,300	40,200	98,500	104,400	1.06	0,59	0,59	-91,63	-10,98
PB-b-PI_{3,4}-4	35,500	72,400	107,900	115,600	1.07	0,32	0,32	-92,00	-17,91
PB-b-PI_{3,4}-5	590,200	420,300	1,010,500	1,111,500	1.10	0,59	0,59	-92,25	-5,12

^aMO in toluene at 35°C, ^bSEC in THF at 30°C, ^cFrom combination of SEC and MO measurements, ^dFrom ¹H-NMR measurements in CDCl₃ at 25°C ,

^eFrom the equation: $\varphi_{PB} = \frac{f_{PB}\rho_{PI}}{f_{PB}\rho_{PI} + (1 - f_{PB})\rho_{PI}}$ and ^fFrom DSC experiments.

$(\overline{M}_n)_{PI}$ was calculated through the equation: $(\overline{M}_n)_{PI} = (\overline{M}_n)_{Total} - (\overline{M}_n)_{PB}$.

5.7 Morphological Characterization Results for the Linear Diblock Copolymers

The morphological characterization of the linear diblock copolymers synthesized for this thesis was accomplished by transmission electron microscopy (TEM) studies. Transmission electron microscopy (TEM)^{168,169} is a technique where an electron beam is used in order to observe images of samples in the nanoscale. The main advantage of using electrons instead of light is that they provide at least three (3) orders of magnitude increased resolution since they are smaller than atoms. The resolution provided by a visible-light microscope is in most approximately 200 nm, while for an electron microscope it can go down as low as 0.1 nm or lower depending on the accelerating voltage. Many of the features that control the properties of materials are in a scale well below 200 nm, therefore, the need in nano-materials science and engineering to image their structure, even down to atomic level is a necessity in order to understand and ultimately control the properties of various types of materials. In electron microscopy, the sample is exposed to an electron beam and through the interaction of the electrons with the sample, information for its structure is received.

Magnetic lenses are used in order to focus the electron beam on the studied specimen each time. Electrons have a wavelength ($<0,1$ nm) up to 100,000 times smaller than visual light (~ 560 nm). The result is that objects can be detected 400-1000 times better than optical microscopes and 200,000 times better than the human eye with magnifications up to 1,000,000 times without the loss of any details. A major issue is that the human eye cannot see these specific wavelengths, therefore, a screen is needed (e.g. monitor or special photographic film) in which the electron collision is transformed to visible irradiation transmittance. It should be noticed that the electron wave length depends on the accelerating voltage of the instrument and therefore higher kV concludes to smaller electron wave lengths and eventually better resolved images even in high magnifications.

The use of electrons instead of X-rays is enforced since it is necessary to focus the beam whereas X-rays interact very weakly with matter and cannot be focused. Electron beams can be focused with the use of special magnetic lenses (e.g. condenser lens).

The image that appears on the viewing screen of a TEM depends on the image contrast. The electron beam can change both its amplitude and phase as it goes through the specimen and both types of change lead to image contrast. Thus, a fundamental distinction that is made in the TEM is between amplitude and phase contrast. In most cases, both contrasts contribute to an image but there is a tendency to select conditions in order for only one to dominate. There are two principal types of amplitude contrast: mass-thickness and diffraction contrast. Mass-thickness contrast is resulted from variations in mass or thickness of the specimen or a combination of both due to the fact that electrons interact, by incoherent elastic scattering, with more or less material which means more or less mass. Alternatively, diffraction contrast rises from coherent elastic scattering and can only vary locally since the

specimen is not a perfect, uniformly thin film. Consequently, thicker or less crystallized areas of the specimen scatter electrons more and appear darker.

Polymers are very sensitive in the electron beam. Enhanced exposure at the electron beam may cause the polymers to degrade, crosslink and loose mass or even loose the whole specimen due to its sensitivity in the electron beam. Furthermore, polymers are composed from compounds which are almost chemically identical and therefore the blocks involved exhibit in most cases almost identical electron density leading to low contrast and microphase separation is not evident. The contrast in bright field microscopy is due to thickness contrast and the change in the atomic number (difference in electron density).

There are several ways to increase mass-thickness contrast by using smaller objective apertures, by alternating the beam accelerating voltage or by chemically staining the sample with specific stainings such as heavy metal oxide compounds [e.g. osmium tetroxide (OsO_4) or ruthenium tetroxide (RuO_4)]. Staining involves the incorporation of electron dense atoms into the polymer structure in order to increase the density through crosslinking and thus enhance the image contrast.

In block copolymers where one of the blocks is a polydiene, the most commonly used staining compound are diluted vapors of osmium tetroxide (OsO_4) in an aqueous solution which react with the carbon-carbon double bonds enhancing the image contrast due to cross-linking and the electron scattering due to the heavy metal. This cross-linking is a chemical reaction which causes hardening and increased density for the stained polymer chains. The high vapor pressure of OsO_4 is beneficial, making vapor staining of sample sections possible. However, this vapor pressure, along with the toxicity of the compound and the limited exposure time, makes it extremely dangerous to handle and appropriate care must be taken. The reaction that takes place is shown in Figure 5.23:

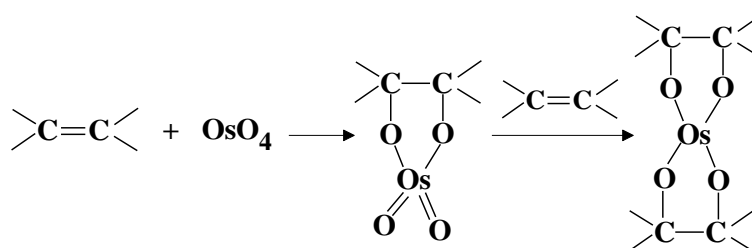


Figure 5.23: Chemical reaction of osmium tetroxide (OsO_4) with the double C-C bonds of a polydiene.

The result of this staining is that the polydiene phases appear darker while the phases of the other blocks appear brighter. This method is commonly used in polystyrene-polydiene copolymers since OsO_4 does not react with polystyrene. Similar results are provided with ruthenium tetroxide (RuO_4) vapors which reacts with polystyrene by destroying the aromatic ring of the PS monomeric units (Figure 5.24) indicating the extreme reactivity of the stainer.

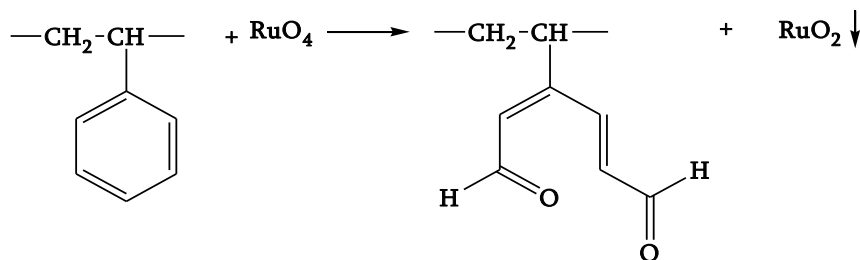


Figure 5.24: Chemical reaction of ruthenium tetroxide (RuO_4) with the aromatic ring of the PS monomeric units indicating its high reactivity.

From this result it is easily understood that RuO_4 cannot be used in cases where all blocks of the specimen bear double bonds since all will be stained and the final TEM image will be a homogeneous dark phase. Therefore, it is evident that the stainers should be used with caution, extreme care but also with understanding of what their result will be in the studied specimen. There are various types of stainers used in polymer science depending on the type of segments and the atoms present per monomeric unit of each block.¹⁶⁹

Except from TEM, small angle X-ray scattering (SAXS) is an important technique for the morphological characterization of block copolymers in order to verify the observed structure by TEM morphology. Both TEM images and SAXS plots can provide unique information concerning the microphase separation of linear diblock copolymers and their structure/properties relationship. Nevertheless, in this study it was not possible to employ SAXS, since the electron densities of PB and PI are considered equivalent.¹⁷⁰

A wide variety of volume fractions was targeted and synthesized in order to study the alternations of microphase separation of PB-*b*-PI_{3,4} type linear diblock copolymers in regard with the variation in composition, the interaction parameter χ and the different values of molecular weight. The total number average molecular weight of the four linear diblock copolymers was kept constant, ranging from 92,000-107,000 g/mol as it is evident from Tables 5.8 and 5.11, where the molecular characteristics of the specific diblock copolymers are given. The degree of polymerization N for a linear diblock copolymer can be easily calculated from the following equation:

$$N_{PB-b-PI_{3,4}} = N_{PB} + N_{PI_{3,4}} = \frac{\overline{M}_n^{PB}}{M_0^{PB}} + \frac{\overline{M}_n^{PI}}{M_0^{PI}} \quad (5.14)$$

where $M_0^{PB} = 54$ g/mol, is the molecular weight of 1,3-butadiene (monomer of PB) and $M_0^{PI} = 68$ g/mol, is the corresponding molecular weight of isoprene (monomer of PI).

As reported previously, five (5) samples were synthesized in an effort to understand the fundamentals of the microphase separation for this system, which have not been reported yet in the literature. The volume fractions for all five samples were calculated by using equation 3.6 (already mentioned in Chapter 3 of this thesis):

$$\varphi_A = \frac{f_A d_B}{f_A d_B + f_B d_A}$$

where, A corresponds to PB and B to PI, while $d_A = 0,900$ g/ml is the density value of PB and $d_B = 0,903$ g/ml is the density value of PI respectively. The volume fractions are presented in Table 5.12.

Table 5.12: Molecular characteristics, volume fractions and degrees of polymerization (N) for the linear diblock copolymers of the PB- b -PI_{3,4} type.

Samples	$(\overline{M}_n)_{PB}^a$ (g/mol)	$(\overline{M}_n)_{PI}^a$ (g/mol)	$(\overline{M}_n)_{Total}^a$ (g/mol)	I_{Total}^b	φ_{PB}^c	φ_{PI}^c	$N_{PB-b-PI_{3,4}}^d$
PB- b -PI _{3,4} -1	38,200	55,400	93,600	1.06	0,42	0,58	1522
PB- b -PI _{3,4} -2	65,100	27,300	92,400	1.05	0,71	0,29	1606
PB- b -PI _{3,4} -3	58,300	40,200	98,500	1.06	0,59	0,41	1670
PB- b -PI _{3,4} -4	35,500	72,400	107,900	1.07	0,32	0,68	1722
PB- b -PI _{3,4} -5	590,200	420,300	1,010,500	1.10	0,59	0,41	17110

^aMO in toluene at 35⁰C, ^bSEC in THF at 30⁰C, ^cFrom ¹H-NMR measurements in CDCl₃ at 25⁰C and

through the equation $\varphi_{PB} = \frac{f_{PB}\rho_{PI}}{f_{PB}\rho_{PI} + (1 - f_{PB})\rho_{PI}}$,

^dFrom the equation: $N_{PB-b-PI_{3,4}} = N_{PB} + N_{PI_{3,4}} = \frac{\overline{M}_n^{PB}}{M_0^{PB}} + \frac{\overline{M}_n^{PI}}{M_0^{PI}}$

$(\overline{M}_n)_{PI}$ was calculated through the equation: $(\overline{M}_n)_{PI} = (\overline{M}_n)_{Total} - (\overline{M}_n)_{PB}$.

Another important aspect of the PB- b -PI_{3,4} copolymers system is that the interaction parameter χ is yet unknown. Furthermore, the restrictions concerning the electron densities of both PB and PI, do not allow SAXS measurements in order to calculate the interaction parameter χ , by studying the order-disorder transition as a function of temperature. The Flory-Huggins interaction parameter χ is inversely proportional to the temperature as already mentioned in Chapter 3 (equation 3.3: $\chi = \alpha T^{-1} + \beta$).

An another equation that is used in order to calculate χ , ignoring the effect of volume fraction φ and the elasticity parameter ϵ and considering only the enthalpic conditions is presented below:

$$\chi = \frac{V}{k_B T} (\delta_A - \delta_B)^2 \quad (5.15)$$

where, V corresponds to the segmental volume of the monomeric units of A and B, considering the densities of A and B chains respectively, k_B corresponds to the Boltzmann's

constant, while δ_A and δ_B are the solubility parameters of A and B polymers respectively. From the above equation, it is obvious that when the solubility parameters of A and B polymers are too close, then the value of the interaction parameter χ is very low and no microphase separation of the two blocks will occur except only when N exhibits very high values. Furthermore, V can be calculated through the equations:

$$V = (V_A V_B)^{1/2} \quad (5.16)$$

$$V_A = \frac{MW_A}{d_A N_A} \quad (5.17)$$

$$V_B = \frac{MW_B}{d_B N_B} \quad (5.18)$$

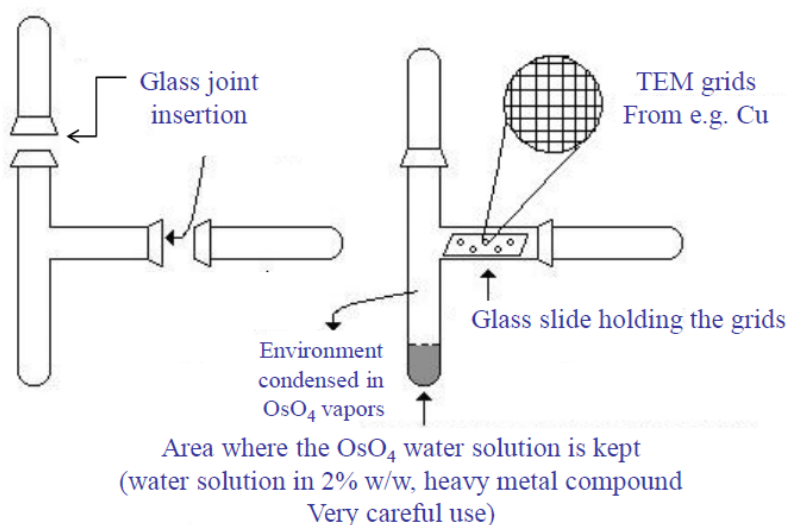
where, MW_A and MW_B are the molecular weights of the monomer unit for A and B block and d_A and d_B the densities of A and B blocks respectively. Through the above equations theoretical calculations of the interaction parameter $\chi_{PB_{1,4}-PI_{1,4}} = 0.0012$ for the PB_{1,4}-PI_{1,4} system, were confirmed experimentally.¹¹⁹

The sample preparation for the molecular characterization results, especially for TEM measurements, is very important. Casting must be performed in a non-selective solvent for several days in order to promote the formation of equilibrium morphologies. All linear diblock copolymers synthesized were cast from a dilute solution (~4 wt%) in toluene (an almost non-selective solvent for both segments) and the procedure for slow evaporation of the solvent was accomplished in approximately 7 days. Then, each film was separated in two equal amounts in order to study morphologically the unannealed and annealed thin sections. Thermal annealing was performed for 5 days at 50⁰C. Then, each film was removed from the annealing oven and quenched in liquid nitrogen in order to avoid any alternation of the formed morphology due to slow cooling to room temperature. As long as casting and annealing are properly accomplished, the films of the samples should be further elaborated by ultramicrotoming and staining in order to be used for TEM studies and images in bright field mode can be taken indicating well resolved microphase separation.

Initially, part of the films was ultra-microtomed in order to obtain very thin sections (~40-50 nm) at -100⁰C and the sections were picked up on 600 mesh copper grids. Cryogenic conditions were employed for increasing the hardness of each sample since the sectioning temperature was below the lower T_g of the blocks (T_g of PB and PI_{3,4} are -90⁰C and -10⁰C respectively). Furthermore, selective staining was necessary, since the intrinsic difference in electron density of PB and PI blocks does not provide adequate mass thickness image contrast (both blocks are exclusively consisted from carbon and hydrogen atoms). The grids were placed on a glass slide and under extreme precautions (glasses, mask and gloves are necessary

to avoid any exposure) the glass slide was inserted in the vapors of a 4% w/w aqueous solution of OsO_4 for selective staining of the two diene domains for approximately 1 h, depending on the quality of the stainer solution (time it has been stored and under which conditions). It should be noted that the staining time in the vapors of a 4% OsO_4 -water solution is very crucial, since the two dienes could be over-stained, yielding to a misleading apparent one-phase contrast. Staining for 1 h or less allows distinction of the two types of polydiene domains.

Figure 5.25 indicates the procedure and device involved for staining the sections already mounted in the Cu grids with OsO_4 .



The use of joints and proper glassware is necessary in order to avoid the loss of the grids

Figure 5.25: Schematic illustration of the device containing the aqueous solution of OsO_4 and the procedure involved for staining the sections on the Cu grids. It is evident that specific glassware is used in order to avoid contamination of the outside environment with OsO_4 (toxic) and of course for avoiding loss of the grids.

Microphase separation was evident in all five diblock copolymers indicating that the choice of the molecular weights leading to relatively high total degree of polymerization per sample was correct. The observation of well identified morphologies leading to alternating lamellae and hcp cylinders in all cases indicates as well that the Flory-Huggins interaction parameter is at least an order of magnitude higher than the one reported above for the case of $\text{PB}_{1,4}\text{-b-PI}_{1,4}$ diblock copolymers which was calculated theoretically and proven experimentally¹¹⁹ as already discussed. If the specific chi ($\chi = 0.0012$ at ambient conditions) is multiplied by the total degree of polymerization (values taken from Table 5.12) for the first four samples the result is below 2 and for the high molecular weight sample the value is approximately 20.5. Furthermore, by doing the annealing at 50°C no microphase should be observed since the χN would have been even lower. The results obtained from the TEM

studies are well resolved phases and actually annealing not only changes the morphology (if the samples were weakly segregated) but improves the order, leading to the important conclusion that the χN of the first four samples are at least in the intermediate segregation limit, whereas the high molecular weight sample is very strongly segregated. The TEM images obtained from the stained sections of the five linear diblock copolymers, thermally annealed and unannealed are presented below in Figures 5.26-5.30.

From Table 5.12 the volume fraction of PB for all samples is evident. Actually what is evident is that despite the fact that the total number average molecular weight of the first four samples (PB-b-PI_{3,4}-1 up to PB-b-PI_{3,4}-4) is kept constant the PB volume fraction varies from 0.32 up to 0.71 (for the fifth sample the comparison is not made with the first four samples since the total number average molecular weight is one order of magnitude higher). The PB volume fractions are 0.32 (sample-4), 0.42 (sample-1), 0.59 (sample-3) and 0.71 (sample-2) leading to the fact that if the theoretical and experimental information on microphase separation of the well-studied PS-b-PI diblock copolymers are adopted the following morphologies should be expected:

Sample-4, $\phi_{PB} = 0.32$: A cubic structure, double gyroid, with networks of the minority component (PB) in the matrix of the majority (PI) should be observed. In contrast, hexagonally closed packed cylinders of the minority component (PB) in the matrix of the majority (PI) is the adopted morphology. Since PB and PI_{3,4} are very flexible chains it seems that the ability to adopt such a complex architecture may not be possible due to entropic as well as enthalpic constraints leading to a less thermodynamically demanding topology such as the hcp cylinders of the minority phase in the matrix of the majority.

Actually, this assumption is verified by the TEM images in Figure 5.26 where dark grey hexagonally packed cylinders of PB in the white/grey matrix of the PI phase is evident. In this case it would be of great interest to prepare binary blends of the diblock copolymers with either homopolymer PB or homopolymer PI_{3,4} in order to explore whether the double gyroid will appear in the volume fraction regime 0.27-0.34. If it will not appear then the specific system studied indicates a major discrepancy with the microphase separation of the well-studied PS-b-PI diblock copolymer system.

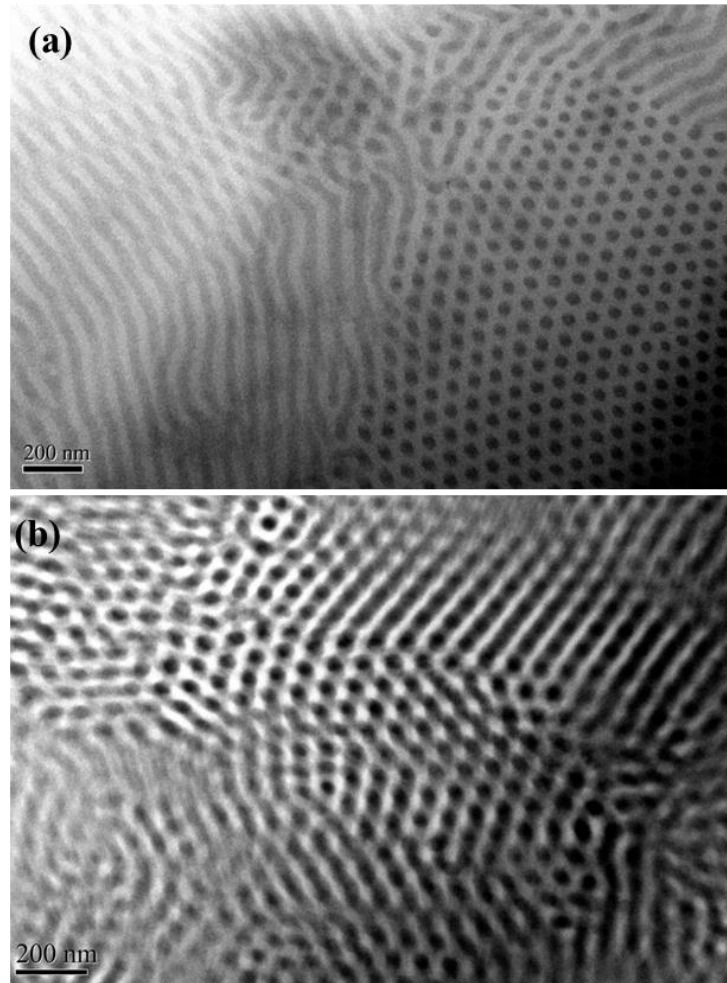


Figure 5.26: Bright field TEM images from thin sections of the: (a) annealed PB-b-PI_{3,4}-4 sample and (b) unannealed PB-b-PI_{3,4}-4 sample with $\phi_{PB} = 0,32$. In both TEM images hexagonally closed packed cylinders of the dark grey phase (PB) in the white matrix (PI_{3,4}) is observed with better order indicated in the annealed sample.

Sample-1, $\phi_{PB} = 0.42$: Alternating lamellae of the two different phases should be adopted. The TEM images in Figure 5.27 completely verify this morphology (alternating dark grey and white/grey layers are evident) in which the one layer (PB) is slightly smaller in dimensions when compared with the other layer, verifying therefore the volume fraction and no discrepancy is encountered with the morphology predicted by the phase diagram of the PS-b-PI diblock copolymer system (as in the case of sample-4).

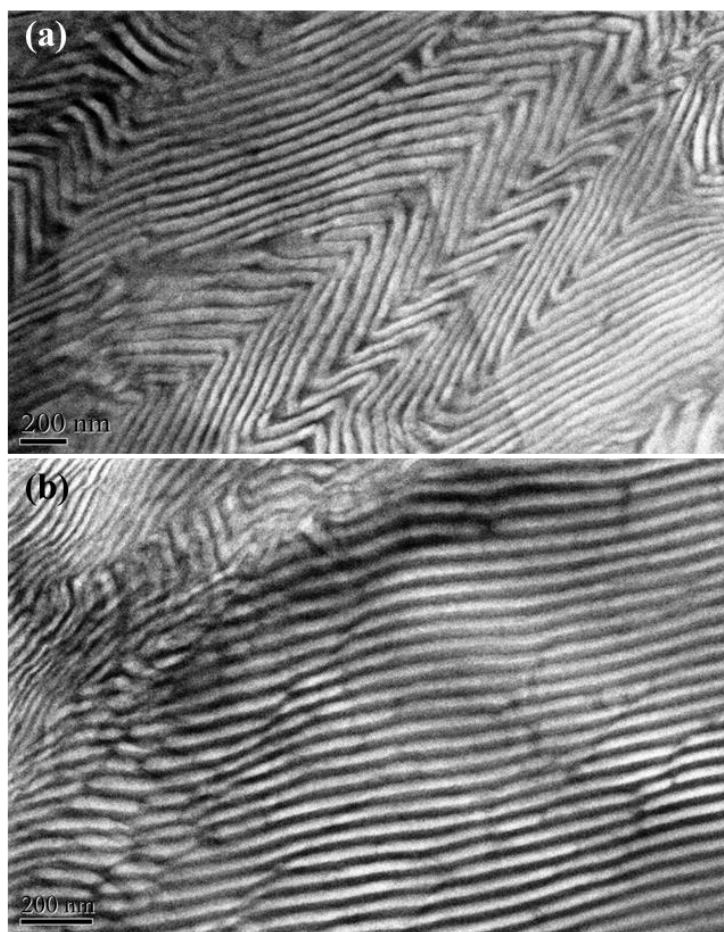


Figure 5.27: Bright field TEM images from thin sections of the: (a) annealed PB-b-PI_{3,4}-1 sample and (b) unannealed PB-b-PI_{3,4}-1 sample with $\phi_{PB} = 0,42$. In both TEM images alternating lamellae morphology is observed. The order is not that different between the annealed and the unannealed sample.

Sample-3, $\phi_{PB} = 0.59$: As in the case of sample-1 alternating lamellae of the two different phases should be evident. The TEM images in Figure 5.28 as well verify this assumption with the only difference when compared with sample - 1, being the reversibility in the layer thickness. In this case the PB layer (dark grey) is slightly larger from the PI layer, verifying, therefore, the volume fraction from the molecular characterization studies and as well no discrepancy is encountered with the morphology predicted by the phase diagram of the PS-b-PI diblock copolymer system (as in the case of sample-4).

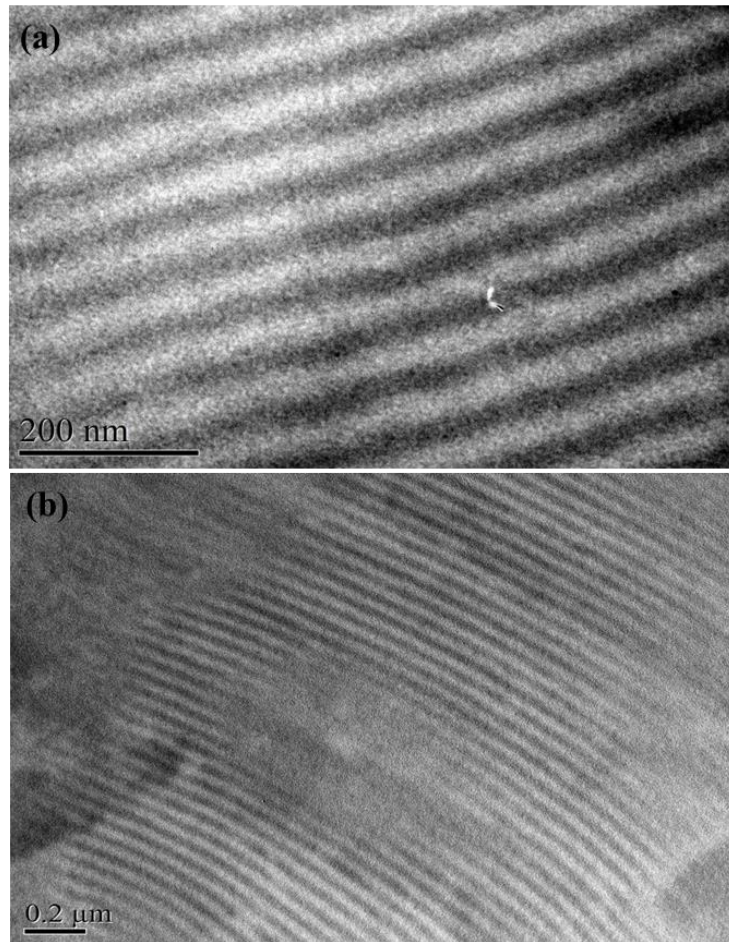


Figure 5.28: Bright field TEM images from thin sections of the: (a) annealed PB-*b*-PI_{3,4}-3 sample and (b) unannealed PB-*b*-PI_{3,4}-3 sample with $\phi_{PB} = 0,59$. In both TEM images alternating lamellae morphology is observed. The order is not that different between the annealed and the unannealed sample.

Sample-2, $\phi_{PB} = 0.71$: Finally for this sample the PB volume fraction is that high leading to the expectation of double gyroid, with networks of the minority component in the matrix of the majority. In contrast, hexagonally closed packed cylinders of the minority component (PI) in the matrix of the majority (PB) is the adopted morphology. The only difference from sample-4 described above is that now the networks should be filled with PI in the PB matrix if the DG structure was adopted for sample-2. Since for the PS-*b*-PI system the phase diagram of χN versus ϕ (volume fraction) is symmetric, this means that the double gyroid morphology is an indicative and stable structure in both sides, whether the volume fraction of the one component is lower or higher than that of the other block. The explanation for the PI hcp cylinders in PB matrix instead of 3D PI networks coincides with what is already mentioned for sample-4, therefore a more comprehensive study through binary blends should be made as well, in order to verify the complete absence of the DG structure or its existence in a more narrow volume fraction regime than 0.27-0.34 and 0.66-0.73 already reported for the PS-*b*-PI diblock copolymer system.

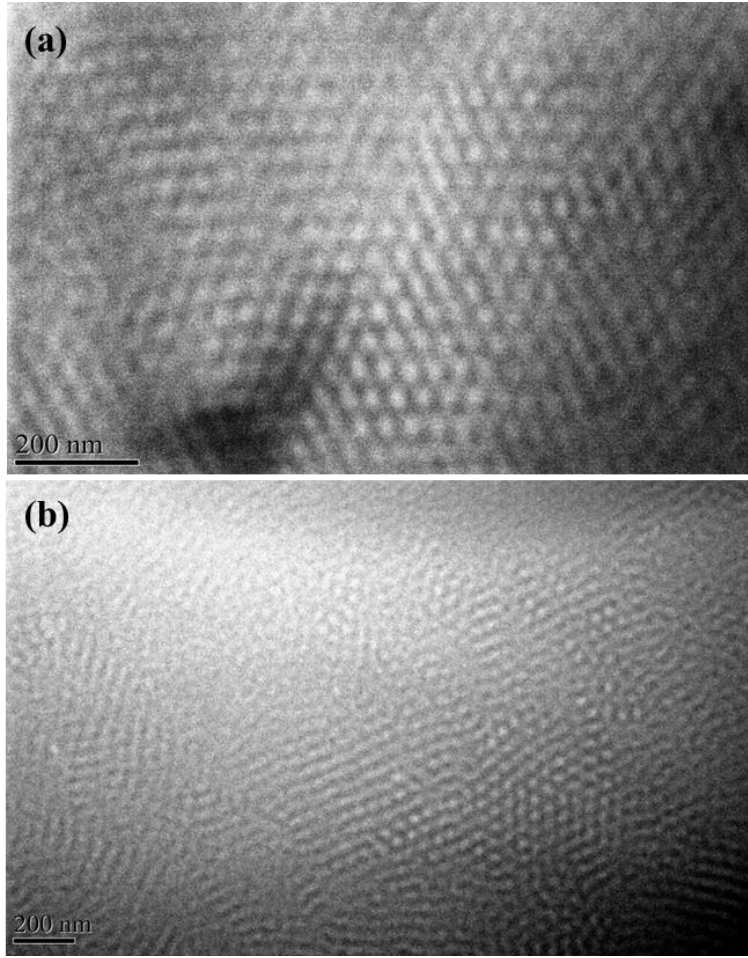


Figure 5.29: Bright field TEM images from thin sections of the: (a) annealed PB-b-PI_{3,4}-2 sample and (b) unannealed PB-b-PI_{3,4}-2 sample with $\phi_{PB} = 0,71$. In both TEM images hexagonally closed packed cylinders of the white phase (PI_{3,4}) in the dark grey matrix (PB) is observed with better order indicated in the annealed sample.

In order to fully comprehend the comparison with the PS-b-PI diblock copolymer, in Figure 5.30 the phase diagram is given as reported in the literature in order to point out the symmetry of the specific phase diagram as well as to indicate where the four samples with the specific volume fractions are located. By taking into consideration the TEM results together with the degree of polymerization values from Table 5.12 for sample PB-b-PI_{3,4}-2 ($\phi_{PB} = 0.71$, $N_{total} = 1606$) and PB-b-PI_{3,4}-4 ($\phi_{PB} = 0.32$, $N_{total} = 1722$) in which hcp cylinders were observed instead of DG structures the χN value should be equal or above 55 in order to observe the cylindrical morphology. It is clearly understood that the χN value will be the lowest in the annealed samples. Therefore:

$$(\chi N)_{sample-2} = 55 \Rightarrow \chi_{sample-2} = \frac{55}{1606} \Rightarrow \chi_{sample-2} = 0.034$$

$$(\chi N)_{sample-4} = 55 \Rightarrow \chi_{sample-4} = \frac{55}{1722} \Rightarrow \chi_{sample-2} = 0.032$$

From the above results it seems that the Flory Huggins interaction parameter at 50⁰C is approximately equal to 0.033 if the average value is taken from the above equations. Since the value is almost identical in both cases and taking into consideration that for the remaining two samples (PB-b-PI_{3,4}-1 / N_{total} = 1522 and PB-b-PI_{3,4}-3 / N_{total} = 1670), which exhibit alternating lamellae, the following calculations can be made:

$$(\chi N)_{\text{sample-1}} = a \Rightarrow a = 0.033 \cdot 1522 \Rightarrow a = 50.2$$

$$(\chi N)_{\text{sample-3}} = b \Rightarrow b = 0.033 \cdot 1670 \Rightarrow b = 55.1$$

These values are as well indicated in Figure 5.30. The conclusion that all these four samples should exhibit approximately equal χN is expected since the total number average molecular weight was kept approximately constant. It is evident that 3 out of 4 samples exhibit almost similar χN values with the only discrepancy in sample-1 which exhibits the lowest N, therefore the lowest χN .

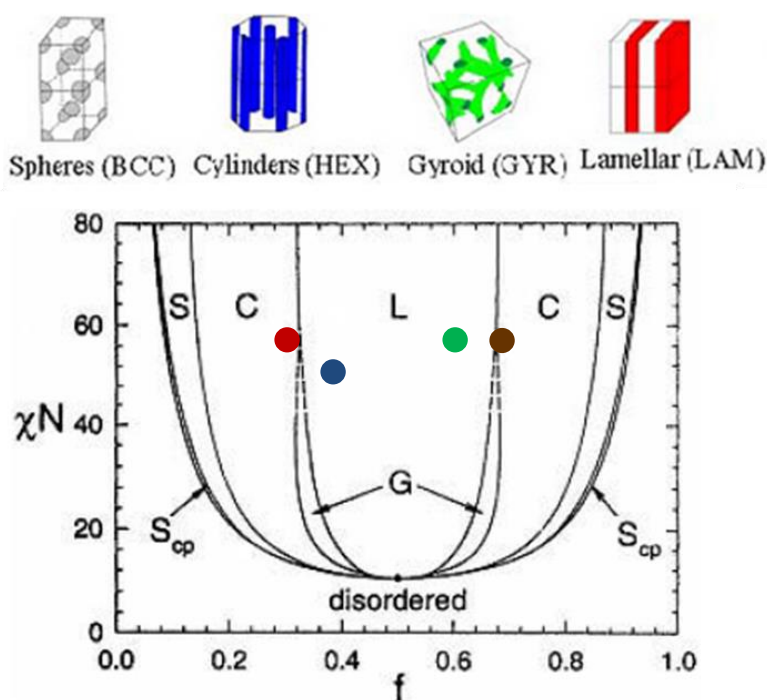


Figure 5.30: Mean field phase diagram within the SCFT approximation for conformationally symmetric diblock copolymers constructed by Matsen. The different phases are: L: lamellar, C: hexagonally close packed cylinders, S: spheres packed in a bcc lattice, G: bicontinuous Ia3d cubic (double gyroid), S_{cp}: closed packed spheres.¹⁰⁷ In the phase diagram with round circles the four diblock copolymers are indicated. The red color corresponds to sample - 4 ($\phi_{PB} = 0.32$), the blue to sample -1 ($\phi_{PB} = 0.42$), the green to sample - 3 ($\phi_{PB} = 0.59$) and finally the brown to sample - 2 ($\phi_{PB} = 0.71$).¹⁰⁷

The main reason for synthesizing the high molecular weight sample was evidently to explore whether microphase separation would occur as well since it is the first time that microphase separation is evident in linear diblock copolymers being exclusively 100%

elastomers. The TEM results suggest that this sample is very well microphase separated and exhibits alternating lamellar morphology as expected since the PB volume fraction is 0.59 identical with sample – 3 in which the same morphology was evident. The darker domains correspond to the heavily stained with vapors of OsO₄ PB_{1,4} chains, while the lighter domains correspond to slightly stained PI_{3,4} segments as explained thoroughly already in the literature (Figure 5.31).¹⁷

Since the electron densities of the two polydiene chains are approximately equal no SAXS results are given for the diblock copolymers. The d_{10} spacing of the observed morphologies can be calculated approximately by the TEM images and varies from 45 to 55 nm for the first 4 samples and 130 nm for the higher molecular weight diblock sample respectively. Therefore, it is evident from the TEM images of the diblock copolymers that the sequence of the polydiene blocks with the specific microstructures leads to well defined topologies almost identical to those reported for PS/PI diblock copolymers in the literature.

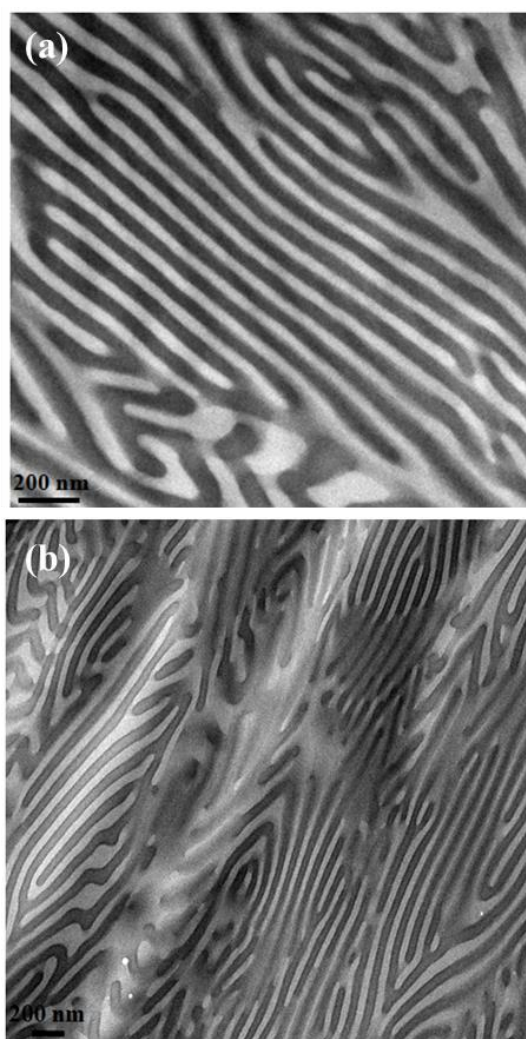


Figure 5.31: TEM images from thin sections of the: (a) annealed PB-*b*-PI_{3,4}-5 sample and (b) lower magnification image again of the annealed PB-*b*-PI_{3,4}-5 sample. In both TEM images alternating lamellae morphology is observed.

5.8 Molecular Characterization Results of Miktoarm Star Copolymers

The molecular characterization results are presented and discussed for the eight (8) miktoarm star copolymers of the PB(PI_{3,4})₂ and PB(PI_{3,4})₃ type respectively. All samples, as already mentioned, were synthesized via anionic polymerization and high vacuum techniques in combination with chlorosilane chemistry. The reagents used were: benzene as solvent, *sec*-BuLi as initiator, THF as the polar media for the achievement of the desirable high 3,4-microstructure for PI, trichloromethylsilane (CH₃SiCl₃) and tetrachlorosilane (SiCl₄) as the linking agents and methanol as the terminating agent for all the polymerizations. ***It is important to mention that these types of miktoarm star copolymers were synthesized for the first time and have never been reported in the literature.***

The eight samples were divided in four (4) sets [four samples per sequence either PB(PI_{3,4})₂ or PB(PI_{3,4})₃]. The volume fraction regime for the PB block as well as the total number average molecular weight of the non-linear copolymers were approximately equal to those documented for the four (4) lower molecular weight diblock copolymers, thus each diblock copolymer corresponds to a set of miktoarm star copolymers. The reason for keeping almost constant both total molecular weight and PB block volume fraction in the linear diblock and the non-linear copolymers was to compare their structure/properties relationship and verify in such systems the influence of non-linear architecture in self-assembly. ***It should be noted here that it is the first time such a study is performed in exclusively 100% elastomers.***

As it was mentioned in previous chapters, several methods were adopted for the molecular characterization of these samples. Size exclusion chromatography (SEC) with THF as the eluent at 30⁰C was used extensively in order to verify the narrow molecular weight distributions of the PB and PI_{3,4} blocks, as well as of the final star copolymers. The instrument was always calibrated with PS standards and the results concerning the PB and PI_{3,4} blocks as well as the final star copolymers are not reliable. In order to verify the total number average molecular weight values for each sample, as well as the values for each PI_{3,4} block, membrane osmometry (MO) in toluene at 35⁰C was adopted. By combining the results from these two characterization methods and using them in equation: $I = \frac{\overline{M}_w}{\overline{M}_n}$, information concerning the weight average molecular weight of the PB and PI_{3,4} homopolymers and of the final star copolymers was obtained. Furthermore, another method used for the molecular characterization of the samples, and especially to verify the high 3,4-microstructure for the PI blocks (~55-65%) as well as the molecular and compositional homogeneity of the samples, was proton nuclear magnetic resonance (¹H-NMR) spectroscopy in CDCl₃ at 25⁰C.

In Table 5.13 the molecular characteristics for the synthesized star copolymers are summarized. The molecular composition or mass fraction, f , was calculated via $^1\text{H-NMR}$ measurements and by using the same equations (5.2 and 5.3), as in the case of the linear diblock copolymers, the values of the volume fractions of each segment were determined.

Table 5.13: Molecular characterization results for the star copolymers of the $\text{PB}(\text{PI}_{3,4})_2$ and $\text{PB}(\text{PI}_{3,4})_3$ types.

Samples	$(\overline{M}_n)_{\text{PB}}^a$ (g/mol)	$(\overline{M}_n)_{\text{PI}}^a$ (g/mol)	$(\overline{M}_n)_{\text{Total}}^a$ (g/mol)	I_{Total}^b	$(\overline{M}_w)_{\text{Total}}^c$ (g/mol)	f_{PB}^d	φ_{PB}^e
PB(PI_{3,4})₂-S₁	43,100	35,300	107,300	1.08	115,900	0,41	0,41
PB(PI_{3,4})₃-S₂	43,100	23,800	109,400	1.07	117,000	0,40	0,40
PB(PI_{3,4})₂-S₃	61,500	16,700	92,400	1.06	97,900	0,67	0,67
PB(PI_{3,4})₃-S₄	61,500	9,800	88,200	1.08	95,200	0,69	0,69
PB(PI_{3,4})₂-S₅	55,200	22,800	98,100	1.06	104,000	0,57	0,57
PB(PI_{3,4})₃-S₆	55,200	15,600	100,300	1.07	107,300	0,56	0,56
PB(PI_{3,4})₂-S₇	27,500	34,500	94,500	1.05	99,200	0,30	0,30
PB(PI_{3,4})₃-S₈	27,500	25,700	101,600	1.05	106,700	0,28	0,28

^aMO in toluene at 35^oC, ^bSEC in THF at 30^oC, ^cFrom combination of SEC and MO measurements,

^dFrom $^1\text{H-NMR}$ measurements in CDCl_3 at 25^oC and ^eFrom the equation $\varphi_{\text{PB}} = \frac{f_{\text{PB}}\rho_{\text{PI}}}{f_{\text{PB}}\rho_{\text{PI}} + (1 - f_{\text{PB}})\rho_{\text{PI}}}$.

A variety of results can be concluded from the values in Table 5.13. The aim of this study, concerning the molecular weight of the polymers, was to keep constant the total number average molecular weight of the star copolymers approximately equal to 100,000 g/mol with volume fractions almost identical with those of the corresponding linear diblock copolymers.

For example, concerning the first set of samples the PB-b-PI_{3,4}-1 linear diblock copolymer exhibited a volume fraction for the PB block equal to 0.42, while φ_{PB} of PB(PI_{3,4})₂-S₁ and PB(PI_{3,4})₃-S₂ was equal to 0.41 and 0.40 respectively. The reason was the molecular and morphological comparison, of the linear diblock copolymers with the corresponding star copolymers.

Furthermore, *it is the first time in the literature that such star copolymers with the specific segments and microstructure content have been synthesized and studied morphologically with transmission electron microscopy*. As it was mentioned previously, the only drawback, that this type of copolymers exhibit, is that they cannot be studied with small-angle X-ray scattering (SAXS) due to the similar and almost identical electron density of the two segments involved.

For all miktoarm star copolymer samples the total number average molecular weight varied in the region of 88,000-109,000 g/mol, in agreement with the corresponding values mentioned already for the linear diblock copolymers. Additionally, the number average molecular weight of the PB arms for each set is identical, as it was mentioned already in Chapter 4 (experimental section). Furthermore, a variety of compositions ranging from 28% up to 69% in mass fraction for the PB segment were obtained in order to compare their morphological behavior with that of the linear diblock copolymers as well as with that of related PS(PI)_n copolymers, where n=1, 2, 3 respectively. It is important to mention that the PS/PI system has been thoroughly studied not only in its linear sequence but also as miktoarm star copolymers of the AB_n type, where n > 1.

The volume fractions (φ) for the two chemically different chains are approximately equal with the mass fractions (f), as they were calculated from ¹H-NMR since, as already mentioned, the densities of PB and PI segments are almost identical (0,900 g/mL and 0,903 g/mL respectively).

Two representative examples, corresponding to samples PB(PI_{3,4})₂-S₇ and PB(PI_{3,4})₃-S₈ (fourth set), are given in Figures 5.32 and 5.33, where the SEC chromatographs of the PB and PI blocks, the unfractionated miktoarm star copolymers and the final fractionated star copolymers are shown. The fractionation technique in a solvent/non-solvent system was necessary in all samples, in order to remove unreacted in excess reagents or intermediate products or unwanted products which were formed during the linking reactions of the living blocks with the appropriate chlorosilane. The results from only two samples were chosen to be presented thoroughly, due to the fact that the chromatographs of all the star copolymers were almost identical.

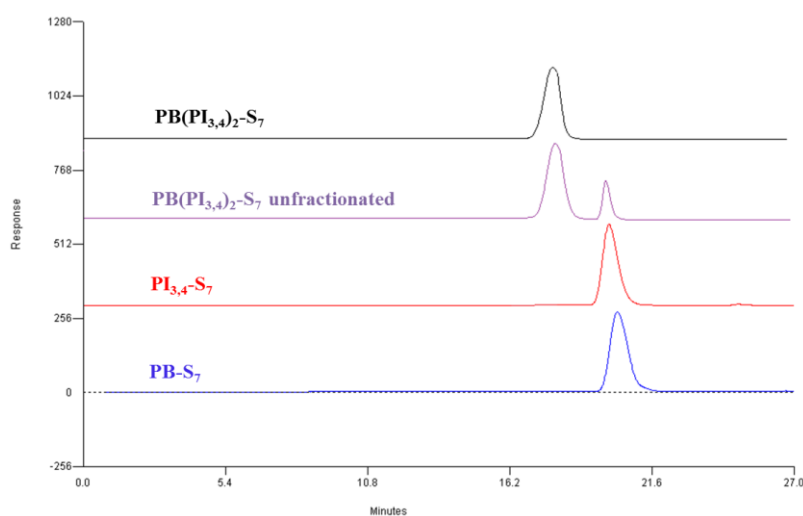


Figure 5.32: SEC chromatographs of homopolymers PB-S₇ (indicated in blue color) and PI_{3,4}-S₇ (indicated in red color), unfractionated star copolymer PB(PI_{3,4})₂-S₇ (indicated in purple color) and the final fractionated miktoarm star copolymer PB(PI_{3,4})₂-S₇ (indicated in black color).

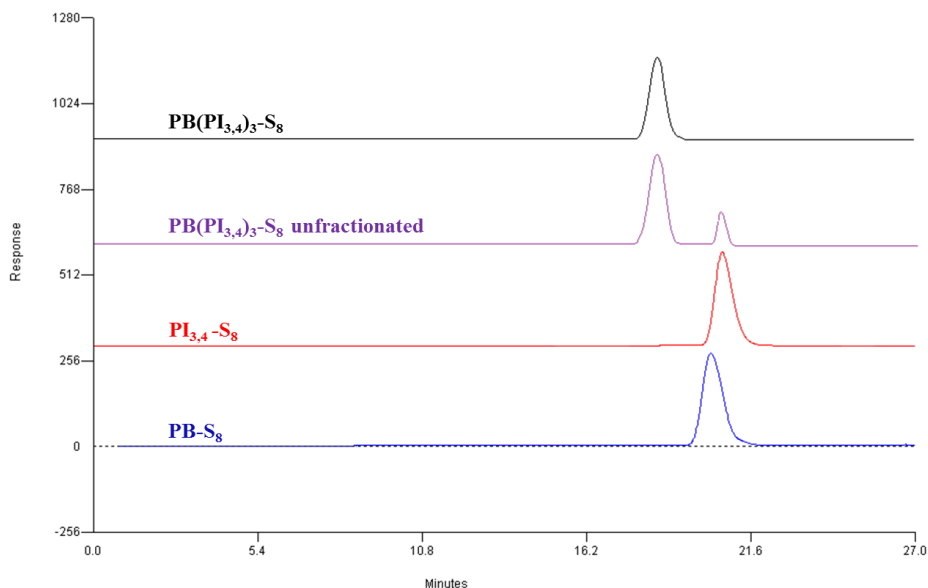


Figure 5.33: SEC chromatographs of homopolymers $PB-S_8$ (indicated in blue color) and $PI_{3,4}-S_8$ (indicated in red color), unfractionated star copolymer $PB(PI_{3,4})_3-S_8$ (indicated in purple color) and the final fractionated miktoarm star copolymer $PB(PI_{3,4})_3-S_8$ (indicated in black color).

By observing the above chromatographs (Figures 5.32 and 5.33), the successful synthesis of the star copolymers $PB(PI_{3,4})_2-S_7$ and $PB(PI_{3,4})_3-S_8$ is confirmed. The presence of only one peak in the final star copolymers SEC chromatographs and the low polydispersity indices indicates their molecular and compositional homogeneity. Anionic polymerization through high vacuum techniques of 1,3-butadiene and isoprene leads to well-defined homopolymers of PB and $PI_{3,4}$, which through linking reactions with CH_3SiCl_3 or $SiCl_4$ and after approximately 4 weeks, the desirable star copolymers of the $PB(PI_{3,4})_2$ and $PB(PI_{3,4})_3$ types were obtained respectively.

As it was mentioned in the experimental part, St end-capping (2-4 monomeric units) was used after the completion of the polymerization of PB, in order to alter the living ends of $PB^{(-)}Li^{(+)}$ to $PS^{(-)}Li^{(+)}$ for better control of the linking reaction with CH_3SiCl_3 or $SiCl_4$ respectively. The additional peak that is presented in the chromatographs of $PB(PI_{3,4})_2-S_7$ and $PB(PI_{3,4})_3-S_8$ unfractionated cases (purple color), corresponds to the excess of living $PI_{3,4}$ (~20%) that was used, during the linking reactions with $PBSiCl_2$ or $PBSiCl_3$ respectively. No other undesirable products were obtained during the linking reactions of the living ends of both homopolymers with the chlorosilanes. The excess of unreacted $PI_{3,4}^{(-)}Li^{(+)}$ was removed by mass fractionation in a solvent (toluene)/non-solvent (methanol) system, leading to monomodal chromatographs (black color chromatographs in Figures 5.32 and 5.33 of the final star copolymers). The peaks of the final star copolymers were eluted in lower elution times compared to those of the corresponding homopolymer PB and $PI_{3,4}$ blocks, indicating the successful linking reactions of both homopolymers with the appropriate chlorosilane.

In Figures 5.34 and 5.35 the SEC chromatographs of all final star copolymers of the $PB(PI_{3,4})_2$ and the $PB(PI_{3,4})_3$ types are presented respectively indicating peaks to approximately similar elution times (due to the similar molecular characteristics needed for the reasons described above).

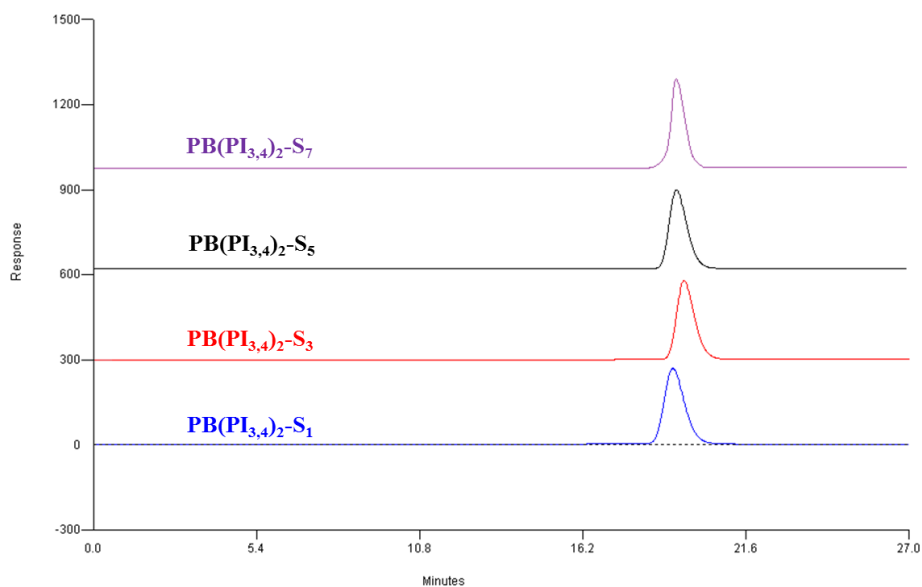


Figure 5.34: SEC chromatographs of all fractionated mikroarm star copolymers of the $PB(PI_{3,4})_2$ type.

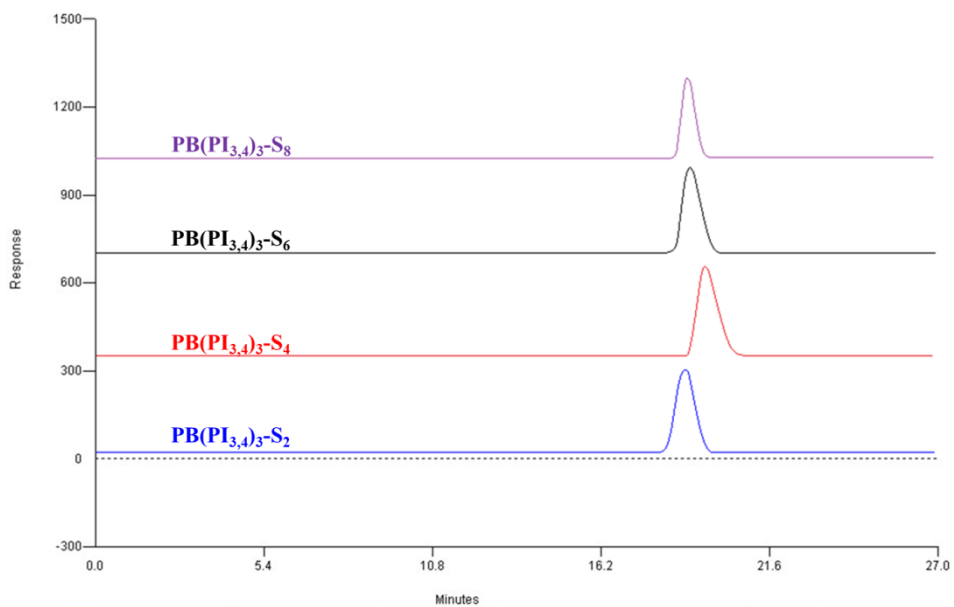


Figure 5.35: SEC chromatographs of all fractionated mikroarm star copolymers of the $PB(PI_{3,4})_3$ type.

The monomodal molecular weight distributions of the eight star copolymers of the PB($\text{PI}_{3,4}$)₂ and PB($\text{PI}_{3,4}$)₃ types (four samples per sequence), indicate high molecular and compositional homogeneity for all samples.

The molecular characterization via proton nuclear magnetic resonance (¹H-NMR) spectroscopy was utilized in order to verify the composition results as produced by the average molecular weights of both blocks through combination of the results from SEC and MO, since the calculation of the mass fraction (f) can be derived from the ¹H-NMR spectra, as well as to confirm the existence of the desirable 3,4-microstructure at high values (> 55%) for the PI segments of the star copolymers.

All the proton chemical shifts for PB and PI have already been thoroughly described in the case of linear diblock copolymers (Table 5.9). In order to calculate the compositions of PB and PI segments of the star copolymers, the equations described previously concerning the linear block copolymers were used (Equations 5.5-5.12). The mass fractions of PB and PI as calculated by ¹H-NMR along with the characteristic microstructure of each block are presented in Table 5.14. In all samples, the 3,4-microstructure of PI is ranging from 58% to 62%, while the mass fraction of the PB obtained values ranging from 0.28 up to 0.69.

Table 5.14: Mass fractions and characteristic microstructure content of each arm (PB and PI), as calculated by ¹H-NMR spectroscopy results.

Samples	f_{PB}	f_{PI}	% 1,4-PB	% 1,2-PB	% 3,4-PI	% 1,4-PI	% 1,2-PI
PB($\text{PI}_{3,4}$) ₂ -S ₁	0,41	0,59	92	8	60	25	15
PB($\text{PI}_{3,4}$) ₃ -S ₂	0,40	0,60	92	8	59	27	14
PB($\text{PI}_{3,4}$) ₂ -S ₃	0,67	0,33	91	8	61	23	16
PB($\text{PI}_{3,4}$) ₃ -S ₄	0,69	0,31	91	8	60	26	14
PB($\text{PI}_{3,4}$) ₂ -S ₅	0,57	0,43	91	9	61	24	15
PB($\text{PI}_{3,4}$) ₃ -S ₆	0,56	0,44	91	9	58	28	14
PB($\text{PI}_{3,4}$) ₂ -S ₇	0,30	0,70	92	8	59	26	15
PB($\text{PI}_{3,4}$) ₃ -S ₈	0,28	0,72	92	8	62	22	16

Two representative examples, corresponding to samples PB($\text{PI}_{3,4}$)₂-S₇ and PB($\text{PI}_{3,4}$)₃-S₈ (one per sequence) are given in Figures 5.36 and 5.37 respectively, where the ¹H-NMR spectra of the PB and PI homopolymers as well as of the final star copolymers are presented. The choice of the samples was made in order to present a full set of star copolymers with approximately the same compositions of PB and PI arms. In the specific set the mass fraction of PI segments obtained high values (0.70 for PB($\text{PI}_{3,4}$)₂-S₇ and 0.72 for PB($\text{PI}_{3,4}$)₃-S₈) respectively.

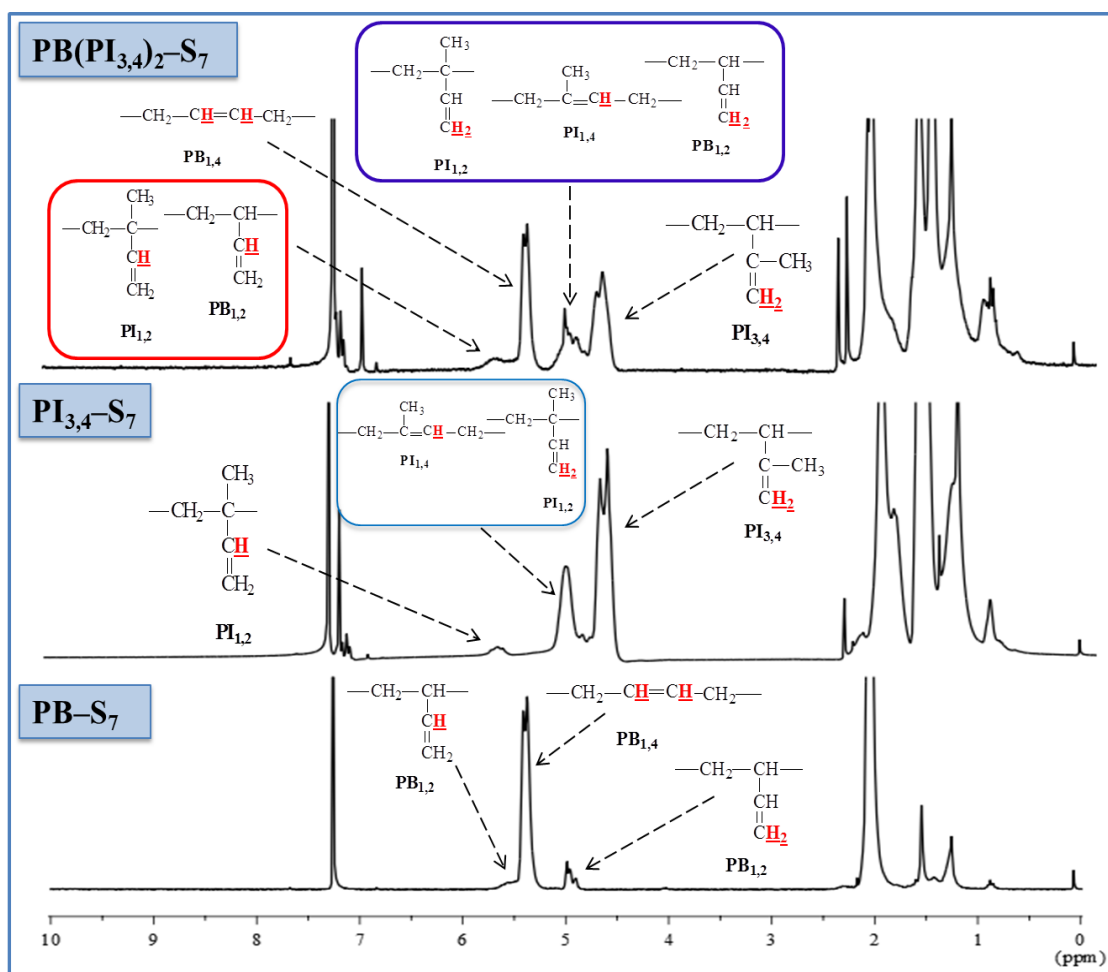


Figure 5.36: $^1\text{H-NMR}$ spectra of the homopolymers PB-S_7 , $\text{PI}_{3,4}\text{-S}_7$ and the final miktoarm star copolymer $\text{PB}(\text{PI}_{3,4})_2\text{-S}_7$.

The intensity of the $^1\text{H-NMR}$ signals is displayed along the vertical axis of a spectrum and is proportional to the molar concentration of the sample. All characteristic chemical shifts corresponding to the olefinic protons of the PB and PI microstructures were observed. It is clearly understood from the above $^1\text{H-NMR}$ spectra that for the miktoarm star copolymer $\text{PB}(\text{PI}_{3,4})_2\text{-S}_7$, PI exhibits high 3,4-content and through calculations by using the equations mentioned above (equations 5.5-5.12), $\text{PB}(\text{PI}_{3,4})_2\text{-S}_7$ sample is enriched in PI 3,4-microstructure by a value of approximately 59%. The same ratio of 3,4-microstructure was also obtained for the $\text{PI}_{3,4}\text{-S}_7$ homopolymer. The value of mass fraction of the PI was calculated to be equal to 0.70 in the specific copolymers.

Furthermore, the PB arm exhibits high 1,4-microstructure $\sim 92\%$ in sample $\text{PB}(\text{PI}_{3,4})_2\text{-S}_7$ and the value of mass fraction of PB was calculated to be 0.30. As mentioned in previous $^1\text{H-NMR}$ spectra, the proton chemical shifts appearing at approximately 7.2-7.3 ppm correspond to the deuterated chloroform (CDCl_3) which is the solvent used for diluting the examined samples.

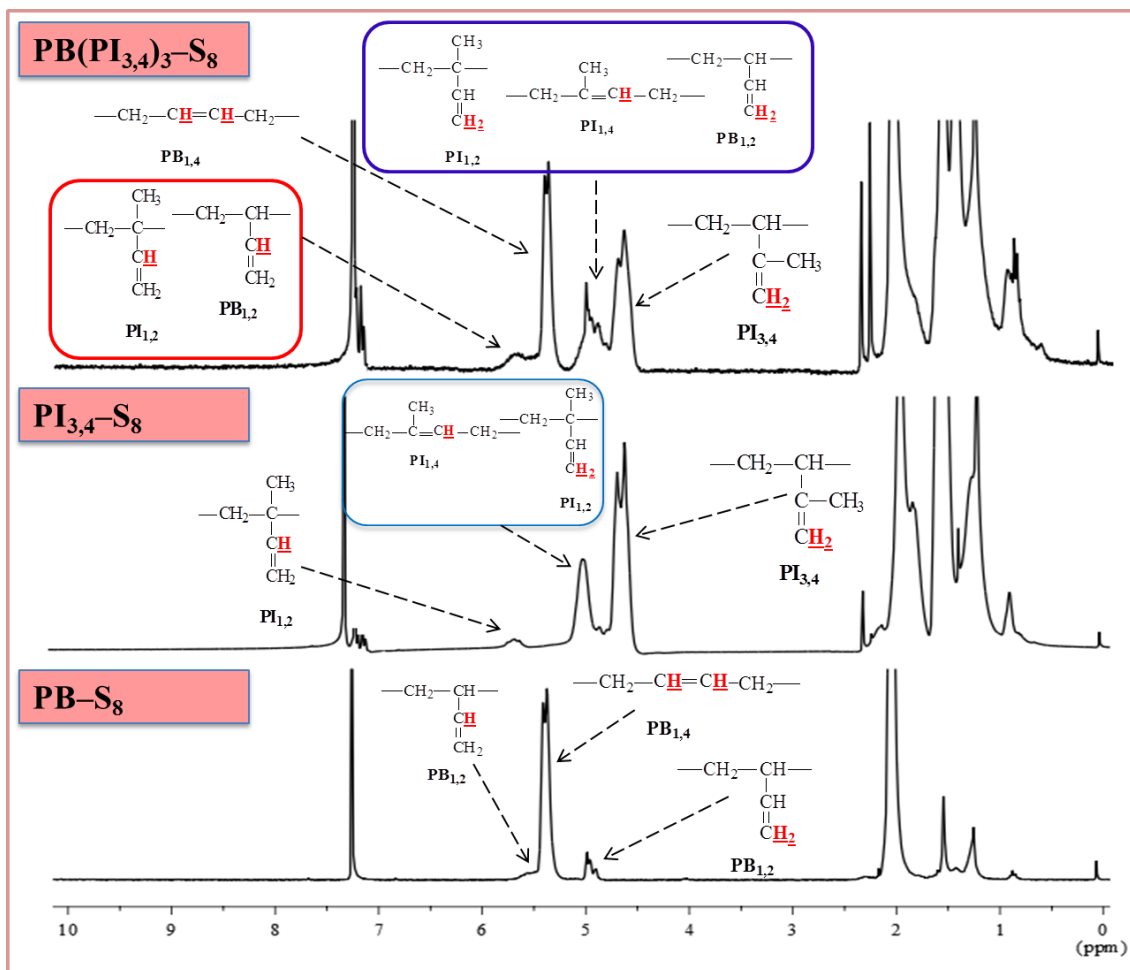


Figure 5.37: $^1\text{H-NMR}$ spectra of the homopolymers PB-S_8 , $\text{PI}_{3,4}\text{-S}_8$ and the final star copolymer $\text{PB}(\text{PI}_{3,4})_3\text{-S}_8$.

Similarly, for the $\text{PB}(\text{PI}_{3,4})_3\text{-S}_8$ mikroarm star copolymer all the characteristic chemical shifts of the olefinic protons, corresponding to PB and PI different microstructures were obtained. In this case, PI also exhibits high 3,4-content ($\sim 62\%$) and the PB mass fraction was calculated equal to 0.28. This star copolymer contained PB arm with the same number average molecular weight with the previous star copolymer $[\text{PB}(\text{PI}_{3,4})_2\text{-S}_7]$, therefore it exhibits the same ratio of 1,4-microstructure with the above sample ($\sim 92\%$). The value of the mass fraction of PB segment was calculated to be 0.28. Similar $^1\text{H-NMR}$ spectra were obtained for the remaining six star copolymers of the $\text{PB}(\text{PI}_{3,4})_2$ and $\text{PB}(\text{PI}_{3,4})_3$ types and the obtained results are thoroughly given in Table 5.14.

5.9 Thermal Analysis Results of Miktoarm Star Copolymers

Differential scanning calorimetry was employed for the thermal analysis of the eight miktoarm star copolymers of the $PB(PI_{3,4})_2$ and $PB(PI_{3,4})_3$ type. DSC can provide very useful information concerning the glass transition temperature, melting point and the crystallization of a polymeric material, as it is already mentioned previously. The measurements were accomplished with a Q20 TA instrument. The heating ramp was $5^{\circ}\text{C}/\text{min}$ and the temperature range from -120°C to 40°C . It should be mentioned that additional measurements to some of the star copolymers were performed, where the heating ramp was $2^{\circ}\text{C}/\text{min}$, but no different results were obtained concerning the values of glass transition temperatures of each segment. The same considerations, concerning the values of the glass transition temperatures as described in the case of the linear diblock copolymers were taken into account for these types of samples.

In Figures 5.38 and 5.39 the DSC thermographs for the first set of star copolymers, corresponding to $PB(PI_{3,4})_2\text{-S}_1$ and $PB(PI_{3,4})_3\text{-S}_2$ are given. The displayed thermographs correspond to the second heating procedure of each measurement. The first heating was performed in order to erase the history of the sample at a specific rate (commonly $10^{\circ}\text{C}/\text{min}$).

1st Set:

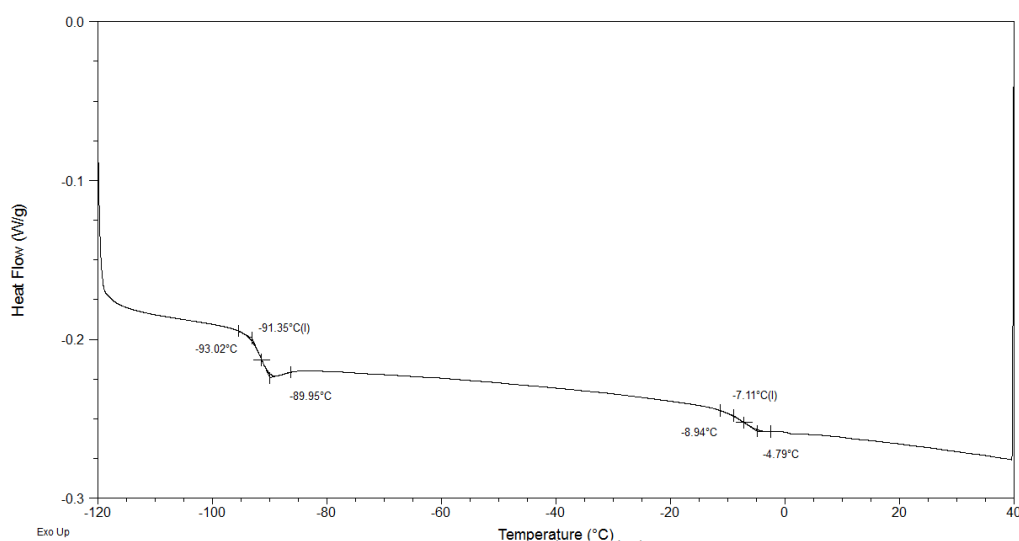


Figure 5.38: DSC thermograph of the $PB(PI_{3,4})_2\text{-S}_1$ star copolymer indicating T_g of PB equal to $-91,35^{\circ}\text{C}$ and T_g of $PI_{3,4}$ equal to $-7,11^{\circ}\text{C}$ respectively.

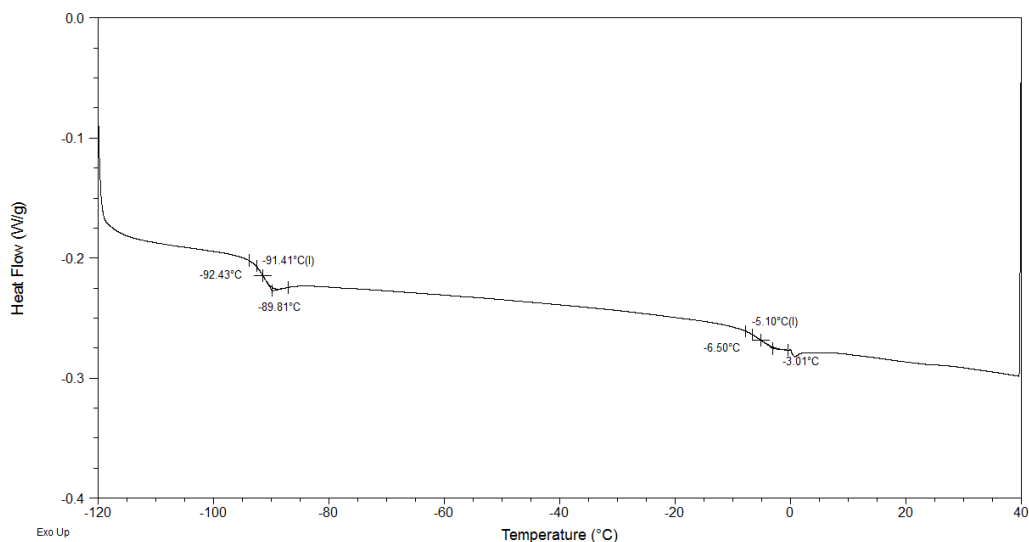


Figure 5.39: DSC thermograph of the $PB(PI_{3,4})_3-S_2$ star copolymer indicating T_g of PB equal to $-91,41^{\circ}C$ and T_g of $PI_{3,4}$ equal to $-5,10^{\circ}C$ respectively.

Analyzing the DSC results for the samples $PB(PI_{3,4})_2-S_1$ and $PB(PI_{3,4})_3-S_2$, which correspond to the first set of the miktoarm star copolymers synthesized, two endothermic transitions were obtained for each star copolymer respectively. Specifically, for the $PB(PI_{3,4})_2-S_1$ sample two endothermic transitions at approximately $-91^{\circ}C$ and $-7^{\circ}C$ and for the $PB(PI_{3,4})_3-S_2$ sample at approximately $-91^{\circ}C$ and $-5^{\circ}C$ were observed corresponding to the glass transition temperatures of PB and $PI_{3,4}$ respectively. The relatively high value of the T_g of $PI_{3,4}$ in both samples is due to the high 3,4-content ($\sim 60\%$ and 59% respectively). The identical value for the T_g of PB in both samples was expected, since the PB precursor is the same for both star copolymers. A slight difference at the value of T_g of $PI_{3,4}$ is obtained in the two star copolymers ($\sim 2^{\circ}C$).

A comparison of the glass transition temperatures of the two star copolymers with the corresponding linear diblock copolymer $PB-b-PI_{3,4}-1$ which exhibits almost the same number average molecular weight and mass fraction, has led to approximately identical values of T_g for both PB and $PI_{3,4}$. Therefore, it can be concluded that the glass transition temperature does not depend on the architecture of a block copolymer. The DSC thermographs of the linear diblock copolymer and the two star copolymers for comparison reasons are presented in Figure 5.40.

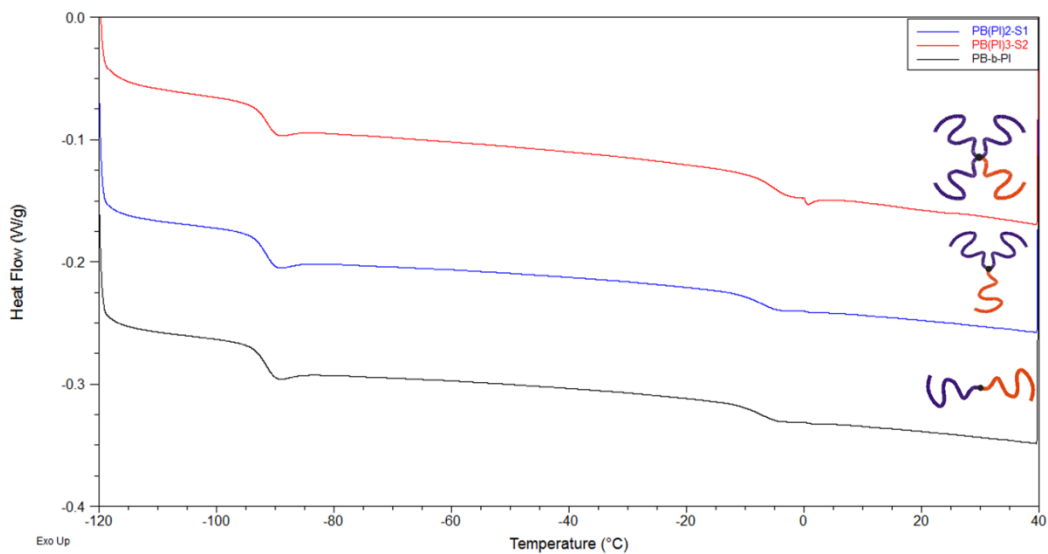


Figure 5.40: DSC thermographs of the PB-*b*-PI_{3,4}-1 linear block copolymer (indicated in black color), PB(PI_{3,4})₂-S₁ star copolymer (indicated in blue color) and PB(PI_{3,4})₃-S₂ star copolymer (indicated in red color) respectively.

In Figures 5.41 and 5.42 the DSC thermographs for the second set of star copolymers, corresponding to PB(PI_{3,4})₂-S₃ and PB(PI_{3,4})₃-S₄ are given.

2nd Set:

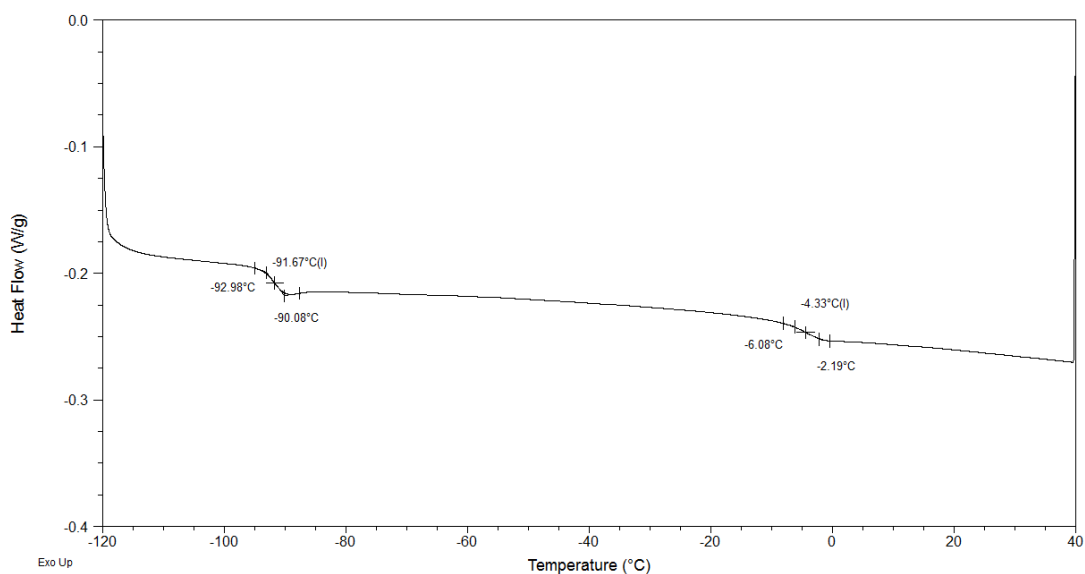


Figure 5.41: DSC thermograph of the PB(PI_{3,4})₂-S₃ star copolymer indicating T_g of PB equal to -91,67°C and T_g of PI_{3,4} equal to -4,33°C respectively.

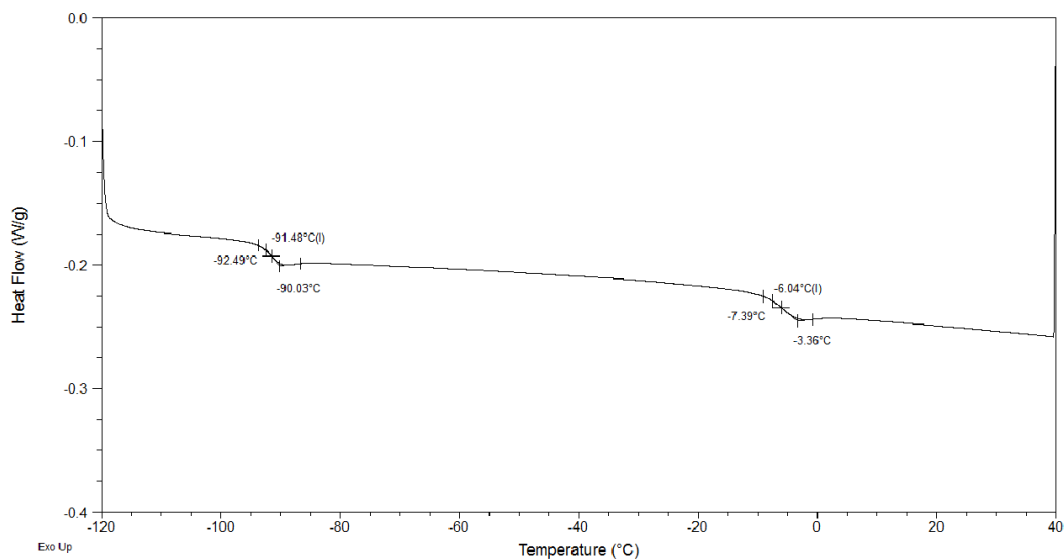


Figure 5.42: DSC thermograph of the $PB(PI_{3,4})_3-S_4$ star copolymer indicating T_g of PB equal to $-91,48^{\circ}C$ and T_g of $PI_{3,4}$ equal to $-6,04^{\circ}C$ respectively.

Analyzing the DSC results for the samples $PB(PI_{3,4})_2-S_3$ and $PB(PI_{3,4})_3-S_4$, which correspond to the second set of star copolymers, it is evident again that for the $PB(PI_{3,4})_2-S_3$ sample, two endothermic transitions at approximately $-92^{\circ}C$ and $-4^{\circ}C$ and for the $PB(PI_{3,4})_3-S_4$ sample at approximately $-91^{\circ}C$ and $-6^{\circ}C$ are observed corresponding to the glass transition temperatures of PB and $PI_{3,4}$ sequences respectively. The relatively high value of the T_g of $PI_{3,4}$ in both samples is due to the high 3,4-content ($\sim 61\%$ and 60% respectively).

Comparing the glass transition temperatures of the two star copolymers with the linear diblock copolymer $PB-b-PI_{3,4}-2$ exhibiting almost similar number average molecular weight and mass fraction, no differences in the T_g values for both PB and $PI_{3,4}$, as it was concluded already for the 1st set above. The combined DSC thermographs of the linear diblock copolymer and the corresponding star copolymers are presented in Figure 5.43.

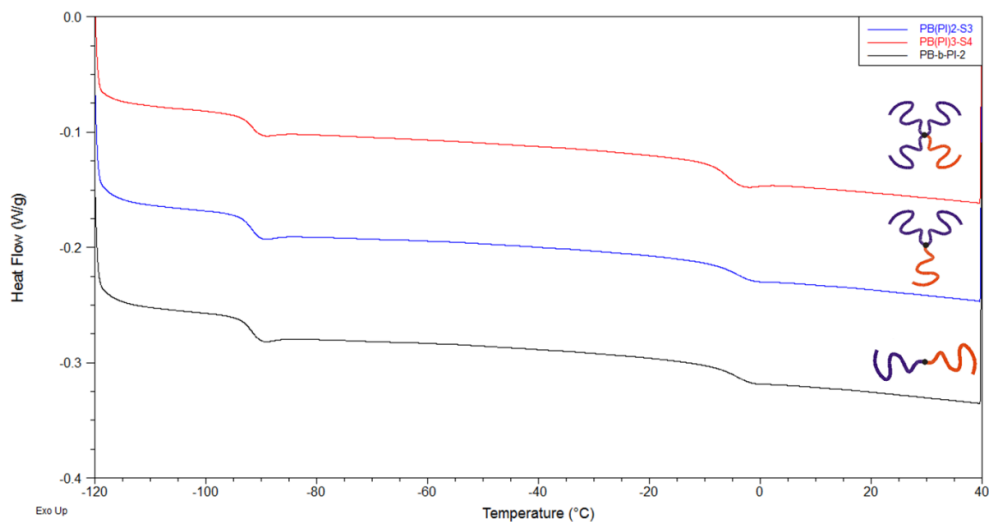


Figure 5.43: DSC thermographs of the PB-*b*-PI_{3,4}-2 linear block copolymer (indicated in black color), PB(PI_{3,4})₂-S₃ star copolymer (indicated in blue color) and PB(PI_{3,4})₃-S₄ star copolymer (indicated in red color) respectively.

In Figures 5.44 and 5.45 the DSC thermographs for the third set of star copolymers, corresponding to PB(PI_{3,4})₂-S₅ and PB(PI_{3,4})₃-S₆ are given.

3rd Set:

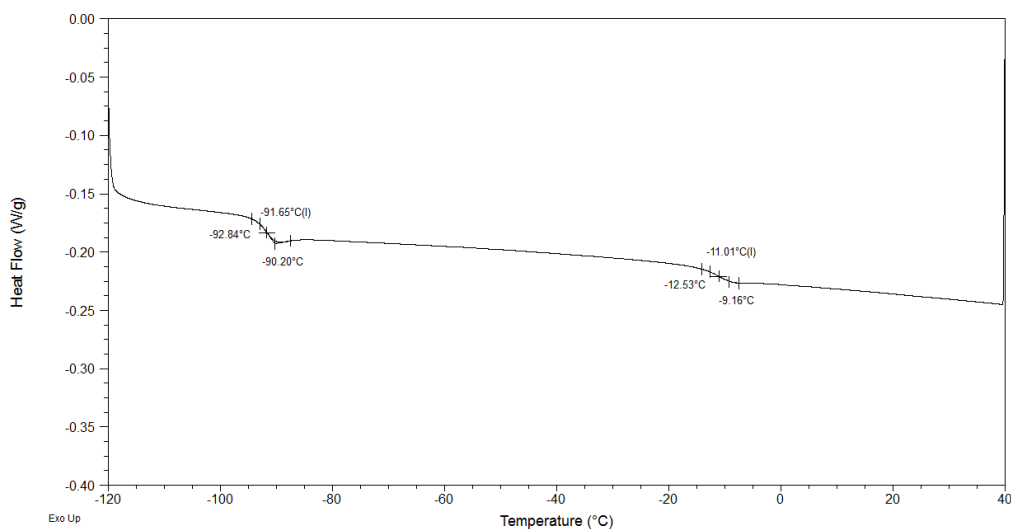


Figure 5.44: DSC thermograph of the PB(PI_{3,4})₂-S₅ star copolymer indicating T_g of PB equal to -91,65^oC and T_g of PI_{3,4} equal to -11,01^oC respectively.

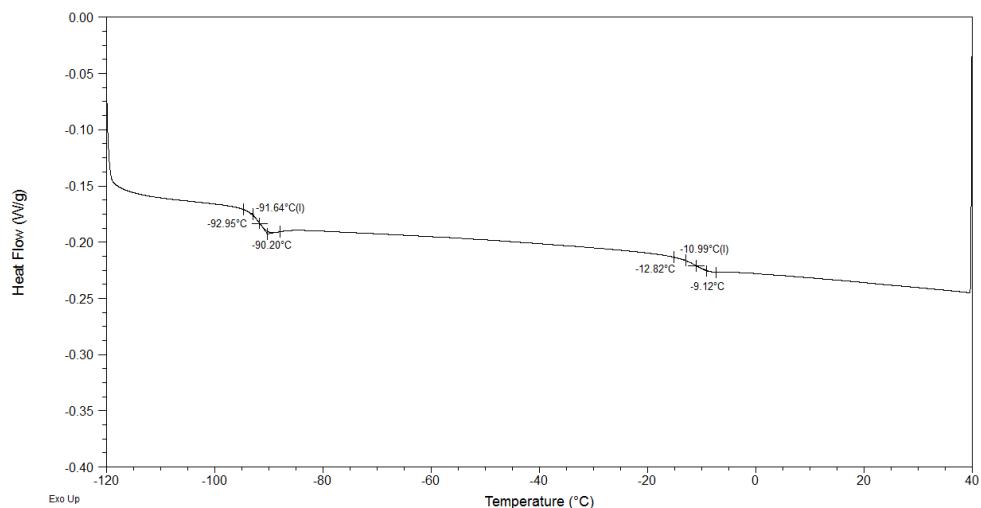


Figure 5.45: DSC thermograph of the $PB(PI_{3,4})_3-S_6$ star copolymer indicating T_g of PB equal to $-91,64^{\circ}C$ and T_g of $PI_{3,4}$ equal to $-10,99^{\circ}C$ respectively.

Analyzing the DSC results for the 3rd set of non-linear copolymers, again two endothermic transitions were obtained for each star copolymer respectively at identical values for both samples: $-92^{\circ}C$ and $-11^{\circ}C$ corresponding to the glass transition temperatures of PB and $PI_{3,4}$ blocks respectively. The relatively high value of the T_g of $PI_{3,4}$ in both samples is due to the high 3,4-content ($\sim 61\%$ and 58% respectively). The comparison of these star copolymers with $PB-b-PI_{3,4}-3$ linear block copolymer, reported also similar T_g values for both PB and $PI_{3,4}$ sequences. The DSC thermographs of the linear diblock copolymer and the corresponding star copolymers are presented in Figure 5.46.

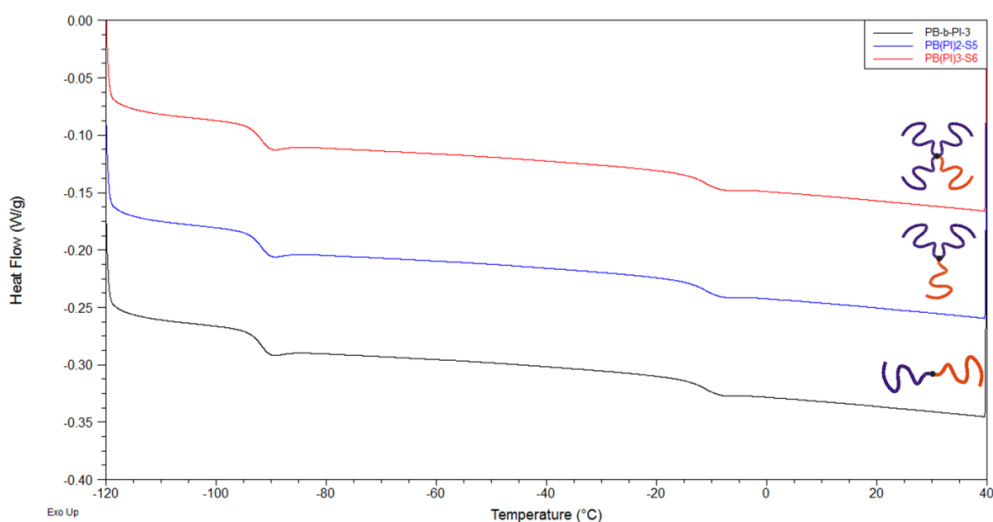


Figure 5.46: DSC thermographs of the $PB-b-PI_{3,4}-3$ linear block copolymer (indicated in black color), $PB(PI_{3,4})_2-S_5$ star copolymer (indicated in blue color) and $PB(PI_{3,4})_3-S_6$ star copolymer (indicated in red color) respectively.

In Figures 5.47 and 5.48 the DSC thermographs for the fourth set of miktoarm star copolymers, corresponding to $PB(PI_{3,4})_2-S_7$ and $PB(PI_{3,4})_3-S_8$ are presented.

4th Set:

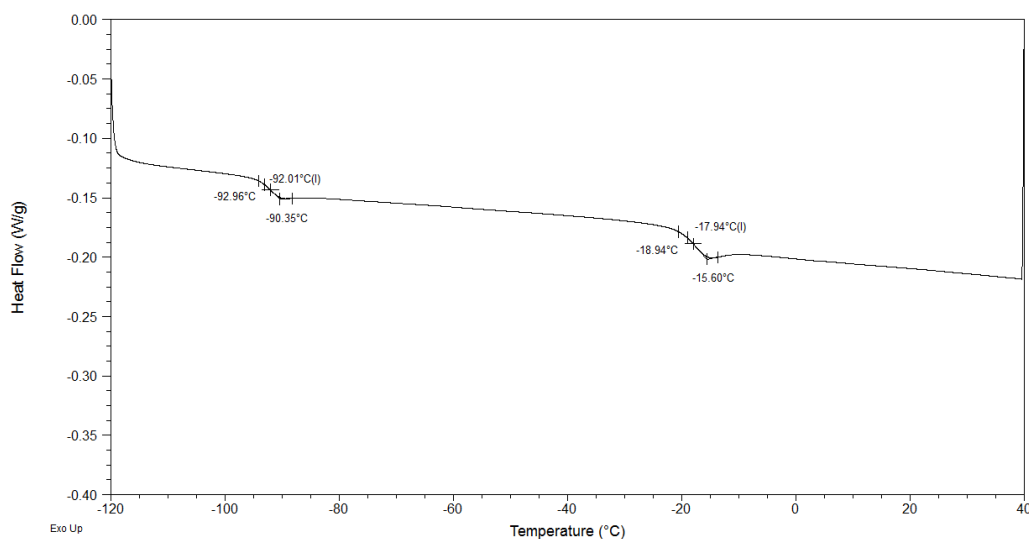


Figure 5.47: DSC thermograph of the $PB(PI_{3,4})_2-S_7$ star copolymer indicating T_g of PB equal to $-92,01^{\circ}C$ and T_g of $PI_{3,4}$ equal to $-17,94^{\circ}C$ respectively.

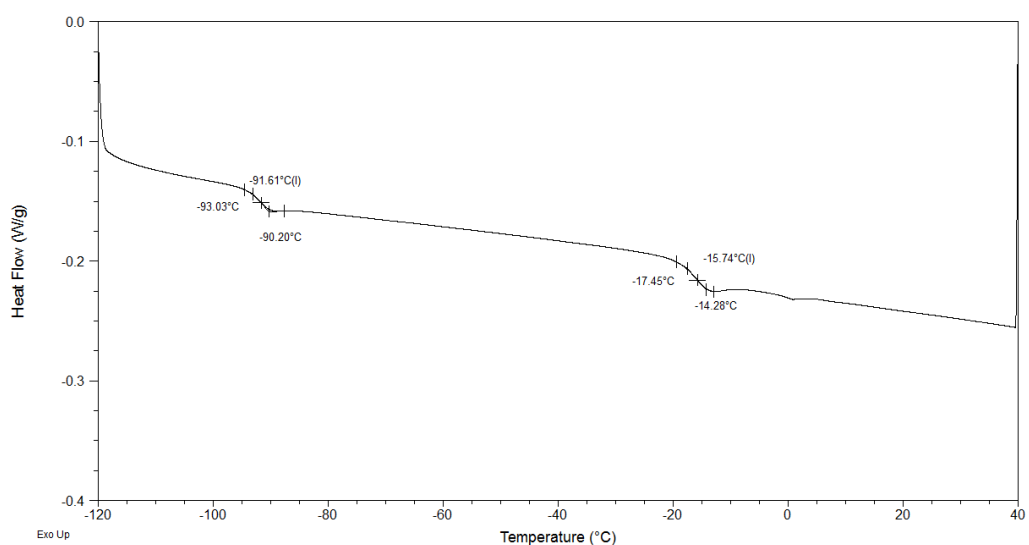


Figure 5.48: DSC thermograph of the $PB(PI_{3,4})_3-S_8$ star copolymer indicating T_g of PB equal to $-91,61^{\circ}C$ and T_g of $PI_{3,4}$ equal to $-15,74^{\circ}C$ respectively.

For this set again two endothermic transitions were obtained for each star copolymer and were almost identical in value: $-92^{\circ}C$ and $-16^{\circ}C$ corresponding to the glass transition temperatures of PB and $PI_{3,4}$ respectively. The relatively high value of the T_g of $PI_{3,4}$ in both samples is due to the high 3,4-content ($\sim 59\%$ and 62% respectively) but it is significantly different to the values reported for the other non-linear samples. The same behavior was evident for the corresponding diblock copolymer $PB-b-PI_{3,4}$ with similar molecular characteristics and mass fraction (T_g value of PI was $\sim -15^{\circ}C$). This slight discrepancy may be attributed to the higher PI mass fraction in this set of samples when compared to the star

copolymers of the other 3 sets and it is the only set in which the PI component is above 70% in mass and volume. Since the 3,4-content in PI is almost identical in all samples with only slight deviations (~2-3%) one should expect that due to the steric hindrance of the substituted vinyl bond per monomeric unit the T_g value would have been expected to be closer to zero and not that low as it is evident in all three samples involved in the fourth set. This behavior is awkward and more detailed studies should be made for giving a more straightforward explanation. The DSC thermographs of the linear diblock copolymer and the corresponding star copolymers are presented in Figure 5.49.

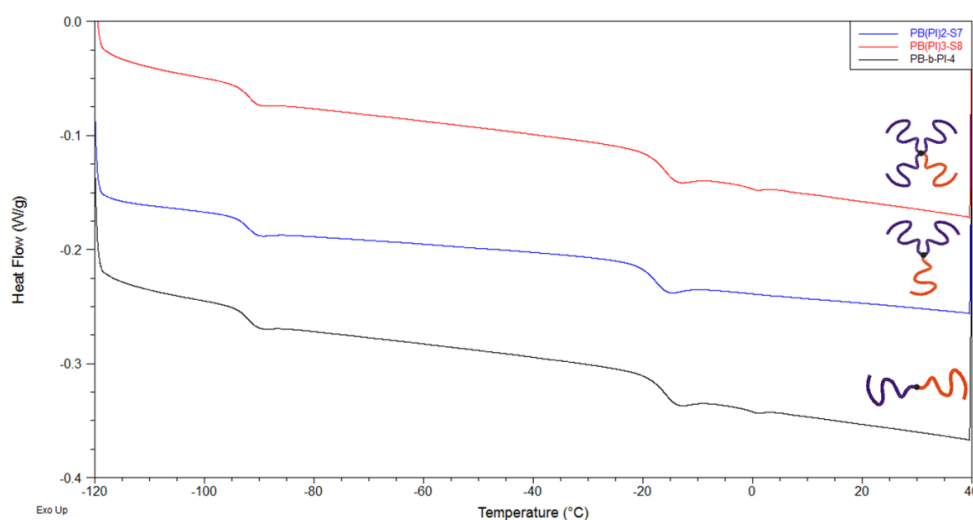


Figure 5.49: DSC thermographs of the PB-*b*-PI_{3,4}-4 linear block copolymer (indicated in black color), PB(PI_{3,4})₂-S₇ star copolymer (indicated in blue color) and PB(PI_{3,4})₃-S₈ star copolymer (indicated in red color) respectively.

Crystallization and melting point temperature (T_m) are not evident in all thermographs, since both PB and PI as synthesized by anionic polymerization with the specific microstructures exhibit T_m above 40⁰C as well as the non-linear microstructures (-1,2 and -3,4) are mostly atactic. The existence of two glass transition temperatures, similar to the glass transition temperatures of the corresponding homopolymers, leads to the conclusion that the two different blocks are completely immiscible. The glass transition temperatures of all miktoarm star copolymers and the corresponding linear diblock copolymers along with their molecular characteristics are summarized in Table 5.15 given below.

Table 5.15: Glass transition temperatures (T_g) of the miktoarm star copolymers and the corresponding linear diblock copolymers along with their molecular characteristics.

	Samples	$(\overline{M}_n)_{PB}^a$ (g/mol)	$(\overline{M}_n)_{PI}^a$ (g/mol)	$(\overline{M}_n)_{Total}^a$ (g/mol)	I_{Total}^b	$(\overline{M}_w)_{Total}^c$ (g/mol)	f_{PB}^d	φ_{PB}^e	$(T_g)_{PB}^f$ ($^{\circ}C$)	$(T_g)_{PI}^f$ ($^{\circ}C$)
1st set	PB-b-PI _{3,4} -1	38,200	55,400	93,600	1.06	99,200	0,42	0,42	-91,46	-7,99
	PB(PI _{3,4}) ₂ -S ₁	43,100	35,300	107,300	1.08	115,900	0,41	0,41	-91,35	-7,11
	PB(PI _{3,4}) ₃ -S ₂	43,100	23,800	109,400	1.07	117,000	0,40	0,40	-91,41	-5,10
2nd set	PB-b-PI _{3,4} -2	65,100	27,300	92,400	1.05	97,000	0,71	0,71	-91,35	-7,17
	PB(PI _{3,4}) ₂ -S ₃	61,500	16,700	92,400	1.06	97,900	0,67	0,67	-91,67	-4,33
	PB(PI _{3,4}) ₃ -S ₄	61,500	9,800	88,200	1.08	95,200	0,69	0,69	-91,48	-6,04
3rd set	PB-b-PI _{3,4} -3	58,300	40,200	98,500	1.06	104,400	0,59	0,59	-91,63	-10,98
	PB(PI _{3,4}) ₂ -S ₅	55,200	22,800	98,100	1.06	104,000	0,57	0,57	-91,65	-11,01
	PB(PI _{3,4}) ₃ -S ₆	55,200	15,600	100,300	1.07	107,300	0,56	0,56	-91,46	-10,99
4th set	PB-b-PI _{3,4} -4	35,500	72,400	107,900	1.07	115,600	0,32	0,32	-92,00	-17,91
	PB(PI _{3,4}) ₂ -S ₇	27,500	34,500	94,500	1.05	99,200	0,30	0,30	-92,01	-17,94
	PB(PI _{3,4}) ₃ -S ₈	27,500	25,700	101,600	1.05	106,700	0,28	0,28	-91,61	-15,74

5.10 Morphological Characterization Results for the Miktoarm Star Copolymers

The morphological characterization of the miktoarm star copolymers was accomplished by transmission electron microscopy (TEM) studies as already reported and analyzed for the case of the corresponding linear diblock copolymers.

A wide variety of volume fractions was targeted and synthesized in order to study the alternations of microphase separation of these non-linear copolymers of the (PB-b-PI_{3,4})_n type where n = 2, 3 with variation in composition. The $(\overline{M}_n)_{Total}$ of the final samples was kept approximately constant (as in the case of the linear diblock copolymers), ranging from 92,400-107,300 g/mol and 88,200-109,400 g/mol for samples (PB-b-PI_{3,4})₂ and (PB-b-PI_{3,4})₃ respectively as it is evident from Table 5.15 where the molecular characteristics, mass/volume fractions and glass transition temperatures are given. The degree of polymerization N for the two types of miktoarm star copolymers can be easily calculated from the following equations:

$$N_{PB(PI_{3,4})_2} = N_{PB} + 2N_{PI_{3,4}} = \frac{\overline{M}_n^{PB}}{M_0^{PB}} + 2 \frac{\overline{M}_n^{PI}}{M_0^{PI}} \quad (5.19)$$

$$N_{PB(PI_{3,4})_3} = N_{PB} + 3N_{PI_{3,4}} = \frac{\overline{M}_n^{PB}}{M_0^{PB}} + 3 \frac{\overline{M}_n^{PI}}{M_0^{PI}} \quad (5.20)$$

where $M_0^{PB} = 54$ g/mol, is the molecular weight of 1,3-butadiene (monomer of PB) and $M_0^{PI} = 68$ g/mol, is the corresponding molecular weight of isoprene (monomer of PI). In Table 5.16 the total degree of polymerization per sample is given together with other important characteristics (polydispersity, volume fractions and numer average molecular weights per block).

Table 5.16: Molecular characteristics, volume fractions and degrees of polymerization (N) for the miktoarm star copolymers of the PB(PI_{3,4})_n type where n is either 2 or 3.

Type of star	Samples	$(\overline{M}_n)_{PB}$ (g/mol)	$(\overline{M}_n)_{PI}$ (g/mol)	$(\overline{M}_n)_{Total}$ (g/mol)	I_{Total}	φ_{PB}	φ_{PI}	$N_{PB/PI_{3,4}}$
PB(PI _{3,4}) ₂	PB(PI _{3,4}) ₂ -S ₁	43,100	35,300	107,300	1.08	0,41	0,59	1836
	PB(PI _{3,4}) ₂ -S ₃	61,500	16,700	92,400	1.06	0,67	0,33	1631
	PB(PI _{3,4}) ₂ -S ₅	55,200	22,800	98,100	1.06	0,57	0,43	1692
	PB(PI _{3,4}) ₂ -S ₇	27,500	34,500	95,500	1.05	0,30	0,70	1523
PB(PI _{3,4}) ₃	PB(PI _{3,4}) ₃ -S ₂	43,100	23,800	109,400	1.07	0,40	0,60	1848
	PB(PI _{3,4}) ₃ -S ₄	61,500	9,800	88,200	1.08	0,69	0,31	1571
	PB(PI _{3,4}) ₃ -S ₆	55,200	15,600	100,300	1.07	0,56	0,44	1709
	PB(PI _{3,4}) ₃ -S ₈	27,500	25,700	101,600	1.05	0,28	0,72	1643

It is evident from the degree of polymerization calculated for the miktoarm star copolymers as exhibited in Table 5.16, that the values are approximately equal for the stars belonging in the same set but also with the corresponding diblock copolymer (the N values for the diblock copolymers are exhibited in Table 5.10 in the subchapter related to the diblock copolymer samples morphological characterization results).

A very thorough description has been given in subchapter 3.6 of this thesis where the microphase separation of non-linear copolymers has been thoroughly discussed. Taking into account the research work by Olvera de la Cruz and Sanchez¹¹³ concerning the phase stability of graft and miktoarm star copolymers of equal number of A and B arms through theoretical calculations has led to the fact that no critical point for any ϕ is evident for such complex architecture copolymers.

In the same study it was concluded that miktoarm star copolymers of the A_nB_n type are predicted to have critical point $(\chi N)_c=10.5$ (as for the diblocks when $\phi=0.5$), which signifies that the microphase separation of nearly symmetrical miktoarm stars depends only on the molecular weight of the associated block copolymer N_0 and not the whole star macromolecule.

For such non-linear copolymers as those synthesized in this thesis, Milner¹¹⁵ predicted a theoretical phase diagram for A_nB_n miktoarm star copolymers in the strong segregation limit, in which the interface between two blocks is very sharp. The morphologies are determined by the competition between the increase of stretching free energy as each arm stretches away from the interface and the reduction of the interfacial tension.

More specifically Milner's theory indicates that when $n_A = n_B = 1$, then the examined sample corresponds to the diblock copolymer (A-b-B). If $n_A = 2$ and $n_B = 1$ then the examined sample corresponds to the miktoarm star copolymer of the A_2B type and if $n_A = 3$ and $n_B = 1$ then A_3B type materials are studied. When an A_2B melt is studied with $\phi = 0.5$ and the A block length is half of B and the radius of gyration for A is half of B then the observed morphology is lamellae at the strong segregation limit (SSL), in which the need for equal density leads to the equal thickness of A and B. In that case the A chains should expand more than B and the surface is curved in order for A to be closer to the interface without stretching. The free energy per chain can be calculated by the following equation 5.21:

$$f_{ch}(r) \approx \frac{h^2}{R^2} \left(1 + \frac{c_1 h}{r} + \dots \right) \quad (5.21)$$

In the above equation $c_1 = \text{constant}$, $h = \text{segment thickness}$, $r = \text{curvature radius}$, $R = \text{radius of gyration}$ and $h = Vs$ ($V = \text{segment volume}$ and $s = \text{number of segments per junction point}$). For the example given (A_2B miktoarm star copolymer) the free energy is described by the following equation (5.22):

$$f_{A_2B}(r) \approx \frac{h_B^2}{R_B^2} \left(1 + \frac{c_1 h_B}{r} + \dots\right) + \frac{2h_A^2}{R_A^2} \left(1 - \frac{c_1 h_A}{r} + \dots\right) \quad (5.22)$$

The parameters involved in the above equation maybe become simpler if the segment volume (V) and the radii of gyration per segment will be used as shown below (equation 5.23-5.24):

$$\frac{c_1 h_B^3}{R_B^2 r} = \frac{2c_1 h_A^3}{R_B^2 r} \Rightarrow \frac{V_B^3}{R_B^2} = \frac{16V_A^3}{R_A^2} \quad (5.23)$$

$$\frac{V_{A,B}}{R_{A,B}^2} = l_{A,B} \quad (5.24)$$

It is well known from the literature that $l_{A,B}$ is a value independent of length and when both blocks A and B are equally flexible then $l_A = l_B$ and the interphase curvature is equal to zero leading to the alternating lamellae structure. The parameters l_A and l_B correspond to the term Kuhn length of segments A and B respectively.

Taking into consideration all the above together with the fact that the total free energy is the sum of the interfacial and stretching free energies (the former contributing due to localization of the junction points on the interface since Milner's theory involves strongly segregated systems in order to consider that the interface is of minimal thickness therefore reduction of interfacial tension occurs and the latter being increased due to overcrowding effects of the multiple identical arms either 2 or 3 in the miktoarm star samples prepared in this thesis), then a calculation for lamellae, hcp cylinders and bcc spheres total free energy values maybe performed through the following equations (5.25-5.27):

$$f_{LAM} = \left[\varepsilon(1-\varphi) + \frac{\varphi}{\varepsilon} \right]^{1/3} \quad (5.25)$$

$$f_{CYL} = \left[\frac{2\varepsilon\varphi(1-\varphi^{1/2})^3(3+\varphi^{1/2})}{(1-\varphi)^2} + \frac{2\varphi}{\varepsilon} \right]^{1/3} \quad (5.26)$$

$$f_{SPH} = \left[\frac{27\varepsilon\varphi^{4/3}(1-\varphi^{1/3})^3(\varphi^{2/3}+3\varphi^{1/3}+6)}{10(1-\varphi)^2} + \frac{27\varphi}{10\varepsilon} \right]^{1/3} \quad (5.27)$$

In equations 5.25-5.27 the new value that should be determined is the value ε which is denoted as the elasticity parameter and involves the influence on morphology from the architecture as well as the asymmetry in the chain elasticity. Parameter ε is calculated by the following equation (5.28) where the number of blocks A and B are involved together with their Kuhn lengths:

$$\varepsilon = \left(\frac{n_A}{n_B} \right) \left(\frac{l_A}{l_B} \right)^{1/2} \quad (5.28)$$

For the specific miktoarm star copolymers synthesized in the framework of this thesis a comparison between them will be presented, in order to verify whether or not these materials behave accordingly to related PS/PI non-linear samples of similar types already reported in the literature.^{115,128} In the following Figure 5.50, the phase diagram indicating the microphase separation for various miktoarm star copolymers as reported by Milner in comparison with experimental data is given.¹⁷¹ It is evident that as the asymmetry increases large deviations occur for the PS/PI corresponding systems (red symbols indicate discrepancies from the theoretically expected structures).

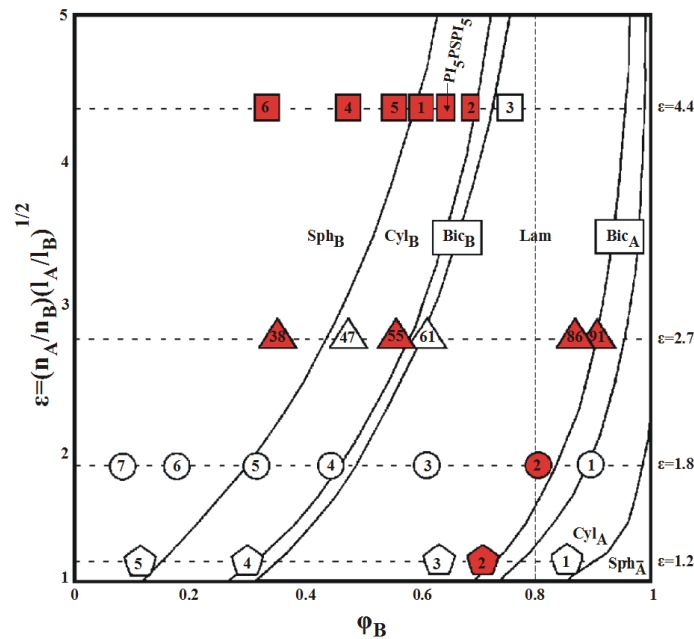


Figure 5.50: Phase diagram of microphase separation for various miktoarm star copolymers: A_2B_2 (pentagons) A_2B (cycles), A_3B (triangles), A_5B and A_5BA_5 (squares).¹⁷¹

5.9.1 Miktoarm Star Copolymers of the $PB(PI_{3,4})_2$ Type

Microphase separation was evident in all four related copolymers indicating that the choice of the molecular weights leading to relatively high total degree of polymerization per sample was correct as reported already for the case of the linear diblock copolymers.

Based on the diagram of ε vs φ_B (where B is the single block, PB in the specific samples) and taking into account that the volume fractions of PB are varying from 0.30 (sample S_7), to 0.41 (sample S_1) to 0.57 (sample S_5) and finally to 0.67 (sample S_3) the morphologies which must be obtained if the elasticity parameter ε as given in y axis is higher than 1.8 and closer to 2 (meaning slightly not equivalent in flexibility chains as expected due to the increased 3,4-content of PI leading to increased steric hindrance caused by the large ligand involving a methyl group vinyl bond per monomeric unit when compared to the high 1,4-content of the PB segments) are: PB hcp cylinders in PI matrix (samples S_3 and S_7) and alternating lamellae (samples S_1 and S_5) as indicated in Table 5.17.

Table 5.17: Molecular characteristics, volume fractions, degrees of polymerization (N) and theoretically predicted morphologies from the phase diagram in Figure 5.50 for the miktoarm star copolymers of the $PB(PI_{3,4})_2$ type.

Samples	$(\overline{M}_n)_{Total}$ (g/mol)	φ_{PB}	φ_{PI}	$N_{PB/PI_{3,4}}$	Morphology
PB(PI_{3,4})₂-S₁	107,300	0,41	0,59	1836	CYL _{PB}
PB(PI_{3,4})₂-S₃	92,400	0,67	0,33	1631	LAM
PB(PI_{3,4})₂-S₅	98,100	0,57	0,43	1692	LAM
PB(PI_{3,4})₂-S₇	95,500	0,30	0,70	1523	CYL _{PB}

The TEM results completely verify the theoretically expected structures. Actually, according to the above discussion as asymmetry increases large deviations occur for the PS/PI corresponding systems (red symbols indicate discrepancies from the theoretically expected structures) in Figure 5.50 phase diagram. The samples of the $PB(PI_{3,4})_2$ type exhibit the lowest asymmetry, flexibility of the segments is different but not as high as in the PS/PI system and therefore not large deviations from theory should be expected. In Figures 5.51–5.54 the TEM images of the thermal annealed $PB(PI_{3,4})_2$ type samples at 50⁰C for 5 days (as it was reported for the PB-b-PI_{3,4} diblock copolymers) are exhibited. It is clear that for the two samples (S_7 and S_1) with the lower PB volume fraction, a structure of hcp PB dark cylinders in an almost white PI matrix is observed (Figures 5.51–5.52), which is the expected morphology according to the samples' molecular characteristics (Table 5.17) whereas for the remaining two samples

(S_5 and S_3) alternating lamellae of dark and white layers is evident (Figure 5.53–5.54) as expected as well from theory.

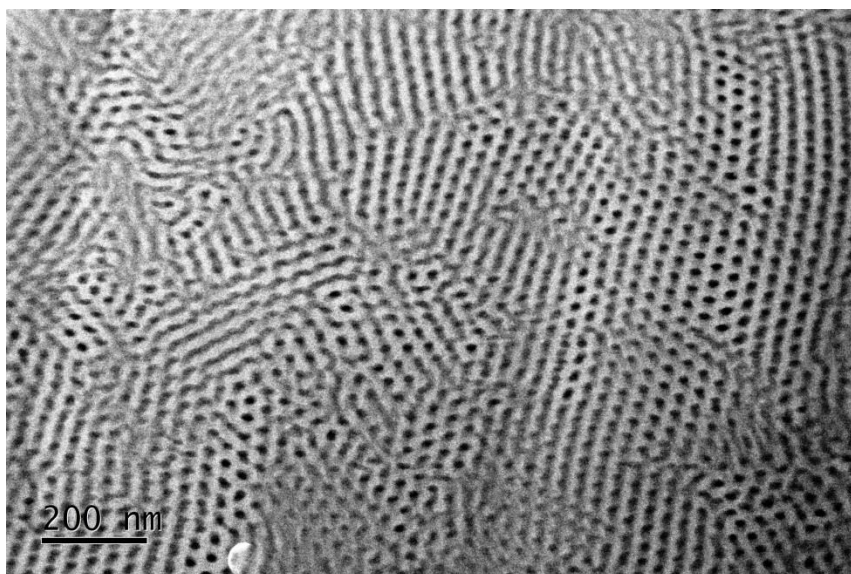


Figure 5.51: TEM image from thin sections of the annealed $PB(PI_{3,4})_2$ sample with PB volume fraction equal to 0.30 (sample S_7) in which hexagonally closed packed cylinders of the dark grey phase (PB) in the white matrix ($PI_{3,4}$) is evident.

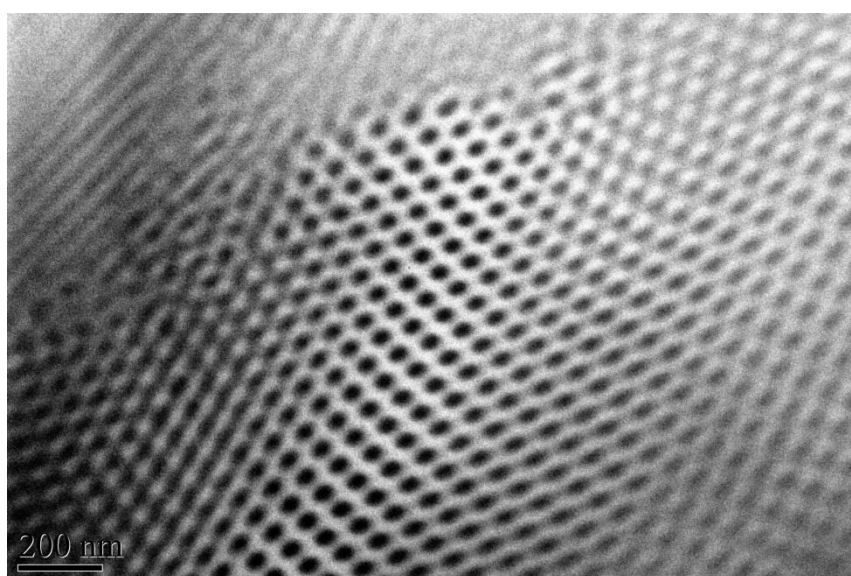


Figure 5.52: TEM image from thin sections of the annealed $PB(PI_{3,4})_2$ sample with PB volume fraction equal to 0.41 (sample S_1) in which hexagonally closed packed cylinders of the dark grey phase (PB) in the white matrix ($PI_{3,4}$) is evident.

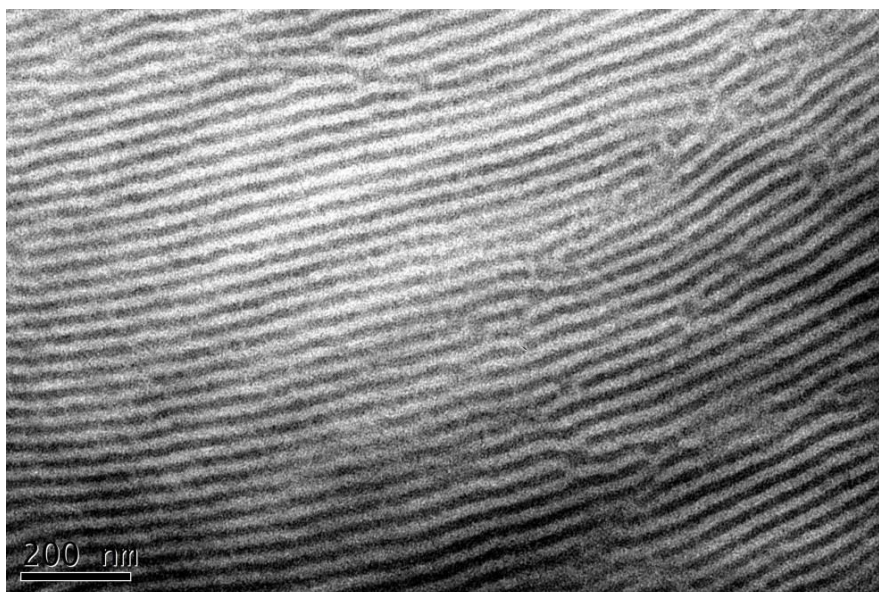


Figure 5.53: TEM image from thin sections of the annealed $PB(PI_{3,4})_2$ sample with PB volume fraction equal to 0.57 (sample S_5) in which alternating lamellae of the dark grey phase (PB) and the white phase ($PI_{3,4}$) is evident.

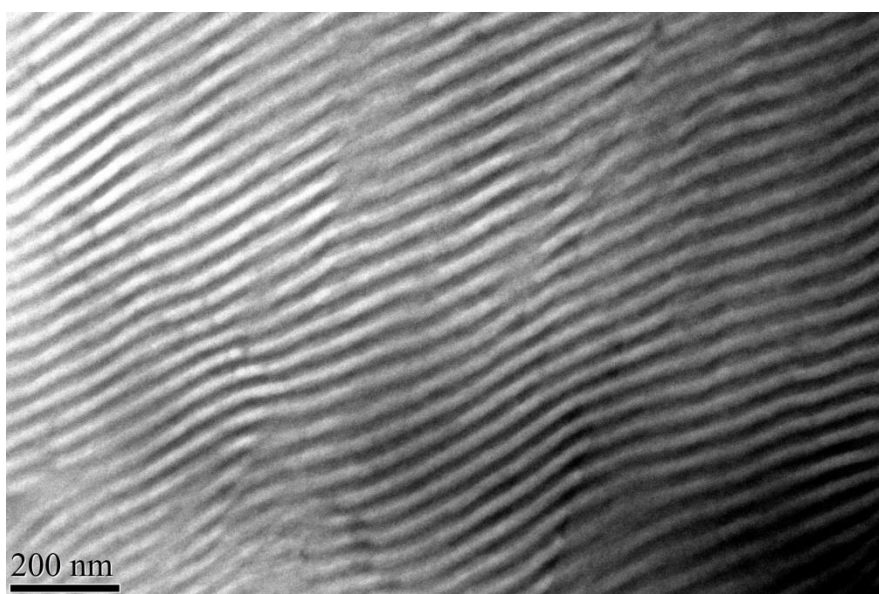


Figure 5.54: TEM image from thin sections of the annealed $PB(PI_{3,4})_2$ sample with PB volume fraction equal to 0.67 (sample S_3) in which alternating lamellae of the dark grey phase (PB) and the white phase ($PI_{3,4}$) is evident.

5.9.2 Miktoarm Star Copolymers of the $PB(PI_{3,4})_3$ Type

Microphase separation was again evident in all four related copolymers indicating that the choice of the molecular weights leading to relatively high total degree of polymerization per sample was correct as reported already for the case of the linear diblock copolymers and the corresponding $PB(PI_{3,4})_2$ type miktoarm stars.

Based on the same phase diagram of ϵ vs ϕ_B (where B is the single segment, PB in the specific samples) and taking into account that the volume fractions of PB are varying from

0.28 (sample S₈), to 0.40 (sample S₂) to 0.56 (sample S₆) and finally to 0.69 (sample S₃) the morphologies which must be obtained, if the elasticity parameter ε as given in y axis is higher than 2.7 and closer to 3 (meaning slight not equivalent in flexibility chains as expected due to the increased 3,4-content of PI leading to increased steric hindrance due to the large ligand involving a methyl group vinyl bond per monomeric unit when compared to the high 1,4-content of the PB segments) are: PB spheres in bcc lattice in PI matrix (samples S₈ and S₂), PB hcp cylinders in PI matrix (sample S₆) and alternating lamellae (sample S₄), as indicated in Table 5.18.

Table 5.18: Molecular characteristics, volume fractions, degrees of polymerization (N) and theoretically predicted morphologies from the phase diagram in Figure 5.45 for the miktoarm star copolymers of the PB(PI_{3,4})₃ type.

Samples	$(\overline{M}_n)_{Total}$ (g/mol)	φ_{PB}	φ_{PI}	$N_{PB/PI_{3,4}}$	Morphology
PB(PI _{3,4}) ₃ -S ₂	109,400	0,40	0,60	1848	SPH _{PB}
PB(PI _{3,4}) ₃ -S ₄	88,200	0,69	0,31	1571	LAM
PB(PI _{3,4}) ₃ -S ₆	100,300	0,56	0,44	1709	CYL _{PB}
PB(PI _{3,4}) ₃ -S ₈	101,600	0,28	0,72	1643	SPH _{PB}

In Figures 5.55–5.58 the TEM images of the thermal annealed PB(PI_{3,4})₃ type samples at 50⁰C for 5 days [as it was reported already for the PB-b-PI_{3,4} diblock copolymers and the PB(PI_{3,4})₂ type samples] are exhibited. It is clear that for the two samples (S₈ and S₂) with the lower PB volume fraction, a structure of PB dark spheres at a bcc lattice in an almost white PI matrix is observed (Figure 5.55–5.56), which is the expected morphology according to the samples' molecular characteristics (Table 5.18) and the phase diagram of Figure 5.50, whereas for the remaining two samples (S₆ and S₄) hcp cylinders of PB in the PI matrix (sample S₆, despite that PB is the majority component) and alternating lamellae of dark and white layers (sample S₄) are evident (Figures 5.57 and 5.58 respectively as expected as well from theory for the corresponding volume fractions of PB).

It can be concluded therefore, that despite the increase in asymmetry (going from A₂B to A₃B samples) the theory predicted by Milner did not lead to discrepancies when a comparison with the experimental results was made, in contrast to what has been reported in the literature for corresponding in volume fraction PS/PI identical systems.¹⁷⁰ This observation signifies that the elasticity parameter, ε , in the PB/PI_{3,4} copolymer non-linear architectures is as high as in the PS/PI case. Therefore, the flexibility of the PB and the PI_{3,4} chains is different due to the increased 3,4- and 1,2-content of the PI (when compared to the PI 1,4-microstructure content, ~90% in the PS/PI studied and well reported in the literature

systems) but still within comparable values. Therefore, the elasticity parameter, ϵ , in the miktoarm star copolymers synthesized in this thesis is exhibiting values closer to 2 and 3 respectively depending mostly in the increased complexity of the architecture ($n_A = 2$ or 3 whereas $n_B = 1$) and much less on the flexibility, leading to a phase diagram slightly different from that in Figure 5.50 since the lines indicating the transition from one morphology to another as volume fraction ϕ_B increases, should be less curved and more vertical to the x axis (corresponding to the volume fraction). This observation can be attributed to the fact that the non-linear copolymers studied in this thesis are 100% elastomers and not thermoplastic elastomers as the related PS/PI systems. Therefore, flexibility plays a significant role and when similar values are exhibited for the different segments involved in the copolymer (as the case of this thesis copolymer samples) the elasticity parameter, ϵ , adopts a value closer to an absolute integer (either 2 or 3) similar to the number of the similar blocks involved in the non-linear architectures either 2 $PI_{3,4}$ or 3 $PI_{3,4}$ chains for $PB(PI_{3,4})_2$ and $PB(PI_{3,4})_3$ type non-linear copolymers respectively.

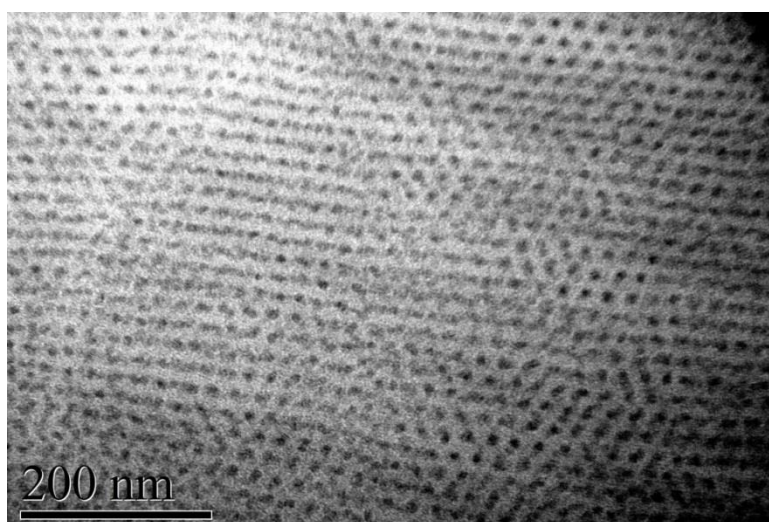


Figure 5.55: TEM image from thin sections of the annealed $PB(PI_{3,4})_3$ sample with PB volume fraction equal to 0.30 (sample S_8) in which bcc spheres of the dark grey phase (PB) in a white matrix ($PI_{3,4}$) is evident. The image does not show any alternating layers (as in the hcp cylinders) and since no SAXS experiments are possible, the TEM is significantly indicating bcc spheres of minority component (PB) in the matrix of the majority (PI).

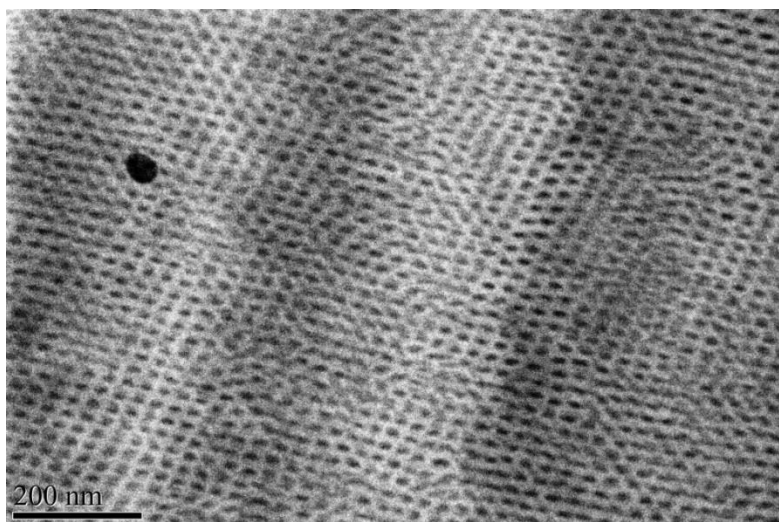


Figure 5.56: TEM image from thin sections of the annealed $PB(PI_{3,4})_3$ sample with PB volume fraction equal to 0.40 (sample S_2) in which bcc spheres of the dark grey phase (PB) in a white matrix ($PI_{3,4}$) is evident. The image does not show any alternating layers (as in the hcp cylinders) and since no SAXS experiments are possible, the TEM is significantly indicating bcc spheres of minority component (PB) in the matrix of the majority (PI).

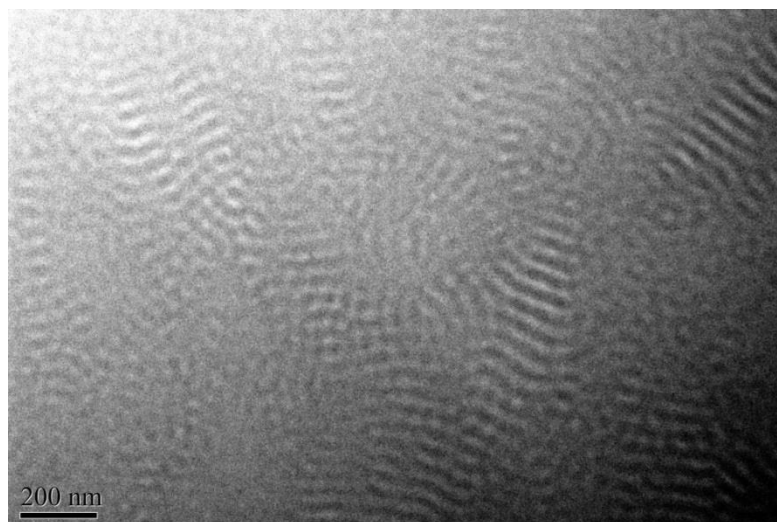


Figure 5.57: TEM image from thin sections of the annealed $PB(PI_{3,4})_3$ sample with PB volume fraction equal to 0.56 (sample S_6) in which hexagonally closed packed cylinders of the dark grey phase (PB) in the white matrix ($PI_{3,4}$) is evident. For this sample not well resolved images could be taken and of major importance is the fact that the cylinders are formed from the majority component (increased asymmetry leading to increased free energy stretching).

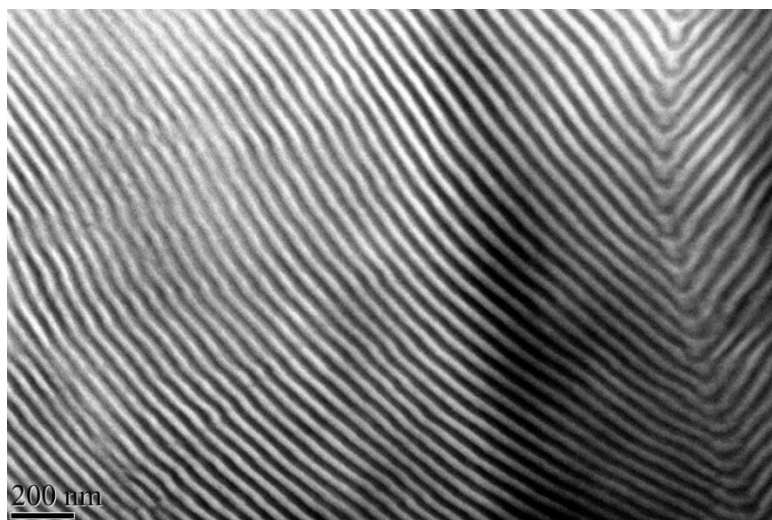


Figure 5.58: TEM image from thin sections of the annealed $PB(PI_{3,4})_3$ sample with PB volume fraction equal to 0.69 (sample S_4) in which alternating lamellae of the dark grey phase (PB) and the white phase ($PI_{3,4}$) is evident.

5.9.3 Comparison of the Morphological Characterization Results Between Linear and Non-Linear Architectures Involving Immiscible Polydienes

By summarizing the morphological characterization results as reported above for the linear PB- b - $PI_{3,4}$ diblock copolymers and the miktoarm star copolymers of the $PB(PI_{3,4})_n$ with $n = 2, 3$ a new Table (Table 5.19) is made in which four (4) new sets can be originated based on the fact that between the linear and the non-linear architectures the volume fraction and total number average molecular weight have remained constant in specific samples for comparison reasons. By this manner the influence of architecture in copolymers involving immiscible polydienes (PB and $PI_{3,4}$) which microphase separate can be studied and compared with the PS/PI related system which has been excessively studied as is evident in the literature as well as in the subchapters involving the analysis of the self-assembly for the various types of copolymers synthesized in the framework of the thesis.

The results between the theoretically predicted morphology and the experimentally obtained did not lead to any discrepancies for the miktoarm stars and as is evident from the last column of Table 5.19 there is an almost absolute agreement between theory and experiment which is not that common especially when many samples are involved (16 in total). It was expected initially that such type of agreement would occur only for the linear diblock copolymers as well as for the least complex architecture [samples of the $PB(PI_{3,4})_2$ type]. The fact that also the remaining $PB(PI_{3,4})_3$ type copolymers showed similar agreement is of great importance in order to conclude that the assumption made in the aforementioned subchapter concerning the fact that the elasticity parameter, ϵ , in the miktoarm star copolymers synthesized in this thesis is exhibiting values closer to 2 and 3 respectively

depending mostly in the increased complexity of the architecture ($n_A = 2$ or 3 whereas $n_B = 1$) and much less on the flexibility, is correct.

The only case where different results were obtained between theory and experiment was in the linear architecture where in both samples the morphology expected was the DG cubic structure (sample-2 and sample-4), with networks of the minority component in the matrix of the majority. In contrast, hexagonally closed packed cylinders of the minority component (PB or PI for $\varphi_{PB} = 0.32$ and 0.71 respectively) in the matrix of the majority (PI or PB) is the adopted morphology for the remaining two diblock copolymers samples as theoretically expected. As mentioned in the previous subchapter related to the morphological characterization of the diblock copolymers since PB and $PI_{3,4}$ are very flexible chains it seems that the ability to adopt such a complex architecture (DG) may not be possible due to entropic as well as enthalpic constrains leading to a less thermodynamically demanding topology such as the hcp cylinders of the minority phase in the matrix of the majority.

Table 5.19: *Molecular characteristics, volume fractions, degrees of polymerization (N) and theoretically predicted morphologies and verification of morphology for all the copolymers synthesized.*

Set of Samples	Samples	$(\overline{M}_n)_{Total}$ (g/mol)	φ_{PB}	φ_{PI}	$N_{PB/PI_{3,4}}$	Morphology from Theory	Verified Morphology
N° 1	PB-b- $PI_{3,4}$ -1	93,600	0,42	0,58	1522	LAM	✓
	PB($PI_{3,4}$) ₂ -S ₁	107,300	0,41	0,59	1836	CYL _{PB}	✓
	PB($PI_{3,4}$) ₃ -S ₂	109,400	0,40	0,60	1848	SPH _{PB}	✓
N° 2	PB-b- $PI_{3,4}$ -2	92,400	0,71	0,29	1606	DG	CYL _{PI}
	PB($PI_{3,4}$) ₂ -S ₃	92,400	0,67	0,33	1631	LAM	✓
	PB($PI_{3,4}$) ₃ -S ₄	88,200	0,69	0,31	1571	LAM	✓
N° 3	PB-b- $PI_{3,4}$ -3	98,500	0,59	0,41	1670	LAM	✓
	PB($PI_{3,4}$) ₂ -S ₅	98,100	0,57	0,43	1692	LAM	✓
	PB($PI_{3,4}$) ₃ -S ₆	100,300	0,56	0,44	1709	CYL _{PB}	✓
N° 4	PB-b- $PI_{3,4}$ -4	107,900	0,32	0,68	1722	DG	CYL _{PB}
	PB($PI_{3,4}$) ₂ -S ₇	95,500	0,30	0,70	1523	CYL _{PB}	✓
	PB($PI_{3,4}$) ₃ -S ₈	101,600	0,28	0,72	1643	SPH _{PB}	✓

It is evident from Table 5.19 that each set of samples involves copolymers with identical molecular characteristics (almost constant number average molecular weight), therefore identical polymerization degree and similar volume fractions. The comparison discussed in the previous subchapters involved the PS/PI related systems since most of the

theoretical predictions and theories concerning self-assembly have been developed for the specific thermoplastic elastomer copolymers.

It is the first time that self-assembly has been studied for copolymers being 100% elastomers and the fact that similar behavior with the PS/PI copolymers or better (since in this thesis samples no discrepancies have been indicated from theoretical predictions) was indicated opens a new field of research and development for the specific linear and non-linear architectures bearing immiscible polydienes.

In Figure 5.59 an attempt has been made to include all samples indicated in Table 5.19 in the phase diagram reported in the literature and already discussed and showed in Figure 5.50.

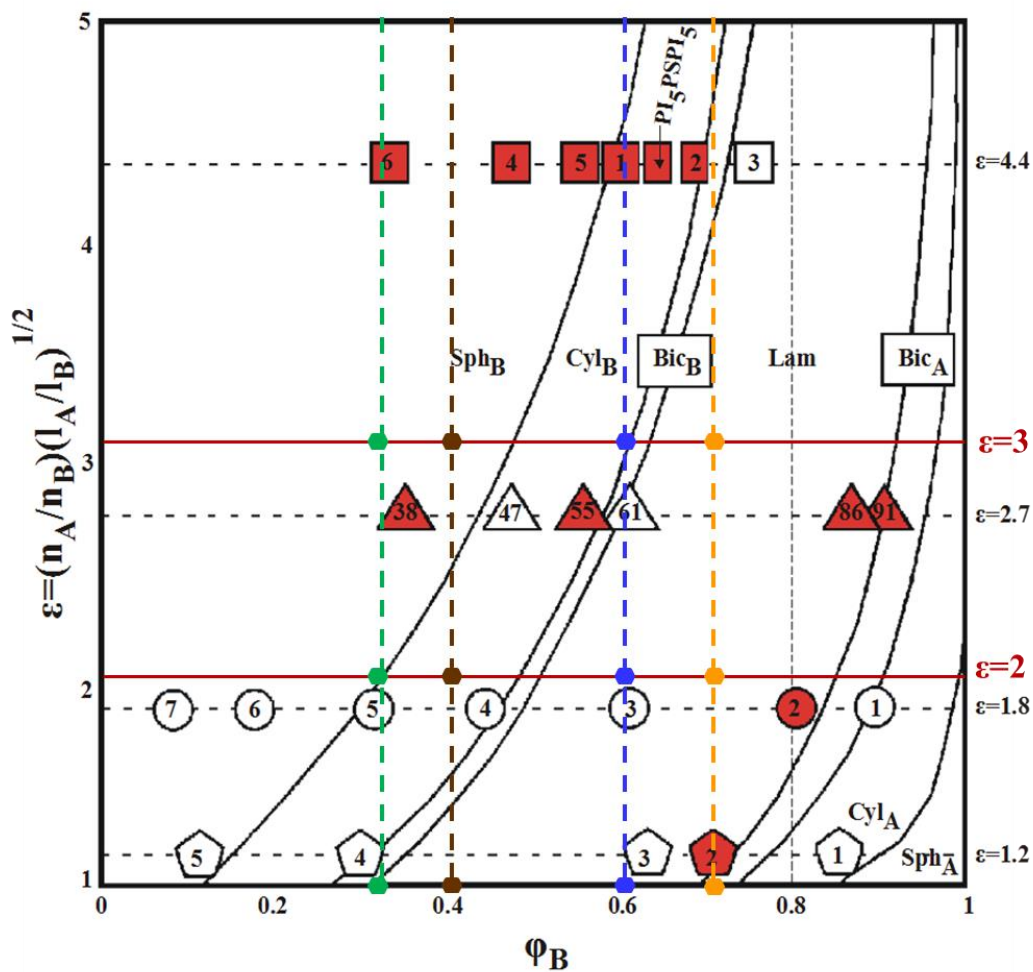


Figure 5.59: Modified phase diagram of microphase separation for various miktoarm star copolymers (initial diagram exhibited in Figure 5.45) in which the self-assembly results of the sixteen linear and non-linear PB/PI_{3,4} copolymers are indicated. Green color corresponds to set N° 4 (volume fraction ~0.3), brown to set N° 1 (volume fraction ~0.4), blue to set N° 3 (volume fraction ~0.6) and orange to set N° 2 (volume fraction ~0.7). It is evident that all miktoarm stars absolutely correspond to the theoretically predicted morphologies and discrepancies appear only for two diblock copolymers which instead of adopting the DG structure, hcp cylinders appear in both sides of the volume fraction axis (PS-*b*-PI_{3,4} of set N° 2 and 4 respectively with PB volume fractions of 0.71 and 0.32).

In Figure 5.59 the literature symbols ascribed to different architecture types for PS/PI systems were kept in order to show the increased discrepancies involved and also the integer values for parameter ε are shown as well for comparison reasons. Also the different 4 sets of samples have been assigned different colors and vertical lines are drawn indicating the volume fraction for each set and the symbols used are hexagons. It is straightforward from the above illustration that the only two samples out of the total sixteen (16) do not agree with theoretical prediction are those for which DG cubic structure (denoted as Bic_B and Bic_A in the schematic) was expected (red and orange hexagon for $\varepsilon=1$). The absence of such three-dimensional bicontinuous morphology should be verified in types of the studied samples by either preparing binary blends with homopolymers (easier approach, least time consuming, most cost effective) or synthesizing new copolymers within the volume fraction regime of 0.27-0.34 and 0.66-0.73 (which is a time consuming process and very difficult to control the volume fraction effectively in order for the new samples to vary just 1% in volume fraction between them).

5.11 Conclusions-Future Work

The synthesis of all samples [nineteen (19) in total] presented in this thesis is considered successful. Four (4) linear homopolymers of PI_{3,4} (55-65% of 3,4-microstructure) with low and high molecular weights, two (2) non-linear H-type PI_{3,4} homopolymers, five (5) linear diblock copolymers of the PB-b-PI_{3,4} type [PB: poly(butadiene) with ~90-92% -1,4] and miktoarm star copolymers of PB(PI_{3,4})₂ and PB(PI_{3,4})₃ types were synthesized. In order to make the necessary conclusions from the molecular and morphological characterization results and discussion, the samples were divided in two categories:

- a) *Linear and non-linear homopolymers of PI_{3,4}*
- b) *Linear diblock copolymers (PB-b-PI_{3,4}) and miktoarm stars [PB(PI_{3,4})₂ and PB(PI_{3,4})₃].*

The molecular characterization via size exclusion chromatography (SEC), membrane osmometry (MO) or vapor pressure osmometry (VPO) and proton nuclear magnetic resonance (¹H-NMR) spectroscopy indicated molecular and compositional homogeneity for all samples. Thermal analysis via differential scanning calorimetry (DSC) was also performed in order to examine the variations of glass transition temperatures and their dependence from the molecular weight and the weight fraction of each segment. Morphological characterization was performed in the linear diblock copolymers as well as in the miktoarm star copolymers, through bright field transmission electron microscopy (TEM), in order to verify the microphase separation and provide significant information concerning the dependence of the architecture (linear or non-linear) on the adopted topology. Furthermore, rheological studies were performed in linear and non-linear PI_{3,4} homopolymers, through the

collaboration with Prof. S.-Q. Wang's group (Morton Institute of Polymer Science and Engineering, The University of Akron, Ohio, USA).

It is important to mention that the non-linear H-PI_{3,4}, the linear PB-b-PI_{3,4} diblock copolymers and the miktoarm star copolymers of PB(PI_{3,4})₂ and PB(PI_{3,4})₃ type were synthesized for the first time and have never been reported in the literature.

5.11.1 Linear and Non-Linear Homopolymers of PI_{3,4}

Specifically, from the molecular characterization results for the linear and non-linear homopolymers of PI_{3,4} type the following conclusions can be made:

- ✓ The number average molecular weights obtained from MO or VPO verified the theoretical calculations of \overline{M}_n for the linear and the H-type homopolymers of PI_{3,4}. The molecular weights in the case of linear homopolymers varied from 5,000 g/mol up to 330,000 g/mol, while for the two (2) H-type PI_{3,4} homopolymers was 192,300 and 210,800 g/mol respectively.
- ✓ The molecular weight distributions of the linear homopolymers as well as of the non-linear H-type PI_{3,4} materials were monomodal since the polydispersity indices varied from 1,03 to 1,10 as indicated from SEC.
- ✓ The use of the difunctional reagent CDMSS [(4-chlorodimethylsilyl)styrene] in combination with the well-established chlorosilane chemistry led to well-defined final complex architecture homopolymers (H-PI_{3,4}).
- ✓ The mass fractionation procedure in a solvent (toluene)/non-solvent (methanol) mixture was necessary due to the synthetic approach requirements (e.g. excess of the living ends to successfully substitute the two chlorine atoms of the chlorosilane reagent) for the two (2) complex architecture homopolymers in order to obtain in high purity the desirable final products.
- ✓ The characteristic ratios of stereo-chemical microstructures of all samples were verified from the ¹H-NMR results, indicating the high 3,4-content (55-65%) of PI in all cases.

The thermal analysis was performed via differential scanning calorimetry and the glass transition temperatures were measured for the H-type PI_{3,4} samples and compared to those referred to linear PI_{3,4} homopolymers in the literature.¹⁶¹ More specifically:

- ✓ The two samples showed T_g values equal to -12^oC (H-PI_{3,4}-1) and -9^oC (H-PI_{3,4}-2) respectively.
- ✓ Glass transition temperature depends on the microstructure of PI and specifically it increases linearly with increasing 3,4-content as already reported in the literature¹⁶¹, even in the complex architecture systems.

Rheological measurements in the linear and non-linear homopolymers were performed by Prof. Wang's group, as previously mentioned, where uniaxial extension measurements were carried out through small amplitude oscillatory shear (SAOS) experiments. More specifically:

- ✓ The elastic modulus G_N^0 and the number of entanglements per chain Z were estimated for the linear PI_{3,4}-4 and the H-type PI_{3,4} homopolymer.
- ✓ Stress relaxation experiments which were carried out in the linear response regime for different temperatures reported that the chain relaxation dynamics showed the same temperature dependence.

The immediate future work and aims for the synthesized linear and non-linear homopolymers of this research work are:

- a) The molecular characterization of the H-type PI_{3,4} homopolymers through dilute solutions viscometry (DSV) in selective and Θ solvents respectively.
- b) Synthesis and molecular characterization of H-type PI_{3,4} samples in higher molecular weights (>400,000 g/mol), in order to examine further the rheological behavior of this architecture (through the collaboration with Prof. S.-Q. Wang's group). It should be noted that preliminary studies have already been in progress using the difunctional reagent 4-(dichloromethylsilyl)diphenylethylene (DCMSDPE), in a similar synthetic strategy obtained for the aforementioned samples synthesized in this thesis.
- c) Synthesis and molecular characterization of super H-type PI_{3,4} samples in various molecular weights, in order to investigate thoroughly the non-linear dynamic behavior of LCB polymers in the presence of large external deformations in either simple shear or uniaxial extension (in collaboration with Prof. S.-Q. Wang's group).

5.11.2 Linear Diblock Copolymers (PB-b-PI_{3,4}) and Miktoarm Stars [PB(PI_{3,4})₂ and PB(PI_{3,4})₃]

In these types of materials the molecular characterization results via SEC, MO and ¹H-NMR spectroscopy indicated molecular and compositional homogeneity for all the samples. More specifically:

- ✓ The number average molecular weights obtained from MO verified the theoretical calculations of \overline{M}_n for the PB and PI blocks as well as for the final diblock and miktoarm star copolymers. The molecular weights of all samples (diblock and star copolymers) were calculated to be in the region of 90,000-110,000 g/mol except of one diblock copolymer (PB-b-PI_{3,4}-5), which exhibited very high value of \overline{M}_n (~1000 kg/mol) approximately one order of magnitude higher than the other copolymers.

- ✓ The molecular weight distributions of the PB block of each diblock copolymer as well as of the final materials were monomodal with values ranging from 1,05 to 1,10.
- ✓ The molecular weight distributions of PB and PI_{3,4} blocks as well as the final star copolymers were monomodal ranging from 1,05 to 1,08. The well-established chlorosilane chemistry led to well-defined final star copolymers.
- ✓ The mass fractionation procedure in a solvent (toluene)/non-solvent (methanol) mixture was necessary due to the synthetic approach requirements (e.g. excess of the living ends to successfully substitute all chlorine atoms of the corresponding chlorosilane reagent in each case) for the eight (8) star copolymers, in order to remove the undesired excess of the PI blocks and obtain in high purity the desirable final products.
- ✓ The mass fractions of PB and PI blocks were also verified from the ¹H-NMR results, indicating molecular and compositional homogeneity for the synthesized samples. The mass fractions as well as the volume fractions varied from 28% v/v to 71% v/v of the PB block (ϕ_{PB}).
- ✓ Furthermore, the characteristic ratios of stereo-chemical microstructures of PB and PI were calculated with ¹H-NMR, indicating the high 3,4-content of PI (57-62%) and the high 1,4-microstructure of the PB (90-92%) respectively.

The thermal analysis was performed via DSC and the glass transition temperatures were measured for all synthesized linear diblock and star copolymers, where the independence of T_g from the molecular weight and the different architecture was obtained. More specifically:

- ✓ The existence of two glass transition temperatures in all samples (linear and non-linear) with values similar to those already reported for the corresponding homopolymers, led to the conclusion that the two different blocks are completely immiscible.
- ✓ The T_g values were approximately -92⁰C to -91⁰C for the PB block and in the region of -11⁰C to to -5⁰C for the PI_{3,4} block in the linear diblock copolymers.
- ✓ Unique is the case of the linear diblock copolymer PB-b-PI_{3,4}-4 which exhibited lower T_g for the PI_{3,4} block than the aforementioned samples (-17,91⁰C). This low value was attributed to the fact that this sample is the only one with very high content in PI ($\phi_{PB} = 0,32$).
- ✓ Linear and non-linear architectures of copolymers of the PB(PI_{3,4})_n type, where n=1, 2, 3 respectively, with approximately the same molecular characteristics (molecular weight and mass or volume fractions) exhibited similar values of T_g for both blocks.

The morphological characterization via transmission electron microscopy (TEM) indicated that the two different blocks can self-assemble leading to known morphologies, where

interesting conclusions raised for both linear diblock and non-linear star copolymers. More specifically:

- ✓ All samples were cast from a dilute solution (~4 wt%) in toluene (an almost non-selective solvent for both segments) and the procedure for slow evaporation of the solvent was accomplished in approximately 7 days.
- ✓ Annealing was performed to the half of the film at 50⁰C for 5 days, in order to study morphologically the unannealed and annealed thin sections.
- ✓ Part of the films was ultra-microtomed in order to obtain very thin sections (~40-50 nm) at -100⁰C.
- ✓ The polydiene blocks (PB and PI_{3,4}) were selectively stained with fresh aqueous solution (4% wt in water) of osmium tetroxide (OsO₄) for approximately 1 h, in order to increase the contrast in TEM. In this manner, the PB chains crosslink more than the PI_{3,4} chains, with the staining media increasing their electron density and therefore they appear darker in TEM micrographs.
- ✓ Microphase separation was evident in all five diblock copolymers indicating that the choice of the molecular weights leading to relatively high total degree of polymerization per sample was correct.
- ✓ The observation of well identified morphologies leading to alternating lamellae and hcp cylinders in all cases indicates that the Flory-Huggins interaction parameter is at least an order of magnitude higher than the one reported for the case of PB_{1,4}-b-PI_{1,4} diblock copolymers ($\chi = 0,0012$).¹¹⁹
- ✓ Thermal annealing improved the order of self-assembly, leading to the important conclusion that the χN value of the first four samples is at least in the intermediate segregation regime, whereas the high molecular weight sample is very strongly segregated.
- ✓ A comparison of the morphologies of PB-b-PI_{3,4} linear diblock copolymers with the theoretical and experimental information on microphase separation of the well-studied PS-b-PI diblock copolymers, indicated that total agreement between them was achieved only in sample-1 ($\phi_{PB} = 0.42$), sample-3 ($\phi_{PB} = 0.59$) and sample-5 ($\phi_{PB} = 0.59$), since alternating lamellae morphology was observed. In both samples -2 and -4 hcp cylinders of the minority component in the matrix of the majority were the adopted morphologies respectively, instead of a cubic network (double gyroid) that was expected. This was attributed to the fact that PB and PI_{3,4} are very flexible chains and the ability to adopt such a complex architecture may not be possible due to entropic as well as enthalpic constraints leading to a less thermodynamically demanding topology such as the hcp cylinders of the minority phase in the matrix of the majority.

- ✓ Microphase separation was evident in all eight star copolymers synthesized, indicating that the choice of the molecular weights leading to relatively high total degree of polymerization per sample was correct.
- ✓ The observation of well identified morphologies leading to alternating lamellae and hcp cylinders in the case of $PB(PI_{3,4})_2$ miktoarm star copolymers, as well as to spheres and hcp cylinders in the case of $PB(PI_{3,4})_3$ star copolymers completely verified the theoretically expected structures according to Milner's phase diagram for PS/PI system.¹¹⁵
- ✓ The elasticity parameter, ϵ , in the $PB/PI_{3,4}$ copolymer non-linear architectures is not that dependent on flexibility as in the PS/PI case. The flexibility of the PB and the $PI_{3,4}$ chains is different due to the increased 3,4- and 1,2-content of the PI when compared to the 1,4-microstructure, ~90% in the PS/PI system but still within comparable values.
- ✓ In this study it was not possible to perform SAXS measurements, since the electron densities of PB and PI are considered equivalent.

The future work and aims for the synthesized diblock copolymers of this research work are listed below:

- a) Synthesis of a diblock copolymer of the $PB-b-PI_{3,4}$ type in which one of the two blocks will be deuterated (d -PB or d -PI), in order to perform small-angle neutron scattering (SANS) measurements and calculate the interaction parameter χ of this system.
- b) Prepare more diblock copolymers of the $PB-b-PI_{3,4}$ type in various volume fractions in order to construct phase diagram χN vs. volume fraction for this system.
- c) Prepare binary blends of the diblock copolymers with either homopolymer PB or homopolymer $PI_{3,4}$ in order to explore whether the double gyroid will appear in the volume fraction regime 0.27-0.34 and 0.66-0.73 as is reported for the PS/PI system.
- d) Investigate the photonic properties and behavior of the high molecular weight sample-5, since it already appears to be photonic.

Finally, the future work and aims concerning the miktoarm star copolymers synthesized in this thesis are listed below:

- a) Further investigation of the molecular characterization of the star copolymer samples via dilute solutions viscometry (DSV) in selective and non-selective solvents.
- b) Synthesis, molecular and morphological characterization of the $PI_{3,4}(PB_{1,4})_2$ and $PI_{3,4}(PB_{1,4})_3$ types of star copolymers, in order to obtain similarities or discrepancies with the synthesized star copolymers in this thesis, concerning the microphase separation of this system.

- c) Synthesis, molecular and morphological characterization of other complex architectures such as $PB(PI_{3,4})_n$ type, where $n > 3$.

References

1. Aleman J., Chadwick A. V., He J., Hess M., Horie K., Jones R. G., Kratoscvil P., Meisel I., Mita I., Moad G., Penczek S., Stepto R. F. T., *Pure Appl. Chem.* **2007**, *79*, 1801.
2. Bhowmick A. K., Stephens H., *Handbook of Elastomers, Second Edition*, Taylor & Francis, **2000**.
3. Visakh P. M., Sabu T., Arup K. C., Aji P. M.: *Advances of Elastomers I*; Springer, **2013**.
4. Drobny J. G., *Handbook of Thermoplastic Elastomers*, William Andrew, Inc., **2007**.
5. Morton M., *Anionic Polymerization: Principles and Practice*; Academic Press, New York., **1983**.
6. Lazzari M., Liu G., Lecommandoux S., *Block Copolymers in Nanoscience*; Wiley-VCH., **2006**.
7. Bates F. S., Frendickson G. H., *Phys. Today* **1999**, *52*, 32.
8. Mark H. F., Kroschwitz J. I., *Encyclopedia of Polymer Science and Technology, 3rd edition*, John Wiley & Sons., **2003**.
9. Hadjichristidis N., Pispas S., Pitsikalis M., Iatrou H., Vlahos C., *Asymmetric Star Polymers: Synthesis and Properties. In Branched Polymers I*; Roovers, J., Ed., Advances in Polymer Science, Springer Berlin Heidelberg, **1999**, *142*, pp 71-127.
10. Hadjichristidis N., *J. Polym. Sci. A: Polym. Chem.* **1999**, *37*, 857.
11. Uhrig D., Mays J., *Polym. Chem.* **2011**, *2*, 69.
12. Perny S., Allgaier J., Cho D., Lee W., Chang T., *Macromolecules* **2001**, *34*, 5408.
13. Iatrou H., Avgeropoulos, A., Hadjichristidis N., *Macromolecules* **1994**, *27*, 6232.
14. Munmaya K., Mishra Shiro K., *Star and Hyperbranched Polymers*, Marcel Dekker, Inc., **1999**.
15. Nikopoulou A., Iatrou H., Lohse D. J., Hadjichristidis N., *J. Polym. Sci. A: Polym. Chem.* **2009**, *47*, 2597.
16. Rangou S., Theodorakis P. E., Gergidis L. N., Avgeropoulos A., Efthymiopoulos P., Smyrniaios D., Kosmas M., Vlahos C., Giannopoulos T., *Polymer* **2007**, *48*, 652.
17. Avgeropoulos A., Paraskeva S., Hadjichristidis N., Thomas E. L., *Macromolecules* **2002**, *35*, 4030.
18. Avgeropoulos A., Rangou S., Krikorian V., Thomas E. L., *Macromol. Symp.* **2008**, *267*, 16.
19. Flory, P., *Principles of Polymer Chemistry*, Cornell University Press, **1953**.
20. Blomquist A. T., Tapp W. J., Johnson J. R., *J. Am. Chem. Soc.* **1945**, *67*, 1519.
21. Beaman R. G., *J. Am. Chem. Soc.* **1948**, *70*, 3115.
22. Szwarc M., Levy M., Milkovich R., *J. Am. Chem. Soc.* **1956**, *78*, 2656.
23. Szwarc M., *Nature* **1956**, *178*, 1168.
24. Fetters L. J., *J. Polym. Sci. C: Polym. Symp.* **1969**, *26*, 1.
25. Lambert C., von Ragué Schleyer P., *Angew. Chem. Int. Ed. in English* **1994**, *33*, 1129.
26. Schade C., von Rague Scheyer P., *Adv. Organom. Chem.* **1987**, *27*, 169.
27. Hsieh H. L., *J. Polym. Sci. A: General Papers* **1965**, *3*, 163.
28. Hadjichristidis N., Iatrou H., Pispas S., Pitsikalis M., *J. Polym. Sci. A: Polym. Chem.* **2000**, *38*, 3211.
29. Brown T. L., *Acc. Chem. Res.* **1968**, *1*, 23.
30. Lewis H. L., Brown T. L., *J. Am. Chem. Soc.* **1970**, *92*, 4664.
31. Margerison D., Newport J. P., *Trans. Far. Soc.* **1963**, *59*, 2058.
32. Margerison D., Pont J. D., *Trans. Far. Soc.* **1971**, *67*, 353.
33. Bywater S., Worsfold D. J., *J. Organom. Chem.* **1967**, *10*, 1.
34. Weiner M., Vogel G., West R., *Inorg. Chem.* **1962**, *1*, 654.
35. Glaze, W. H., Freeman C. H., *J. Am. Chem. Soc.* **1969**, *91*, 7198.
36. Hsieh H. L., Glaze W. H., *Rub. Chem. Technol.* **1970**, *43*, 22.
37. Altares T., Wyman D. P., Allen V. R., *J. Polym. Sci. A: General Papers* **1964**, *2*, 4533.
38. Mays J., Hadjichristidis N., *Polym. Bull.* **1989**, *22*, 471.

39. Conlon D. A., Crivello J. V., Lee J. L., O'Brien M. J., *Macromolecules* **1989**, *22*, 509.
40. Morton M., Bostick E. E., Clarke R. G., *J. Polym. Sci. A: General Papers* **1963**, *1*, 475.
41. Kuntz I., Gerber A., *J. Polym. Sci.* **1960**, *42*, 299.
42. Mavroudis A., Avgeropoulos A., Hadjichristidis N., Thomas E. L., Lohse D. J., *Chem. Mat.* **2003**, *15*, 1976.
43. Xu Z., Mays J., Chen X., Hadjichristidis N., Schilling F. C., Bair H. E., Pearson D. S., Fetters L. J., *Macromolecules* **1985**, *18*, 2560.
44. Natori I., *Macromolecules* **1997**, *30*, 3696.
45. Hong K., Mays J. W., *Macromolecules* **2001**, *34*, 782.
46. Allen R. D., Long T. E., McGrath J. E., *Polym. Bull.* **1986**, *15*, 127.
47. Ekizoglou N., Hadjichristidis N., *J. Polym. Sci. A: Polym. Chem.* **2001**, *39*, 1198.
48. Bellas V., Iatrou H., Hadjichristidis N., *Macromolecules* **2000**, *33*, 6993.
49. Paul, D. R., Barlow J. W., *J. Macromol. Sci. Rev. Chem.* **1980**, *C(18)*, 109.
50. Bahary W. S., Sapper D. I., *Rub. Chem. Tech.* **1967**, *40*, 1529.
51. Burfield D. R., Lim K. L., *Macromolecules* **1983**, *16*, 1170.
52. Natori, I., Imaizumi K., Yamagishi H., Kazunori M., *J. Polym. Sci. B: Polym. Phys.* **1998**, *36*, 1657.
53. Imaizumi K., Ono T., Natori I., Sakurai S., Takeda K., *J. Polym. Sci. B: Polym. Phys.* **2001**, *39*, 13.
54. Morton M., Fetters L. J., *Rub. Chem. Tech.* **1975**, *48*, 359.
55. Bywater S., Firat Y., Black P. E., *J. Polym. Sci.: Polym. Chem. Ed.* **1984**, *22*, 669.
56. Duck E. W., Locke J. M., *Polydienes by Anionic Catalyst*, John Wiley & Sons, New York, **1977**.
57. Hsieh H. L., Quirk R. P., *Anionic Polymerization: Principles and Practical Applications*, Marcel Dekker, Inc., New York, **1996**.
58. Worsfold D. J., Bywater S., *Can. J. Chem.* **1964**, *42*, 2884.
59. Bywater S., Johnson A. F., Worsfold D. J., *Can. J. Chem.* **1964**, *42*, 1255.
60. Bywater S., Worsfold D. J., *Can. J. Chem.* **1967**, *45*, 1821.
61. Gebert W., Hinz J., Sinn H., *Die Makromol Chem.* **1971**, *144*, 97.
62. Salle R., Pham Q.-T., *J. Polym. Sci.: Polym. Chem. Ed.* **1977**, *15*, 1799.
63. Dyball C. J., Worsfold D. J., Bywater S., *Macromolecules* **1979**, *12*, 819.
64. Hsu W. L., Halasa A. F., US.Patent No 5,239,023, **1993**.
65. Bower D. I., *An Introduction to Polymer Physics*, Cambridge University Press, New York, **2002**.
66. Roovers, J., Toporowski P. M., *Macromolecules* **1981**, *14*, 1174.
67. Hakiki A., Young R. N., McLeish T. C. B., *Macromolecules* **1996**, *29*, 3639.
68. Rahman M. S., Aggarwal R., Larson R. G., Dealy J. M., Mays J. W., *Macromolecules* **2008**, *41*, 8225.
69. Chen X., Rahman M. S., Lee H., Mays J. W., Chang T., Larson R., *Macromolecules* **2011**, *44*, 7799.
70. Rahman M. S., Lee H., Chen X., Chang T., Larson R., Mays J. W., *ACS Macro Letters* **2012**, *1*, 537.
71. Chen X., Lee H., Rahman M. S., Chang T., Mays J. W., Larson R., *Macromolecules* **2012**, *45*, 5744.
72. Knauss D. M., Al-Muallem H. A., Huang T., Wu D. T., *Macromolecules* **2000**, *33*, 3557.
73. Al-Muallem H. A., Knauss D. M., *J. Polym. Sci. A: Polym. Chem.* **2001**, *39*, 3547.
74. Vazaios A., Lohse D. J., Hadjichristidis N., *Macromolecules* **2005**, *38*, 5468.
75. Chalari I., Hadjichristidis N., *J. Polym. Sci. A: Polym. Chem.* **2002**, *40*, 1519.
76. Hamley I. W., *Developments in block copolymer science and technology*, J. Wiley, **2004**.
77. Darling S. B., *Prog. Polym. Sci.* **2007**, *32*, 1152.
78. Bang J., Jeong U., Ryu D. Y., Russell T. P., Hawker C. J., *Advanced Materials* **2009**, *21*, 4769.

79. Park C., Yoon J., Thomas E. L., *Polymer* **2003**, *44*, 6725.
80. Ross C. A., Cheng J. Y., *MRS Bull.* **2008**, *33*, 838.
81. Jackson E. A., Hillmyer M. A., *ACS Nano* **2010**, *4*, 3548.
82. Deng T., Chen C., Honeke, C., Thomas E. L., *Polymer* **2003**, *44*, 6549.
83. Uhrig D., Mays J. W., *J. Polym. Sci. A: Polym. Chem.* **2005**, *43*, 6179.
84. Hadjichristidis N., Pitsikali, M., Pispas S., Iatrou H., *Chem. Rev.* **2001**, *101*, 3747.
85. Ruzette A.-V., Leibler L., *Nat Mater* **2005**, *4*, 19.
86. Morton M., *Anionic Polymerization: Principles and Practice*, Academic Press, New York., **1973**.
87. Antkowiak T. A., Oberster A. E., Halasa A. F., Tate, D. P., *J. Polym. Sci. A-1: Polym. Chem.* **1972**, *10*, 1319.
88. Tsoukatos T., Avgeropoulos A., Hadjichristidis N., Hong K., Mays J. W., *Macromolecules* **2002**, *35*, 7928.
89. Hautekeer J. P., Varshney S. K., Fayt R., Jacobs C., Jerome R., Teyssie P., *Macromolecules* **1990**, *23*, 3893.
90. Zilliox J. G., Roovers J., Bywater S., *Macromolecules* **1975**, *8*, 573.
91. Ciolino A., Sakellariou G., Pantazis D., Villar M. A., Vallés E., Hadjichristidis N., *J. Polym. Sci. A: Polym. Chem.* **2006**, *44*, 1579.
92. Mays J. *Polym. Bull.* **1990**, *23*, 247.
93. Iatrou H., Siakali-Kioulafa E., Hadjichristidis N., Roovers J., Mays J., *J. Polym. Sci. B: Polym. Phys.* **1995**, *33*, 1925.
94. Avgeropoulos A., Hadjichristidis N., *J. Polym. Sci. A: Polym. Chem.* **1997**, *35*, 813.
95. Tselikas Y., Iatrou, H., Hadjichristidis N., Liang K. S., Mohanty K., Lohse D. J., *J. Chem. Phys.* **1996**, *105*, 2456.
96. Bates F. S., Fredrickson G. H., *Ann. Rev. Phys. Chem.* **1990**, *41*, 525.
97. Bates F. S., *Science* **1991**, *251*, 898.
98. Leibler L., *Macromolecules* **1980**, *13*, 1602.
99. Helfand E., *Macromolecules* **1975**, *8*, 552.
100. Helfand E., Wasserman Z. R., *Macromolecules* **1976**, *9*, 879.
101. Helfand E., Wasserman Z. R., *Macromolecules* **1978**, *11*, 960.
102. Semenov, A. N., *J. Exper. Theor. Phys.* **1985**, *61*, 733.
103. Papadakis C. M., Almdal K., Mortensen K., Posselt D., *J. Phys. II France* **1997**, *7*, 1829.
104. Hasegawa H., Tanaka H., Yamasaki K., Hashimoto T., *Macromolecules* **1987**, *20*, 1651.
105. Mayes A. M., Olvera de la Cruz M., *Macromolecules* **1991**, *24*, 3975.
106. Matsen M. W., Schick M., *Phys. Rev. Lett.* **1994**, *72*, 2660.
107. Matsen M. W., Bates F. S., *Macromolecules* **1996**, *29*, 1091.
108. Hajduk D. A., Takenouchi H., Hillmyer M. A., Bates F. S., Vigild M. E., Almdal K., *Macromolecules* **1997**, *30*, 3788.
109. Matsen M. W., Bates F. S., *J. Polym. Sci. B: Polym. Phys.* **1997**, *35*, 945.
110. Khandpur A. K., Foerster S., Bates F. S., Hamley I. W., Ryan A. J., Bras W., Almdal K., Mortensen K., *Macromolecules* **1995**, *28*, 8796.
111. Park J., Jang S., Kon Kim J., *J. Polym. Sci. B: Polym. Phys.* **2015**, *53*, 1.
112. Hadjichristidis N., Pispas S., Floudas G., *Structure Factor and Chain Architecture. In Block Copolymers*, John Wiley & Sons, Inc., **2003**, 268-285.
113. Olvera de la Cruz M., Sanchez I. C., *Macromolecules* **1986**, *19*, 2501.
114. Mayes A. M., Olvera de la Cruz M., *J. Chem. Phys.* **1989**, *91*, 7228.
115. Milner S. T., *Macromolecules* **1994**, *27*, 2333.
116. Matsen M. W., Schick M., *Macromolecules* **1994**, *27*, 6761.
117. Thomas E. L., Alward D. B., Kinning D. J., Martin D. C., Handlin D. L., Fetters L. J., *Macromolecules* **1986**, *19*, 2197.
118. Hashimoto T., Ijichi Y., Fetters L. J., *J. Chem. Phys.* **1988**, *89*, 2463.

119. Floudas G., Hadjichristidis N., Iatrou H., Pakula T., Fischer E. W., *Macromolecules* **1994**, *27*, 7735.
120. Floudas G., Pispas S., Hadjichristidis N., Pakula T., Erukhimovich I., *Macromolecules* **1996**, *29*, 4142.
121. Floudas G., Hadjichristidis N., Iatrou H., Avgeropoulos A., Pakula T., *Macromolecules* **1998**, *31*, 6943.
122. Pochan D. J., Gido S. P., Pispas S., Mays J. W., *Macromolecules* **1996**, *29*, 5099.
123. Floudas G., Hadjichristidis N., Tselikas Y., Erukhimovich I., *Macromolecules* **1997**, *30*, 3090.
124. Grason G. M., Kamien R. D., *Macromolecules* **2004**, *37*, 7371.
125. Matsen M. W., *Macromolecules* **2012**, *45*, 2161.
126. Bailey T. S., Hardy C. M., Epps T. H., Bates F. S., *Macromolecules* **2002**, *35*, 7007.
127. Takenaka M., Wakada T., Akasaka S., Nishitsuji S., Saijo K., Shimizu H., Kim M. I., Hasegawa H., *Macromolecules* **2007**, *40*, 4399.
128. Hadjichristidis N., Iatrou H., Behal S. K., Chludzinski J. J., Disko M. M., Garner R. T., Liang K. S., Lohse D. J., Milner S. T., *Macromolecules* **1993**, *26*, 5812.
129. Pochan D. J., Gido S. P., Pispas S., Mays J. W., Ryan A. J., Fairclough J. P. A., Hamley I. W., Terrill N. J., *Macromolecules* **1996**, *29*, 5091.
130. Cohen R. E., Ramos A. R., *Macromolecules* **1979**, *12*, 131.
131. Cohen R. E., Wilfong D. E., *Macromolecules* **1982**, *15*, 370.
132. Neumann C., Abetz V., Stadler R., *Colloid Polym Sci* **1998**, *276*, 19.
133. Neumann C., Loveday D. R., Abetz V., Stadler R., *Macromolecules* **1998**, *31*, 2493.
134. Mogi Y., Kotsuji H., Kaneko Y., Mori K., Matsushita Y., Noda I., *Macromolecules* **1992**, *25*, 5408.
135. Gido S. P., Schwark D. W., Thomas E. L., de Carmo Goncalves M., *Macromolecules* **1993**, *26*, 2636.
136. Zapsas G., Moschovas D., Ntetsikas K., Rangou S., Lee J. H., Thomas E. L., Zafeiropoulos N. E., Avgeropoulos, A., *Accepted in J. Polym. Sci. B: Polym. Phys.* **4/2015**.
137. Carreau P. J., Degee D. C. R., Chhaabla R. P., *Rheology of Polymeric Systems. Principles and Applications*; Gardner Publications, Inc.: Cincinnati, **1997**.
138. Larson, R. G., *The Structure and Rheology of Complex Fluids*, OUP USA, **1999**.
139. Rohn C. L., *Analytical Polymer Rheology: Structure-processing-property Relationships*, Hanser, **1995**.
140. Goodwin J., Hughes R. W., *Rheology for Chemists: An Introduction*, Royal Society of Chemistry, Cambridge, **2000**.
141. Archer L. A., *J. Rheol.* **1999**, *43*, 1555.
142. Doi M., Edwards S. F., *The theory of polymer dynamics*; Clarendon Press, **1986**.
143. Watanabe H., *Prog. Polym. Sci.* **1999**, *24*, 1253.
144. McLeish T. C. B., *Adv. Phys.* **2002**, *51*, 1379.
145. Tapadia P., Wang S.-Q., *Phys. Rev. Lett.* **2006**, *96*, 016001.
146. Ravindranath S., Wang S.-Q., *J. Rheol.* **2008**, *52*, 957.
147. Ravindranath S., Wang S.-Q., Olechnowicz M., Quirk R. P., *Macromolecules* **2008**, *41*, 2663.
148. Lee C., Gido S. P., Poulos Y., Hadjichristidis N., Tan N. B., Trevino S. F., Mays, J. W., *J.Chem.Phys.* **1997**, *107*, 6460.
149. Münstedt H., Laun H. M., *Rheol. Acta* **1981**, *20*, 211.
150. Münstedt H., Kurzbeck S., Egersdörfer L., *Rheol. Acta* **1998**, *37*, 21.
151. Wagner M. H., Bastian H., Hachmann P., Meissner J., Kurzbeck S., Münstedt H., Langouche F., *Rheol. Acta* **2000**, *39*, 97.
152. Rasmussen H. K., Nielsen J. K., Bach A., Hassager O., *J. Rheol.* **2005**, *49*, 369.
153. McLeish T. C. B., *Phys. Today* **2008**, 40.
154. McLeish T. C. B., Larson R. G., *J.Rheol.* **1998**, *42*, 81.

155. McLeish T. C. B., Allgaier J., Bick D. K., Bishko G., Biswas P., Blackwell R., Blottière B., Clarke N., Gibbs B., Groves D. J., Hakiki A., Heenan, R. K., Johnson J. M., Kant R., Read D. J., Young R. N., *Macromolecules* **1999**, 32, 6734.
156. Daniels D. R., McLeish T. C. B., Kant R., Crosby B. J., Young R. N., Pryke A., Allgaier J., Groves D. J., Hawkins R. J., *Rheol. Acta* **2001**, 40, 403.
157. Wang S.-Q., *Soft Matter* **2015**, 11, 1454.
158. Colvin I. C. *Scientific Glassblowing: An Introduction*, **2008**.
159. Francuskiewicz, F., *Polymer fractionation*, Springer, Berlin, **1994**.
160. Ito K., *Prog. Polym. Sci.* **1998**, 23, 581.
161. Widmaier J. M., Meyer G. C., *Macromolecules* **1981**, 14, 450.
162. Liu G., Sun H., Rangou S., Ntetsikas K., Avgeropoulos A., Wang, S.-Q., *J.Rheol.* **2013**, 57, 89.
163. Sun H., Ntesikas K., Avgeropoulos A., Wang S.-Q., *Macromolecules* **2013**, 46, 4151.
164. Sentmanat M., *Rheol. Acta* **2004**, 43, 657.
165. Sentmanat M., Wang B. N., McKinley G. H., *J.Rheol.* **2005**, 49, 585.
166. Brandrup J., Immergut E. H., Clarke E. A., *Polymer Handbook*, 4th edition ed., **2003**.
167. Fox T. G., Flory P. J., *J.Polym. Sci.* **1954**, 14, 315.
168. Williams D. B., Carter B. C., *Transmission Electron Microscopy: A Textbook for Materials Science*; Springer, **2009**.
169. Sawyer L. C., Grubb D. T., *Polymer Microscopy*; Chapman & Hall, **2008**.
170. Schacher F., Yuan J., Schoberth H. G., Müller A. H. E., *Polymer* **2010**, 51, 2021.
171. Beyer, F. L., Gido S. P., Velis G., Hadjichristidis N., Tan N. B., *Macromolecules* **1999**, 32, 6604.

Abstract

In the present research thesis, the synthesis of nineteen (19) samples of linear and non-linear homopolymers and copolymers containing PI_{3,4} [where PI_{3,4}: poly(isoprene) enriched in 3,4-microstructure (55-65%)] is reported. Specifically, four (4) linear homopolymers of the PI_{3,4} type exhibiting low and high molecular weights, two (2) non-linear homopolymers of the H-PI_{3,4} type, five (5) linear diblock copolymers of the PB-b-PI_{3,4} type [where PB: poly(butadiene) with ~90-92% 1,4-content] exhibiting high (~100,000 g/mol) and very high molecular weights (~1,000,000 g/mol) as well as eight (8) miktoarm star copolymers of the PB(PI_{3,4})₂ and PB(PI_{3,4})₃ types [four (4) samples per architecture] with approximately similar molecular characteristics with the linear diblock copolymers were synthesized.

The synthesis of the PI_{3,4} linear homopolymers was accomplished by the use of anionic polymerization through high vacuum techniques. For the successful polymerization of isoprene, *sec*-BuLi was used as the initiator and benzene as the solvent, while a small amount of THF (~1 mL) was added in order for the PI to obtain high 3,4-microstructure (55-65%).

The complete synthesis of the complex architecture of the H-PI_{3,4} type involved initially the preparation of the difunctional reagent 4-(chlorodimethylsilyl)styrene (CDMSS) in order to synthesize a macroinitiator in combination with living ends of PI_{3,4}⁽⁻⁾Li⁽⁺⁾. Through this macroinitiator a living 3-arm star of the (PI_{3,4})₂PI_{3,4}' type was prepared and by a linking reaction with the appropriate chlorosilane [(CH₃)₂SiCl₂], the desirable model H-type PI_{3,4} samples were synthesized.

The preparation of linear diblock copolymers were achieved utilizing anionic polymerization via high vacuum techniques and sequential monomer addition. Again, *sec*-BuLi was used as the initiator, benzene as the solvent, while a small amount of THF (~1 mL) was added prior to the polymerization of isoprene, in order for the PI to obtain high 3,4-microstructure. A variety of volume fractions was chosen and accomplished (0,30 < φ_{PB} < 0,70). For the synthesis of the star copolymers chlorosilane chemistry in combination with anionic polymerization techniques were used. The linking reactions of the appropriate chlorosilane (CH₃SiCl₃ or SiCl₄) with living PB and PI blocks, led to the final miktoarm stars under absolutely controlled conditions. The molecular weights (~100,000 g/mol) as well as the volume fractions of PB and PI blocks were approximately equal with those for the linear diblock copolymers.

The molecular characterization was performed via size exclusion chromatography (SEC) and membrane osmometry (MO) or vapor pressure osmometry (VPO) in order to confirm the molecular weight distributions and the number average molecular weight \overline{M}_n of the samples.

Also, proton nuclear magnetic resonance ($^1\text{H-NMR}$) spectroscopy was adopted to calculate the characteristic ratios of stereochemical microstructures for both poly(dienes) as well as to identify the composition of each segment in the copolymers and stars.

Thermal analysis via differential scanning calorimetry (DSC) was also performed in order to examine the variation of glass transition temperature and its dependence from the molecular weight and the weight fraction of each segment. The results indicated that all samples exhibited low molecular weight distributions and molecular as well as compositional homogeneity.

Morphological characterization was performed through bright field transmission electron microscopy (TEM), in order to verify microphase separation and provide significant information concerning the dependence of the architecture (linear or non-linear) on the adopted morphology.

Furthermore, rheological studies were performed in linear and non-linear $\text{PI}_{3,4}$ homopolymers, through the collaboration with Prof. S.-Q. Wang (Morton Institute of Polymer Science and Engineering, The University of Akron, Ohio, USA), leading to new theoretical considerations for the non-linear dynamic behavior of LCB polymers and their mixtures with the corresponding linear chains in the presence of large external deformations in either simple shear or uniaxial extension.

Περίληψη

Στη συγκεκριμένη ερευνητική εργασία περιγράφεται η σύνθεση συνολικά δεκαεννέα (19) γραμμικών και πολύπλοκης αρχιτεκτονικής ομοπολυμερών και συμπολυμερών πολυ(ισοπρενίου) υψηλής περιεκτικότητας σε μικροδομή -3,4 ($PI_{3,4}$). Συγκεκριμένα, συντέθηκαν τέσσερα (4) ομοπολυμερή $PI_{3,4}$ χαμηλού και υψηλού μοριακού βάρους, δύο ομοπολυμερή πολύπλοκης αρχιτεκτονικής του τύπου $H-PI_{3,4}$, πέντε (5) γραμμικά δισυσταδικά συμπολυμερή του τύπου $PB-b-PI_{3,4}$ (όπου PB : πολυ(βουταδιένιο) μικροδομής -1,4) ενδιάμεσου (~100,000 g/mol) και υψηλού μοριακού βάρους (~1,000,000 g/mol) καθώς και μικτόκλωνων αστεροειδών συμπολυμερών των τύπων $PB(PI_{3,4})_2$ και $PB(PI_{3,4})_3$ με περίπου τα ίδια μοριακά χαρακτηριστικά με αυτά των γραμμικών δισυσταδικών συμπολυμερών αντίστοιχα.

Η σύνθεση των γραμμικών ομοπολυμερών πολυ(ισοπρενίου) πραγματοποιήθηκε μέσω του ανιοντικού πολυμερισμού με χρήση τεχνικών υψηλού κενού. Ο πολυμερισμός του ισοπρενίου επιτεύχθηκε χρησιμοποιώντας τον απαρχητή *sec*-BuLi σε διαλύτη βενζόλιο και προσθέτοντας μία μικρή ποσότητα THF (~1 mL), ώστε να εμφανίζει το πολυ(ισοπρένιο) υψηλή περιεκτικότητα σε μικροδομή -3,4 (55-65%).

Η σύνθεση των πολύπλοκης αρχιτεκτονικής ομοπολυμερών του τύπου $H-PI_{3,4}$ αρχικά περιελάμβανε την παρασκευή του διδραστικού αντιδραστήριου σύζευξης 4-(chlorodimethylsilyl)styrene (CDMSS), το οποίο χρησιμοποιήθηκε για την σύνθεση ενός μακροαπαρχητή από την σύζευξη του με ζωντανούς κλάδους $PI_{3,4}$. Στη συνέχεια παρασκευάστηκε ένα αστεροειδές ομοπολυμερές τριών κλάδων του τύπου $(PI_{3,4})_2PI_{3,4}'$ όπου μέσω αντιδράσεων σύζευξης με το κατάλληλο χλωροσιλάνιο $[(CH_3)_2SiCl_2]$, προέκυψαν τα επιθυμητά ομοπολυμερή πολύπλοκης αρχιτεκτονικής του τύπου $H-PI_{3,4}$.

Για την σύνθεση των γραμμικών δισυσταδικών συμπολυμερών χρησιμοποιήθηκε η μέθοδος του ανιοντικού πολυμερισμού με τεχνικές υψηλού κενού μέσω διαδοχικής προσθήκης μονομερών. Ως απαρχητής του πολυμερισμού χρησιμοποιήθηκε το *sec*-BuLi σε διαλύτη βενζόλιο και προσθέτοντας μία μικρή ποσότητα THF (~1 mL) πριν τον πολυμερισμό του ισοπρενίου, για την επίτευξη της υψηλής σε περιεκτικότητα μικροδομής -3,4. Συντέθηκε ένα μεγάλο εύρος κλασμάτων όγκου για το PB κυμαινόμενο από 0,30 έως 0,70 ($0,30 < \phi_{PB} < 0,70$). Για την παρασκευή των αστεροειδών συμπολυμερών χρησιμοποιήθηκε η μέθοδος του ανιοντικού πολυμερισμού σε συνδυασμό με την χημεία χλωροσιλανίων. Οι αντιδράσεις σύζευξης του κατάλληλου χλωροσιλανίου (CH_3SiCl_3 ή $SiCl_4$) με τους ενεργούς κλάδους του PB και του PI , οδήγησαν στην επιτυχή σύνθεση των μικτόκλωνων αστεροειδών υπό απόλυτα ελεγχόμενες συνθήκες. Τα μοριακά βάρη όπως και τα κλάσματα όγκου των συστάδων ήταν περίπου ίσα με αυτά των γραμμικών δισυσταδικών συμπολυμερών.

Ο μοριακός χαρακτηρισμός των δειγμάτων πραγματοποιήθηκε με τις τεχνικές της χρωματογραφίας αποκλεισμού μεγεθών (size exclusion chromatography, SEC) και ωσμωμετρίας μεμβράνης (membrane osmometry, MO) για τον υπολογισμό των κατανομών μοριακών βαρών και των μέσων μοριακών βαρών κατ' αριθμό. Επιπλέον, χρησιμοποιήθηκε η φασματοσκοπία πυρηνικού μαγνητικού συντονισμού πρωτονίου ($^1\text{H-NMR}$) ώστε να επιβεβαιωθούν τα κλάσματα μάζας και η ομοιογένεια ως προς την σύσταση και το μοριακό βάρος, καθώς και τα ποσοστά των μικροδομών των πολυδιενίων. Επίσης έγινε χρήση της διαφορικής θερμιδομετρίας σάρωσης (differential scanning calorimetry, DSC) ώστε να προσδιοριστούν οι θερμοκρασίες υαλώδους μετάπτωσης (T_g) των τελικών δειγμάτων και να μελετηθεί η εξάρτηση της από το μοριακό βάρος.

Ο μορφολογικός χαρακτηρισμός των γραμμικών δισυσταδικών συμπολυμερών καθώς και των αστεροειδών συμπολυμερών πραγματοποιήθηκε με την χρήση της ηλεκτρονικής μικροσκοπίας διέλευσης φωτεινού πεδίου (bright field transmission electron microscopy, TEM), όπου πιστοποιήθηκε ο μικροφασικός διαχωρισμός των συστάδων.

Τέλος, μέσω της συνεργασίας με την ερευνητική ομάδα του Καθηγητή S.-Q. Wang (Morton Institute of Polymer Science and Engineering, The University of Akron, Ohio, USA), διεξήχθησαν μελέτες ως προς την ρεολογική συμπεριφορά των γραμμικών και πολύπλοκης αρχιτεκτονικής ομοπολυμερών πολυ(ισοπρενίου) υψηλής περιεκτικότητας σε μικροδομή -3,4 ($\text{PI}_{3,4}$) με πολλά ενδιαφέροντα αποτελέσματα.

Curriculum Vitae

Fullname: Ntetsikas Konstantinos, DEng, MSc
Title: PhD Candidate
Address: Department of Materials Science Engineering
University of Ioannina
University Campus
Ioannina 45110
Greece
Communication: Tel: +30 26510 09028-9
Cell: +30 6945225153
Email: kntetsik@cc.uoi.gr

Personal Information

- **Date of Birth:** November 12th 1984
- **Place of Birth:** Ioannina
- **Nationality:** Greek
- **Marital Status:** Single

Languages

- English (“First Certificate in English”)

Studies

- **Sep. 2002- Sep. 2008:** Undergraduate Studies at the Department of Materials Science Engineering, University of Ioannina.
- **Nov. 2008- Nov. 2010:** MSc Thesis in Chemistry and Technology of Materials through the interdepartmental collaboration between Department of Materials Science Engineering and Department of Chemistry, University of Ioannina. MSc advisor: Associate Professor A. Avgeropoulos
MSc Thesis Title: ‘*Synthesis and Characterization of Methacrylate Diblock Copolymers - Studies of Chemically Modified and Non Modified Polymers – Properties*’
- **Nov.2010- May 2015:** PhD candidate in Polymer Science at Polymers Laboratory, Department of Materials Science Engineering, University of Ioannina. PhD advisor: Professor A. Avgeropoulos
Completion date of PhD: May 2015
PhD Thesis Title: ‘*Macromolecular Architecture for Complex Structures of Elastomers. Synthesis-Characterization-Properties*’

Educational Experience

2009-2015 (6 semesters in total)

- **Teaching Assistant**

“Materials Laboratory V (Polymer Materials)” in the Polymer Materials Laboratory, Department of Materials Science Engineering, University of Ioannina

Research Interests

- a). Synthesis of novel polymers via anionic polymerization using high vacuum techniques, linear and non-linear types of homopolymers, copolymers and terpolymers exhibiting low and high molecular weight. Chemical modifications of methacrylate diblock copolymers.
- b). Characterization and properties of polymers in dilute solutions via Size Exclusion Chromatography (SEC), Membrane Osmometry (MO), Vapor Pressure Osmometry (VPO), automated Viscometry (V), Proton and Carbon Nuclear Magnetic Resonance Spectroscopy ($^1\text{H-NMR}$, $^{13}\text{C-NMR}$).
- c). Morphological Characterization via Transmission Electron Microscopy (TEM), Scanning Electron Microscopy (SEM), Differential Scattering Calorimetry (DSC).
- d). Thin films, Nanolithography Techniques, Nanopatterning, Direct Self-Assembly (DSA) methods

Publications

1. “*Studying the Origin of “Strain Hardening”: Basic Difference Between Extension and Shear*”
Liu G., Sun H., Rangou S., Ntetsikas K., Avgeropoulos A., Wang S-Q.
***Journal of Rheology*, 2013, 57, 89-104.**
2. “*Breakdown of Time-Temperature Equivalence in Startup Uniaxial Extension of Entangled Polymer Melts*”
Sun H., Ntetsikas K., Avgeropoulos A., Wang SQ.
***Macromolecules*, 2013, 46, 4151-4159.**
3. “*Achieving Structural Control with Thin Polystyrene-b-Polydimethylsiloxane Block Copolymer Films: The Complex Relationship of Interface Chemistry, Annealing Methodology and Process Conditions*”
B.M.D. O’Driscoll, Kelly R.A., Shaw M., Mokarian-Tabari P., Lontos G., Ntetsikas K., Avgeropoulos A., Petkov N., Morris M.A.
***European Polymer Journal*, 2013, 49, 3445-3454.**
4. “*Rheology of Entangled Polymers Not Far above Glass Transition Temperature: Transient Elasticity and Intersegmental Viscous Stress*”
Sun H., Liu G., Ntetsikas K., Avgeropoulos A., Wang SQ.
***Macromolecules*, 2014, 47, 5839-5850.**

5. “*Thin Film Morphologies of Bulk-Gyroid Polystyrene-block-Polydimethylsiloxane Under Solvent Vapor Annealing*”
W. Bai, A.F. Hannon, K.W. Gotrik, H.K. Choi, K. Aissou, G. Lontos, K. Ntetsikas, A. Alexander-Katz, A. Avgeropoulos, C.A. Ross.
***Macromolecules*, 2014, 47, 6000-6008.**
6. “*High Throughput Sub-10 nm Metallic Particles Organization on Templates Made by Block Copolymer Self-Assembly and Nanoimprint*”
J. Arias-Zapata, J. Cordeiro, S. Bohme, C. Girardot, J. Garnier, P. Bezard, K. Ntetsikas, G. Lontos, A. Avgeropoulos, D. Peyrade, M. Zelsmann.
***Microelectronic Engineering*, 2015, 141, 155-159.**
7. “*Failure behavior after stepwise uniaxial extension of entangled polymer melts*”
H. Sun, P. Lin, G. Liu, K. Ntetsikas, K. Misichronis, N. Kang, J. Liu, A. Avgeropoulos, J. Mays, S-Q. Wang.
***Journal of Rheology*, 2015, 59, 751-767.**
8. “*Soft Graphoepitaxy for Large Area Directed Self-assembly of Polystyrene-block-poly(dimethylsiloxane) Block Copolymer on Nanopatterned POSS Substrates Fabricated by Nanoimprint Lithography*”
D. Borah, S. Rasappa, M. Salaun, M. Zellsman, O. Lorret, G. Lontos, K. Ntetsikas, A. Avgeropoulos, and M. A. Morris.
***Accepted in Advanced Functional Materials*, DOI: 10.1002/adfm.201500100**
9. “*Immiscible Polydiene Blocks in Linear Copolymer and Terpolymer Sequences*”
G. Zapsas, D. Moschovas, K. Ntetsikas, S. Rangou, J.-H. Lee, E. L. Thomas, N. E. Zafeiropoulos and A. Avgeropoulos.
Accepted in Journal of Polymer Science, Part B: Polymer Physics
10. “*Nanoscale Silicon Substrate Patterns From Self-Assembly of Cylinder-Forming Polystyrene-block-Poly(dimethylsiloxane) Block Copolymer on Silane Functionalized Surfaces*”
D. Borah, S. Rasappa, C. Cummins, S. M. D. Watson, A. R. Pike, B. R. Horrocks, D. A. Fulton, A. Houlton, G. Lontos, K. Ntetsikas, A. Avgeropoulos, and M. A. Morris.
Submitted in Langmuir
11. “*Nanopatterning via Self-Assembly of a Lamellar-Forming Polystyrene-block-Poly(dimethylsiloxane) Diblock Copolymer on Topological Substrates Fabricated by Nanoimprint Lithography*”
D. Borah, S. Rasappa, C. Cummins, M. Salaun, M. Zellsman, O. Lorret, G. Lontos, K. Ntetsikas, A. Avgeropoulos, M. A. Morris
Submitted in Advanced Functional Materials

12. “Combining Graphoepitaxy and Electric Fields Towards Uniaxial Alignment of Solvent-Annealed Poly(styrene)-*b*-Poly(dimethylsiloxane) Block Copolymers”
C. C. Kathrein, W. Bai, J. A. Currivan Incorvia, G. Lontos, K. Ntetsikas, A. Avgeropoulos, A. Boker, L. Tsarkova, C. A. Ross.
Submitted in ACS Nano

Participation in National Conferences

1. **7th Panhellenic Polymers Conference** (Ioannina, Greece, September 28–October 1, 2008)
2. **26th Panhellenic Conference of Solid State Physics and Materials Science** (Department of Physics, University of Ioannina, Ioannina, Greece, September 26-29, 2010)
3. **8th Hellenic Polymers Conference** (Hersonissos, Crete, Greece, October 24-29, 2010)
*Title: Synthesis, Molecular Characterization and Chemical Modification of Poly(Trimethylsilyloxymethyl Ether Methacrylate)-*b*-Poly(Methyl Methacrylate)”*
Ntetsikas K., Constantinou M. and Avgeropoulos A. (poster)
4. **E-MRS 2012 Spring Meeting** (Strasbourg, France, May 15-17, 2012)
Title: “Polydimethylsiloxane (PDMS)-based nanocomposite coatings: morphology, structure, thermal stability and optical properties”
L. E. Koutsokeras, K. Ntetsikas, G. Lontos, A. Avgeropoulos, P. Patsalas (poster)
Title: “Evaluation of the sp^2/sp^3 ratio of carbon materials from X-ray emission spectra”
D. F. Anagnostopoulos, L. E. Koutsokeras, D. Katsigiannopoulos, K. Ntetsikas, A. Avgeropoulos, P. Patsalas (oral presentation by L. E. Koutsokeras)
5. **APS March Meeting, 2012** (February 27- March 2, 2012, Boston, Massachusetts, USA)
Title: “Exploring the role of long-chain branching in large deformation of entangled melts”
Liu G., Ntetsikas K., Avgeropoulos A., Wang SQ. (oral presentation by Liu G.)
6. **9th Hellenic Polymer Conference** (Thermi, Thessaloniki, Greece, November 29-December 1, 2012)
Title: “Nanoimprint Lithography on Diblock Copolymer Thin Films”
K. Ntetsikas, D. Moschovas, C. Delgado Simao, N. Kehagias, C. M. Sotomayor Torres, A. Avgeropoulos (oral presentation by K. Ntetsikas)
7. **The Society of Rheology, 85th Annual Meeting** (October 13-17, 2013, Montreal, QC, Canada)
Title: “A rheo-optical study of monodisperse H-polyisoprenes to delineate the nature ‘strain hardening’ in uniaxial extension”
Liu G., Ntetsikas K., Avgeropoulos A., Wang SQ. (poster)

8. **2013 MRS Fall Meeting** (December 1-6, 2013, Boston, Massachusetts, USA)
Title: "Thin Film Morphology of a Bulk-Gyroid Block Copolymer"
 Bai W., Hannon A., Gotrik K., Aissou K., Choi H. K., Lontos G., Ntetsikas K., Avgeropoulos A., Katz A. A., Ross C. A. (poster)
9. **APS March Meeting 2014** (March 3–7, 2014, Denver, Colorado, USA)
Title: 'Shear and extensional rheology of model branched polymer melts (H shaped and grafted)' (oral presentation by Liu G.)
 Liu G., Ntetsikas K., Misichronis K., Mays J., Avgeropoulos A., Wang SQ.
10. **APS March Meeting 2014** (March 3–7, 2014, Denver, Colorado, USA)
Title: 'Thin Film Morphologies of Bulk-Gyroid Polystyrene-block-Polydimethylsiloxane under Solvent Vapor Annealing'
 W. Bai, A. Hannon, K. Gotrik, H.K. Choi, K Aissou, Lontos G., Ntetsikas K., Avgeropoulos A., Katz A. A., Ross C. A. (oral presentation by W. Bai)
11. **3rd International Conference on Industrial Technologies Research and Innovation** (April 9-11, 2014, Athens, Greece)

Participation in Research Programs

- **Funded by the European Union under the Call identifier: FP7-NMP-2009-SMALL-3 with Proposal No: CP-FP 245565-2 LAMAND (36 months, 1/7/2010-30/6/2013), title: "Large Area Molecularly Assembled Nanopatterns for Devices" and Acronym: "LAMAND", as *Researcher*.**
- **Funded by the European Union under the Call identifier:FP7-NMP-2007-LARGE-1, with Proposal No: CP-IP 213939-1 POCO (48 months, 1/11/2008-31/10/2012), title: "Carbon Nanotube Confinement Strategies to Develop Novel Polymer Matrix Composites" με το ακρωνύμιο "POCO", as *Researcher*.**

Visits to Foreign Institutes-Universities

- **February 4-9, 2012:** Participation together with PhD advisor at University of Newcastle Upon Tyne, Department of Chemistry for the 18-Month Meeting for the EU funded proposal (LAMAND).
- **May 15-29, 2012:** Visiting Researcher, *Phononics and Photonics Nanostructures Group, Catalan Institute of Nanotechnology, Campus de la UAB, Barcelona, Spain, Collaboration through EU funded proposal (LAMAND):* Training and research on nanolithography techniques for diblock copolymers of PS-b-PDMS, PS-b-PMMA, PS-b-PEO, PS-b-PB, PI-b-PPMDSS types.

Supervisor: Professor Clivia Sotomayor Torres

- **June 3-16, 2013:** Visiting Researcher, *Phononics and Photonics Nanostructures Group, Catalan Institute of Nanotechnology, Campus de la UAB, Barcelona, Spain*, **Collaboration through EU funded proposal (LAMAND):** Research on nanolithography techniques for triblock copolymers of PS-b-PDMS-b-PS type and comparison with results from PS-b-PDMS type.

Supervisor: Professor Clivia Sotomayor Torres